Publishing House ASV

begell house, inc. publishers

PAACH

Scientific coordination is carried out by the Russian Academy of Architecture and Construction Sciences (RAACS)

Volume 18 • Issue 4 • 2022

ISSN 2588-0195 (Online)
ISSN 2587-9618 (Print) Continues ISSN 1524-5845

International Journal for

Computational Civil and Structural Engineering

Международный журнал по расчету гражданских и строительных конструкций

http://raasn.ru/public.php
http://ijccse.iasv.ru/index.php/IJCCSE

DOI: 10.22337/2587-9618
GICID: 71.0000.1500.2830

PUBLISHER

ASV Publishing House
(ООО «Издательство АСВ»)
19/1,12, Yaroslavskoe Shosse, 120338, Moscow, Russia
Tel. +7(925)084-74-24; E-mail: iasv@iasv.ru; Интернет-сайт: http://iasv.ru/

ADVISORY EDITORIAL BOARD

TECHNICAL EDITOR

EDITORIAL TEAM

INVITED REVIEWERS

AIMS AND SCOPE

The aim of the Journal is to advance the research and practice in structural engineering through the application of computational methods. The Journal will publish original papers and educational articles of general value to the field that will bridge the gap between high-performance construction materials, large-scale engineering systems and advanced methods of analysis.

The scope of the Journal includes papers on computer methods in the areas of structural engineering, civil engineering materials and problems concerned with multiple physical processes interacting at multiple spatial and temporal scales. The Journal is intended to be of interest and use to researches and practitioners in academic, governmental and industrial communities.

ОБЩАЯ ИНФОРМАЦИЯ О ЖУРНАЛЕ

International Journal for Computational Civil and Structural Engineering

(Международный журнал по расчету гражданских и строительных конструкций)

Международный научный журнал "International Journal for Computational Civil and Structural Engineering (Международный журнал по расчету гражданских и строительных конструкций)" (IJCCSE) является ведущим научным периодическим изданием по направлению «Инженерные и технические науки», издаваемым, начиная с 1999 года (ISSN 2588-0195 (Online); ISSN 2587-9618 (Print) Continues ISSN 1524-5845). В журнале на высоком научно-техническом уровне рассматриваются проблемы численного и компьютерного моделирования в строительстве, актуальные вопросы разработки, исследования, развития, верификации, апробации и приложений численных, численно-аналитических методов, программно-алгоритмического обеспечения и выполнения автоматизированного проектирования, мониторинга и комплексного наукоемкого расчетно-теоретического и экспериментального обоснования напряженно-деформированного (и иного) состояния, прочности, устойчивости, надежности и безопасности ответственных объектов гражданского и промышленного строительства, энергетики, машиностроения, транспорта, биотехнологий и других высокотехнологичных отраслей.

В редакционный совет журнала входят известные российские и зарубежные деятели науки и техники (в том числе академики, члены-корреспонденты, иностранные члены, почетные члены и советники Российской академии архитектуры и строительных наук). Основной критерий отбора статей для публикации в журнале − их высокий научный уровень, соответствие которому определяется в ходе высококвалифицированного рецензирования и объективной экспертизы, поступающих в редакцию материалов.

Журнал входит в Перечень ВАК РФ ведущих рецензируемых научных изданий, в которых должны быть опубликованы основные научные результаты диссертаций на соискание ученой степени кандидата наук, на соискание ученой степени доктора наук по научным специальностям и соответствующим им отраслям науки:

- 1.1.8 – Механика деформируемого твердого тела (технические науки),
- 1.2.2 – Математическое моделирование численные методы и комплексы программ (технические науки),
- 2.1.1 – Строительные конструкции, здания и сооружения (технические науки),
- 2.1.2 – Основания и фундаменты, подземные сооружения (технические науки),
- 2.1.5 – Строительные материалы и изделия (технические науки),
- 05.23.07 – Гидротехническое строительство (технические науки),
- 2.1.9 – Строительная механика (технические науки)

В Российской Федерации журнал индексируется Российским индексом научного цитирования (РИНЦ).

Журнал входит в базу данных Russian Science Citation Index (RSCI), полностью интегрированную с платформой Web of Science. Журнал имеет международный статус и высылается в ведущие библиотеки и научные организации мира.

Издатели журнала – *Издательство Ассоциации строительных высших учебных заведений /АСВ/* (Россия, г. Москва) и до 2017 года *Издательский дом Begell House Inc*. (США, г. Нью-Йорк). Официальными партнерами издания является *Российская академия архитектуры и строительных наук* (РААСН), осуществляющая научное курирование издания, и *Научно-исследовательский центр СтаДиО* (ЗАО НИЦ СтаДиО).

Цели журнала – демонстрировать в публикациях российскому и международному профессиональному сообществу новейшие достижения науки в области вычислительных методов

решения фундаментальных и прикладных технических задач, прежде всего в области строительства.

Задачи журнала:

• предоставление российским и зарубежным ученым и специалистам возможности публиковать результаты своих исследований;

• привлечение внимания к наиболее актуальным, перспективным, прорывным и интересным направлениям развития и приложений численных и численно-аналитических методов решения фундаментальных и прикладных технических задач, совершенствования технологий математического, компьютерного моделирования, разработки и верификации реализующего программно-алгоритмического обеспечения;

• обеспечение обмена мнениями между исследователями из разных регионов и государств.

Тематика журнала. К рассмотрению и публикации в журнале принимаются аналитические материалы, научные статьи, обзоры, рецензии и отзывы на научные публикации по фундаментальным и прикладным вопросам технических наук, прежде всего в области строительства. В журнале также публикуются информационные материалы, освещающие научные мероприятия и передовые достижения Российской академии архитектуры и строительных наук, научно-образовательных и проектно-конструкторских организаций.

Тематика статей, принимаемых к публикации в журнале, соответствует его названию и охватывает направления научных исследований в области разработки, исследования и приложений численных и численно-аналитических методов, программного обеспечения, технологий компьютерного моделирования в решении прикладных задач в области строительства, а также соответствующие профильные специальности, представленные в диссертационных советах профильных образовательных организациях высшего образования.

Редакционная политика. Политика редакционной коллегии журнала базируется на современных юридических требованиях в отношении авторского права, законности, плагиата и клеветы, изложенных в законодательстве Российской Федерации, и этических принципах, поддерживаемых сообществом ведущих издателей научной периодики.

За публикацию статей плата с авторов не взымается. Публикация статей в журнале бесплатная. На платной основе в журнале могут быть опубликованы материалы рекламного характера, имеющие прямое отношение к тематике журнала.

Журнал предоставляет непосредственный открытый доступ к своему контенту, исходя из следующего принципа: свободный открытый доступ к результатам исследований способствует увеличению глобального обмена знаниями.

Индексирование. Публикации в журнале входят в системы расчетов индексов цитирования авторов и журналов. «Индекс цитирования» – числовой показатель, характеризующий значимость данной статьи и вычисляющийся на основе последующих публикаций, ссылающихся на данную работу.

Авторам. Прежде чем направить статью в редакцию журнала, авторам следует ознакомиться со всеми материалами, размещенными в разделах сайта журнала (интернет-сайт Российской академии архитектуры и строительных наук (http://raasn.ru); подраздел «Издания РААСН» или интернет-сайт Издательства АСВ (http://iasv.ru); подраздел «Журнал IJCCSE»): с основной информацией о журнале, его целями и задачами, составом редакционной коллегии и редакционного совета, редакционной политикой, порядком рецензирования направляемых в журнал статей, сведениями о соблюдении редакционной этики, о политике авторского права и лицензирования, о представлении журнала в информационных системах (индексировании), информацией о подписке на журнал, контактными данными и пр. Журнал работает по лицензии Creative Commons типа cc by-nc-sa (Attribution Non-Commercial Share Alike) – Лицензия «С указанием авторства – Некоммерческая – Копилефт».

Рецензирование. Все научные статьи, поступившие в редакцию журнала, проходят обязательное двойное слепое рецензирование (рецензент не знает авторов рукописи, авторы рукописи не знают рецензентов).

Заимствования и плагиат. Редакционная коллегия журнала при рассмотрении статьи проводит проверку материала с помощью системы «Антиплагиат». В случае обнаружения многочисленных заимствований редакция действует в соответствии с правилами COPE.

Подписка. Журнал зарегистрирован в Федеральном агентстве по средствам массовой информации и охраны культурного наследия Российской Федерации. Индекс в общероссийском каталоге РОСПЕЧАТЬ − 18076.

По вопросам подписки на международный научный журнал “International Journal for Computational Civil and Structural Engineering (Международный журнал по расчету гражданских и строительных конструкций)” обращайтесь в Агентство «Роспечать» (Официальный сайт в сети Интернет: http://www.rosp.ru/) или в издательство Ассоциации строительных вузов (АСВ) в соответствии со следующими контактными данными:

ООО «Издательство АСВ»

Юридический адрес: 129337, Россия, г. Москва, Ярославское ш., д. 26, офис 705;

Фактический адрес: 129337, Россия, г. Москва, Ярославское ш., д. 19, корп. 1, 5 этаж, офис 12 (ТЦ Соле Молл);

Телефоны: +7 (925) 084-74-24, +7 (926) 010-91-33;

Интернет-сайт: www.iasv.ru. Адрес электронной почты: iasv@iasv.ru.

Контактная информация. По всем вопросам работы редакции, рецензирования, согласования правки текстов и публикации статей следует обращаться к главному редактору журнала члену-корреспонденту РААСН *Сидорову Владимиру Николаевичу* (адреса электронной почты: sidorov.vladimir@gmail.com, sidorov@iasv.ru, iasv@iasv.ru, sidorov@raasn.ru) или к техническому редактору журнала советнику РААСН *Кайтукову Таймуразу Батразовичу* (адреса электронной почты: tkaytukov@gmail.com; kaytukov@raasn.ru). Кроме того, по указанным вопросам, а также по вопросам размещения в журнале рекламных материалов можно обращаться к генеральному директору ООО «Издательство АСВ» *Никитиной Надежде Сергеевне* (адреса электронной почты: iasv@iasv.ru, nsnikitina@mail.ru, ijccse@iasv.ru).

Журнал становится технологичнее. Издательство АСВ с сентября 2016 года является членом Международной ассоциации издателей научной литературы (Publishers International Linking Association (PILA)), осуществляющей свою деятельность на платформе CrossRef. Оригинальным статьям, публикуемым в журнале, будут присваиваться уникальные номера (индексы DOI – Digital Object Identifier), что значительно облегчит поиск метаданных и местонахождение полнотекстового произведения. DOI – это система определения научного контента в сети Интернет.

С октября 2016 года стал возможен прием статей на рассмотрение и рецензирование через онлайн систему приема статей Open Journal Systems на сайте журнала (электронная редакция): http://ijccse.iasv.ru/index.php/IJCCSE.

Автор имеет возможность следить за продвижением статьи в редакции журнала в личном кабинете Open Journal Systems и получать соответствующие уведомления по электронной почте.

В феврале 2018 года журнал был зарегистрирован в Directory of open access journals (DOAJ) (это один из самых известных поисковых сервисов в мире, который предоставляет открытый доступ к материалам и индексирует не только заголовки журналов, но и научные статьи), в сентябре 2018 года включен в продукты EBSCO Publishing.

В ноябре 2020 года журнал начал индексироваться в международной базе Scopus.

International Journal for
Computational Civil and Structural Engineering
(Международный журнал по расчету гражданских и строительных конструкций)
Volume 18, Issue 4 ***2022***

Scientific coordination is carried out by the Russian Academy of Architecture and Construction Sciences (RAACS)

CONTENTS

International Journal for
Computational Civil and Structural Engineering
(Международный журнал по расчету гражданских и строительных конструкций)
Volume 18, Issue 4 ***2022***

Scientific coordination is carried out by the Russian Academy of Architecture and Construction Sciences (RAACS)

СОДЕРЖАНИЕ

DOI:10.22337/2587-9618-2022-18-4-14-22

EXPERIMENTAL METHOD FOR STRUCTURAL CONCRETE DAMPING PROPERTIES EVALUATION

Vladimir A. Smirnov, Michail Yu. Smolyakov

Moscow State University of Civil Engineering (MGSU), Moscow, RUSSIA

Abstract. This article proposes a solution for structural materials such as concrete and cement mortars dynamic properties investigation using experimental modal analysis technique. The studied dynamic characteristics of structural materials include the dynamic modulus of elasticity and the loss factor or its derivatives: the logarithmic oscillation decrement or the relative damping coefficient. Closed expressions are presented for determining the loss factor of mechanical vibrations, obtained on the basis of solving the differential equation for vibrations of a single-mass dynamic system. A method for calculating the loss factor based on the analysis of the spectrum of the transfer function of an oscillatory system loaded with an impulsive dynamic force is presented, in which the results of measuring accelerations at various points of the sample are used as a response. The experiments were carried out on short and long samples made from samples of structural materials - cement mortars with a density of 1500 - 1900 kg/m^3 with special aggregates. Based on the solution of the equation of oscillations of a beam with distributed masses, a formula is presented for determining the dynamic modulus of elasticity of the beam material.

Keywords: dynamic tests, modal analysis, loss factor, modulus of elasticity, damping

ЭКСПЕРИМЕНТАЛЬНОЕ ОПРЕДЕЛЕНИЕ ДЕМПФИРУЮЩИХ ХАРАКТЕРИСТИК КОНСТРУКЦИОННЫХ МАТЕРИАЛОВ

В.А. Смирнов, М.Ю. Смоляков

Национальный исследовательский Московский Государственный Университет, г. Москва, РОССИЯ

Аннотация. В работе с применением метода экспериментального модального анализа исследуется возможность определения динамических характеристик конструкционных материалов, таких как бетоны и цементные растворы. К исследуемым динамическим характеристикам конструкционных материалов относят динамический модуль упругости и коэффициент потерь или его производные: логарифмический декремент колебаний или коэффициент относительного демпфирования. Представлены замкнутые выражения для определения коэффициента потерь механических колебаний, полученные на основании решения дифференциального уравнения колебаний одномассовой динамической системы. Представлен метод вычисления коэффициента потерь на основании анализа спектра передаточной функции колебательной системы, нагруженной импульсной динамической силой, в которой в качестве отклика использованы результаты измерения ускорений в различных точках образца. Эксперименты проводили на коротких и длинных образцах, выполненных из образцов конструкционных материалов – цементных растворов плотностью 1500 – 1900 кг/м^3 со специальными заполнителями. На основании решения уравнения колебаний балки с распределёнными массами представлена формула для определения динамического модуля упругости материала балки.

Ключевые слова: динамические испытания, модальный анализ, коэффициент потерь, модуль упругости, демпфирование

INTRODUCTION

The main parameters necessary for calculating the amplitudes of forced vibrations of structures are their dynamic characteristics - primarily the coefficient of mechanical energy loss, as well as the dynamic modulus of elasticity of the structural material. As a result of the application of external or internal loads, finite deformations will occur in the structural elements, which, under certain conditions, will lead to oscillations with very large amplitudes or to the loss of stability of the processes of static or dynamic deformation. It is very important for modern engineering practice to be able to predict the occurrence of such movements, instability or vibrations with large amplitudes in order to be able to control the level of static and dynamic stresses, the magnitude of the amplitudes during dynamic behavior, as well as the levels of transmitted or radiated noise in accordance with the needs of practical applications [1].

The importance of taking into account damping parameters is also due to the fact that the presence of damping can cause the process of energy transfer between the forms of oscillations of superstructures, which can, under certain conditions, lead to their destruction. Such an effect was noted and studied in [2, 3].

DYNAMIC MODEL

To determine the dynamic characteristics of samples of structural materials, ultrasonic research methods [16], methods of experimental modal analysis [11, 13–15], as well as methods with the application of a given forced external load [7, 8, 12] are used.

Consider the simplest single-mass model of vibrations of a damped system, shown in Fig. 1.

The equation of oscillations of the system under consideration under the action of a harmonic load is written as:

$$m\frac{d^2w}{dt^2}+C\frac{dw}{dt}+kw=F\cos\omega t\,. \qquad (1)$$

A particular solution w_p is a certain function w(t) that satisfies an inhomogeneous differential equation and, in particular, has the form [1, 2]:

$$w_p=\frac{F\cos\left(\omega t-\varepsilon\right)}{\sqrt{\left(k-m\omega^2\right)^2+\omega^2C^2}},\qquad \varepsilon=arctg\left[C\omega/\left(k-m\omega^2\right)\right]. \qquad (2)$$

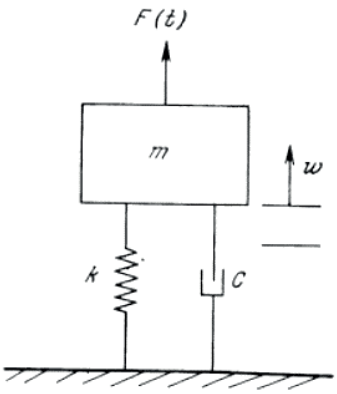

Figure 1. System with one degree of freedom and viscous damping

Then the general solution of equation (1) can be written as:

$$w=w_c+w_p=e^{-at}\left(C_1\sin\omega_Dt+C_2\cos\omega_Dt\right)+A_1\cos\left(\omega t-\varepsilon\right),\qquad A_1=F/\sqrt{\left(k-m\omega^2\right)^2+\omega^2C^2}\,. \qquad (3)$$

Arbitrary constants C_1 and C_2 are determined by the initial conditions.

One of the general methods for assessing damping, as noted in [1, 7, 10], is to determine the width of the resonant peak of oscillations at those points of the curve for dynamic displacements, at which the dynamic displacement makes up a certain proportion of

the resonant dynamic displacements of the system, for example, points A and B in figure 2. It is usually assumed that points A and B correspond to frequencies at which the amplitude of dynamic displacements is several times less than the maximum amplitude.

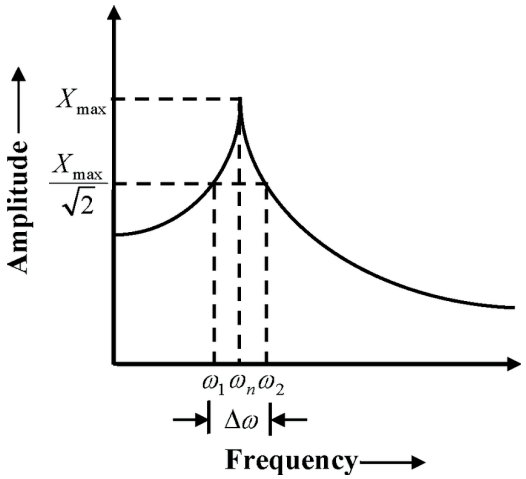

Figure 2. Frequencies that determine the bandwidth of the resonant amplitude

Consider the viscous damping of the system. The frequency of resonant vibrations is determined by the expression [1, 9, 11]:

$$\omega_{рез} = \sqrt{\frac{k}{m}\left(1-\frac{C^2}{2km}\right)} \tag{4}$$

Substituting (4) into (3), we find the oscillation amplitude at resonance:

$$W_{p,рез} = \frac{F}{k}\left[2\left(C/2\sqrt{km}\right)\left(1-C^2/4km\right)^{1/2}\right]^{-1} \tag{5}$$

In order to find the frequencies corresponding to points A and B, in which the amplitude is n times less than the resonant $W_{p,res}$, the dynamic displacement determined by the expression $\left|w_p/F\right| = 1/\sqrt{\left(k-m\omega^2\right)^2+\omega^2C^2}$ should be equated to the dynamic displacement (5) multiplied by 1/n at resonance, as a result of which we obtain:

$$\left(\frac{m\omega_i^2}{k}\right)^2 - 2\left(1-\frac{2C^2}{4km}\right)\frac{m\omega_i^2}{k} + 1 - 4n^2\frac{C^2}{4km}\left(1-\frac{C^2}{4km}\right) = 0. \tag{6}$$

When $C^2/4km << 1$, we obtain:

$$\omega_{1,2}\sqrt{m/k} = 1 \pm \sqrt{n^2-1}\,\frac{C}{2\sqrt{km}}, \tag{7}$$

Where do we get ratio:

$$\frac{\Delta\omega}{\omega_{рез}} = \frac{\omega_2-\omega_1}{\omega_{рез}} = 2\sqrt{n^2-1}\,\frac{C}{2\sqrt{km}}. \tag{8}$$

By $n=\sqrt{2}$ we obtain:

$$\frac{\Delta\omega}{\omega_{рез}} = 2\frac{C}{2\sqrt{km}} = 2\xi, \tag{9}$$

where $\xi = C/2\sqrt{km} = C/C_c$ - damping ratio; $C_c = 2\sqrt{km}$ - critical damping of the system.

Similar transformations can be performed for a system with hysteresis damping.
In this case, the amplitude at resonance is equal to:

$$W_{p,рез} = \frac{F}{k\eta}. \tag{10}$$

The frequencies corresponding to points A and B in Figure 2, in which the amplitude of dynamic displacements is n times less than the resonant amplitude $W_{p,res}$, are equal to:

$$\omega_{1,2} = \sqrt{\frac{k}{m}\left(1 \pm \eta\sqrt{n^2-1}\right)}. \tag{11}$$

Then with $n=\sqrt{2}$ we get:

$$\frac{\Delta\omega}{\omega_{рез}} = \sqrt{1+\eta} - \sqrt{1-\eta}\,, \qquad (12)$$

And with η << 1:

$$\frac{\Delta\omega}{\omega_{рез}} \approx \left(1+\frac{\eta}{2}\right) - \left(1-\frac{\eta}{2}\right) = \eta\,. \qquad (13)$$

The relation between $\Delta\omega / \omega_{рез}$ and η is linear only for small values of η. Note that for η > 1 there is no frequency ω1 under the assumption of hysteresis damping, at which the amplitude of dynamic displacements would be equal to $\left|W_p\right| / \sqrt{2}$. In fact, for n > 1, the "peak" amplitude will be less than the static displacement F/k. This is true not only for the case of hysteresis damping, but also for those cases where the parameters η(ω) and k(ω) are determined from experiments with real materials.

The dynamic modulus of elasticity reflects only the elastic properties of the material without the influence of creep, since when the sample vibrates, stresses appear in it, which are very small in magnitude. For this reason, the dynamic modulus of elasticity is approximately equal to the initial modulus of elasticity determined during static tests, and is much higher than the static modulus of deformation [4, 9]. The difference in the values of the dynamic and static modules is also due to the fact that the heterogeneity of concrete affects these modules by a different mechanism.

Within the framework of this study, the parameters of the frequencies of natural vibrations were determined using the methods of experimental modal analysis [7, 8], according to the results of which the frequencies of bending vibrations of the samples were determined.

The modulus of elasticity of the structural material was determined by the well-known formula for a hinged beam:

$$\omega_k = \left(\frac{k\pi}{l}\right)^2 \sqrt{\frac{EI}{m}}\,, \qquad (14)$$

where m is the mass per unit length of the beam, l is the span of the beam, EI is the bending stiffness of the beam, k is the shape number.

Based on formula (14) and the relationship between the circular and technical frequency in the form $\omega = 2\pi f$, we get an expression for determining the modulus of elasticity of the specimen in the form:

$$E = \frac{4mf^2l^4}{k^4\pi^2 I}\,. \qquad (15)$$

EXPERIMENTAL MODEL

The tests were carried out on samples made from different concrete compositions obtained in [5, 6]. The size of the samples in the first batch was 40x40x160 mm, and the second - 800x50x30 mm, which were installed on a tooling with hinged support at the ends.

The tests were carried out according to the method of GOST ISO 7626-5-99. The perturbation was created by exciting vibrations of a concrete prism with an impact hammer, applying 5 successive pulses at each location of the acceleration sensors.

A Bruel&Kjaer 8202 impact hammer (with a Bruel&Kjaer 8200 force sensor) was used to register the applied load, Bruel&Kjaer 4375 charge miniature accelerometers were used to register the response. does not affect test results. Synchronous recording of the excitation and response parameters was carried out by the SCADAS Mobile-I measuring system. The sample test scheme is shown in Figure 3.

After each impact, the signals from the force and vibration sensors are fed to low-pass filters (LPF), which allow avoiding the transfer of high-frequency components to the measurement frequency range during sampling, after which they are analog-to-digital conversion (ADC) to form a sample.

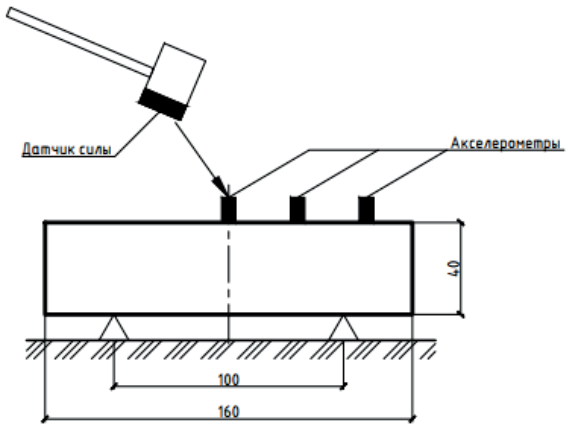

Figure 3. Experimental set-up for short specimen

Each digital entry corresponds to one impact. For each entry, the DFT is calculated. To improve the estimate, averaging over the frequency domain of several implementations of the frequency response obtained for the same measurement and excitation points can be applied.

For each point, at least 5 impulse actions were carried out with an impact hammer and the parameters of the input action - the applied force and the response of the structure - accelerations at different points were recorded, as shown in Figure 4 for one of the episodes of dynamic tests.

To obtain transfer functions, we analyzed the spectrum of the applied load, for which we built its auto spectral characteristic. For each block of impulse actions, the frequency response of the sample was built, which was averaged using a weighted average over several implementations.

a)

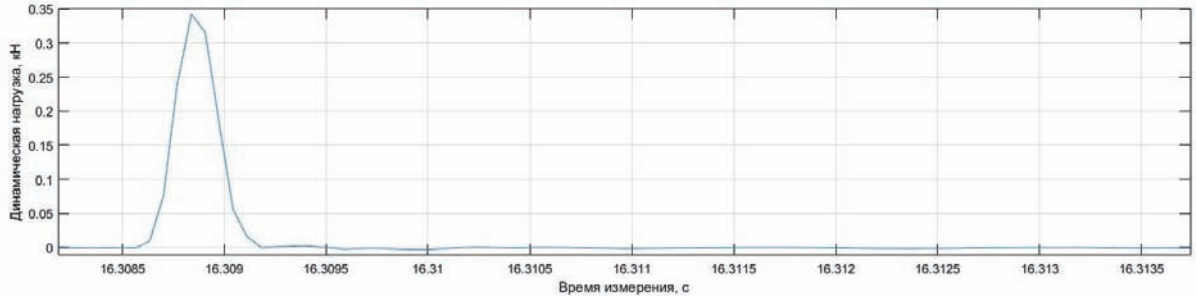

b)

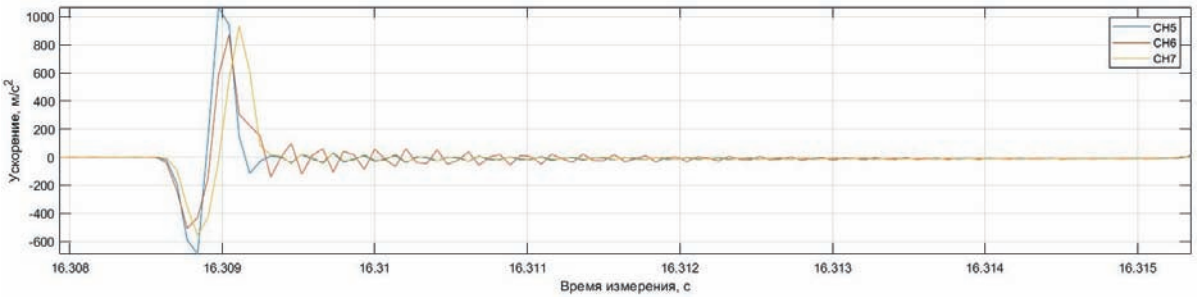

Figure 4. Dependence of applied force (a) on time and measured acceleration (b) on time

An example of the computed transfer function for a rack of one of the samples is shown in Figure 5, together with a signal coherence plot (a value close to 1 indicates a high signal-to-noise ratio, which improves measurement accuracy).

Based on the results of determining the frequency response - modal analysis, a stabilization diagram is constructed, within the framework of which the oscillation modes that are stable in frequency and damping are determined.

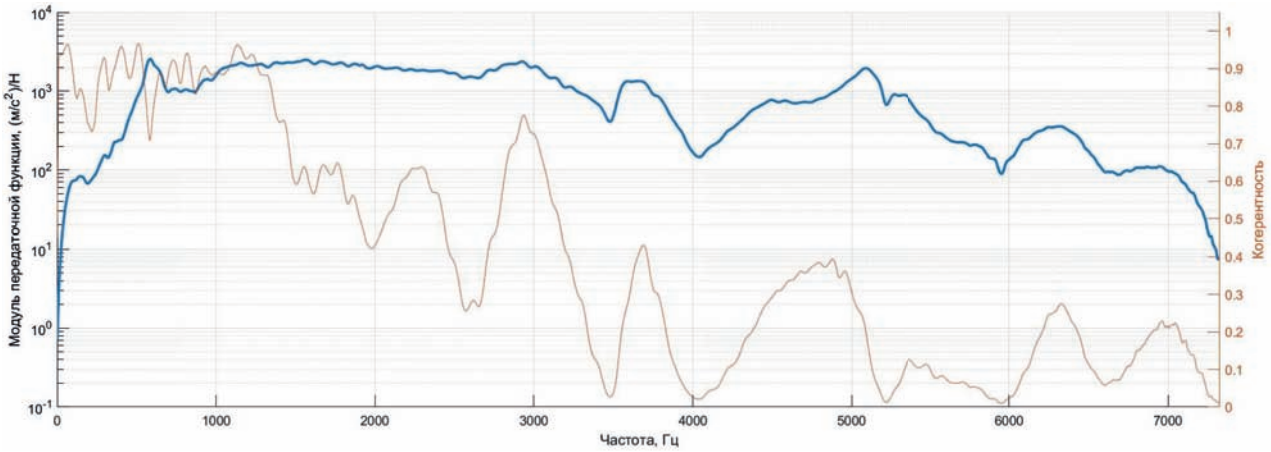

Figure 5. Representation of the results of calculating the frequency response of the sample

EXPERIMENTAL RESULTS

Based on the determination of a stable oscillation frequency corresponding to the bending shape, in which the maximum of the real part of the oscillation form corresponds to the antinode in the sensor located in the middle of the span of the test sample, and the phase shift (the imaginary part of the shape vector) between the sensor located in the middle and in thirds of the span the sample differs by π/2, the loss coefficient η and the relative damping coefficient ξ are determined. The test results for short specimens are shown in Table 1 and for long specimens in Table 2.

Table 1. Test results for short specimens

Specimen name	Avg value		
	η	ξ	Dynamic modulus, Pa
1500к	0.042	0.021	1.69E+10
1500к-ф	0.028	0.014	1.88E+10
1500с	0.133	0.067	1.02E+10
1500с-ф	0.171	0.085	9.93E+09
1700к	0.051	0.025	1.98E+10
1700к-ф	0.038	0.019	2.19E+10
1700с	0.091	0.045	1.51E+10
1700с-ф	0.109	0.054	1.61E+10
1900к	0.070	0.035	2.56E+10
1900к-ф	0.071	0.035	2.73E+10
1900с	0.034	0.017	2.09E+10
1900с-ф	0.025	0.013	2.01E+10
ТБ	0.020	0.010	3.74E+10
ТБ-ф	0.017	0.008	3.95E+10

Table 2. Test results for long specimens

Specimen name	Avg value		
	η	ξ	Dynamic modulus, Pa
1500к	0.126	0.063	2.91E+10
1500к-ф	0.124	0.062	3.27E+10
1500с	0.157	0.079	1.94E+10
1500с-ф	0.161	0.080	1.94E+10
1700к	0.153	0.076	7.85E+10
1700к-ф	0.104	0.052	3.71E+10
1700с	0.105	0.053	1.06E+12
1700с-ф	0.358	0.179	1.43E+10
1900к	0.094	0.047	4.14E+10
1900к-ф	0.080	0.040	4.63E+10
1900с	0.136	0.068	3.08E+10
1900с-ф	0.088	0.044	3.77E+10
ТБ	0.069	0.035	6.27E+10
ТБ-ф	0.078	0.039	8.07E+10

The results of comparing tests of short and long samples are shown in Figure 6.

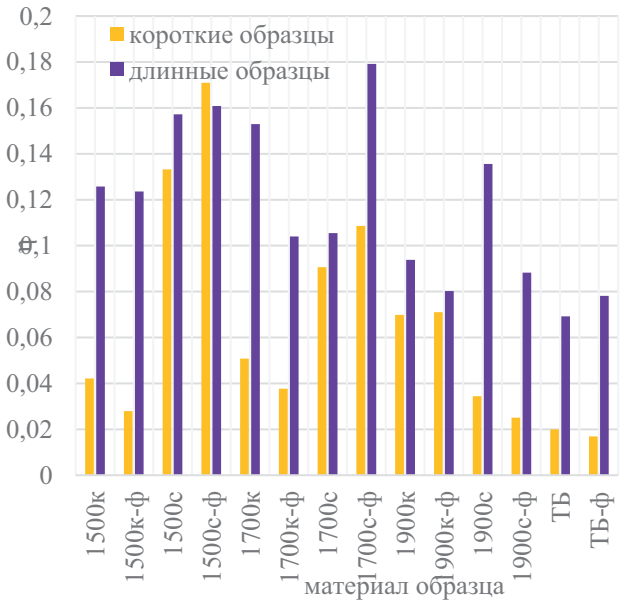

Figure 6. The results of comparing the damping parameters obtained on samples of different sizes

CONCLUSION

As the test results show, the introduction of ceramic microspheres increases the loss factor by 1.75 times with an increase in the density of the composition from 1500 to 1900 kg/m3. the introduction of spherical microspheres at the same time reduces the loss factor by 9 times. At the same time, the introduction of fiber into compositions with silicon spheres leads to a proportional decrease in the loss factor by a factor of 1.5 relative to compositions without fiber with an increase in the density of the composition. the introduction of fiber into compositions with glass microspheres increases the loss factor by 1.28 times relative to compositions without fiber.

The elastic modulus increases for all compositions with increasing sample density. At the same time, compositions with ceramic microspheres have a 30–40% higher elastic modulus than compositions with glass microspheres. The introduction of fibers into compositions with glass microspheres has very little effect on the change in their modulus of elasticity. The introduction of fiber into compositions with ceramic microspheres increases their modulus of elasticity by 11% compared to compositions without fiber.

For the base composition of heavy concrete (marking "TB"), the presence of fiber reduces the average value of the loss factor from 0.02 to 0.017 (34% reduction). In this case, the value of the modulus of elasticity increases by 12%.

The loss factor for samples depends on their shape and size. With an increase in the span of the sample (decrease in the first resonant frequency), the value of the loss factor increases.

To obtain adequate values of the damping coefficients, they should be determined on similar samples with close values of the frequencies of free oscillations. To take into account the dependence on frequency, it is recommended to carry out measurements on several samples with approximation of the results.

ACKNOWLEDGEMENT

This research has been supported by the Russian Science Foundation (Project No 21-19-00634).

REFERENCES

1. **Ahid D. Nashif and David I. G. Jones**. Vibration damping.Wiley, 1991 – 480 p.
2. **Rossikhin Yu.A, Shitikova M.V.** (2014b) Nonlinear dynamic response of a thin plate embedded in a fractional viscoelastic medium under combinational internal resonances. Appl Mech Mat 595: 105—110
3. **Rossikhin Yu.A., Shitikova M.V.** (1998) Application of fractional calculus for analysis of nonlinear damped vibrations of suspension bridges. ASCE J Eng Mech 124:1029—1036A.
4. **M. Neville.** properties of concrete. Abridged translation from English tech. Sciences V. D. PARFENOVA and T. Yu.

YAKUB. Publishing house of literature on construction. M.: - 1972, 345 pages.
5. **Inozemtsev A.S., Korolev E.V.** Deformations of high-strength lightweight concretes on hollow microspheres and a way to reduce them // Stroitelnye materialy. 2015. No. 9. pp. 23-30.
6. **Inozemtsev A.S., Korolev E.V.** Comparative analysis of the influence of nanomodification and microdispersed reinforcement on the process and parameters of destruction of high-strength lightweight concretes. Stroitel'nye materialy. 2017. No. 7. pp. 11-15.
7. **O. Døssing,** "Structural Testing 1 (Mechanical Mobility Measurements)." Brüel & Kjær, 1988.
8. **O. Døssing**, "Structural Testing 2 (Modal Analysis and Simulation)." Brüel & Kjær, 1988.
9. **Myklestad, N.O.** (1952) The concept of complex damping, J. of Applied Mechanics, pp. 284-286.
10. **Lazan, B.J.** (1968). Damping of Materials and Members in Structural Mechanics, Pergamon Press.
11. **Kohoutek, R**. (1992). Damping of concrete beams of different mix design, Proceedings of Materials Week'92, 2–5 November, Conference at Hyatt Regency, Chicago, pp95-102.
12. **Zaveri, K. and Olsen, H.P.** (1972). Measurement of elastic modulus and loss factor of asphalt, Technical Review No.4, Bruel & Kjaer, pp. 3-15.
13. **Kohoutek, R,** (1985). Analysis of beams and frames, Chapter 4 in Analysis and Design of Foundations for Vibrations, pp. 99-156; P. Moore, ed., 512pp, 1985, published by A.A. Balkema.
14. Khemapat Tontiwattanakul, Jirawin Sanguansin, Vatanavongs Ratanavaraha, Vanchai Sata, Suchart Limkatanyu, Piti Sukontasukkul, Effect of viscoelastic polymer on damping properties of precast concrete panel, Heliyon, Volume 7, Issue 5, 2021, e06967, ISSN 2405-8440, https://doi.org/10.1016/j.heliyon.2021.e06967.
15. **Lei B, Liu H, Yao Z, Tang Z**. 2019 Experimental study on the compressive strength, damping and interfacial transition zone properties of modified recycled aggregate concrete. R. Soc. open sci. 6: 190813. http://dx.doi.org/10.1098/rsos.190813
16. **Van Velsor, Jason & Premkumar, Laxmikanth & Chehab, Ghassan & Rose, J.** (2011). Measuring the Complex Modulus of Asphalt Concrete Using Ultrasonic Testing. Journal of Engineering Science and Technology Review. 4. 10.25103/jestr.042.08.

СПИСОК ЛИТЕРАТУРЫ

1. **Нашиф А., Джоунс Д., Хендерсон Дж.** Демпфирование колебаний: Пер. с англ. — М.: Мир, 1988. — 448 с., ил.
2. **Россихин Ю.А, Шитикова М.В.** (2014b) Нелинейный динамический отклик тонкой пластины, погруженной в частичную вязкоупругую среду, при комбинационных внутренних резонансах. Приложение Mech Mat 595: 105-110
3. **Россихин Ю.А., Шитикова М.В.** (1998) Применение дробного исчисления для анализа нелинейных затухающих колебаний подвесных мостов. ASCE J Eng Mech 124:1029-1036
4. **А. М. Невилль.** Свойства бетона. Сокращённый перевод с английского канд. техн. наук В. Д. ПАРФЕНОВА и Т. Ю. ЯКУБ. Изд-во литературы по строительству. М.: - 1972 г., 345 стр.
5. **Иноземцев А.С., Королев Е.В.** Деформации высокопрочных лёгких бетонов на полых микросферах и способ их снижения // Строительные материалы. 2015. № 9. С. 23-30.
6. **Иноземцев А.С., Королев Е.В.** Сравнительный анализ влияния наномодифицирования и микро-

дисперсного армирования на процесс и параметры разрушения высокопрочных лёгких бетонов // Строительные материалы. 2017. № 7. С. 11-15.
7. **О. Дессинг**, "Структурные испытания 1 (измерения механической подвижности)".Brüel & Kjær, 1988
8. **О. Дессинг,** "Структурное тестирование 2 (Модальный анализ и моделирование)."Брюэль и Кьер, 1988
9. **Миклестад, Н.О.** (1952) Концепция комплексного демпфирования, Журнал прикладной механики, стр. 284-286
10. **Лазан, Б.Дж.** (1968). Демпфирование материалов и элементов в строительной механике, Пергамский пресс.
11. **Кохутек Р.** (1992). Демпфирование бетонных балок различной конструкции, Материалы Недели материалов'92, 2-5 ноября, Конференция в Hyatt Regency, Чикаго, стр. 95-102
12. **Завери К. и Олсен Х.П.** (1972). Измерение модуля упругости и коэффициента потерь асфальта, Технический обзор № 4, Bruel & Kjaer, стр. 3-15.
13. **Кохутек, Р.,** (1985). Анализ балок и рам, глава 4 в разделе Анализ и проектирование фундаментов для вибраций, стр. 99-156; P. Moore, ред., 512 стр., 1985, опубликовано A.A. Balkema.
14. **Кхемапат Тонтиваттанакуль, Джиравин Сангуансин, Ватанавонгс Ратанавараха, Ванчай Сата, Сучарт Лимкатанью, Пити Суконтасуккуль,** Влияние вязкоупругого полимера на демпфирующие свойства сборных железобетонных панелей, Heliyon, Том 7, Выпуск 5, 2021, e06967, ISSN 2405-8440, https://doi.org/10.1016/j.heliyon.2021.e06967
15. **Лей Б, Лю Х, Яо З, Тан З.** 2019 Экспериментальное исследование прочности на сжатие, демпфирования и свойств межфазной переходной зоны модифицированного бетона из переработанного заполнителя. R. Soc. open sci. 6: 190813. http://dx.doi.org/10.1098/rsos.190813
16. **Ван Вельсор, Джейсон и Премкумар, Лаксмикант и Чехаб, Гассан и Роуз, Дж.** (2011). Измерение комплексного модуля упругости асфальтобетона с помощью ультразвукового контроля. Journal of Engineering Science and Technology Review. 4. 10.25103/jestr.042.08.

Smirnov Vladimir, Ph.D., Associate Professor of the Department of Structural and Theoretical Mechanics, Head of the Laboratory of Structural Dynamics, National Research Moscow State University of Civil Engineering (MGSU), 129337, Russia, Moscow, Yaroslavskoe shosse, 26, tel. +7 (495) 781-80-07, e-mail: belohvost@list.ru.

Смирнов Владимир Александрович, кандидат технических наук, доцент кафедры «Строительная и теоретическая механика», заведующий лабораторией динамики сооружений НИИ ЭМ, Национальный исследовательский Московский государственный строительный университет (НИУ МГСУ), 129337, Россия, г. Москва, Ярославское шоссе, д. 26, тел. +7 (495) 781-80-07, e-mail: belohvost@list.ru.

Smolyakov Michail, PhD student of the Department of Structural and Theoretical Mechanics, Engineer of the Laboratory of Structures Dynamics, National Research Moscow State University of Civil Engineering (MGSU), 26, Yaroslavskoe shosse, Moscow, 129337, Russia, tel. +7 (495) 781-80-07, e-mail: smolakovmu@gmail.com.

Смоляков Михаил Юрьевич, аспирант кафедры «Строительная и теоретическая механика», инженер лаборатории динамики сооружений НИИ ЭМ, Национальный исследовательский Московский государственный строительный университет (НИУ МГСУ), 129337, Россия, г. Москва, Ярославское шоссе, д. 26, тел. +7 (495) 781-80-07, e-mail: smolakovmu@gmail.com.

DOI:10.22337/2587-9618-2022-18-4-23-38

NUMERICAL MODELLING OF SNOW DEPOSITS AND SNOW TRANSPORT ON LONG-SPAN ROOFS FOR STEADY AND UNSTEADY FLOW

Nikita A. Britikov [1,2]

[1] National Research Moscow State University of Civil Engineering, Moscow, RUSSIA
[2] Russian University of Transport (RUT-MIIT), Moscow, RUSSIA

Abstract: This paper presents the methodologies for numerical modelling of snow deposits and snow transport on long-span roofs for steady and unsteady flow. The calculation of snow loads on long-span roofs is a complex problem, solving which often involves deviating from the building code recommendations. Experiments in wind tunnels, although widely used, do not allow reproducing the full-scale effects of all snow accumulation processes. At the same time, the continuous improvement of mathematical models, numerical methods, software and computer technologies makes the development and implementation of numerical modelling technologies in real construction practice and regulatory documents inevitable. In this paper it is shown that the use of the well-known erosion-deposition model, supported by field observations and experimental data, allows reproducing reasonably accurate snow distributions on long-span roofs. The importance of the "synthesis" between physical and mathematical modelling and the application of the building codes is emphasized, as only the joint use of approaches can comprehensively describe modelling of snow accumulation and snow transport and provide better solutions to a wider range of related problems.

Keywords: computational fluid dynamics, numerical modelling, snow accumulation, snow deposits, snow transport, structure roofs, numerical methods.

МЕТОДИКА ЧИСЛЕННОГО МОДЕЛИРОВАНИЯ СНЕГООТЛОЖЕНИЙ И СНЕГОПЕРЕНОСА НА ПОКРЫТИЯХ БОЛЬШЕПРОЛЁТНЫХ ЗДАНИЙ И СООРУЖЕНИЙ В СТАЦИОНАРНОЙ И НЕСТАЦИОНАРНОЙ ПОСТАНОВКАХ

Бритиков Н.А. [1,2]

[1] Национальный исследовательский Московский государственный строительный университет, г. Москва, РОССИЯ
[2] Российский университет транспорта (МИИТ), г. Москва, РОССИЯ

Аннотация: В данной работе представлена методика численного моделирования снегоотложений и снегопереноса на покрытиях большепролётных зданий и сооружений в стационарной и нестационарной постановках. Расчёт снеговых нагрузок на большепролётные покрытия является сложной задачей, для решения которой часто недостаточно одних лишь рекомендаций строительных норм. Эксперименты в аэродинамических трубах, хотя и применяются повсеместно, не позволяют воспроизвести полномасштабные эффекты всех процессов снегонакопления. В то же время, постоянное развитие математических моделей, численных методов, программного обеспечения и вычислительной техники делает безальтернативным развитие и внедрение технологий математического моделирования в реальную строительную практику и нормативные документы. В данной работе показано, что использование известной модели уноса-отложения, подкреплённое натурными наблюдениями и экспериментальными данными, способно воспроизводить достаточно точные картины распределений снега на большепролётные покрытия. Отдельно подчёркнута важность «синтеза» между физическим и математическим моделированием и применением нормативных рекомендаций, поскольку только

совместное использование подходов способно всесторонне раскрыть проблему моделирования снегоотложений и снегопереноса и дать наилучшее её решение для широкого спектра задач.

Ключевые слова: вычислительная аэродинамика, математическое моделирование, снегонакопление, снегоотложения, снегоперенос, покрытия сооружений, численные методы.

1. INTRODUCTION

Calculating the snow load on the roofs of large-span buildings and structures, including unique ones, often involves deviating from the building code recommendations for the shape coefficient and using experimental methods to determine the possible location of snowdrifts. Due to the fact that snow accumulation is a complex, highly non-linear and multi-scale phenomenon, the simulation of which is subject to different approaches depending on the problem in question, the development of a unified, verified and validated methodology for its numerical modelling is non-trivial. However, for most construction problems, the main interest is the snow transport, the greatest contribution to which (according to [4], from 50% to 75%) is made by saltation. In this regard, a methodology has been developed that allows to model snow transport and snow accumulation on large-span roofs of by means of numerical simulation of saltation, the results of which can then be used in combination with the building code recommendations for determining the design roof shape coefficient μ. Based on our previous studies ([1, 2, 3]), a decision was made to use the erosion-deposition model to simulate saltation. Since it describes the change of the height of the snow surface in time, the methodology was initially developed for unsteady flow. Then, to reduce resource intensity and increase efficiency, the methodology was developed for steady flow. The results of the verification and validation of the methodologies showed that, due to the extremely stochastic nature of the snow accumulation process, the use of modelled snow distribution maps alone is not sufficient to set the design shape coefficient μ. Nevertheless, numerical modelling makes it possible to identify areas of snow accumulation dangerous from the point of view of mechanical safety of the building, which cannot be predicted by the building code recommendations. Therefore, the symbiosis of the numerical modelling with the guidelines from the building code makes it possible to obtain the most crucial snow distributions on a particular roof.

2. UNDERLYING PRINCIPLES

Both methodologies utilize the erosion-deposition model (described in [6]), developed on the basis of some previous works of the early 1990s. The aforementioned model is based on the assumption that snow mass entrainment is the result of aerodynamic forces, while deposition is the result of settling and attachment of snow particles brought by wind flow. The change in snow cover height over time is described by the expression:

$$\frac{\partial h}{\partial t} = \frac{q_g}{\gamma}, \tag{1}$$

where h is the height of the snow surface, t is time, and γ is the bulk density of snow.
The snow mass exchange flux between air and snow cover q_g is given by:

$$q_g = q_+ - q_- \tag{2}$$

$$q_+ = C w_f \left(1 - \frac{u_*^2}{u_t^2}\right) \theta(u_t - u_*) \tag{3}$$

$$q_- = A \rho_a (u_*^2 - u_t^2) \theta(u_* - u_t), \tag{4}$$

where q_+ is the deposition flux, q_- is the erosion flux, C is the snow concentration in the air near the snow accumulation surface, w_f is the average snowfall velocity, A is the coefficient depending on the degree of cohesion (snow particles intergranular bonding), ρ_a is the air density, u_* is the friction velocity, u_t is the threshold friction

velocity, and θ is the Heaviside function. The friction velocity is determined by the following formula:

$$u_* = \sqrt{\frac{\tau_w}{\rho_a}} \quad (5)$$

where τ_w is the local shear stress on the surface calculated by numerical simulation of wind flows over the surface in question. Threshold friction velocity u_t is determined experimentally. If the friction velocity u_* is lower than the threshold velocity u_t, deposition is observed, otherwise, erosion is observed.

3. METHODOLOGY FOR UNSTEADY FLOW

The flowchart of the methodology for unsteady flow can be represented as the following list:

1. Analysis of the object
Analysis of climatic characteristics at the location, identification of possible snow accumulation and snow drift zones.
2. Problem statement
Selection of blowing directions and velocities, specifying the flow characteristics for each phase (snow concentration, friction velocity, etc.).
3. Computational model generation
Creation of a geometric model of the computational domain and a computational mesh that takes into account the points of interest of the object.
4. Selection and tuning of the turbulence model
Bearing in mind the computational optimization considerations.
5. Definition of the calculation parameters
Initial and boundary conditions, timestep size, numerical schemes and solvers.
6. Aerodynamic analysis
Transient analysis which utilizes custom code to calculate the change in snow height.
7. Engineering analysis of the calculation results
The equation (1) is solved at each timestep Δt with help of custom code, where $\partial t = \Delta t$, and the snow-surface mesh is deformed by moving each node in z direction by $\partial h = \Delta h$ provided by the equation. The problem is solved until a satisfactory result has been achieved.

4. VERIFICATION OF THE METHODOLOGY FOR UNSTEADY FLOW

Two problems were considered as verification problems:
1) The model problem (flow around a cube), for which snow accumulation is investigated qualitatively, with the formation of characteristic structures (windward and leeward snowdrifts and a horseshoe-shaped trace);
2) The building code problem (snow distribution on a gable roof), for which snow accumulation is investigated both qualitatively and quantitatively, with calculation of the shape coefficient μ for each slope.

4.1 Solution of the model problem for unsteady flow: a two-phase flow around a cube

In a rectangular computational domain of 10×10×5 m a Eulerian two-phase flow around a 1×1×1 m cube (primary phase is air, secondary phase is solid particles) with a logarithmic velocity profile at the inlet is simulated for 60 min with timestep of 1 s. In this problem the density of the secondary phase is 150 kg/m^3. An aerodynamic domain (Fig. 1c) is formed from the finite-volume mesh (Fig. 1b). A series of additional steady-state calculations were carried out to select the initial value of the snow volume fraction at the inlet and the initial friction velocity. Based on the results, they were set to $1 \cdot 10^{-4}$% and 0.3 m/s, respectively. Realizable *k-ε* model was used for turbulence modelling.
The calculated snow accumulation (Fig. 1d) in general agrees with the field experiment (Fig. 1a): two characteristic drifts on the windward and leeward sides and a horseshoe-shaped trace of the erosion flow are observed. The results suggest that the application of the erosion-deposition model for the saltation is sufficient to produce

snow drifts of characteristic shapes and to simulate snow transport. However, they also demonstrate the stochasticity of the snow accumulation and the resource-intensive nature of the modelling itself, for a very small timestep is required for problem's adequate convergence.

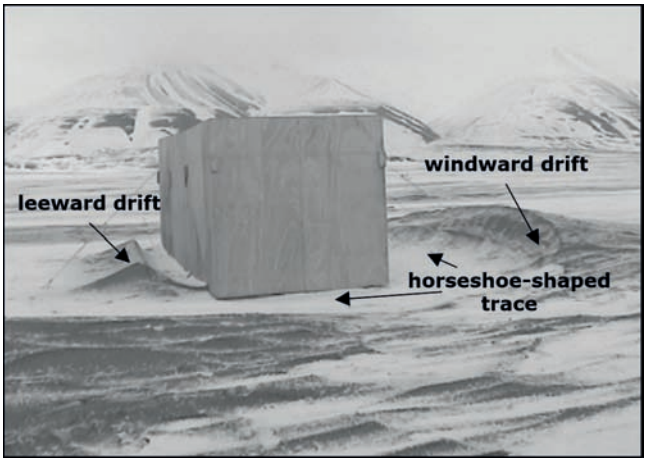

a) snowdrift around a low-rise construction (from [8])

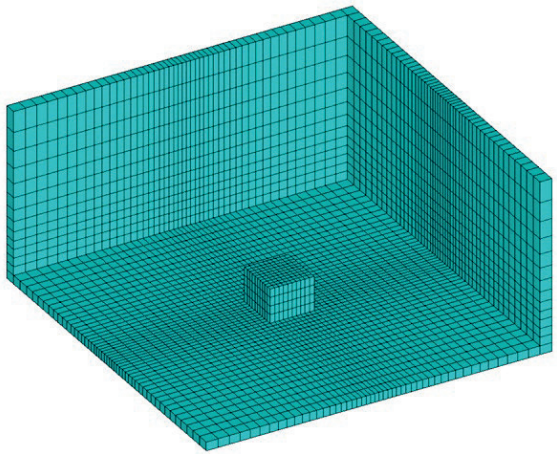

b) outer layer of the finite-volume mesh (~35.8k cells)

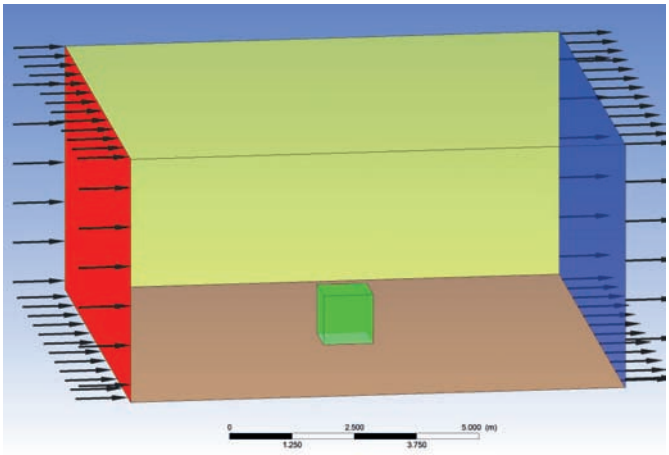

c) layout of the aerodynamic domain

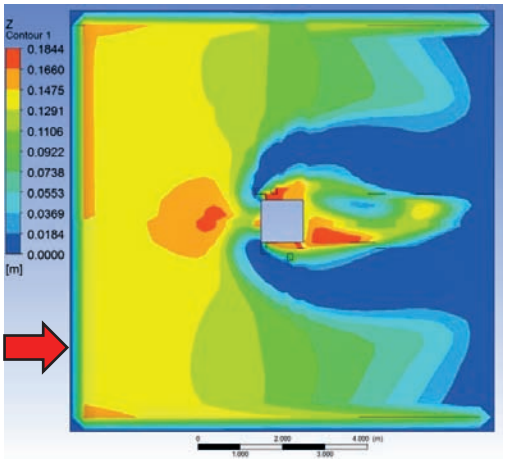

d) snowdrift around the cube at the end of the simulation (t = 3600 s)

Figure 1. Unsteady numerical modelling of snow accumulation and snow transport around a cube

4.2 Solution of the building code problem for unsteady flow: a two-phase flow around a gable roof

In a rectangular computational domain of 40×38×15 m, a Eulerian two-phase flow around a 10×8×6 m building with the same characteristics as given in paragraph 4.1 is simulated for 50 min with timestep of 1 s. An aerodynamic domain (Fig. 2c) is formed from the finite-volume mesh (Fig. 2b). In this problem, a series of additional steady-state calculations were also carried out to select the initial value of the snow inlet volume fraction and the initial friction velocity. Realizable k-ε model was used for turbulence modelling, as well.

The calculated snow accumulation (Fig. 2d) allows to conclude that *qualitatively* snow erosion was obtained on the windward side of the roof, snow deposition was obtained on the leeward side, and a horseshoe-shaped trace was

obtained around the building, but *quantitatively* the result does not agree with the building codes, because snow erosion is almost complete (in contrast to the expected $\mu = 0.75$ according to the code).

In conclusion, based on the results of the verification, it is demonstrated that the erosion-deposition model can be applied to simulate snow accumulation and snow transport for unsteady flow and allows to obtain a *qualitative* result; however, obtaining adequate *quantitative* result requires multiple calculations with varying initial conditions and analysis of intermediate results, which are special cases of snow accumulation.

a) snow distribution on a gable roof (from [9])

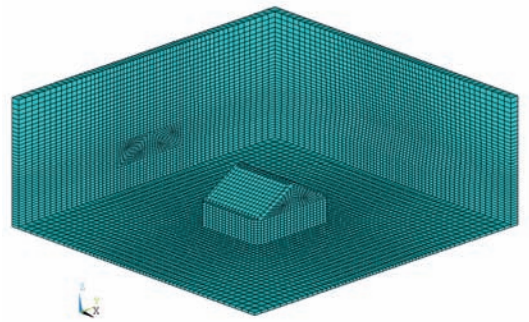

b) outer layer of the finite-volume mesh (~143k cells)

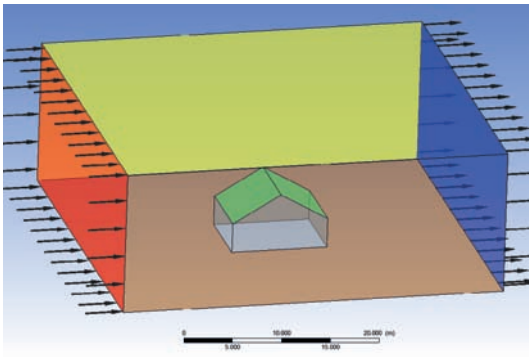

c) layout of the aerodynamic domain

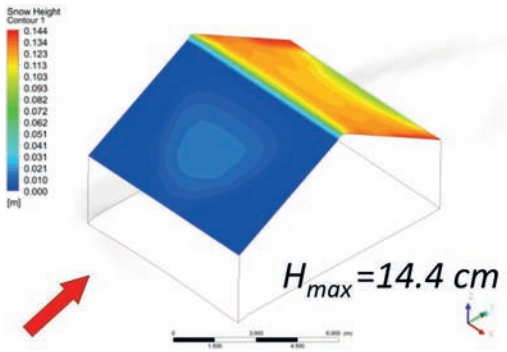

d) snow distribution on a gable roof at the end of the simulation (t = 3000 s)

Figure 2. Unsteady numerical modelling of snow accumulation and snow transport on a gable roof

5. VALIDATION OF THE METHODOLOGY FOR UNSTEADY FLOW

The validation is performed for a real building under construction for which snow accumulation on the roof is to be investigated.

In a rectangular computational domain of 519×953×125 m, a two-phase flow around an industrial building with the same characteristics as in paragraph 4.1 is simulated for 40 min with timestep of 1 s. In this problem the density of the secondary phase is 300 kg/m^3. An aerodynamic domain (Fig. 3c) is formed from the finite-volume mesh (Fig. 3b & 3d). Initial conditions, the inlet velocity and snow volume fraction, were varied to obtain different snow accumulation patterns on the roof. The parameters are presented in Table 1.

As a result, three snow accumulation distributions were obtained on the roof. Although qualitatively they allow determining the direction of snow transport and quantitatively the height of snow cover, it is not possible to draw a general

conclusion for the value of the design shape coefficient μ from them, as individual cases of snow accumulation are obtained.

In conclusion, the results suggest that it is not possible to directly use the data from the unsteady flow modelling to determine the design shape coefficient μ.

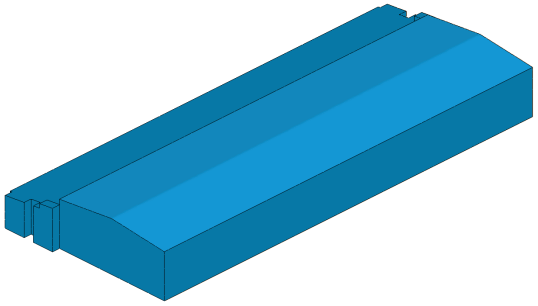

a) geometry of the industrial building

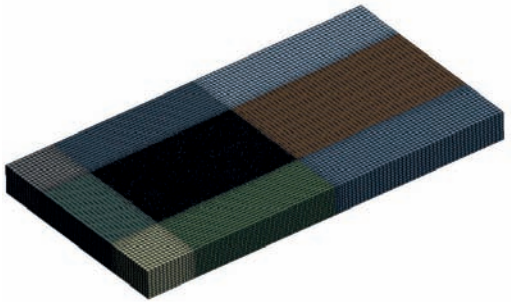

b) finite-volume mesh (~1.7m cells)

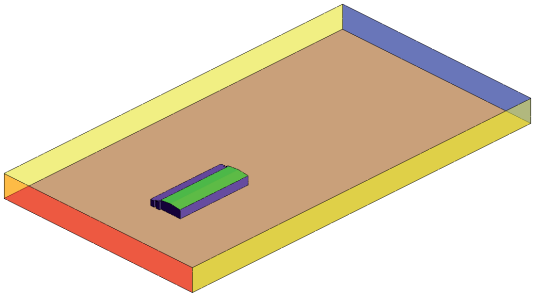

c) layout of the aerodynamic domain

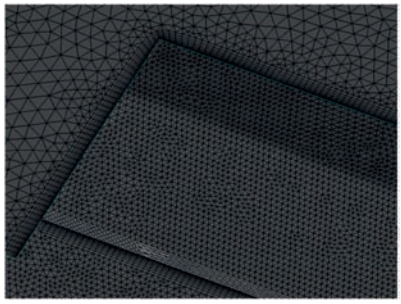

d) inflation in the boundary layer

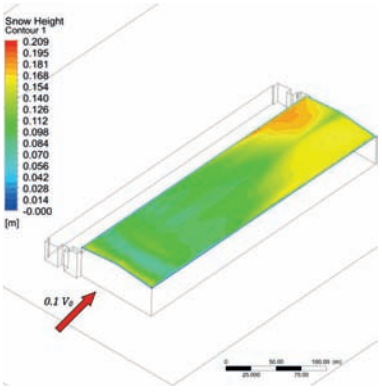

e) final snow distribution for case 1 (see table 1 for details)

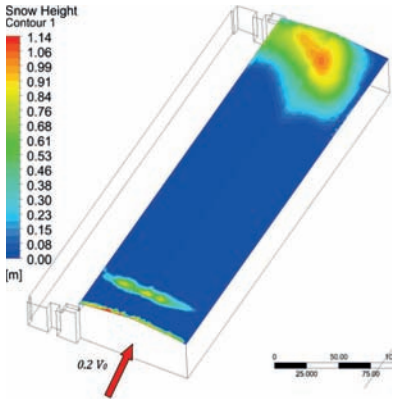

f) final snow distribution for case 2

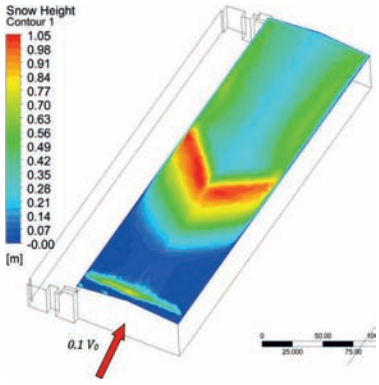

g) final snow distribution for case 3

Figure 3. Unsteady numerical modelling of snow accumulation and snow transport around an industrial building

Table 1. Validation cases summary

Case number	***Simulated snowfall***	***Velocity at 10 m above ground [m/s]***	***Snow surface maximum height [cm]***	***Snow phase maximum concentration [%·10^{-3}]***	***Snow distribution***
1	Mild	0.84	20.9	0.19	Close to even
2	Mild	1.69	114	1.34	Uneven
3	Moderate	0.84	105	1.2	Uneven

6. METHODOLOGY FOR STEADY FLOW

Due to the problems identified during verification and testing of the methodology for unsteady flow, it was necessary to change the approach and develop a methodology for steady flow, reducing resource intensity but not losing accuracy.

For these reasons, the erosion-deposition model is supplemented by two hypotheses:

Hypothesis 1: There is initially some amount of snow $\mu_0 = const$ on the roof;

Hypothesis 2: The flux q_g and its constituent parameters are time-independent.

The *modelled shape coefficient* μ_m is also introduced to emphasize the difference between it and the design shape coefficient μ.

Then, integrating expression (1), we obtain:

$$\int_0^H dh = \frac{1}{\gamma}\int_0^T q_g dt, \qquad (6)$$

where $H = (\mu_m - \mu_0)S_n/\gamma$ is the change in snow cover height, T is the observed time period, and S_n is the characteristic value of snow on the ground at the relevant site.

Assuming q_g to be time-independent, (6) can be rewritten as:

$$\frac{(\mu_m - \mu_0)}{\gamma} = \frac{T}{\gamma} q_g$$
$$\mu_m = \mu_0 + \frac{T}{\gamma} q_g \qquad (7)$$

Separate *observing time periods* for snow deposition T_+ and for snow erosion T_-. are also introduced. Finally:

$$\mu_m = \mu_0 + \frac{q_+ T_+ - q_- T_-}{S_n} \qquad (8)$$

By varying the initial amount of snow μ_0, the observing time periods T_+ и T_-, and the wind speed at the inlet, different snow accumulation distributions and different contours of the modelled shape coefficient μ_m on the roof can be obtained to find the most unfavourable ones, which are determined from the mechanical safety considerations for the building.

It is important to note, with reference to the conclusions of the validation of the methodology for unsteady flow, that the obtained distributions of the modelled shape coefficient μ_m are used *qualitatively in conjunction with the building code recommendations*. Based on the synthesis of these approaches, the design shape coefficient μ is obtained.

For turbulence modelling, the Generalized *k-ω* model (see [5]) is used. Through adjustments of certain coefficients, it can be tuned for particular objects and can predict the boundary layer flow more accurately, which is crucial for determining the shear stress and, subsequently, the friction velocity. It comprises the capabilities of previously used *k-ε* and *k-ω* models, which at this point renders their further use redundant.

The flowchart of the methodology for steady flow can be represented as the following list:

1. ***Analysis of the object***
Analysis of climatic characteristics at the location, identification of possible snow accumulation and snow drift zones.

2. ***Problem statement***
Selection of blowing directions and velocities, specifying the flow characteristics (friction velocity, etc.).

3. ***Computational model generation***
Creation of a geometric model of the computational domain and a computational mesh that takes into account the points of interest of the object.

4. ***Tuning of the turbulence model***
Adjustment of the GEKO coefficients for proper simulation of the flow around the particular object.

5. ***Definition of the calculation parameters***
Initial and boundary conditions, numerical schemes and solvers.

6. ***Aerodynamic analysis***
Steady-state analysis which utilizes the modified erosion-deposition model, supplemented by hypotheses 1 and 2.

*7. **Engineering analysis of the calculation results***
Derivation of the design shape coefficient μ through the synthesis of numerical modelling and building codes.

7. VERIFICATION OF THE METHODOLOGY FOR STEADY FLOW

Similar problems were considered for verification but the geometry of the dynamic contour of the CSTB wind tunnel (Fig. 4a) was used for the computational domain, as the data from [7] was utilized.

7.1 Solution of the model problem for steady flow: a one-phase flow around a cube

In a computational domain of 23×10×6 m, the one-phase flow around a 1×1×0.5 m cube with a logarithmic velocity profile at the inlet is simulated for 150 iterations. As with the previous simulations, an aerodynamic domain is formed from the finite-volume mesh (Fig. 4b & 4c).
The calculated snow accumulation (Fig. 4d & 4e) is consistent with both field observations, physical modelling in the wind tunnel and numerical modelling results for unsteady flow. The snow distribution on the top face of the cube is also observed, although not taken into account during the verification procedure. Similar to the unsteady flow case, two characteristic drifts on the windward and leeward sides and a horseshoe-shaped trace of the erosion flow are observed. The results allow to conclude that the modified erosion-deposition model can adequately simulate snow accumulation and snow transport for steady flow.

7.2 Solution of the building code problem for unsteady flow: a one-phase flow around a gable roof

In the same computational domain from the paragraph 7.1, the one-phase flow around a 1×1×0.92 m building with a logarithmic velocity profile at the inlet is simulated for 150 iterations. An aerodynamic domain (Fig. 5a) is formed from the finite-volume mesh (Fig. 5b).
The calculated snow accumulation (Fig. 5d) suggests that *qualitatively* an uneven distribution of snow on the roof and a horseshoe-shaped trace around the building is obtained. *Quantitatively*, the result is close to the physical modelling (Fig. 5c), but not close enough to the building code distribution (see Table 2, total discrepancy ~22%).
In conclusion, the advantage of the steady-state approach over the transient approach is demonstrated, but the modelling results still *cannot be used directly* for the design shape coefficient. It should be also noted that the absolute height of the snow surface depends on the observing time periods T_+ and T_- and can be adjusted, but the pattern of the snow accumulation and snow transport itself remains unchanged and depends entirely on the shear stress pattern on the roof.

8. VALIDATION OF THE METHODOLOGY FOR STEADY FLOW

The methodology for steady flow has been validated on several real objects under construction, for which the synthesis of numerical modelling and building code recommendations has given the design shape coefficient μ. For all simulations, the following values of experimental constants were taken: $A\rho_a$ = 10^{-4} kg·s/m^4, w_f = 0.5 m/s, u_t = 0.25 m/s.

8.1 Community Centre

In a cylindrical computational domain of 600×100 m, the one-phase flow around a civil building (Fig. 6a) is simulated for 200 iterations. Ten simulations were carried out for the two wind directions due to the symmetry of the building (180° and 210°; 20 simulations total) using the numerical methodology for steady flow with varying wind speed without considering the surrounding buildings. According to Table 7.1 of SP 131.13330.2020 *Construction Climatology*, the average wind velocity at a height of 10 m

during the winter period for the centre's location is 2.6 m/s. Simulations were carried out in the velocity range from 1 m/s to 10 m/s in steps of 1 m/s. The snow concentration C was assumed to be 5 g/m^3, which corresponds to a moderate snowfall. The contours of modelled shape coefficient μ_m obtained by numerical simulation for steady flow (Fig. 6c & 6e) were then analyzed to identify the most unfavourable cases from the mechanical safety point of view and summarized in the form of contours of the design shape coefficient μ.

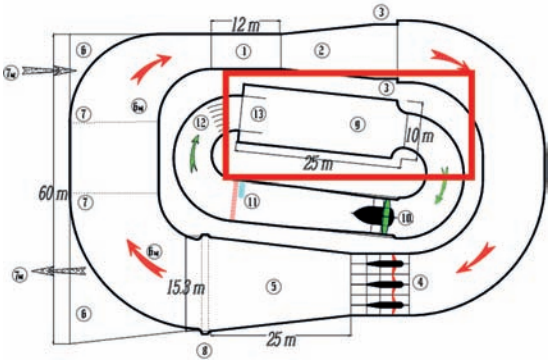

a) modelled part of the dynamic contour of the CSTB wind tunnel

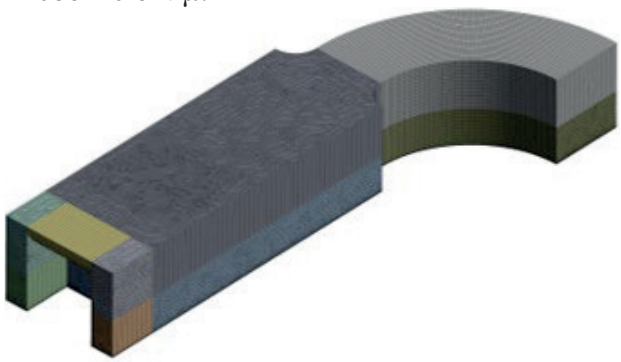

b) finite-volume mesh (~1.47m cells)

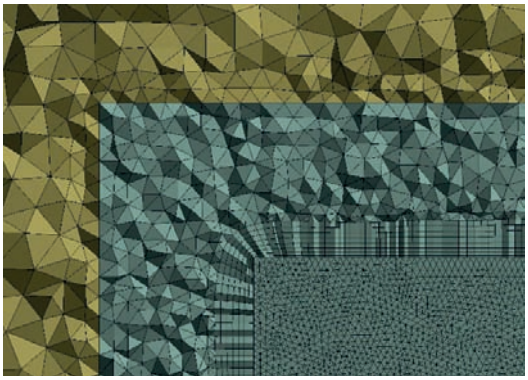

c) inflation in the boundary layer

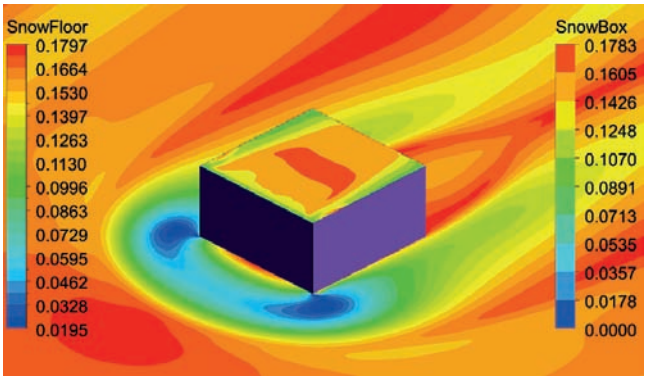

d) snow distribution on and around the cube at the end of the simulation (150 iterations, T_+=3600 s)

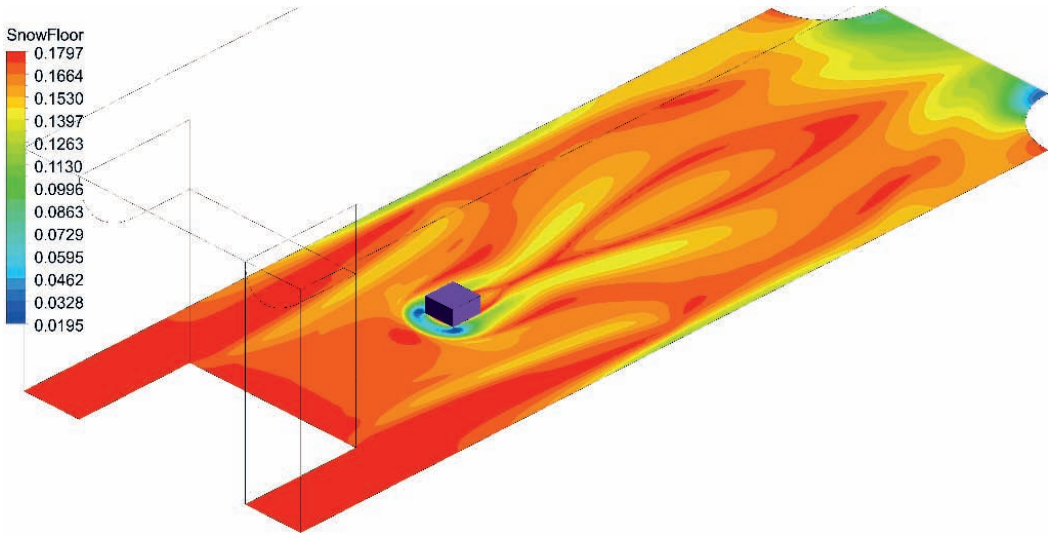

e) snow distribution in the whole aerodynamic domain

Figure 4. Steady numerical modelling of snow accumulation and snow transport around a cube

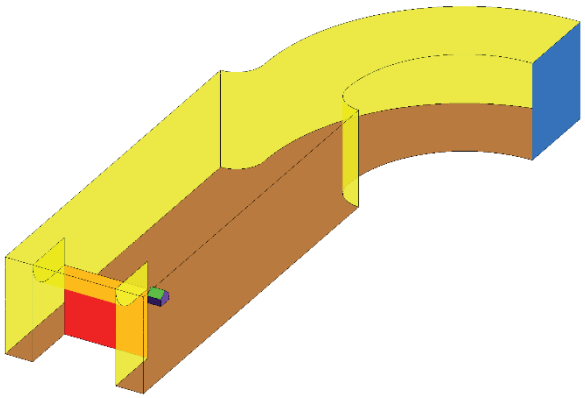

a) layout of the aerodynamic domain

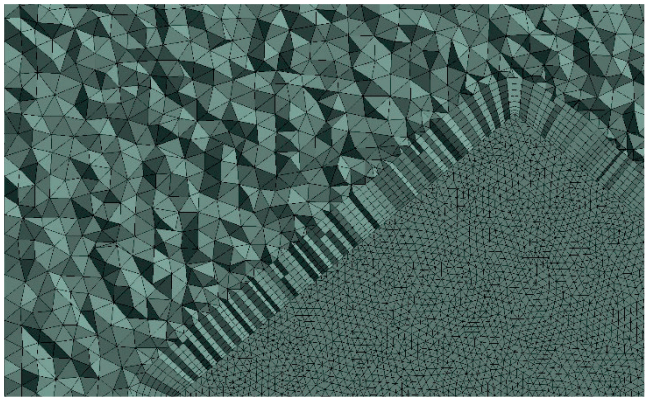

b) inflation in the boundary layer of the finite-volume mesh (~1.65m cells total)

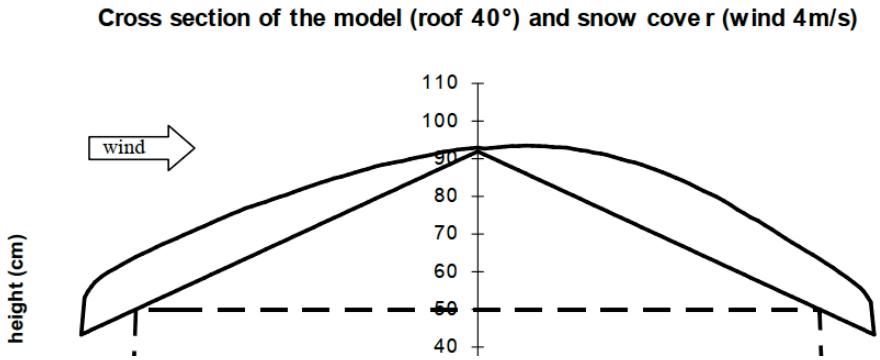

c) physical modelling of snow distribution on a gable roof (from [])

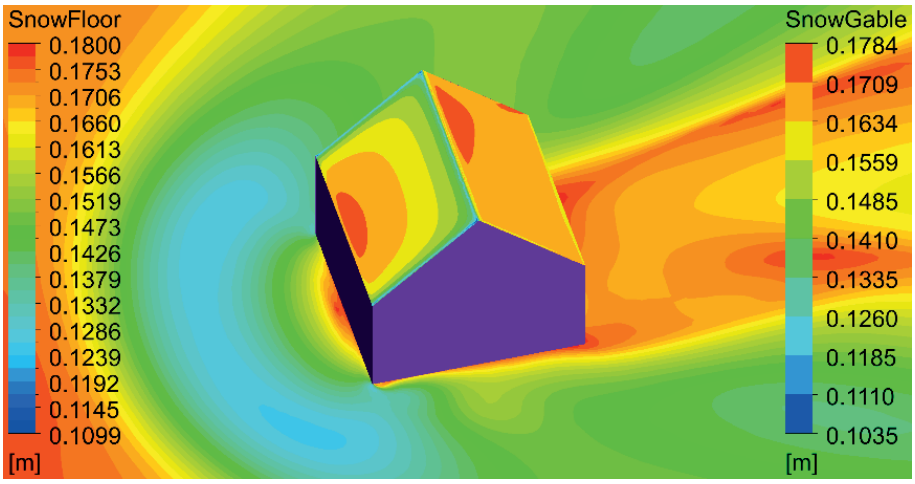

d) snow distribution on a gable roof at the end of the simulation (150 iterations, T_+=3600 s)

Figure 5. Steady numerical modelling of snow accumulation and snow transport on a gable roof

Table 2. Comparison of physical and numerical modelling of snow on a gable roof

Modelling approach	***Windward shape coefficient***	***Leeward shape coefficient***
Physical	0.88	1.13
Numerical	0.96	1.03
Discrepancy	9.1%	8.8%

The Community Centre simulations allowed thorough adjustments to the methodology. As such, they revealed that such a wide range of inlet velocities was excessive, and fewer velocities (as well as study cases) can be utilized in obtaining the contours of the modelled shape coefficient μ_m. It was also shown that an average value of 0.25 m/s for the threshold friction velocity is sufficient for achieving plausible snow distributions for real buildings.

8.2 Sports Centre

In a cylindrical computational domain of 1500×1200 m, the one-phase flow around a civil building (Fig. 7a) is simulated for 200 iterations. For this problem, two setups were considered: the one that includes the surrounding buildings and terrain around the Sports Centre (Fig. 7b) and the one that doesn't. This was made to both demonstrate the influence of the environment on the snow distribution and obtain more varied distributions in search of the most unfavourable ones.

In numerical modelling, three simulations were carried out for eight wind directions for the Sports Centre (0°, 36°, 90°, 144°, 180°, 213°, 270°, 327°; 24 simulations total) using the numerical methodology for steady flow with varying wind speed. With reference to the conclusions of the previous case, simulations were only made for wind speeds of 1 m/s, 3 m/s and 6 m/s. To simulate a longer snowfall, in which an uneven snow distribution can be obtained, the deposition time T_+ was assumed to be 6 h and the erosion time T_- to be 240 h.

A more traditional physical modelling in the wind tunnel was also carried out for the Sports Centre, which allowed to both compare the results given by two approaches and validate one through the other. In physical modelling, the same wind directions were investigated as for the numerical, and the characteristic wind speeds at which snow transport was analyzed on the model ranged from 3.4 to 8 m/s. The modelling was performed at 3.5-4% humidity using wood flour with a particle size of 50÷250 μm as a snow-like material, which was shifted from a smooth painted surface at a wind speed of 3.4 m/s. As a result of prolonged exposure of the model covered with a thin layer of wood flour in the air flow at a speed of 6÷7 m/s, the patterns of snow transport were formed. Analysis of the obtained snow distributions was performed to zone the roof and obtain the *physically-modelled shape coefficient* μ_{mp} for the zones. As with the numerical modelling, the simulations were carried out with and without taking into account the surrounding buildings, albeit in a lesser radius due to the wind tunnel test chamber size.

Through the comparison of the results, it was clearly observed that both the physical and the numerical modelling provide mostly similar snow distributions. The overall distribution pattern, as well as some local snow drifts, were in agreement with each other (compare Fig. 7c vs. 7e & Fig. 7d vs. 7f and Fig. 8a vs. 8c & Fig. 8b vs. 8d). A similar influence of the surrounding buildings on the obtained contours was also noted. As per the methodology, the results given by the two approaches were summarized and used qualitatively in the engineering analysis in conjunction with the building code recommendations, which provided the final contours of design shape coefficient μ (Fig. 7e; note a small μ = 2.7÷0.6 zone on the right side of the picture, which was specified by the code).

In conclusion, the use of numerical modelling for both validation cases made it possible to provide the design shape coefficient μ, as well as identify some non-obvious and hazardous distributions of said coefficient, which could not be obtained solely by following the recommendations of the Russian building code or any other building codes. The physical modelling carried out for the Sports Centre also evidently showed that numerical modelling is capable of providing similar and thus plausible results, which are true to the nature of the snow accumulation and snow transport processes.

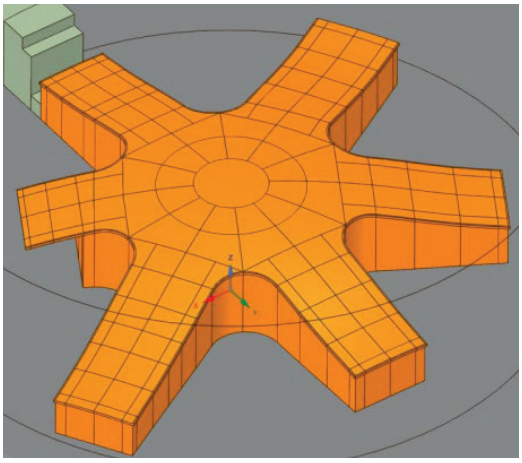

a) geometry of the Community Centre

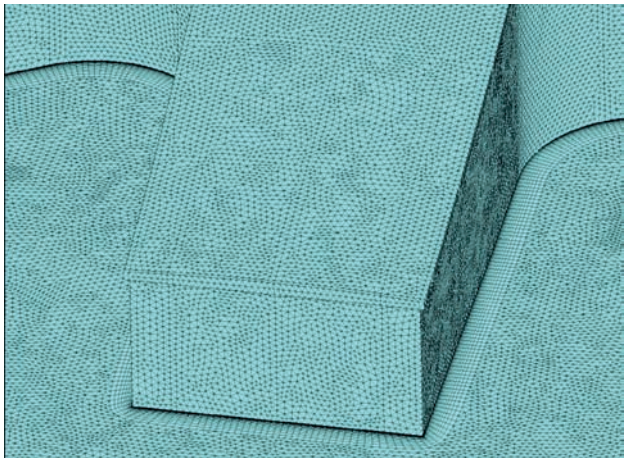

b) inflation in the boundary layer of the finite-volume mesh (~5m cells total)

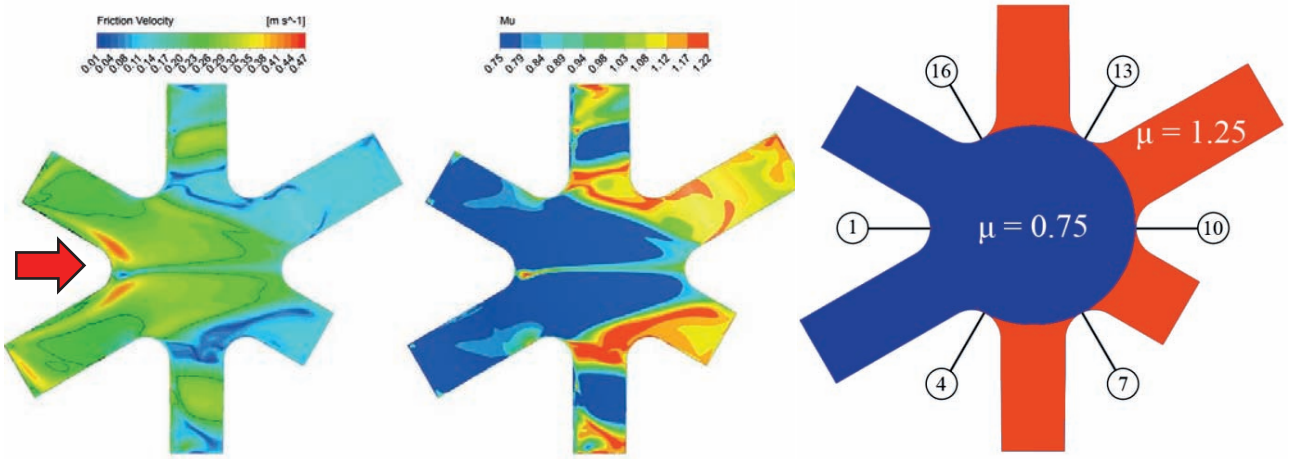

c) contours of friction velocity and modelled shape coefficient for wind direction 180° at 7 m/s

d) design shape coefficient for wind direction 180°

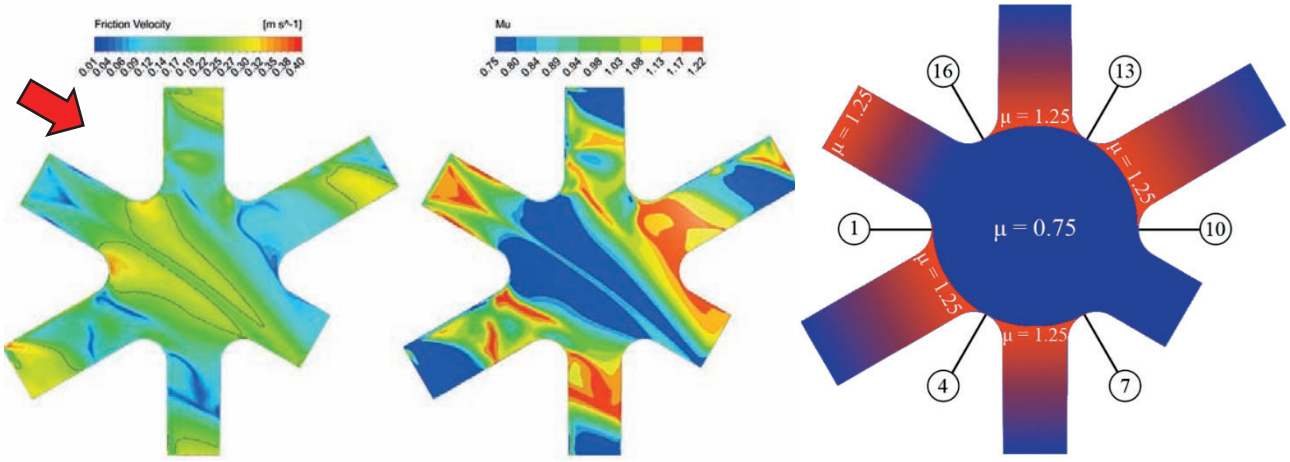

e) contours of friction velocity and modelled shape coefficient for wind direction 210° at 7 m/s

f) design shape coefficient for wind direction 210°

Figure 6. Steady numerical modelling of snow accumulation and snow transport for the Community Centre

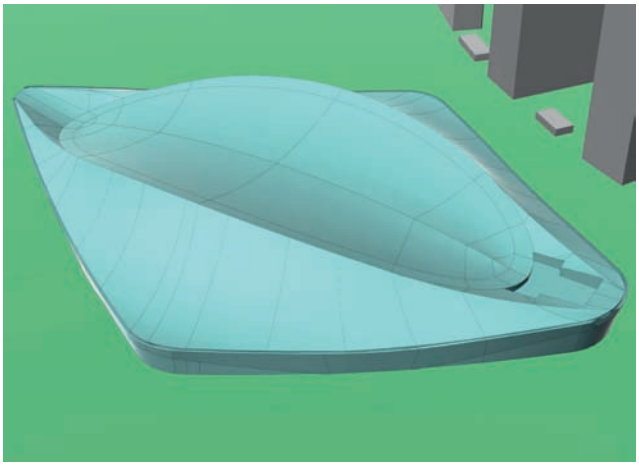

a) geometry of the Sports Centre

b) surrounding buildings and terrain

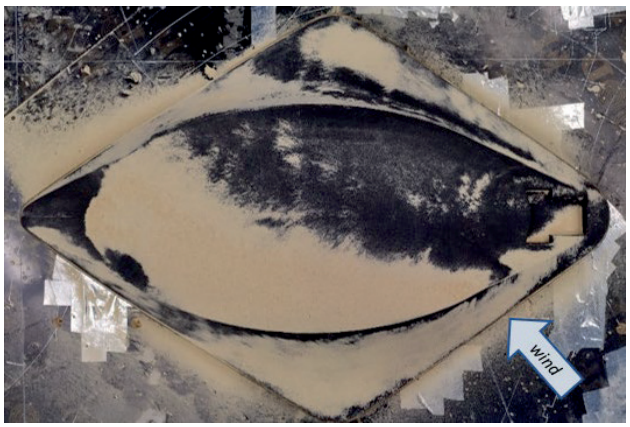

c) physical modelling for wind direction 144°

d) physical modelling for wind direction 213°

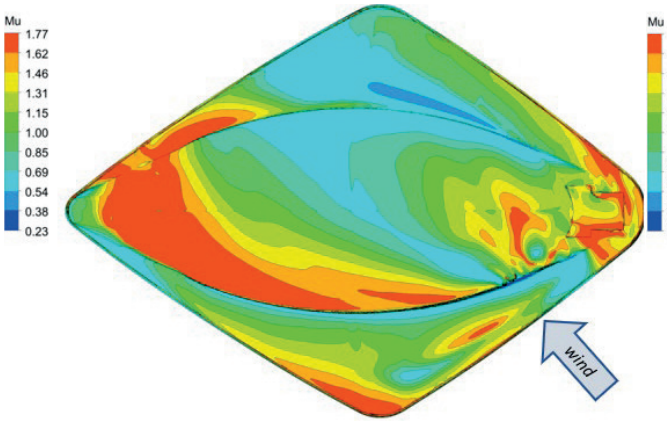

e) numerical modelling for wind direction 144°

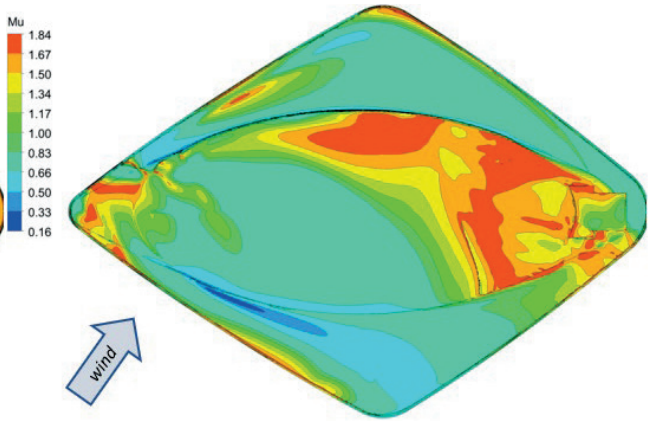

f) numerical modelling for wind direction 213°

Figure 7. Steady numerical modelling of snow accumulation and snow transport for the Sports Centre
(provided design shape coefficient contours for these wind directions are not given in this paper)

a) physical modelling for wind direction 90° (surrounding buildings ignored)

b) physical modelling for wind direction 90° (surrounding buildings considered)

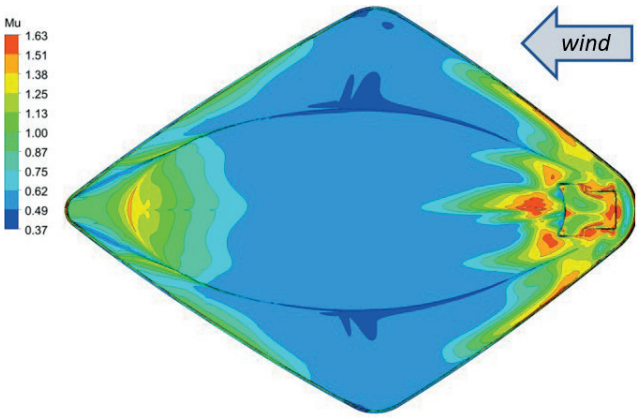

c) numerical modelling for wind direction 90° (surrounding buildings and terrain ignored)

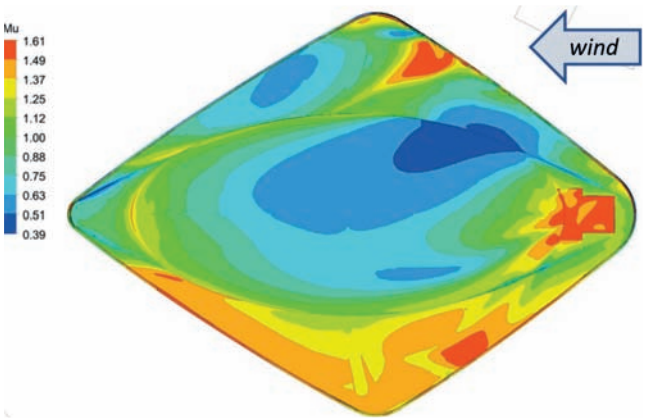

d) numerical modelling for wind direction 90° (surrounding buildings and terrain considered)

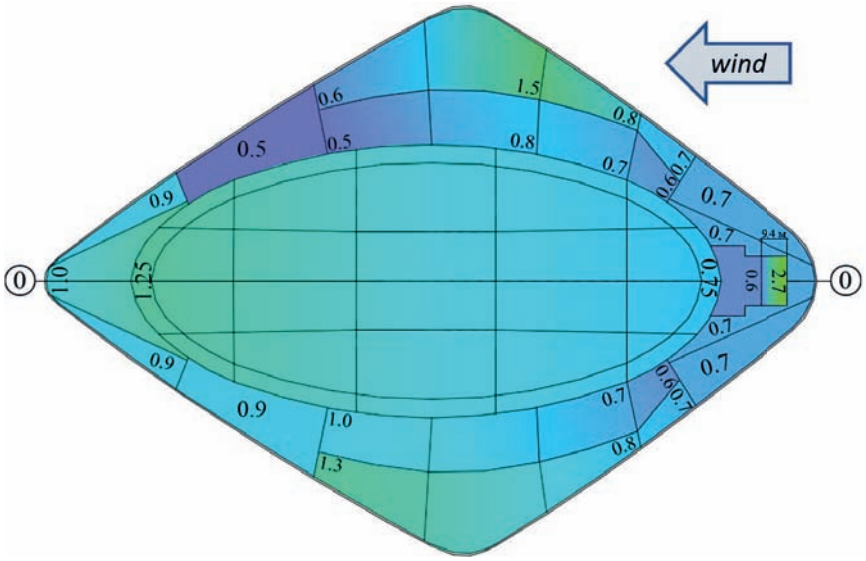

e) design shape coefficient based on the results of physical and numerical modelling and the building code recommendations for wind direction 90°

Figure 8. Steady numerical modelling of snow accumulation and snow transport for the Sports Centre

9. CONCLUSION

The methodologies of numerical modelling of snow loads for unsteady and steady flows have been developed, verified, and validated. The specifics of the erosion-deposition model used at their basis have been studied, the limits of the applicability have been determined.

The methodology for unsteady flow has proven to be capable of producing plausible results that agree with field experiment. The validation process also revealed its high sensitivity to initial conditions and ability to provide a wide variety of snow distributions for the same geometry under different flow regimes. With that said, this methodology is unlikely to become practically applicable in the nearest future. High resource intensity and computational time demands all make it difficult to apply the methodology to everyday engineering problems, especially when multiple study cases need to be examined and multiple simulations are required. Its ability to produce special cases of snow accumulation and snow transport also appears to be its disadvantage in this sense, as producing a more general snow distribution on the roof requires varying the initial conditions and summarizing the results.

The methodology for steady flow, on the other hand, successfully combines the strengths of its unsteady counterpart and benefit of being time-independent without losing too much in accuracy. For a wide range of long-span roof geometries, the steady-state approach appeared to be sufficient in producing plausible results. Comparisons with field experiments and physical modelling make it clear that numerical modelling is in no way less efficient in simulating snow accumulation and snow transport and may be used for obtaining the design shape coefficient μ if applied reasonably. In the case of the methodology for steady flow, the results of the numerical modelling are considered qualitatively to gain insight into the snow behaviour and used in conjunction with the building code recommendations to assign the coefficient values for the roof. With this approach, the methodology for steady flow can be applied in engineering practice due to its lower resource intensity and efficiency and a more generalized nature of the snow distributions it provides.

Unsolved problems remain that the methodologies do not consider. For example, at current time they don't account for snowmelt, the impact of which may be detrimental for many roofs and buildings, specifically for translucent constructions. We believe that the methodology may and will be expanded to take other snow accumulation phenomena into consideration and thus allow to obtain higher-quality results and further secure the mechanical safety of buildings.

REFERENCES

1. **Belostotsky, A. M., Britikov, N. A., & Goryachevsky, O. S.** (2021). Comparison of determination of snow loads for roofs in building codes of various countries. International Journal for Computational Civil and Structural Engineering, 17(3), 39-47.
2. **Belostotsky, A. M., Britikov, N. A., & Goryachevsky, O. S.** (2021). Critical review of modern numerical modelling of snow accumulation on roofs with arbitrary geometry. International Journal for Computational Civil and Structural Engineering, 17(4), 40-59.
3. **Belostotsky, A. M., Goryachevsky, O. S., & Britikov, N. A.** (2021). Critical review of physical modelling of snow accumulation on roofs with arbitrary geometry. International Journal for Computational Civil and Structural Engineering, 17(4), 22-39.
4. **Gromke, C., Horender, S., Walter, B., & Lehning, M.** (2014). Snow particle characteristics in the saltation layer. Journal of Glaciology, 60(221), 431-439.
5. **Menter, F. R., Matyushenko, A., & Lechner, R.** (2018, November). Development of a generalized k-ω two-equation turbulence model. In Symposium der Deutsche

Gesellschaft für Luft-und Raumfahrt (pp. 101-109). Springer, Cham.
6. **Naaim, M., Naaim-Bouvet, F., & Martinez, H.** (1998). Numerical simulation of drifting snow: erosion and deposition models. Annals of Glaciology, 26, 191-196.
7. **Sanpaolesi, L., Currie, D., Sims, P., Sacré, C., Stiefel, U., Lozza, S., ... & Formichi, P.** (1998). Scientific support activity in the field of structural stability of civil engineering works: Snow loads. Final Report Phase II. Report, Commission of the European Communities. DGIII-D3, 2.
8. **Thiis, T. K.** (2003). Large scale studies of development of snowdrifts around buildings. Journal of Wind Engineering and Industrial Aerodynamics, 91(6), 829-839.
9. **Thiis, T. K., & O'Rourke, M.** (2015). Model for snow loading on gable roofs. Journal of Structural Engineering, 141(12), 04015051.

СПИСОК ЛИТЕРАТУРЫ

1. **Белостоцкий А., Битиков Н., Горячевский О.** Comparison of determination of snow loads for roofs in building codes of various countries //International Journal for Computational Civil and Structural Engineering. – 2021. – Т. 17. – №. 3. – С. 39-47.
2. **Белостоцкий А., Битиков Н., Горячевский О.** Critical review of modern numerical modelling of snow accumulation on roofs with arbitrary geometry //International Journal for Computational Civil and Structural Engineering. – 2021. – Т. 17. – №. 4. – С. 40-59.
3. **Белостоцкий А., Горячевский О., Битиков Н.** Critical review of physical modelling of snow accumulation on roofs with arbitrary geometry //International Journal for Computational Civil and Structural Engineering. – 2021. – Т. 17. – №. 4. – С. 22-39.
4. **Gromke C. et al.** Snow particle characteristics in the saltation layer //Journal of Glaciology. – 2014. – Т. 60. – №. 221. – С. 431-439.
5. **Menter F. R., Matyushenko A., Lechner R.** Development of a generalized k-ω two-equation turbulence model //Symposium der Deutsche Gesellschaft für Luft-und Raumfahrt. – Springer, Cham, 2018. – С. 101-109.
6. **Naaim M., Naaim-Bouvet F., Martinez H.** Numerical simulation of drifting snow: erosion and deposition models //Annals of glaciology. – 1998. – Т. 26. – С. 191-196.
7. **Sanpaolesi L. et al.** Scientific support activity in the field of structural stability of civil engineering works: Snow loads //Final report phase I. Report, Commission of the European Communities. DGIII-D3. – 1998. – С. 2.
8. **Thiis T. K.** Large scale studies of development of snowdrifts around buildings //Journal of Wind Engineering and Industrial Aerodynamics. – 2003. – Т. 91. – №. 6. – С. 829-839.
9. **Thiis T. K., O'Rourke M.** Model for snow loading on gable roofs //Journal of Structural Engineering. – 2015. – Т. 141. – №. 12. – С. 04015051.

Britikov Nikita Aleksandrovich, engineer of the A.B. Zolotov NICCM of the National Research Moscow State University of Civil Engineering; postgraduate student of the Russian University of Transport (MIIT); 129337, Russia, Moscow, Yaroslavskoe shosse, 26. E-mail: n.a.britikov@gmail.com

Битиков Никита Александрович, инженер НОЦ КМ им. А.Б. Золотова Национального исследовательского Московского государственного строительного университета; аспирант Российского университета транспорта (МИИТ); 129337, Россия, г. Москва, Ярославское шоссе, д. 26. E-mail: n.a.britikov@gmail.com

DOI:10.22337/2587-9618-2022-18-4-39-48

MODEL OF THERMOMECHANICAL VIBRATIONS OF CURRENT-CARRYING CONDUCTORS

Alexander N. Danilin [1], ***Egor S. Onuchin*** [2], ***Valery A. Feldshteyn*** [2]

[1] Institute of Applied Mechanics of the Russian Academy of Sciences
[2] JSC "Central Research Institute for Machine Building"

Abstract. In the operation practice of overhead power transmission lines (OHL), the phenomenon of "galloping" of conductors is well known – vibrations with frequencies of ~ 1 Hz and with amplitudes of the order of the static sag [1, 2]. This phenomenon is observed, as a rule, when the symmetry of the conductor section is violated due to icy deposits, which gives the conductor some aerodynamic efficiency. However, this model does not explain all the observed cases of galloping. In this regard, it is advisable to pay attention to the little-known experience of Academician Abram F. Ioffe, who experimentally discovered the self-excitation of a current-carrying conductor – a stretched string that heats up when connected to an electrical circuit. Solving this issue can significantly expand the understanding of the nature of conductor galloping and open up new ways to fend off this phenomenon, which poses a danger to the stability of the functioning of energy systems. This requires a mathematical model of the OHL conductor describing the interaction of mechanical and thermal processes. The purpose of this work is to construct the simplest version of this model, on the basis of which the condition of self-excitation of thermomechanical self-excitation of real OHL conductors can be justified.

Keywords: power transmission, sagging conductor, heat generation, heat transfer, thermomechanical processes, vibrations, self-excitation, galloping

МОДЕЛЬ ТЕРМОМЕХАНИЧЕСКИХ КОЛЕБАНИЙ ТОКОНЕСУЩИХ ПРОВОДНИКОВ

А.Н. Данилин [1], ***Е.С. Онучин*** [2], ***В.А. Фельдштейн*** [2]

[1] ФГБУН Институт прикладной механики Российской академии наук
[2] АО «Центральный научно-исследовательский институт машиностроения»

Аннотация. В практике эксплуатации воздушных линий электропередачи (ВЛЭ) известен феномен «пляски» проводов – колебания с частотами ~1 Гц и с амплитудами порядка стрелы статического провисания провода [1, 2], наблюдаемые, как правило, при потере симметрии сечения провода вследствие гололедных отложений, что придает проводу некоторое аэродинамическое качество. Однако эта модель не объясняет всех наблюдаемых случаев пляски. В связи с этим целесообразно обратить внимание на малоизвестный опыт академика А.Ф. Иоффе, экспериментально обнаружившего самовозбуждение токонесущего проводника – натянутой струны, нагревающейся при включении в электрическую цепь. Решение этого вопроса может существенно расширить представления о природе пляски проводов и открыть новые пути парирования этого феномена, представляющего опасность для стабильности функционирования энергетических систем. Для этого необходима математическая модель провода ВЛЭ, описывающая взаимодействие механических и тепловых процессов. Целью данной работы является построение наиболее простого варианта этой модели, на базе которого может быть обосновано условие самовозбуждения термомеханического самовозбуждения реальных проводов ВЛЭ.

Ключевые слова: электропередача, провисающий провод, тепловыделение, теплоотдача, термомеханические процессы, колебания, самовозбуждение, галопирование

INTRODUCTION

Open mechanical oscillatory systems interacting with energy sources and the environment are widely known in technology. These include, for example, relay thermoregulators that include current only in a given range; their mode of operation is relaxation self–oscillation. In thermistor generators, self-oscillations do not occur as a result of circuit interruption, but due to the dependence of resistance on temperature. A special class of thermomechanical self-oscillations was experimentally discovered by A.F. Ioffe, who demonstrated, as an illustration for a lecture course in physics, the self-excitation of a conductor – a stretched string that heats up when it is connected to a DC electric circuit.

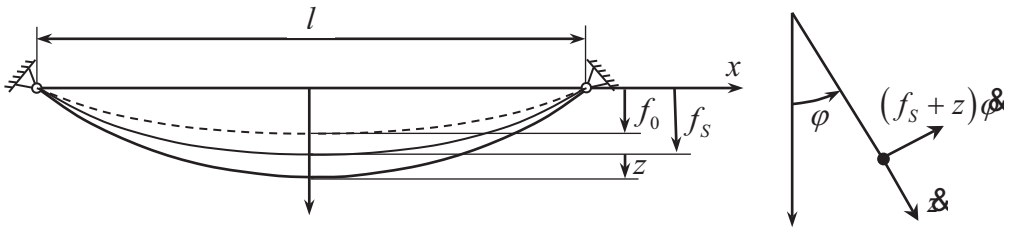

Figure 1. Kinematic parameters of three conductor states

The works devoted to the construction of a theory explaining this phenomenon are [3-7]. It is shown that self-oscillations in such systems can be caused by the interaction of a number of thermomechanical factors: Joule heat release, thermal and deformation changes in the electrical resistance of the conductor (thermoresistive effect), dependence of heat transfer to the medium on the vibration amplitude. In [7] there are indications of a repetition of the experience of A.F. Ioffe. Of practical interest is the question of whether the concept of thermomechanical vibrations can serve as an explanation for the phenomenon of conductor galloping – low-frequency vibrations of overhead power line (OHL) conductors with frequencies of ~ 1 Hz and with amplitudes of the order of static sag. The authors of the cited works have made such an assumption, but it has not yet received convincing confirmation: there is no transfer of the effect, modeled theoretically and observed in a laboratory model, to the full-scale OHL conductors. The purpose of this work is to build, if possible, an elementary model suitable for assessing the conditions for self-excitation of vibrations and transferring them to the actual operating conditions of OHL.

1. MODEL OF CONDUCTOR VIBRATION

The conductor is considered as an elastic flexible heavy thread in a homogeneous field of gravity (Figure 1). With a static sag that is small compared to the span length $\left(f_S << l\right)$, the curvature and tension of the conductor can be considered constant, and the conductor configuration in the equilibrium state is a parabola $y_S = f_S\left(1 - 4x^2 / l^2\right) = f_S\sigma\left(x\right)$.

It is assumed that the shape of vertical oscillations relative to the static equilibrium position coincides with the shape function $\sigma\left(x\right)$: $y\left(t,s\right) - y_S\left(s\right) = z\left(t\right)\sigma\left(x\right)$. The state parameters are: the sag variation $z\left(t\right)$, the angle of deviation of the conductor plane from the vertical $\varphi\left(t\right)$, temperature $\theta\left(t\right)$. Ambient air temperature θ_B is at the moment of self-excitation of vibrations.

There are three conductor states:

- natural:

$$f = f_0,\ \varphi = 0,\ \theta = \theta_0,$$

when there are no deformations (θ_0 – installation temperature before static deformations occur in it);
- stationary:

$$f = f_S,\ \varphi = 0,\ \theta = \theta_S,$$

when the deformations and temperature correspond to equilibrium with the electric voltage switched on and stationary heat release Q_S;
- perturbed (vibration mode):

$$f = f_S + z,\ \varphi \neq 0,\ \theta = \theta_S + \eta,$$

when perturbations are imposed on static deformations and temperature z, η, due to changes in configuration, heat release $Q_V(t)$ and heat transfer.
The lengths of the conductor in the natural, static and perturbed states are respectively equal to:

$$L_0 = l\left(1 + \frac{8f_0^2}{3l^2}\right),\ L_S = l\left(1 + \frac{8f_S^2}{3l^2}\right),$$
$$L_t = l\left[1 + \frac{8(f_S + z)^2}{3l^2}\right].$$

Static and total deformations are:

$$\varepsilon_S = \frac{8}{3l^2}\left(f_S^2 - f_0^2\right),$$
$$\varepsilon = \frac{8}{3l^2}\left[(f_S + z)^2 - f_0^2\right] = \tag{1}$$
$$= \varepsilon_S + \frac{8}{3l^2}\left(z^2 + 2zf_S\right) = \varepsilon_S + \varepsilon.$$

When describing coupled thermomechanical vibrations, the role of the elastic potential W passes to the free energy [8]:

$$F = W - 3k\alpha_T\theta e,$$

where $k = E/3(1-2\nu)$ is modulus of volume elasticity, e is volume strain, α_T is coefficient of linear thermal expansion. Expressing the volume strain in terms of the elongation strain by the formula $e = (1-2\nu)\varepsilon$, find the free energy expression for the entire volume of the conductor:

$$F = Bl\left[\frac{1}{2}(\varepsilon_S + \varepsilon)^2 - \alpha_T(\theta_S + \eta - \theta_0)(\varepsilon_S + \varepsilon)\right] +$$
$$+ \frac{2}{3}mgl\left[(f + z)(1 - \cos\varphi) - z - f_S + f_0\right].$$

Here $B = ES$ is tensile conductor stiffness; $S = \pi a^2$ – effective conductor cross section with section radius a; m – linear mass.
Kinetic energy is

$$K = m\frac{V_0^2}{2}\int_{-l/2}^{l/2}\sigma^2(x)dx = \frac{4}{15}mlV_0^2,$$

where $V_0 = \sqrt{\dot{z}^2 + (f_S + z)^2\dot{\phi}^2}$ – the speed of the midpoint of the span.
Let's limit ourselves to taking into account the aerodynamic drag. With normal flow, the linear aerodynamic force is equal to $F = -\rho_B \boldsymbol{V}|\boldsymbol{V}|C_D a$, where ρ_B, $\boldsymbol{V}$ – density and velocity vector of incoming air. The drag coefficient for a circular cylinder in the current range of Reynolds numbers $\mathrm{Re} = 10^3 - 10^5$ changes slightly and can be taken equal to $C_D = 1,2$.
Dissipative function [9] is

$$\Phi = \rho_B C_D a\frac{|V_0|^3}{3}\int_{-l/2}^{l/2}\sigma^3(x)dx = \frac{16}{105}\rho_B C_D a l|V_0|^3.$$

We write the vibration equations in the Lagrange form:

$$\frac{8}{15}ml\left[\ddot{z} - (f + z)\dot{\phi}^2\right] + \frac{16}{35}\rho_в a l c_L V_0\dot{z} +$$

$$+Bl[\varepsilon+\varepsilon_S-\alpha_T(\theta_S-\theta_0)-\alpha_T\eta]\frac{d\varepsilon}{dz}-$$
$$-\frac{2}{3}mgl+\frac{2}{3}mgl(1-\cos\phi)=0,$$
$$\frac{8}{15}ml\left[\ddot{\phi}(z+f)^2+2\dot{\phi}\dot{z}(z+f)\right]+$$
$$+\frac{16}{35}\rho_B alc_l V_0(f_S+z)^2\dot{\phi}^2+$$
$$+\tfrac{2}{3}mgl(z+f)\sin\phi=0. \quad (2)$$

2. CONDUCTOR TEMPERATURE

The conductor heating occurs due to Joule heat generation, the power of which is uniform in volume. When the conductor oscillates, it acquires a velocity relative to the air, as a result of which heat transfer occurs, uneven on the surface. Taking into account the unevenness would dramatically complicate the model, so the heat transfer is taken into account according to Newton's law with an averaged heat transfer coefficient over the cross section and over the span length. In this approximation, the temperature distribution is axisymmetric and constant along the conductor length, and the first law of thermodynamics takes the form [8, 10]:

$$\rho c\frac{\partial\eta}{\partial t}+3k\alpha_T\theta_0\frac{de}{dt}=$$
$$=\lambda\frac{1}{r}\frac{\partial}{\partial r}\left(r\frac{\partial(\theta_S+\eta-\theta_0)}{\partial r}\right)+Q_S+Q_V(t), \quad (3)$$

where ρ and c – density and specific heat capacity of the conductor.

The stationary component of the temperature satisfies the equation and the boundary conditions:

$$\lambda\frac{1}{r}\frac{\partial}{\partial r}\left(r\frac{\partial(\theta_S-\theta_0)}{\partial r}\right)+Q_S=0;$$
$$\left.\frac{\partial(\theta_S-\theta_0)}{\partial r}\right|_0=0, \quad (4)$$
$$\left.\frac{\partial(\theta_S-\theta_0)}{\partial r}\right|_a+\alpha(\theta_S-\theta_0-\theta_B)\big|_a=0.$$

Passing, as before, from e to ε and taking into account (4), we transform (3) to the form

$$\rho c\frac{\partial\eta}{\partial t}+E\alpha_T\theta_0\frac{d\varepsilon}{dt}=$$
$$=\lambda\frac{1}{r}\frac{\partial}{\partial r}\left(r\frac{\partial\eta}{\partial r}\right)+Q_V(t). \quad (5)$$

Let us apply to both parts of this equation the averaging over the cross-sectional area:

$$\rho c\int_0^a\frac{\partial\eta}{\partial t}rdr=\lambda\int_0^a\frac{\partial}{\partial r}\left(r\frac{\partial\eta}{\partial r}\right)dr+$$
$$+\int_0^a Q_V rdr-\int_0^a\alpha_T E\theta_0\,\dot{\varepsilon}rdr.$$

On the surface $r=a$, Newton's heat transfer condition must be satisfied both for the total temperature $\theta_S-\theta_0+\eta$ and for its stationary component; hence it follows that the variable component must satisfy the condition $-\lambda\partial\eta/\partial r=\alpha\eta$. Taking this into account and introducing the cross-sectional average temperature $\tilde{\eta}=2a^{-2}\int_0^a r\eta dr$, we arrive at an equation for its change:

$$\rho c\dot{\tilde{\eta}}=Q_V-\frac{2\alpha}{a}\tilde{\eta}-\alpha_T E\tilde{\theta}_0\dot{\varepsilon}. \quad (6)$$

Here, omitting for brevity a rather elementary justification, the result is used: for the Fourier numbers $\mathrm{Fo}=\lambda/\rho ca^2\omega$, characteristic of the modes of dancing of the OHL, the amplitude of the periodic temperature component is almost constant over the conductor cross section, which gave reason to replace the surface temperature $\eta(a)$ in (6) with its average value $\tilde{\eta}$.

3. HEAT RELEASE AND HEAT TRANSFER

The power of heat release in the span of a conductor with electrical resistance R is equal to $W^+=U^2/R=I^2R$. In the general case, a

change in resistance changes the current and voltage simultaneously, but two limiting cases can be distinguished: a circuit with a stabilized voltage and a circuit with a stabilized current.
In the first case, as the resistance increases, the heat release decreases, and in the second case, it increases. Small fluctuations in resistance cannot change the current in the OHL conductors, which is determined by the large load resistance, so the second option is of practical importance $W^+ = I^2R(1+\cos 2\omega_e t)$, where I – effective current, ω_e – its frequency. Since the oscillation frequency of the conductor is small compared to ω_e, we can neglect the variable component in the expression for W^+.
The change in conductor resistance R depends on the change in length, cross-sectional area (tensoresistive effect [11]), and the temperature dependence of resistivity:

$$\frac{dR}{R} = \left(\frac{d\rho_e}{\rho_e} + \frac{dl}{l} - \frac{dS}{S} \right);$$
$$\frac{dl}{l} = \varepsilon + \alpha_T \eta, \quad \frac{d\rho_e}{\rho_e} = \beta_1 \eta,$$
$$\frac{dS}{S} = 2\left(\alpha_T \eta - \nu\varepsilon\right);$$

where ρ_e – resistivity, $\beta_1 \approx 4.10^{-3}\,\mathrm{K}^{-1}$ – coefficient of temperature dependence of electrical resistivity, $\beta_2 = 1 + 2\nu$ – coefficient characterizing the tensoresistive effect, ν – Poisson's ratio of conductor material. As a result, taking into account that $\alpha_T << \beta_1$, we find

$$R = 4\rho_e\left(\beta_1\theta + \beta_2\varepsilon\right)l/\pi d^2,$$

and the variable component of the heat release power per unit volume of the conductor is (hereinafter, the tilde sign above the variable η is omitted):

$$Q_V(t) = 16\frac{I^2\rho_e}{\pi^2 d^4}\left(\beta_1\eta + \beta_2\varepsilon\right). \qquad (7)$$

Heat transfer depends on the speed of blowing with ambient air and on the presence of icy deposits on the surface of the wire. Let's look at the first of these factors. Heat transfer from the wire surface is taken into account according to Newton's law. The heat transfer coefficient is determined by the Nusselt number $\alpha = \mathrm{Nu}\cdot\lambda_B/d$, depending on the Reynolds and Grashof numbers

$$\mathrm{Re} = Vd/\nu_B,$$
$$\mathrm{Gr} = g\beta_B d^3\left(\eta_S - \eta_B\right)/\nu_B^2.$$

Here: $\lambda_B, \nu_B, \beta_B$ are coefficient of thermal conductivity, kinematic viscosity and the coefficient of volumetric thermal expansion of air, d – conductor diameter. Approximation of the data contained in [12, 13] leads to the following relationship (at a constant flow rate):

$$\alpha = 0{,}47\frac{\lambda_B}{d}\sqrt{\mathrm{Re} + \sqrt{\mathrm{Gr}/2}}. \qquad (8)$$

We assume that this dependence is also true for the instantaneous values of the Reynolds number with its periodic change (quasi-stationary model), and the conductor speed during vibrations will be replaced by its average value over the span $\tilde{V} = 2V_0/3$. At low velocities $\tilde{V}$, which are characteristic of the initial stage of soft self-excitation of oscillations ($\mathrm{Re} << \sqrt{\mathrm{Gr}/2}$), the determining factor is the free convection effect and $\alpha = 0.39\sqrt[4]{\mathrm{Gr}}\,\lambda_B/d$.
The reason for the dance is traditionally associated with the icing of the wire [1, 2], as a result of which its cross section becomes similar to a wing profile, and the excitation of the dance is likened to a flutter. However, practice shows [1] that dancing can also occur with a uniform deposition of a thin layer of ice, in which the section does not acquire an aerodynamic quality. From the standpoint of the thermomechanical model, the role of the ice sheath may be to change the thermal regime of the wire. In this

regard, it is necessary to assess the degree of this influence.

Taking into account the significant uncertainty in the shape of ice deposits, for evaluation we consider a simplified auxiliary problem, replacing the axisymmetric model with a flat one: an infinite plate with a thickness of $2a$ (analogous to a wire) contacts with plates with a thickness δ (analogous to an ice shell). Considering, due to symmetry, half of the region and placing the origin of coordinates on the contact surface, we write down the equations of heat conduction:

$$\dot{T}_1 = \chi_1 T_1'' + \frac{Q}{\rho_1 c_1} e^{i\omega t} \ (-a \le x \le 0);$$
$$\dot{T}_2 = \chi_2 T_2'' \ \ (0 < x < \delta).$$

Assuming $T_1 = e^{i\omega t}\eta_1(x)$, $T_2 = e^{i\omega t}\eta_2(x)$, we arrive at the equations for the amplitudes

$$-i\omega\eta_1 + \chi_1\eta_1'' + q = 0, \ -i\omega\eta_2 + \chi_2\eta_2'' = 0;$$

$\chi_{1,2} = \lambda_{1,2} / \rho_{1,2}c_{1,2}$ – coefficients of thermal conductivity of the conductor and ice, $q = Q / \rho_1 c_1$. The solutions of the equations have the form of heat waves $\eta_{1,2} = \exp\left(\pm\nu_{1,2}x\right)$, where $\nu_{1,2} = \sqrt{i\omega/\chi_{1,2}}$.

The characteristic values of the thermal parameters of ice are [14, 16]:

$$\rho_2: \ 200 \ \mathrm{kg/m^3}, \ c_2: \ 2 \ \mathrm{kJ/kg \cdot K},$$
$$\lambda_2: \ 0.1 \ \mathrm{W/m \cdot K} \ \text{(granular frost)},$$
$$\rho_2: \ 900 \ \mathrm{kg/m^3}, \ c_2: \ 2 \ \mathrm{kJ/kg \cdot K},$$
$$\lambda_2: \ 2.2 \ \mathrm{W/m \cdot K} \ \text{(ice)}.$$

At vibration frequencies ~1 Hz the value $|\nu_2| \approx 10^3 - 10^4$ 1/m, $|\nu_1| \approx 250$. It follows that the variable temperature component does not penetrate deeply into the ice shell and attenuates at a distance of less than 1 mm from the wire surface. This allows us to represent the temperature amplitudes in the form:

$$\eta_1 = \left| -\frac{iq}{\omega} + A_1 e^{\nu_1 x} + A_2 e^{-\nu_1 x} \right|, \quad \eta_2 = B\left|e^{-\nu_2 x}\right|,$$

under boundary conditions:

$$\eta'(-a) = 0, \ \lambda_1\eta_1'(0) = \lambda_2\eta_2'(0),$$
$$\eta_1(0) = \eta_2(0).$$

Determining the constants, we find

$$\eta_1 \approx -\frac{q}{\omega}\left(1 - \frac{\varepsilon}{1+\varepsilon}e^{|\nu_1|x} - \frac{\varepsilon}{1+\varepsilon}e^{-|\nu_1|(2a+x)}\right).$$

Taking into account that $\varepsilon = \nu_2\lambda_2/\nu_1\lambda_1 = 0.01 \div 0.1$, as well as the estimate $\nu_1 a \approx 2 \div 5$, we will make up for the interface $x = 0$ the ratio of the type of heat transfer condition from the conductor to the icy shell $-\lambda_1\eta_1' = \alpha_{ecv}\eta_1$, from which follows an approximate estimate of the equivalent heat transfer coefficient:

$$\alpha_{экв} = -\lambda_1\frac{\eta_1'}{\eta_1}(0) \approx \lambda_1\nu_1\varepsilon = \lambda_2\nu_2. \qquad (9)$$

Therefore, for an iced wire, the variable temperature can be calculated in the same way as for a bare conductor when using the value α_{ecv} as the heat transfer coefficient in equation (6). Note that for $\nu_2\delta > 2$, which is already achieved at $\delta > 1$ mm, the heat transfer with respect to the variable temperature does not depend on the speed of blowing the conductor with the air flow.

4. RESOLUTION SYSTEM OF EQUATIONS AND SIMILARITY PARAMETERS

Let's move on to compiling a resolving system of equations. Let us transform (2), substituting expressions for deformations (1) into them and passing to dimensionless variables:

$$q = \frac{z}{f_S},\ \ \overline{t} = t/\tau,\ \ \tau = \sqrt{\frac{4f_S}{5g}},\ \ \vartheta = \frac{\eta}{\theta_S}. \quad (10)$$

Note that the accepted time scale differs by only 10% from the oscillation period of a mathematical pendulum with length f_S. Let us represent the heat transfer coefficient (8) as

$$\alpha = \lambda_B \mu(q,\varphi)/d \text{, где } \mu(\dot{q},\dot{\phi}) = \sqrt{\alpha_1 v(\dot{q},\dot{\phi}) + \alpha_2^2},$$
$$v(\dot{q},\dot{\phi}) = \sqrt{\dot{q}^2 + (1+q)^2\dot{\phi}^2},,$$
$$\alpha_1 = 0.44 f_S a/\nu_B\tau,\ \ \alpha_2^2 = 0.15\sqrt{Gr}.$$

Considering that in static equilibrium the tension in the conductor $T = B(\varepsilon_S - \varepsilon_T)$, where $\varepsilon_T = \alpha_T(\theta_S - \theta_0)$, is related to the sag by the ratio $8Tf_S = mgl^2$, we finally obtain

$$\ddot{q} + \varsigma v(\dot{q},\dot{\phi})\dot{q} - (1+q)\dot{\phi}^2 + \\ +(1+2\beta)q + \beta(3q^2+q^3) + 1 - \\ -cos\,\phi - \gamma\vartheta(1+q) = 0, \quad (11)$$

$$(1+q)\ddot{\phi} + \varsigma v(\dot{q},\dot{\phi})(1+q)\dot{\phi} + \\ +2\dot{q}\dot{\phi} + sin\,\phi = 0, \quad (12)$$

Substituting (7), (8) or (9) into equation (6), taking into account expression (1) for strains and passing to the previously accepted dimensionless values, we finally obtain:

$$\dot{\vartheta} = \vartheta\xi_1 + \xi_2(q^2+2q) - \\ -\chi\dot{q}(1+q) - \vartheta\Delta\mu(\dot{q},\dot{\phi}). \quad (13)$$

The parameters ς, β, γ, ξ_1, ξ_2, ϑ are determined by the formulas (14) below.

The first and second terms in the right part determine the change in the heat output power due to the dependence of the electrical resistance on temperature and on the conductor deformation (strain-resistive effect); the third term describes thermoelastic connectivity – cooling by increasing the deformation (downward movement) and heating by decreasing it (upward movement); the last term determines the heat transfer due to the conductor movement relative to the air during vibrations.

Thus, the system is described by equations (11)–(13) and a set of dimensionless similarity parameters:

$$\alpha_1 = 0.22\frac{f_S d}{\nu_B\tau},\ \ \alpha_2^2 = 0.15\sqrt{Gr},$$
$$\beta = \frac{64Bf_S^3}{3mgl^4},\ \ \xi = 16\frac{I^2\rho_e\tau}{\rho c\theta_S\pi^2 d^4},$$
$$\xi_1 = \xi\theta_S\beta_1,\ \ \xi_2 = \frac{8f_S^2}{3l^2}\xi\beta_2, \quad (14)$$
$$\Delta = 4\frac{\lambda_B\tau}{d^2\rho c},\ \ \chi = \frac{16f_S^2}{3l^2}\frac{\alpha_T E\theta_0}{\rho c\theta_S},$$
$$\gamma = \frac{8f_S\alpha_T\theta_S B}{mgl^2} = \frac{\varepsilon_T}{\varepsilon_S - \varepsilon_T},$$
$$\varsigma = \frac{3\rho_e f_S d c_L}{7m}.$$

In the presence of icy deposits with the parameters indicated above λ_2, ρ_2, c_2 heat transfer to air is replaced by heat transfer to ice and parameter Δ in (14) is taken as $\Delta = 4\tau\sqrt[4]{1+2\beta}\sqrt{\lambda_2\rho_2 c_2}\,/\rho cd$ and the parameter μ in (13) is assumed to be 1.

It is advisable to express the similarity parameters (14) in terms of operational and easily measured values in the experiment, fixing the design parameters and characteristics of aluminum as the predominant conductor material:

$$\alpha_1 = 5.5\cdot10^4 d\sqrt{f_S},\ \ \alpha_2 = 44\sqrt[4]{d^3(\theta_S - \theta_B)},$$
$$\beta = 1.09\cdot10^4\frac{f_S^3}{l^4},\ \ \xi = 5.33\cdot10^{-15}\frac{I^2\sqrt{f_S}}{\theta_S d^4},$$
$$\xi_1 = 21.3\cdot10^{-18}\frac{I^2\sqrt{f_S}}{d^4}, \quad (15)$$
$$\xi_2 = 22.7\cdot10^{-15}\frac{I^2\sqrt{f_S^5}}{d^4 l^2\theta_S},$$
$$\Delta = 1.6\cdot10^{-8}\frac{\sqrt{f_S}}{d^2},\ \ \chi = 3.69\frac{f_S^2\theta_0}{l^2\theta_S},$$
$$\gamma = 490\frac{f_S\theta_S}{l^2},\ \ \varsigma = 0.67\frac{f_S d}{m};$$

in the presence of ice

$$\Delta = \Delta_0 \frac{\sqrt{f_S}}{d}, \quad \Delta_0 = 10^{-4} - 10^{-3}.$$

In an experimental study of the excitation of vibrations on a laboratory model, it is most convenient to vary the measurable operational parameters of the model: the conductor temperature before turning on the current θ_0, current I, temperature θ_S and sag f_S in the heated state, leaving the design parameters of the model unchanged.

Under the conditions of a laboratory experiment, the air temperature θ_B and the conductor temperature in the natural (installation) state θ_0 are naturally considered to be the same. Therefore, the entire set of coefficients in (15) is expressed in terms of current I, sag f_S, and stationary temperature θ_S. In this case, it is advisable to empirically establish the dependence of the temperature and the sagging arrow on the current. This will allow, in the experimental study of self-excitation, to express all similarity parameters (14), (15) related to a given physical model, through a single and easily adjustable quantity – the current.

CONCLUSION

The resulting system of equations and a set of dimensionless similarity parameters are intended for the primary analytical analysis of the conditions for self-excitation of thermomechanical oscillations on a laboratory scale model and for transferring the results to natural conductors of overhead lines. In the future, it is planned to use the results obtained on the analytical model to build a detailed model that more fully takes into account the features of overhead power lines and their operating conditions.

ACKNOWLEDGMENT

The work was supported by a grant from the Russian Science Foundation No 22-19-00678.

REFERENCES

1. **Yakovlev L.V.** Plyaska provodov na vozdushnyh liniyah elektroperedachi i sposoby bor'by s neyu / Prilozhenie k zhurnalu «Energetik» [Galloping of overhead power lines conductors and ways to deal with it / Appendix to the magazine "Energetik"], Iss. 11 (47). Moscow, NTF «Energoprogress» Publ., 2002. 96 p. (in Russian).
2. **Alexandrov G.P.** (ed.) Proektirovanie linij elektroperedachi sverhvysokogo napryazheniya [Design of ultra-high voltage power transmission lines]. St. Petersburg, "Energoatomizdat" Publ., 1993. 368 p. (in Russian).
3. **Landa P.S.** Nelinejnye kolebaniya i volny [Nonlinear vibrations and waves]. Moscow, Nauka-Fizmatlit Publ., 1997. 495 p. (in Russian).
4. **Babitsky V.I., Landa P.S.** Avtokolebaniya v sistemah s inercionnym vozbuzhdeniem [Self-vibrations in systems with inertial excitation] // Dokl. USSR Academy of Sciences, 1982, Vol. 266, No. 5. Pp. 1087–1089. (in Russian).
5. **Penner D.I., Duboshinsky Ya.B., Duboshinsky D.B., Petrosov V.A., Porotnikov A.A.** Parametricheskie termomekhanicheskie kolebaniya [Parametric thermomechanical vibrations]. In book: Nekotorye voprosy vozbuzhdeniya nezatuhayushchih kolebanij [Some issues of excitation of undamped oscillations]. Vladimir, VGPI Publ., 1974. Pp. 168–183 (in Russian).
6. **Galkin Yu.V., Duboshinsky D.B., Vermel A.S., Penner D.I.** Vertikal'nye termomekhanicheskie kolebaniya [Vertical thermomechanical vibrations]. Ibid. Pp. 150–158. (in Russian).

7. **Feldshteyn V.A.** Termomekhanicheskie kolebaniya tokonesushchih provodnikov [Thermomechanical vibrations of current-carrying conductors] // Journal of Applied Mechanics and Technical Physics, 2017, Vol. 58, No. 6. Pp. 158–166. (in Russian). DOI: 10.15372/PMTF20170615
8. **Lurie A.I.** Teoriya uprugosti [Theory of elasticity]. Moscow, "Nauka" Publ., 1970. 940 p. (in Russian).
9. **Lurie A.I.** Analiticheskaya mekhanika [Analytical mechanics]. Moscow, GIFML Publ., 1961. 824 p. (in Russian).
10. **Sneddon I.N., Berry D.S.** Klassicheskaya teoriya uprugosti [Classical theory of elasticity]. Moscow, "Fizmatgiz" Publ., 1961. 219 p. (in Russian).
11. **Klokova N.P.** Tenzorezistory: teoriya, metody rascheta, razrabotki [Tensoresistors: theory, calculation methods, development]. Moscow, "Mashinostroenie" Publ., 1990. 224 p. (in Russian).
12. **Wang H.** Osnovnye formuly i dannye po teploobmenu dlya inzhenerov. Spravochnik [Basic formulas and heat exchange data for engineers. Guide]. Moscow, "Atomizdat" Publ., 1979. 216 p. (in Russian).
13. Metodika rascheta predel'nyh tokovyh nagruzok po usloviyam sohraneniya mekhanicheskoj prochnosti provodov i dopustimyh gabaritov vozdushnyh linij / Standart organizacii «FSK EES» 56947007-29.240.55.143-2013 [The method of calculating the maximum current loads under the conditions of maintaining the mechanical strength of wires and the permissible dimensions of overhead lines / The standard of FGC UES 56947007-29.240.55.143-2013]. Moscow, "FGC UES" Publ., 2013. 67 p. (in Russian).
14. **Osokin N.I., Sosnovsky A.V., Chernov R.A.** Koefficient teploprovodnosti snega i ego izmenchivost' [Coefficient of thermal conductivity of snow and its variability] // Cryosphere of the Earth. 2017, Vol. XXI, No. 3. – Pp. 60-68. (in Russian).
15. GOST 839-80. Provoda neizolirovannye dlya vozdushnyh linij elektroperedachi. Tekhnicheskie usloviya [GOST 839-80. Non-insulated wires for overhead power lines. Technical conditions]. Moscow, Branch of IPK Standards Publ., Printing House "Moskovsky Pechatnik", 2002. 21 p. (in Russian).
16. Rukovodstvo po raschyotu rezhimov plavki gololeda na grozozashchitnom trose so vstroennym opticheskim kabelem (OKGT) i primeneniyu raspredelyonnogo kontrolya temperatury OKGT v rezhime plavki / Standart organizacii «FSK EES» 56947007-29.060.50.122-2012 [Guidelines for the calculation of ice melting modes on a lightning-proof cable with a built-in optical cable (OCGT) and the use of distributed temperature control of OCGT in the melting mode / The standard of FGC UES 56947007-29.060.50.122-2012]. Moscow, "FGC UES" Publ., 2012. 119 p. (in Russian).

СПИСОК ЛИТЕРАТУРЫ

1. **Яковлев Л.В.** Пляска проводов на воздушных линиях электропередачи и способы борьбы с нею / Приложение к журналу «Энергетик», выпуск 11 (47). – М.: Изд-во НТФ «Энергопрогресс», 2002. – 96 стр.
2. **Александров Г.П.** (ред.). Проектирование линий электропередачи сверхвысокого напряжения. – С-Пб.: Изд-во «Энергоатомиздат», 1993. – 368 с.
3. **Ланда П.С.** Нелинейные колебания и волны. – М.: Изд-во «Наука. Физматлит», 1997. – 495 с.
4. **Бабицкий В.И., Ланда П.С.** Автоколебания в системах с инерционным возбуждением // ДАН СССР. 1982. Т. 266. № 5. – С. 1087–1089.
5. **Пеннер Д.И., Дубошинский Я.Б., Дубошинский Д.Б., Петросов В.А., Поротников А.А.** Параметрические термо-

механические колебания. / В кн. Некоторые вопросы возбуждения незатухающих колебаний. – Владимир: Изд-во ВГПИ, 1974. – С. 168–183.
6. **Галкин Ю.В., Дубошинский Д.Б., Вермель А.С., Пеннер Д.И.** Вертикальные термомеханические колебания / Там же. – С. 150–158.
7. **Фельдштейн В.А.** Термомеханические колебания токонесущих проводников // ПМТФ. 2007. Т. 58. № 6. – С. 158–166.
8. **Лурье А.И.** Теория упругости. – М.: Изд-во «Наука», 1970. – 940 с.
9. **Лурье А.И.** Аналитическая механика. – М.: Изд-во ГИФМЛ, 1961. – 824 с.
10. **Снеддон И.Н., Берри Д.С.** Классическая теория упругости. – М.: Изд-во «Физматгиз», 1961. – 219 с.
11. **Клокова Н.П.** Тензорезисторы: теория, методы расчета, разработки. – М.: Изд-во «Машиностроение». 1990. – 224 с.
12. **Уонг Х.** Основные формулы и данные по теплообмену для инженеров. Справочник. – М.: Изд-во «Атомиздат», 1979. – 216 с.
13. Методика расчета предельных токовых нагрузок по условиям сохранения механической прочности проводов и допустимых габаритов воздушных линий / Стандарт организации «ФСК ЕЭС» 56947007-29.240.55.143-2013. – М.: Изд-во ОАО «ФСК ЕЭС». 2013. – 67 с.
14. **Осокин Н.И, Сосновский А.В., Чернов Р.А.** Коэффициент теплопроводности снега и его изменчивость // Криосфера Земли. 2017. Т. XXI. № 3. – С. 60–68. DOI: 10.21782/KZ1560-7496-2017-3(60-68)
15. ГОСТ 839-80. Провода неизолированные для воздушных линий электропередачи. Технические условия. – М.: Филиал ИПК Изд-во стандартов, типография «Московский печатник». 2002. – 21 с.
16. Руководство по расчёту режимов плавки гололеда на грозозащитном тросе со встроенным оптическим кабелем (ОКГТ) и применению распределённого контроля температуры ОКГТ в режиме плавки / Стандарт организации «ФСК ЕЭС» 56947007-29.060.50.122-2012. – М.: Изд-во ОАО «ФСК ЕЭС». 2012. – 119 с.

Danilin Alexander Nikolaevich, Doctor of Physical and Mathematical Sciences, Chief Researcher of the Institute of Applied Mechanics of the Russian Academy of Sciences (IAM RAS), Professor of the Moscow Aviation Institute; 125040, Moscow, Leningradsky Prospekt, 7, p. 1; +7 (495) 946-18-06; andanilin@yandex.ru

Onuchin Egor Sergeevich, Head of the Department of JSC "Central Research Institute for Machine Building" (JSC "TsNIIMash"), postgraduate student of the Moscow Institute of Physics and Technology (MIPT); Russia, 141070, Moscow region, Korolev, Pionerskaya str., 4; +7 (495) 513-59-51; oes92@yandex.ru

Feldshteyn Valery Adolfovich, Doctor of Technical Sciences, Chief Researcher of JSC "TsNIIMash", Professor of MIPT; Russia, 141070, Moscow region, Korolev, Pionerskaya str., 4; +7 (495) 513-59-51; dinpro@mail.ru

Данилин Александр Николаевич, доктор физико-математических наук, главный научный сотрудник Института прикладной механики РАН (ИПРИМ РАН), профессор Московского авиационного института; 125040, г. Москва, Ленинградский проспект, д.7, стр. 1; +7 (495) 946-18-06; andanilin@yandex.ru

Онучин Егор Сергеевич, начальник отдела АО «Центральный научно-исследовательский институт машиностроения» (АО «ЦНИИмаш»), аспирант ФГАОУ Московского физико-технического института (МФТИ); Россия, 141070, Московская область, г. Королёв, ул. Пионерская, д. 4; +7 (495) 513-59-51; oes92@yandex.ru

Фельдштейн Валерий Адольфович, доктор технических наук, главный научный сотрудник АО «ЦНИИмаш», профессор МФТИ; Россия, 141070, Московская область, г. Королёв, ул. Пионерская, д. 4; +7 (495) 513-59-51; dinpro@mail.ru

DOI:10.22337/2587-9618-2022-18-4-49-61

POWDER-ACTIVATED CONCRETE WITH A GRANULAR SURFACE TEXTURE

Vladimir T. Erofeev [1], Nikolai I. Vatin [2], Irina. N. Maksimova [3], Oleg V. Tarakanov [3], Yana A. Sanyagina [1], Irina V. Erofeeva [4], Oleg V. Suzdaltsev [5]

[1] N.P. Ogarev National Mordovian State University (Ogarev Moscow State University), Saransk, RUSSIA
[2] St. Petersburg Polytechnic University named after Peter the Great, St. Petersburg, RUSSIA
[3] Penzensky State University of Architecture and Construction, Penza, RUSSIA
[4] National Research Moscow State University of Civil Engineering, Moscow, RUSSIA
[5] Asia Cement LLC, Penza, RUSSIA

Abstracts. In recent years, self-compacting concrete mixtures have been widely used. Such mixtures are characterized by high workability without the use of vibration exposure. The application of innovative technologies allows manufactoring of various materials and products for architectural and construction purposes with improved decorative properties. The paper provides the results of a study on the selection of compositions for decorative-finishing powder-activated concrete with a granular surface texture according to rheological properties, strength and frost resistance had been adopted.

The following components were adopted for the research. Egyptian white cement was used as a binder, microquartz as a microfiller, screenings of crushing granite and cooper slag of 0–0.63 mm fraction was used as a finely dispersed component, granite cuts 0.63–5.0 mm and cooper slag of 0.63–2.5 mm fraction as an aggregate sand. A new generation superplasticizer of domestic and foreign productionplasticized the mixtures. Structural and rheotechnological parameters of powder-activated concretes were calculated.

From the obtained values of the conditional rheological criteria of powder-activated concretes, it follows that all of them are much greater than unity and characterize a significant excess of the volumes of rheological matrиces over the volumes of fine-grained, coarse-grained components that fit into them with large separation of particles and grains.

Strength as a complex mechanical characteristic, including a combination of strength, reliability and durability criteria, is the most important quality parameter of the concrete structure as an active and the most massive building material for structural purposes. A significant number of facilities made of concrete and reinforced concrete are being built in the southern and northern regions, characterized by extreme climatic conditions. Buildings and structures are exposed to cyclic loadings of various types and climatic influences, characterized by cyclic manifestations of negative and alternating temperatures. The research revealed high indicators of strength and frost resistance of decorative powder-activated concretes with a granular surface texture.

Keywords: decorative concrete, powder activation, composition selection, structural and rheotechnological indicators, strength, frost resistance

ПОРОШКОВО-АКТИВИРОВАННЫЕ БЕТОНЫ С ЗЕРНИСТОЙ ФАКТУРОЙ ПОВЕРХНОСТИ

В.Т. Ерофеев [1], Н.И. Ватин [2], И.Н. Максимова [3], О.В. Тараканов [3], Я.А. Санягина [1], И.В. Ерофеева [4], О.В. Суздальцев [5]

[1] Национальный мордовский государственный университет им. Н. П. Огарева (МГУ им. Н. П. Огарева), г. Саранск, РОССИЯ
[2] Санкт-Петербургский политехнический университет им. Петра Великого, г. Санкт-Петербург, РОССИЯ
[3] Пензенский государственный университет архитектуры и строительства, г. Пенза, РОССИЯ
[4] Национальный исследовательский Московский государственный строительный университет, г. Москва, РОССИЯ
[5] ООО «Азия Цемент», г. Пенза, РОССИЯ

Аннотация. Показано, что в последние годы в отечественной и мировой практике широкое применение нашли самоуплотняющиеся бетонные смеси отличающиеся высокой удобоукладываемостью без применения вибрационного воздействия. С применением инновационных технологий могут быть изготовлены разнообразные материалы и изделия архитектурно-строительного назначения с улучшенными декоративными свойствами. Приведены результаты исследования по подбору составов декоративно-отделочных порошково-активированных бетонов зернистой фактурой поверхности по реологическим свойствам, показателям прочности и морозостойкости.

При проведении исследований в качестве вяжущего использовался египетский белый цемент, микронаполнителя – микрокварц, тонкодисперсного компонента – отсевы дробления гранита и купершлака фр. 0–0,63 мм, песка-заполнителя – гранитные высевки фр. 0,63–5 мм и купершлак фр. 0,63–2,5 мм. Смеси пластифицировались суперпластификаторами нового поколения отечественного и зарубежного производства. Рассчитаны структурные и реотехнологические показатели порошково-активированных бетонов.

Из полученных значений условных реологических критериев порошково-активированных бетонов следует, что все они значительно больше единицы и характеризуют существенное превышение объемов реологических матриц над объемами тонкозернистых, грубозернистых компонентов, которые вмещаются в них с большими раздвижками частиц и зерен.

Прочность как комплексная механическая характеристика, включающая сочетание критериев прочности, надежности и долговечности, является важнейшим параметром качества структуры бетона как активного и самого массового строительного материала конструкционного назначения. Здания и сооружения в условиях эксплуатации подвергаются циклическим механическим нагрузкам различного вида и климатическим воздействиям, характеризующимся циклическими проявлениями отрицательных и знакопеременных температур. В результате выполнения исследований выявлены высокие показатели прочности и морозостойкости декоративных порошково-активированных бетонов с зернистой фактурой поверхности.

Ключевые слова: декоративные бетоны, порошковая активация, подбор составов, структурные и реотехнологические показатели, прочность, морозостойкость

INTRODUCTION

In recent years, self-compacting concrete mixtures have been widely used. Such mixtures are characterized by high workability and do not require the use of vibration exposure [1, 2]. Modern construction is already impossible to imagine without it. Due to the unique rheological properties, such as good flowability, high resistance to delamination and effective air removal, self-compacting concrete is actively used primarily in those areas of construction where the use of vibration compacting is difficult. For example, it is relevant for work in residential areas where the requirements for sound insulation are stringent, as well as when forming products with high reinforcement density or complex geometry [3]. The production of self-compacting concrete mixtures is less expensive.

To date, it is relevant the studies aimed to obtaining construction materials and products with new properties, for example, ensuring environmental safety, expanding the use of additives that give surfaces special properties, etc. Among them, chemically resistant, biostable, self-cleaning decorative and other products and coatings are known [2]. One of the effective technologies for implementation in construction is also 3D printing, which is carried out by layer-by-layer extrusion in accordance with a given three-dimensional digital model [4].

The usage of innovative technologies allowsmanufacturing of various materials and products with improved decorative properties for architectural and construction purposes. Decorative concrete with a granular surface texture can be obtained using waste screenings from stone crushing quarries, which have accumulated more than 6 billion tons in the Russian Federation. These all allow obtaining fine aggregates and aggregate sand.

A large number of works [5] are devoted to the selection of concrete compositions with a rational binder consumption. In concretes of optimal structure, the cement paste not only covers the surface of the aggregate grains, but also fills the remaining voids between them. For this purpose, the principle of successive filling of voids is used. According to this principle, the grains

of finer fractions fall into voids between coarse aggregate grains without causing its expansion. It is known that a decrease in the voidness between the grains of fine aggregate (sand) causes descending of the consumption of the binder, and the strength of the solution increases [6].

One of the most effective ways to control the rheological properties and aggregate stability of cement composites, including decorative ones, is the use of substances that have surface activity at the solid-solution interface. In the industry of construction materials, these additives are called as plasticizers and superplasticizers (SP). The introduction of plasticizing additives helps to increase the strength of cement stone by reducing the water-cement ratio [7].

As it follows from the basics of physical chemistry, a concrete mixture must contain a sufficient amount of a highly concentrated water-dispersed mixture (matrix), which can be converted from aggregation-unstable to aggregation-stable using a plasticizer. In this case, it is necessary to meet the basic rule: an increase in the volume of the dispersed phase should be provided without increasing the consumption of cement, but by adding powder filler in an amount of 40–70%, and in low-cement concrete - up to 90–100%. [8]. Such a high content of dispersed powder, for example, ground quartz sand, leads to increase the volume of the water-cement-mineral mixture and achievement of a high thinning effect of the superplasticizers. In this case, it is also necessary to take into account the limiting values of the volume concentration of the solid phase C_V:

$$C_V = \frac{V_{SP}}{V_{SP} + V_W}, \quad (1)$$

where V_{SP} – is thevolume of the solid phase (cement, ground sand, fine sand, aggregate sand, crushed stone); V_W – is the water volume.

Kalashnikov V.I. noted that an important task of choosing mineral additives as microfillers of cement concretes is to determine not only their rheotechnological activity in comparison with cement systems, but also their reactive activity in relation to cement systems in terms of binding hydrolytic lime released during cement hydration, and the possibility of formation of intergrowth contacts on defect-free surfaces of microcrystals formed on the surface of hydrated particles of cement and microfiller.

Structural strength as a complex mechanical characteristic is the most important parameter of the quality of the concrete structure as an active and most widespread construction material for structural purposes [9]. It includes a combination of strength, reliability and durability criteria.

Modern construction shows more pronounced the tendency to use high-strength materials, in particular concrete. Over the past decades, the strength of used ready-mixed concrete has increased 1.5 times in some countries. And there is a task to increase it up 2–3 times (to the level of 100–150 MPa) in the coming decades [9].

A significant number of construction projects are being built in the southern and northern regions, which have extreme natural and climatic conditions. Buildings and structures under operating conditions are subjected to cyclic mechanical loadings and climatic influences. For this conditions, special operational requirements are imposed on construction materials and products. For example, the durability of pavement and similar elements of transport communications and landscaping is mainly estimated by indicators of frost resistance and strength.

In the construction industry, decorative concretes are used in the manufacture of various building products [10, 11]. Based on this, complex studies on the formation of a dense and time-stable structure of decorative concretes under cyclic physical and mechanical impacts have a particular interest. As well know, it is also necessary to ensure the required workability of concrete mixtures in addition to the requirements of strength and frost resistance of hardened concrete. The workability is more consistent with powder-activated concrete.

Decorative powder-activated concrete is one of the most promising materials for use in the construction of buildings and structures of increased architectural expressiveness since it allows choosing a rational recipe composition.

The reason for the high strength of new generation concrete is not only the presence of a powder component. To enhance the action of the superplasticizer (SP) in new generation concretes (NGC), there should be fine-grained sand of 0.16–0.63 mm fraction, capable of being liquefied by plasticizers in an aqueous extract of cement paste.

One of the main quality criteria in assessing durability and service life without loss of strength and aesthetic characteristics of architectural and decorative concretes operating under atmospheric conditions is the frost resistance. A large number of studies in this field are devoted to the investigation of the resistance of concrete to the effects of frost in a water-saturated state and to increase their frost resistance [12]. Most researchers note that the fundamental reason for the frost destruction of cement concrete is the phase transition of water into ice, accompanied by an increase in its volume and the appearance of stresses in a rigid frame. The water to cement ratio significantly affects the porosity and frost resistance of concrete. At the same time, it was also found that finely ground additives introduced in an amount of up to 25–30% by weight of cement contribute to an increase the frost resistance of concrete due to better filling of voids between fine aggregate grains. In addition, a decrease in the specific consumption of cement per unit volume of concrete reduces the relative volume of cement stone and reduces internal stresses from unmanifested capillary shrinkage. Thereby, it increases the crack resistance of the concrete matrix and its frost resistance.

As a rule, the frost resistance grade of the old generation concretes does not exceed F 300–400, which is quite sufficient for the predicted high durability of concretes [13]. However, the period of operation before the disappearance of the decorative expressiveness of surfaces significantly reduced for architectural and decorative concretes in this case.

For hard operating conditions, the developed concretes must perceive more than 1000 cycles of alternating freeze-thaw. At the initial stage of selecting the composition of concrete, it is necessary to evaluate the rheotechnological properties of the components for their liquefaction using various superplasticizers, not only individual cement and mineral suspensions, but also their compositions.

In this regard, studies aimed to creation of construction materials with increased strength, density and high frost resistance are urgent. The task of the composition selectingwas not only to obtain high-strength concrete with a low water absorption value, but also to significantly increase frost resistance without the use of special air-entraining additives that increase the cost of concrete.

AIMS AND SCOPE OF THE RESEARCH

The present research aims to the selection of compositions of decorative and finishing powder-activated concretes with a granular surface texture according to rheological properties, strength and frost resistance indicators.

The tasks of the Research:

1. Analysis of the state of art in researches on concretes of a new generation with the allocation of structural and rheotechnological properties of powder-activated concretes.
2. Selection of the components for the formation of powder-activated concrete, considering cost minimization, providing the required view of the granular texture of the concrete surface, and ensuring high rheology of concrete mixtures based on the selected components.
3. Calculation of the structural and rheotechnological indicators of decorative and finishing powder-activated concrete and selection of the optimal compositions for technological properties.
4. Experimental studies of powder-activated concrete, depending on the type of superplasticizer and various fillers.
5. Determination of the volumes of various matrices, volumetric content of water-dispersed, water-dispersed-fine-grained and mortar components, relative excesses of volumes of conditional rheological matrices in decorative powder-activated concretes.

6. Experimental studies of powder-activated concrete strength and frost resistance, depending on the type of superplasticizer (SP) and fillers used.

MATERIALS AND METHODS

In these studies, the rheotechnological properties of cement composites of several types and several types of dispersed fillers in suspensions plasticized with plasticizers of various types were investigated at the first stage. And at the second stage, the strength and frost resistance of cement composites plasticized by superplasticizer such as Melflux-1641 were studied. The selection of components was carried out in regard with the combination of the following parameters: the cost of the components, providing the required view of the granular texture of the concrete surface, ensuring high rheology of concrete mixtures based on the selected components.

Fillers including those of the above type, were used as a finely dispersed component that increases the volume of the rheological matrix of the first row, which was microquartz from the Lebedinsky Mining and Processing Plant. And as filling components, that provide a granular surface texture, screenings of crushed granite of 0–5.0 mm fracture and cooper slag of 0–2.5 mm were adopted. The binder was Egyptian white cement (CEM 52.5). Materials of both domestic and foreign production were used as SP and GP, including Melflux 1641 and Khidetal γ-9.

We used a standard cone (GOST 10181–2014) to determine the rheotechnological parameters of the concrete mixture. The relevant regulatory documents (GOST 18105-2018; GOST 10060-2012) were used to determine the strength indicators and frost resistance of concrete.

Based on experiments, four most optimal compositions were proposed with optimized rheological matrices in terms of the content of cement, microquartz (ground sand), fine sand of 0.16–0.63 fracture and aggregate sand.

The studied compositions that differ in the type of superplasticizer and the quantitative content of filling components are given in [14]. In addition to mass contents, the volume content of the components, as well as the sediments of a standard cone, are indicated there.

The volumes of various matrices, the volume content of water-dispersed, water-dispersed fine-grained and mortar components in new generation concretes were calculated. These results are also in [15].The technology for calculating indicators is given below.

Frost resistance was determined according to GOST 10060-2012 “Concretes. Methods for determination of frost-resistance" according to the 3rd accelerated method, for which the samples are saturated with a 5% aqueous solution of sodium chloride. The tests were carried out in an independent laboratory of the production enterprise Penza Construction Department LLC in a freezer of the KTX-14 type at a temperature of minus 50 °C. The test mode was as follows: 8 hours of freezing, 16 hours of thawing.

CALCULATION OF STRUCTURAL AND RHEOTECHNOLOGICAL INDICATORS OF DECORATIVE AND FINISHING POWDER-ACTIVATED CONCRETE

The calculation of structural and rheotechnological indicators of decorative and finishing powder-activated concretes of a new generation, as well as relative excess volumes of conditional rheological matrices, was carried out using methods developed by V.I. Kalashnikov.

The volumes of various matrices, depending on their type, are calculated using the following formulas:

$$\text{I kind: } V_{\text{I}} = V_{\text{C}} + V_{\text{P}_{\text{M}}} + V_{\text{W}}; \quad (2)$$

$$\text{II kind: } V_{\text{II}} = V_{\text{I}} + V_{\text{P}_{\text{T}}}; \quad (3)$$

$$\text{III kind: } V_{\text{III}} = V_{\text{II}} + V_{\text{P}_{\text{Z}}}, \quad (4)$$

where V_{C} – isthe volume of cement per 1000 liters of concrete mix; $V_{\text{P}_{\text{M}}}$ – is thevolume of microquartz (ground sand) per 1000 liters; V_{W} – is

the water volume per 1000 liters; V_{P_T} – isthe volume of fine sand based on stone crushing screenings of granite stone and cooper slag of 0–0.63 mm fraction per 1000 liters; V_{P_Z} – isthe volume of aggregate sand based on a fraction of 0.63–2.5 mm per 1000 liters.

For comparison, the volumes of matrices in concrete of the old generation with the above composition can be calculated as follows:

$$\text{Ikind: } V_{\text{I}} = V_{\text{C}} + V_{\text{W}}; \quad (5)$$

$$\text{III kind: } V_{\text{III}} = V_{\text{I}} + V_{P_T}. \quad (6)$$

Taking into account the established volumes, the volume content of water-dispersed, water-dispersed-fine-grained mortar suspension components in plasticized powder-activated concrete of a new generation is calculated. The calculation of the volume content of water-dispersed (C^V_{WD}), water-dispersed fine-grained ($C^V_{\text{WDP}_T}$) and solution ($C^V_{\text{sol.}}$) suspension components in plasticized powder-activated crushed stone concrete of a new generation is carried out according to the formulas:

$$C^V_{\text{WD}} = \frac{V_{\text{C}} + V_{P_M} + V_{\text{W}}}{V_{\text{conc.mix}}} \cdot 100\%; \quad (7)$$

$$C^V_{\text{WDP}_T} = \frac{V_{\text{C}} + V_{P_M} + V_{\text{W}} + V_{P_T}}{V_{\text{conc.mix}}} \cdot 100\%; \quad (8)$$

$$C^V_{\text{sol.}} == \frac{V_{\text{C}} + V_{P_M} + V_{\text{W}} + V_{P_T} + V_{P_Z}}{V_{\text{conc.mix}}} \cdot 100\%. \quad (9)$$

The limits of volume concentrations of the studied concrete mixes are: C^V_{WD} varies from 39.91 to 43.94%, $C^V_{\text{WDP}_T}$ varies from 63.85 to 66.19% and for $C^V_{\text{sol.}}$ from 99.61 to 99.76%.

Only one composition in self-compacting mixtures has the volume concentration of a water-dispersed suspension less than 40%. Moreover, even in those mixtures, the rigid consistency of which is associated with a change in the content of the filler, the volume concentration of the water-dispersed suspension is more than 60%. Concrete mixtures of optimal composition have an equal volume concentration of the mortar component (over 60%). This is the fundamental difference between the developed concretes and traditional ones, in which the volumetric concentrations C^V_{WD} and $C^V_{\text{sol.}}$ are in the range of 24–26% and 54–57%, respectively.

For the topological analysis of all types of new concretes, developed and traditional concretes of the old generation, it is effective to use dimensionless rheological criteria. For powder concrete, the first criterion is the relative excess of the volume of the conditional rheological matrix of the I kind $I^{\text{WD}}_{P_T}$, i.e., relative excess of the volume of the water-dispersed system V_{WD} over the absolute volume of fine sand V_{P_T}. It is calculated by the following formula:

$$I^{\text{WD}}_{P_T} = V_{\text{WD}} / V_{P_T} = \left(V_{\text{C}} + V_{P_M} + V_{\text{W}}\right) \Big/ V_{P_T}, \quad (10)$$

where V_{C}, V_{P_M}, V_{W}, V_{P_T} – areabsolute volumes of cement, ground sand, water, fine sand, respectively.

There are two rheological matrices in powder-activated sandy concretes of the new generation: a water-dispersed matrix of the I kind and a water-dispersed fine-grained matrix of the II kind, including cement, microquartz (ground sand), fine sand and water. Fine sand in this matrix participates in the rheological process, providing the displacement of aggregate sand grains in the matrix of the I kind. The latter one is located discretely in a matrix of the II kind, ensuring the fluidity of the system without steric obstacles. The relative excess of the volume of the rheological matrix of the II kind over the absolute volume of aggregate sand is calculated by the formula:

$$I^{\text{WDP}_T}_{P_Z} = V_{\text{WDP}_T} / V_{P_Z} = \left(V_{\text{C}} + V_{P_M} + V_{\text{W}} + V_{P_T}\right) \Big/ V_{P_Z}, \quad (11)$$

where V_C, V_{P_M}, V_W, V_{P_T}, V_{P_Z} – are absolute volumes of cement, ground sand, water, fine sand, aggregate sand, respectively.

The excess rheological matrix of the II kind also provides the necessary distances between the aggregate sand grains. For narrow granulometry of sand, the theoretical calculation of distances can be close to the real one. For a wider granulometry, a distribution curve of the granulometric composition should be constructed, and then the distances between grains in narrow fractions can be calculated. Topological patterns of particle placement in narrow fractions are then combined into a single topological pattern with the free space maximization algorithm. This approach belongs to the problems of computer materials science, which can be useful for studying the topology of new generation concretes and optimizing the granulometric composition of components.

For concretes of the old generation, these criteria may not be excess volumes of rheological matrices over the volumes of sand and crushed stone, but shortcomings. They are calculated according to the formulas:

$$I_{P_Z}^{CD} = V_{CD} / V_{P_Z} = \left(V_C + V_W\right) / V_{P_Z}, \quad (12)$$

$$I_{SH}^{CDP} = V_{CDP} / V_{SH} = \left(V_C + V_W + V_{P_Z}\right) / V_{SH}. \quad (13)$$

ANALYSIS OF EXPERIMENTAL RESULTS

From the point of view of rheotechnological indicators, all compositions showed a fairly high quality as follows from the results of the study. According to the calculated values of conditional rheological matrices of the I and II kind, compositions 2 and 1 seem to be the most qualitative, compositions 4 and 3 are slightly less qualitative. Compositions 2 and 1 are self-compacting concretes with a cone draft of 27.4 and 28.5 cm, which corresponds to the American SF2 standard. There is a regularity in achieving close values of conditional rheological matrices ($I_{P_T}^{WD}$, $I_{P_Z}^{WDP_T}$), equal to 1.67–1.97 and 1.78–1.98, respectively. Thus, the volume content of the water-dispersed-fine-grained suspension component ($C_{WDP_T}^{V}$) for self-compacting powder-activated sand concrete should be in the range of 60–70%. The self-flowing can be ensured only at a high content of water-dispersed-fine-grained suspension.

The difference between compositions 2 and 1 is that the composition 1contains the increased volume of the conditional rheological matrix of the I kind due to a larger amount of microquartz (300 kg/m^3) relative to composition 2 (200 kg/m^3). While maintaining the sum of the masses of all components in composition 2, a part of microquartz is replaced by screening of stone crushing for greater saturation with granular components of the concrete mix and providing the most complete visual picture of the surface. As a result of this, rheotechnological, physical and technical indicators fall very slightly (see tables 1, 2). At the same time, in such self-compacting concrete mixtures, it is important to ensure aggregative stability and prevent sedimentation of particles.

As can be seen from the values of the conditional rheological criteria of powder-activated concretes, all of these values are much greater than unity and characterize a significant excess of the volumes of rheological matrices over the volumes of fine-grained, coarse-grained components that fit into them with large separation of particles and grains.

The physical and technical properties of powder-activated concretes of four compositions were studied. Indicators of compressive and bending strength and complex indicators for evaluating the effectiveness of materials of 4 compositions were obtained from testing of standard samples.

To assess the economic indicators of individual compositions, we determine the specific consumption of cement per unit of compressive and flexural strength as follows:

$$C_{R_c}^{S} = \frac{C}{R_c}, \; kg/MPa, \quad (14)$$

$$C_{R_b}^{S} = \frac{C}{R_b}, \; kg/MPa. \quad (15)$$

The specific strength per unit of cement consumption was determined by the formulas:

$$R^{\mathrm{S}}_{CR_{\mathrm{c}}} = \frac{R_{\mathrm{c}}}{C},\ MPa/kg; \quad R^{\mathrm{S}}_{CR_{\mathrm{b}}} = \frac{R_{\mathrm{b}}}{C},\ MPa/kg. \quad (16)$$

The ratio of strength indicators in compression and bending was also determined as follows:

$$K = R_{\mathrm{c}} / R_{\mathrm{b}}. \quad (17)$$

According to the data from [15] it follows that composition No. 3 [15] has improved performance. The table 1 presents the results of comprehensive studies of the properties of concrete, taking into account the data from table 3 in [15].

Table 1. Properties of decorative powder-activated sand concretes

Components	Disperse-fractional composition	Per 1 m^3, *kg*	Volum eper 1 m^3, l	*W*/*C*, *W*/*T*	*P*, *kg*/m^3	$\frac{P_{\mathrm{M}}}{C}$	$\frac{P_{\mathrm{T}}}{C}$	$\frac{P_{\mathrm{Z}}}{C}$	Strength *MPa*, at days	
									1	28
1	2	3	4	5	6	7	8	9	10	11
Cement 600 DO Egyptian	3800 cm^2/g	500	161	0,4	P_w1 days 2415	0,4	1,4	2,1 1	R_{c}=37 R_{b}= 6,1	R_{c}=90 R_{b}= 11
Melflux 1641 0,9 % ofC	—	4,5	3			$\frac{\Sigma P}{C} = 3,916$			$C^{\mathrm{s}}_{R_{\mathrm{c}}} = 5,55$	
Microquartz	3400 cm^2/g	200	75,5	0,081	P_{theor} 2434	$I^{\mathrm{WD}}_{\mathrm{P_T}} = 1,67$			$R^{\mathrm{s}}_{CR_{\mathrm{c}}} = 0,18$	
Screening stone crushing granite	0-0,63 mm	450	165			$I^{\mathrm{WDT}}_{\mathrm{P_Z}} = 1,78$			$C^{\mathrm{s}}_{R_{\mathrm{b}}} = 45,4$	
	0,63-5,0 mm	930	344		K_{seal} 0,992	$V_{\mathrm{WD}} = 436,5$ $V_{\mathrm{WDP_T}} = 698,4$ $V_{\mathrm{sol.}} = 1090,8$ $C^{V}_{\mathrm{WD}} = 39,91\ \%$ $C^{V}_{\mathrm{WDP_T}} = 63,85\ \%$ $C^{V}_{\mathrm{sol.}} = 99,73\ \%$			$R_{\mathrm{c}}/R_{\mathrm{b}} = 8,18$	
Cooperslag	0-0,63 mm	252	96,9							
	0,63-2,5 mm	126	48,4		CS_{sm}=11cm					
$\sum M_{\mathrm{dry}}$ $\sum V_{\mathrm{dry}}$ Water	—	2464 — 200	— 894,4 200							
$M_{\mathrm{conc.mix}}$		2664	—							
$V_{\mathrm{conc.mix}}$		—	1094							

We calculated the dimensionless parameters of raw components' ratios and criteria of conditional rheological matrices, which have the following values: $P/C = 3,55$; $R_C^s = 0,418$ MPa/kg; $I_{P_T}^{WD} = 1,67$; $I_{P_Z}^{CDP} = 1,78$.

It should be noted that a change in these criteria in the direction of a slight decrease or increase leads to a decrease in strength indicators by 10–20%. It is important that an extremely low specific consumption of cement per unit of concrete strength in compression ($C_{R_c}^s = 5.55$ *kg / MPa*) and tension in bending ($C_{R_b}^s = 45.4$ *kg / M*Pa) has been achieved. Strength ratio of indicators is $R_b / R_c = 0.112$.

The supposed correctness of the forecast of high frost resistance depending on the kinetics of water absorption was accounted. It was less than 1.5% by weight after four days of exposure. After two weeks of testing, this value was 1.98% and exceeded the 4-day water absorption by approximately 25–28%. That is, such a kinetics of water absorption for a sufficiently long time causes a large number of free pores which remain after water saturation of concrete for four days before testing for frost resistance. It is known that the volume of water increases by 9.6% at freezing. Thus, it can be safely predicted that an almost threefold excess of the volume of free pores over the increment in the volume of water when it passes into ice contributes to extremely high frost resistance.

The results of the experiment showed that after 1000 cycles of alternating freezing and thawing the weight of the samples decreased by an average of 0.7%. At the same time, there were no obvious signs of external destruction such as chipping of the corners of the samples, peeling of the surface, which shows the presence just of minimal destructive processes in the concrete structure and a slight change in strength. Besides, this result guarantees the preservation of the visual architectural appeal of the concrete surface over a long period of operation under the influence of harsh environmental factors.

After 1000 cycles of alternating freeze-thaw, the samples were tested for strength. The standard compressive strength of the test concrete after 28 days of hardening in normal humidity conditions was 85 MPa. By the end of the test, the samples stored in saline had a strength of 92 MPa. In this case, the samples that were tested had a strength of 90 MPa (after 1000 freeze-thaw cycles). That is, the loss of strength was slightly more than 2%, which is within the experimental error and meets the requirements of GOST.

Thus, the composition of architectural and decorative concrete proposed for implementation corresponds to the required properties in terms of strength and frost resistance. The results provide a basis for setting the limit levels of loads on concrete of various coatings, as well as for establishing requirements for the properties of concrete when designing it for operating conditions.

CONCLUSIONS

1. In recent years, self-compacting concrete mixtures have been widely used. Such mixtures are characterized by high workability without the usage of vibration compacting. Using innovative technologies, various materials and products for architectural and construction purposes with improved decorative properties can be manufactured.
2. According to physical chemistry, it follows necessity for the concrete mixture to have a sufficient amount of highly concentrated water-dispersed mixture (matrix), which can be converted from aggregation-unstable to aggregation-stable with the help of a plasticizer. In this case, it is required to stay the basic rule: an increase in the volume of the dispersed phase is provided without increasing the consumption of cement, but by adding powder filler in an amount of 40–70%, and in low-cement concrete - up to 90–100%.
3. The studies have been performed to select the compositions of decorative and finishing concretes with a granular surface texture according to rheological properties. Egyptian white cement served as a binder, micro-quartz as a microfiller, and screenings of crushed granite and cooper-slag of 0–0.63 mm fraction and the same components as filler sand of 0.63–5.0 mm and 0.63–2.5 mm fractions. The new generation su-

perplasticizers plasticized the mixture. At the initial stage of selecting the concrete composition, it is necessary to evaluate the rheotechnological properties of the components for their liquefaction using various superplasticizers, not only individual cement and mineral suspensions, but also their compositions.

4. The paper provides determined in the study structural and rheotechnological indicators of powder-activated concretes such as volumes of various matrices, volumetric contents of water-dispersed, water-dispersed-fine-grained and mortar components, relative excesses of volumes of conditional rheological matrices in decorative powder-activated concretes.

5. The research results shows that all compositions showed a fairly high quality in terms of rheotechnological indicators. According to the calculated values of conditional rheological matrices of the I and II kind, compositions 2 and 1 seem to be the most qualitative, compositions 4 and 3 are slightly less qualitative. Compositions 2 and 1 are self-compacting concretes with a cone draft of 27.4 and 28.5 cm, which corresponds to the American SF2 standard. There is a regularity in achieving close values of conditional rheological matrices ($I_{P_T}^{WD}$, $I_{P_Z}^{WDP_T}$), equal to 1.67–1.97 and 1.78–1.98, respectively. Thus, the volume content of the water-dispersed-fine-grained suspension component ($C_{WDP_T}^{V}$) for self-compacting powder-activated sand concrete should be in the range of 60–70%. Only a high content of water-dispersed-fine-grained suspension ensure absolute self-flowing.

6. The difference between compositions 2 and 1 is that in composition 1, the volume of the conditional rheological matrix of the I kind increases due to a larger amount of microquartz (300 kg/m^3) relative to composition 2 (200 kg/m^3). While maintaining the sum of the masses of all components in composition 2, part of the microquartz is replaced by screening of stone crushing for greater saturation with the granular components of the concrete mixture and ensuring the most complete visual picture of the surface (while the sum of the masses of all components is preserved). This leads to a slight decrease in rheotechnological and physical and technical indicators. It is essential to ensure aggregative stability and prevent particle sedimentation in such self-compacting concrete mixtures.

7. All values of the conditional rheological criteria of powder-activated concretes are significantly greater than one and characterize a significant excess of the volumes of rheological matrices over the volumes of fine-grained, coarse-grained components that fit into them with large separation of particles and grains.

8. The second stage included studies of the strength and frost resistance of concrete. As a result of testing for strength and frost resistance, high rates of these properties were revealed for decorative concretes.

9. The reason for the high strength of new generation concrete is not only the presence of a powder component. New generation concrete should contain fine-grained sand of a fraction of 0.16–0.63 mm capable of being liquefied by plasticizers in an aqueous extract of cement paste to enhance the action of the SP.

10. The results of the experiment showed that the weight of the samples decreased by an average of 0.7% after 1000 cycles of alternate freezing and thawing. At the same time, there were no obvious signs of external destruction, which allows us to assume the presence of minimal destructive processes in the concrete structure and a slight change in strength. Besides, this result guarantees the preservation of the visual architectural appeal of the concrete surface over a long period of operation under the influence of harsh environmental factors.

11. The samples were tested for strength after 1000 cycles of alternate freezing-thawing. The characteristic compressive strength of the test concrete after 28 days of hardening under normal humidity conditions was 85 MPa. The samples stored in saline had a strength of 92 MPa. In this case, the samples that were tested had a strength of 90 MPa (after 1000 freeze-thaw cycles). That is, the loss of strength was slightly more than 2%, which is within the experimental error and meets the requirements of GOST.

12. Thus, the composition of architectural and decorative concrete developed and proposed for

implementation corresponds to the properties in terms of strength and frost resistance. The obtained results allow setting the limit levels of loads on concrete of various coatings, as well as establishing the requirements and properties of concrete for designing with regard to operating conditions.

REFERENCIES

1. Intelligent dynamic concrete / B. Barragan, X. Roncero, R. Magarotto [et al.] // CP1 Int. Concrete production. 2011. № 2. P. 58–67.
2. **Kalashnikov V.I., Erofeev V.T., Tarakanov O.V.** Suspenzionno-napolnennye betonnye smesi dlya poroshkovo-aktivirovannyh betonov novogo pokoleniya [Technical and economic efficiency of the implementation of architectural and decorative powder-activated carbonate sand concrete] // Izvestija vuzov. Stroitel'stvo. 2016. No. 6 (690). pp. 39–46 (In Russian).
3. **Volpi E., Foiadelli C., Trasatti S.** Development of Smart Corrosion Inhibitors for Reinforced Concrete Structures Exposed to a Microbial Environment // Industrial and Engineering Chemistry Research. Volume 56, Issue 20, 24 May 2017, pp. 5778-5794. DOI: 10.1021/acs.iecr.7b00127.
4. **Mukhametrakhimov R.** Influence of the technological properties of cement-sand mortar on the quality of 3D printed products / R. Mukhametrakhimov, L. Lukmanova // IOP Conference Series: Materials Science and Engineering. 2020. Vol. 890. P. 012082.
5. **Jonkers H.M. and Schlangen E.** Development of a bacteria-based self-healing concrete // Tailor Made Concrete Structures – New Solution for Society. 2008. pp. 425–30.
6. **Zhang G.D., Zhang X.Z., Zhou Z.H., Cheng X.** Preparation and properties of concrete containing iron tailings manufactured sand as fine aggregate // Advanced Materials Research. 2014. Vol. 838-841 P. 152–155. DOI: 10.4028/www.scientific.net/AMR.838-841.152.
7. Study of effects of redispersable latex powders on hardening kinetics of cement-sand composites / A.A. Bobrishev, L.N. Shafigullin, V.T. Erofeev, (...), M.I. Sotnikov, Vyacheslav A. // Research Journal of Pharmaceutical, Biological and Chemical Sciences, 2016.7(4). pp. 795–802.
8. **Senhadji Y., Escadeillas G., Mouli M., Khelafi H.** Benosman Influence of natural pozzolan, silica fume and limestone on strength, acid resistance and microstructure of mortar // Powder Technology. 2014. Vol. 254. pp. 314–323. DOI: 10.1016/j.powtec.2014.01.046.
9. **Kalashnikov V.I.** Selecting the type of control setting composite cement-ash binder / V.I. Kalashnikov, E.A. Belyakova, R.N. Moskvin // Procedia Engineering. 2016. Vol. 150. P. 1631–1635. Doi:10.1016/j.proeng.2016.07.143.
10. **Resner O.** New opportunities in the field of design of architectural facades / O. Resner// Intern. Concreteproduction. 2013. No. 6. pp. 152–155.
11. Visualization of photos and graphics on a concrete surface / Reckli Gmbh, 44268, Herne, Germany // Intern. concrete.pr-in. 2014. No. 3. P. 173.
12. **Jiang G., Keller J., Bond P.L.** Determining the long-term effects of H_2S concentration, relative humidity and air temperature on concrete sewer corrosion // Water Research. 2014. Vol. 65. P. 157–169. DOI: 10.1016/j.watres.2014.07.026.
13. Density of structure and extent of saturation by water of composites as a factor of change of their durability when freezing and thawing / Y.V. Trofimovich, F.A. Petrovich, N.P. Ignatyevich, (...), L.V. Stanislavovich, R.V. Ivanovich // International Journal of Applied Engineering Research, 2015, 10(10), pp. 25711–25720.
14. **Erofeev V. T., Sanyagina Ya. A., Erofeeva I. V., Maksimova I. N.** Podbor sostavov dekorativno-otdelochnyh poroshkovo-aktivirovannyh betonov s zernistoj fakturoj poverhnosti po reologicheskim

svojstvam [The selection of compositions of the decorative and finishing powder-activated concrete with a granular surface texture according to the rheological properties]. // Regional'naya arhitektura i stroitel'stvo. – 2022. – № 3 (52).– pp. 16–31 (In Russian).

15. **Erofeev V.T., Sanyagina Ya. A., Erofeeva I.V., Maksimova I.N.** Prochnost' i morozostojkost' dekorativno-otdelochnyh poroshkovo-aktivirovannyh betonov s zernistoj fakturoj poverhnosti [The durability and frost resistance of the decorative and finishing powder-activated concrete with a granular surface texture]. // Regional'naya arhitektura i stroitel'stvo. – 2022. – № 3 (52). – pp. 32–45 (In Russian).

СПИСОК ЛИТЕРАТУРЫ

1. Intelligent dynamic concrete / B. Barragan, X. Roncero, R. Magarotto [et al.] // CP1 Int. Concrete production. 2011. № 2. P. 58–67.
2. **Калашников В. И.** Суспензионно-наполненные бетонные смеси для порошково-активированных бетонов нового поколения / В. И. Калашников, В. Т. Ерофеев, О. В. Тараканов // Изв. вузов. Стр-во. – 2016. – № 4. – С. 38–37.
3. **Volpi E., Foiadelli C., Trasatti S.** Development of Smart Corrosion Inhibitors for Reinforced Concrete Structures Exposed to a Microbial Environment // Industrial and Engineering Chemistry Research. Volume 56, Issue 20, 24 May 2017, pp. 5778-5794. DOI: 10.1021/acs.iecr.7b00127.
4. **Mukhametrakhimov R.** Influence of the technological properties of cement-sand mortar on the quality of 3D printed products / R. Mukhametrakhimov, L. Lukmanova // IOP Conference Series: Materials Science and Engineering. 2020. Vol. 890. P. 012082.
5. **Jonkers H.M. and Schlangen E.** Development of a bacteria-based self-healing concrete // Tailor Made Concrete Structures – New Solution for Society. 2008. P. 425–30.
6. **Zhang G.D., Zhang X.Z., Zhou Z.H., Cheng X.** Preparation and properties of concrete containing iron tailings manufactured sand as fine aggregate // Advanced Materials Research. 2014. Vol. 838-841 pp. 152–155. DOI: 10.4028/www.scientific.net/AMR.838-841.152.
7. Study of effects of redispersable latex powders on hardening kinetics of cement-sand composites / A.A. Bobrishev, L.N. Shafigullin, V.T. Erofeev, (...), M.I. Sotnikov, Vyacheslav A. // Research Journal of Pharmaceutical, Biological and Chemical Sciences, 2016.7(4). pp. 795–802.
8. **Senhadji Y., Escadeillas G., Mouli M., Khelafi H.** Benosman Influence of natural pozzolan, silica fume and limestone on strength, acid resistance and microstructure of mortar // Powder Technology. 2014. Vol. 254. pp. 314–323. DOI: 10.1016/j.powtec.2014.01.046.
9. **Kalashnikov V.I.** Selecting the type of control setting composite cement-ash binder / V.I. Kalashnikov, E.A. Belyakova, R.N. Moskvin // Procedia Engineering. 2016. Vol. 150. pp. 1631–1635. Doi:10.1016/j.proeng.2016.07.143.
10. **Resner O.** New opportunities in the field of design of architectural facades / O. Resner// Intern. Concreteproduction. 2013. No. 6. pp. 152–155.
11. Visualization of photos and graphics on a concrete surface / Reckli Gmbh, 44268, Herne, Germany // Intern. concrete.pr-in. 2014. No. 3. P. 173.
12. **Jiang G., Keller J., Bond P.L.** Determining the long-term effects of H_2S concentration, relative humidity and air temperature on concrete sewer corrosion // Water Research. 2014. Vol. 65. P. 157–169. DOI: 10.1016/j.watres.2014.07.026.
13. Density of structure and extent of saturation by water of composites as a factor of change of their durability when freezing and thawing / Y.V. Trofimovich, F.A. Pe-

trovich, N.P. Ignatyevich, (...), L.V. Stanislavovich, R.V. Ivanovich // International Journal of Applied Engineering Research, 2015, 10(10), P. 25711–25720.
14. **Ерофеев В. Т., Санягина Я. А., Ерофеева И. В., Максимова И. Н.** Подбор составов декоративно-отделочных порошково-активированных бетонов с зернистой фактурой поверхности по реологическим свойствам // Региональная архитектура и строительство. 2022. № 3 (52). С. 16–31.
15. **Ерофеев В. Т., Санягина Я. А., Ерофеева И. В., Максимова И. Н.** Прочность и морозостойкость декоративно-отделочных порошково-активированных бетонов с зернистой фактурой поверхности // Региональная архитектура и строительство. 2022. № 3 (52). С. 32–45.

Vladimir T. Erofeev, Academician of the RAACS, Professor, Doctor of Technical Sciences, Director of the Institute of Architecture and Construction, National Research Mordovian State University name N.P. Ogaryov; 430005, Republic of Mordovia, Saransk, st. Bolshevik, d. 68; tel. +7(8342) 48-25-64; E-mail: erofeevvt@bk.ru.

Nikolai I. Vatin, Professor, Doctor of Technical Sciences, Chief Researcher, St. Petersburg Polytechnic University name Peter the Great; 109992, Moscow, st. Solyanka, 14; E-mail: vatin_ni@spbstu.ru

Irina N. Maksimova, Associate Professor, Candidate of Technical Sciences, Associate Professor of the Department of Quality Management and Technology of Construction Production, Penza State University of Architecture and Construction; tel. +7(903) 324-95-02; E-mail: maksimovain@mail.ru.

Oleg V. Tarakanov, Professor, Doctor of Technical Sciences, Dean of the Faculty of Territory Management, Penza State University of Architecture and Construction; tel. +7 (927) 384-72-64; E-mail: tarov60@mail.ru.

Yana A. Sanyagina, Competitor of the Department of Building Materials and Technologies, National Research Mordovian State University name N.P. Ogaryov; 430005, Republic of Mordovia, Saransk, st. Bolshevik, d. 68; E-mail: sanyagina@mail.ru.

Irina V. Erofeeva, Candidate of Technical Sciences, Senior Lecturer of the Department "Fundamentals of Architecture and Artistic Communications", National Research Moscow State University of Civil Engineering; 129337, Moscow, Yaroslavl highway, 26; E-mail: ira.erofeeva.90@mail.ru.

Oleg V. Suzdaltsev, Candidate of Technical Sciences, Head of the Concrete Technology Department, Asia Cement LLC; 440000, Penza, st. Bakunin/Plekhanova d.20"B"/34; E-mail: spartak88ru@mail.ru.

Ерофеев Владимир Трофимович, академик РААСН, профессор, доктор технических наук, директор Института архитектуры и строительства, Национальный исследовательский Мордовский государственный университет им. Н.П. Огарёва; 430005, Республика Мордовия, г. Саранск, ул. Большевистская, д. 68; тел. +7(8342) 48-25-64; E-mail: erofeevvt@bk.ru.

Ватин Николай Иванович, профессор, доктор технических наук, главный научный сотрудник, Санкт-Петербургский политехнический университет им. Петра Великого; 109992, г. Москва, ул. Солянка, д. 14; E-mail: vatin_ni@spbstu.ru.

Максимова Ирина Николаевна, доцент, кандидат технических наук, доцент кафедры «Управление качеством и технология строительного производства», Пензенский государственный университет архитектуры и строительства; тел. +7(903) 324-95-02; E-mail: maksimovain@mail.ru.

Тараканов Олег Вячеславович, профессор, доктор технических наук, декан факультета Управления территориями, Пензенский государственный университет архитектуры и строительства; тел. +7 (927) 384-72-64; E-mail: tarov60@mail.ru.

Санягина Яна Андреевна, соискатель кафедры «Строительные материалы и технологии», Национальный исследовательский Мордовский государственный университет им. Н.П. Огарёва; 430005, Республика Мордовия, г. Саранск, ул. Большевистская, д. 68; E-mail: sanyagina@mail.ru.

Ерофеева Ирина Владимировна, кандидат технических наук, старший преподаватель кафедры «Основы архитектуры и художественных коммуникаций», Национальный исследовательский Московский государственный строительный университет; 129337, г. Москва, Ярославское шоссе, д. 26; E-mail: ira.erofeeva.90@mail.ru.

Суздальцев Олег Владимирович, кандидат технических наук, начальник отдела технологии бетонов, ООО «Азия Цемент»; 440000, г. Пенза, ул. Бакунина/Плеханова д.20«Б»/34; E-mail: spartak88ru@mail.ru

International Journal for Computational Civil and Structural Engineering, 18(4) 62–70 (2022)

DOI:10.22337/2587-9618-2022-18-4-62-70

THE EFFECT OF THE AXIAL AND SHEAR STIFFNESSES ON ELASTIC ROD'S STABILITY

Daria A. Kuznetsova [1], Vladimir V. Lalin [2], Nikolay M. Malkov [1]

[1] Far Eastern Federal University, Vladivostok, RUSSIA
[2] Peter the Great St.Petersburg Polytechnic University, Saint Petersburg, RUSSIA

Abstract. This article is about the nonlinear problems of the theory of elastic Cosserat – Timoshenko's rods in the material (Lagrangian) description. The variational definition for the problem as finding the stationary point of the Lagrangian functional and differential formulation of static problems were given. The exact stability functional and stability equations of the plane problem for physically linear elastic rods taking into account the axial, shear and bending stiffnesses were received. The exact value of the critical load was obtained taking into account the axial, shear and bending deformations in the problem of the stability of a rod compressed by an axial force. In the present paper the stability of classical simplified rod's models such as the Timoshenko beam and the Euler–Bernoulli beam was investigated. Also, the stability of third simplified rod's model, based on beam's axial and bending stiffnesses, was explored. The stability functionals, the stability equations and critical loads formulations for this three types of simplified models were derived as a particular case of the general theory. There were made the comparisons of described solutions which regards all the rod's stiffnesses and solutions, based on simplified models. The effect of the axial and shear stiffnesses on rod's stability was analyzed.

Keywords: stability of structures; variational formulation; the stability functional; the stability equations; the critical load

ВОЗДЕЙСТВИЕ ЖЕСТКОСТЕЙ НА РАСТЯЖЕНИЕ – СЖАТИЕ И СДВИГ НА УСТОЙЧИВОСТЬ УПРУГИХ СТЕРЖНЕЙ

Д.А. Кузнецова [1], В.В. Лалин [2], Н.М. Малков [1]

[1]Дальневосточный федеральный университет, Владивосток, РОССИЯ
[2]Санкт-Петербургский политехнический университет Петра Великого, Санкт-Петербург, РОССИЯ

Аннотация. Данная статья посвящена нелинейным задачам теории упругих стержней Коссера – Тимошенко в материальном (Лагранжевом) описании. Приведено вариационное определение задачи в виде поиска точки стационарности функционала типа Лагранжа и дифференциальные постановки статических задач. Получены точные функционал устойчивости и уравнения устойчивости плоской задачи для физически линейных упругих стержней с учетом продольной, сдвиговой и изгибной жесткостей. Точное значение критической нагрузки получено с учетом продольных, сдвиговых и изгибающих деформаций в задаче устойчивости стержня, сжатого осевой силой. В настоящей работе исследована устойчивость классических упрощенных стержневых моделей, таких как балка Тимошенко и балка Бернулли - Эйлера. Также была исследована устойчивость третьей упрощенной модели стержня, основанной на учете продольной и изгибной жесткостей балки. Функционалы устойчивости, уравнения устойчивости и формулы критических сил для этих трех типов упрощенных моделей были выведены в качестве частного случая общей теории. Проведены сравнения описанных решений с учетом всех жесткостей стержня и решений, основанных на упрощенных моделях. Проанализировано влияние осевой и сдвиговой жесткости на устойчивость стержня.

Ключевые слова: устойчивость конструкций; вариационная формулировка; функционал устойчивости; уравнения устойчивости; критическая нагрузка

1. INTRODUCTION

The desire to reduce the material consumption of structures leads to the use of more flexible structural elements in modern construction. This increases the possibility of loss of stability of these elements. Traditional assessment methods of the rod's stability based on the classical Euler's formula, give only approximate values of critical loads for compliant elements. This is due to the fact that only the bending stiffness of the rods is taken into account in the Euler's formula. In this paper, we obtain exact solutions to the stability problems of rods that take into account, in addition to bending stiffness, also axial and shear stiffnesses.

The apparatus of the classical variational calculus is used to solve this problem. The traditional approach to the variational formulation of the problem of rod's nonlinear deformation is to use the variational equation in the form of the principle of possible displacements [1-18]. In this paper, it is shown that the variational problem can be formulated as a problem of finding the stationarity point of a Lagrange-type functional, using energetically conjugate vectors of forces and deformations [19]. In this case, it becomes possible to obtain exact stability equations as the Euler's equations for the second variation of the Lagrangian functional for the first time. From the exact stability functional and stability equations, it is possible as a consequence to obtain an approximate stability functional and stability equations, in which only bending stiffness (the Euler–Bernoulli beam) or only bending and shear stiffnesses (the Timoshenko beam) or only bending and axial stiffnesses (the Euler–Bernoulli beam taking into account the axial stiffness) are considered.

2. VARIATIONAL FORMULATIONS OF THE NONLINEAR STABILITY PROBLEMS OF ELASTIC RODS

Formulation of the geometrically nonlinear problem for the physically linear rod consists of three groups of differential equations: equilibrium equations, geometrical equations and physical equations.

Equilibrium equations for the plane problem are:

$$\begin{cases} (N\cos\varphi - Q\sin\varphi)' + q_x = 0; \\ (N\sin\varphi + Q\cos\varphi)' + q_y = 0; \\ M' + x'(N\sin\varphi + Q\cos\varphi) + \\ +y'(Q\sin\varphi - N\cos\varphi) + m = 0, \end{cases} \quad (1)$$

where N is axial force; Q is shear force; M is bending moment; q_x, q_y and m are distributed power and moment loads respectively. Functions $x(s)$, $y(s)$, and $\varphi(s)$ are three degrees of freedom in the plane problems of the geometrically nonlinear deformation of the rod. In the reference unstressed configuration every point of the rod can be identified by the s coordinate, where $0 \le s \le L$, L is length of the unstrained rod. (...)' denote derivative with respect to s.

The components of axial, shear and bending deformations ε, γ, ψ are defined through the functions $x(s)$, $y(s)$, and $\varphi(s)$ by geometrical equation:

$$\begin{cases} \varepsilon = x'\cos\varphi + y'\sin\varphi - 1; \\ \gamma = -x'\sin\varphi + y'\cos\varphi; \\ \psi = \varphi'. \end{cases} \quad (2)$$

Physical equations for the linear elastic material are:

$$N = k_1\varepsilon;\ Q = k_2\gamma;\ M = k_3\psi, \quad (3)$$

where k_1 = EA is axial stiffness; k_2 = GAk is shear stiffness; k_3 = EI is bending stiffness; E is Young's modulus; A is cross-section area of the rod; G is shear modulus; k is cross-section form coefficient; I is moment of inertia.

The Lagrange functional can be written in the following way:

$$L(x,y,\varphi) = \int_0^L \left[\frac{1}{2}\left(k_1\varepsilon^2 + k_2\gamma^2 + k_3\psi^2 - \right.\right. \\ \left.\left. -q_x(x-s) - q_y y - m\varphi\right)\right] ds - F_1(x(L) - \\ -L) - F_2 y(L) - M_1\varphi(L), \quad (4)$$

where: F_1 is "dead" load parallel to the X axis; F_2 is "dead" load, parallel to the Y axis; M_1 - external moment applied at the end of the rod at s = L.

In [20 - 23], it was proved that the differential formulation of the problem (1)-(3) is equivalent to the L→ STAT variational problem of the search of the stationary point of functional (4).

The stability functional of the plane problem for physically linear elastic rods taking into account the axial, shear and bending stiffnesses, resulting from the second variation the Lagrange functional, can be written in the following way:

$$\Phi_{\text{ст}}(u,\upsilon,\theta) = \frac{1}{2}\int_0^L \big[N_B\varepsilon_B + N\theta\big(2\gamma_B + \\ +\theta(\varepsilon+1)\big) + Q_B\gamma_B + Q(\theta\gamma - 2\varepsilon_B) + \\ +M_B\psi_B\big]\,ds, \qquad (5)$$

where the following notation is used:

$$N_{\text{в}} = k_1\varepsilon_{\text{в}}; \quad Q_{\text{в}} = k_2\gamma_{\text{в}}; \quad M_{\text{в}} = k_3\psi_{\text{в}}; \\ \varepsilon_{\text{в}} = u'\cos\varphi - x'\theta\sin\varphi + \upsilon'\sin\varphi + \\ +y'\theta\cos\varphi; \qquad (6) \\ \gamma_{\text{в}} = -u'\sin\varphi - x'\theta\cos\varphi + \upsilon'\cos\varphi - \\ -y'\theta\sin\varphi; \\ \psi_{\text{в}} = \theta'.$$

The quantities x, y, φ, ε, γ, ψ, N, Q, M denote the equilibrium state characteristics, satisfying the system of equations (1) - (3), as well as boundary conditions. These quantities are characteristics of the equilibrium state, whose stability is studied. The quantities with the subscript "B" are denoted variations; $u(s)$, $\upsilon(s)$, and $\theta(s)$ variations of coordinates x, y and angle of rotation φ, respectively.

The stability equations are the Euler's equations for the variational problem $\Phi_{\text{ст}}$→ STAT. Euler's equations resulting from the condition $\delta\Phi_{\text{ст}} = 0$ are the further equations:

$$\begin{cases} (N_{\text{в}}\cos\varphi - Q_{\text{в}}\sin\varphi)' - \\ -\big(\theta(N\sin\varphi + Q\cos\varphi)\big)' = 0; \\ (N_{\text{в}}\sin\varphi + Q_{\text{в}}\cos\varphi)' + \\ +\big(\theta(N\cos\varphi - Q\sin\varphi)\big)' = 0; \\ \text{M}_{\text{в}}' + u'(N\sin\varphi + Q\cos\varphi) + \\ +\upsilon'(Q\sin\varphi - N\cos\varphi) + x'(N_{\text{в}}\sin\varphi + \\ +Q_{\text{в}}\cos\varphi + \theta(N\cos\varphi - Q\sin\varphi)\big) + \\ +y'(Q_{\text{в}}\sin\varphi - N_{\text{в}}\cos\varphi + \\ +\theta(N\sin\varphi + Q\cos\varphi)\big) = 0. \end{cases} \qquad (7)$$

System (7) is a system of equations for the functions u, υ, and θ. Functions x, y and φ, as well as N, Q, M are fixed and are solutions to problem (1) - (3).

Equations (7) are the exact equations of the problem of the equilibrium state of the rod for the case of the plane problem. We would like to stress that the derived system of the stability equations is exact. No simplifying assumptions were made about the displacement and rotation angles quantity, and the character of the equilibrium state of the rod. The resulting functional (5) and equations (7) are written in general terms and are applicable for any type of load and boundary conditions.

In [20 - 23], stability equations (7) were also obtained by the second way like the equations in variations of the equilibrium equations (1).

The classic Euler problem (hinged rod under the axial potential dead load shown in Figure 1) is considered as an example. The equilibrium configuration is rectilinear.

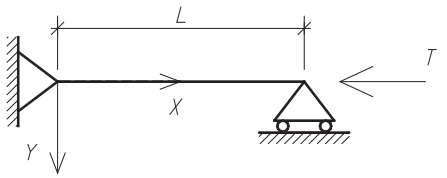

Figure 1. Design model of the rod

Boundary values for this example are:

$$s = 0:\ x(0) = 0;\ \ y(0) = 0;\ \ M(0) = 0; \\ s = \text{L}:\ (N\cos\varphi - Q\sin\varphi)|_{s=L} + \\ T;\ \ y(\text{L}) = 0;\ \ M(\text{L}) = 0. \qquad (8)$$

The exact solution of the nonlinear problem (1) - (3) and (8) is described by the formulas:

$$y = 0; \quad \varphi = 0; \quad \varepsilon = \frac{N}{k_1} = -\frac{T}{k_1};$$
$$\gamma = 0; \quad \psi = 0;$$
$$N = -T; \quad Q = 0; \quad M = 0. \qquad (9)$$
$$x' = \varepsilon + 1 = \frac{N}{k_1} + 1 = 1 - \frac{T}{k_1}.$$

Substitute equations (9) into the stability functional (5) using expressions (6). The functional components containing u describes the axial deformations, not associated with the load T, and can be omitted when studying stability. Finally, the stability functional for this example can be written as:

$$\Phi_{\text{ст}}(v,\theta) = \frac{1}{2}\int_0^L \left[k_2 \left(v' - \theta\left(1 - \frac{T}{k_1}\right)\right)^2 + \right.$$
$$\left. + k_3\theta'^2 + T\theta\left(\left(1 - \frac{T}{k_1}\right)\theta - 2v'\right)\right] ds. \qquad (10)$$

The stability equations, which follow from the condition $\delta\Phi_{\text{ст}} = 0$, have the form:

$$\begin{cases} k_2\left(v' - \left(1 - \frac{T}{k_1}\right)\theta\right)' - T\theta' = 0; \\ k_3\theta'' + k_2\left(v' - \left(1 - \frac{T}{k_1}\right)\theta\right)\cdot \\ \quad \cdot\left(1 + T\left(\frac{1}{k_2} - \frac{1}{k_1}\right)\right) = 0. \end{cases} \qquad (11)$$

A detailed solution to the system of equations (11) was considered in [20 - 23].

The critical (minimal) force value is calculated from the quadratic equation [20 - 23]:

$$T^2\left(\frac{1}{k_2} - \frac{1}{k_1}\right) + T - T_E = 0, \qquad (12)$$

where $T_E = \frac{\pi^2 k_3}{L^2}$ – Euler's force for the hinged rod [24].

It is easy to show that the only positive value of the critical load, following from equation (12) is:

$$T_{cr} = \frac{\sqrt{1 + 4T_E\left(\frac{1}{k_2} - \frac{1}{k_1}\right)} - 1}{2\left(\frac{1}{k_2} - \frac{1}{k_1}\right)}, \qquad (13)$$

Solution (13) is the exact solution of the problem of the hinged rod when axial, shear and bending stiffnesses are taken into account.

3. THE STABILITY OF SIMPLIFIED ROD'S MODELS

3.1. The Timoshenko beam

The Timoshenko beam theory is based on taking into account the effect of shear deformation on the stress and strain state of the rod. The classic Euler problem (hinged rod under the axial potential dead load shown in Figure 1) is considered as an example. When analyzing the stability of the Timoshenko beam, the assumption is made that the change in the geometric dimensions of the rod under subcritical deformations is considered negligible. For instance, the length of the rod is unchanged in the process of loading. Thus, the rod is stressed but not deformed. So:

$$N = k_1\varepsilon = -T; \ \varepsilon = 0; \ \rightarrow \ k_1 \rightarrow \infty \ \rightarrow$$
$$\rightarrow \ (k_1)^{-1} = 0.$$

The stability functional for the Timoshenko beam follows from the stability functional in equation (10), taking $(k_1)^{-1} = 0$:

$$\Phi_{\text{ст}}(v,\theta) = \frac{1}{2}\int_0^L [k_3\theta'^2 + k_2(v' - \theta)^2 +$$
$$+ T\theta(\theta - 2v')]ds. \qquad (14)$$

The stability equations for the Timoshenko beam, arising from the stability functional in equation (14), can be written in the following way:

$$\begin{cases} k_2(v' - \theta)' - T\theta' = 0; \\ k_3\theta'' + k_2(v' - \theta)\left(1 + \frac{T}{k_2}\right) = 0. \end{cases} \qquad (15)$$

The solution to the system of equations (15), which is an exact solution to the stability problem for the Timoshenko beam, taking into account

the shear and bending stiffnesses, can be written in the following way:

$$T_{cr} = \frac{k_2}{2}\left(\sqrt{1 + \frac{4T_E}{k_2}} - 1\right). \quad (16)$$

To assess the effect of the axial stiffness of an initially rectilinear rod compressed by an axial dead load T, as shown in Figure 1, let us compare the values of the critical load calculated by the exact formula, according to equation (13), taking into account the axial, shear and bending stiffnesses, with values, calculated by equation (16) for the Timoshenko beam, taking into account only the shear and bending stiffnesses. Figure 2 shows the graphs for the strut, made of the I-beam, as an example.

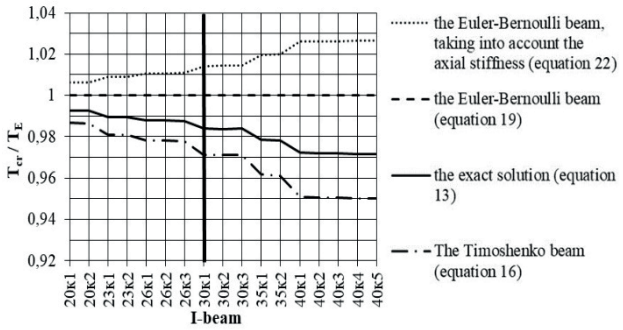

Figure 2. The effect of the axial and shear stiffnesses on values of the critical load

Based on the analysis of the results, we can conclude that the inclusion of the axial stiffness increases the critical load. Thus, we take into account the rod's internal "reserves" under the action of the "dead" axial load, adding the axial stiffness to the calculation of the rod's stability.

3.2. The Euler–Bernoulli beam

Let us consider the stability of the Euler-Bernoulli beam, which does not take into account the effect of shear deformation on the stress and strain state of the rod, as well as the hypothesis of non-deformability of the rod in the subcritical state is accepted. The classic Euler problem (hinged rod under the axial potential dead load shown in Figure 1) is considered as an example, as for the Timoshenko beam.

The stability functional for the Euler-Bernoulli beam follows from the stability functional in equation (10), taking $(k_1)^{-1} = 0; (k_2)^{-1} = 0$:

$$\Phi_{\text{ст}}(v, \theta) = \frac{1}{2}\int_0^L [k_3 v''^2 - T v'^2] ds. \quad (17)$$

Euler's equation, which follows from the condition $\delta\Phi_{\text{ст}} = 0$, can be written as:

$$k_3 v^{IV} + T v'' = 0. \quad (18)$$

The solution to the stability equation (18) is the classical common Euler formula for the critical load exclude the axial and shear stiffnesses.

$$T_E = \frac{\pi^2 k_3}{L^2}. \quad (19)$$

To assess the effect of the axial and shear stiffnesses of an initially rectilinear rod compressed by an axial dead load T, as shown in Figure 1, let us compare the values of the critical load calculated by the exact formula, according to equation (13), taking into account the axial, shear and bending stiffnesses, with values, calculated by equation (19) for the Euler-Bernoulli beam, taking into account only the bending stiffness. Figure 2 shows the graphs for the strut, made of the I-beam, as an example. For illustrative purposes, the figure 2 also shows the graph of the critical load values for the Timoshenko beam, calculated by equation (16), and the graph of the critical load values for the Euler-Bernoulli beam, taking into account axial stiffness, calculated by equation (22).

Based on the analysis of the results, we can conclude that the inclusion of the axial and shear stiffnesses significantly reduces the critical load. Thus, the use of the classical Euler formula in equation (19) leads to the risk of loss of stability by the rod even before reaching the critical load calculated by the equation (13).

3.3. The Euler–Bernoulli beam taking into account the axial stiffness

Let us consider the stability of the Euler-Bernoulli beam, which takes into account the

axial stiffness, but does not take into account the effect of shear deformation on the stress and strain state of the rod. However, the hypothesis of non-deformability of the rod in the subcritical state is not accepted in contrast to the classic the Euler-Bernoulli beam. The classic Euler problem (hinged rod under the axial potential dead load shown in Figure 1) is considered as an example, as for the Timoshenko beam.

The stability functional for this simplified rod's model follows from the stability functional in equation (10), taking $(k_2)^{-1} = 0$:

$$\Phi_{\text{ст}}(v,\theta) = \frac{1}{2}\int_0^L \left[\frac{k_3 v''^2}{\left(1-\frac{T}{k_1}\right)^2} - \frac{T v'^2}{\left(1-\frac{T}{k_1}\right)}\right] ds. \quad (20)$$

Euler's equation, which follows from the condition $\delta\Phi_{\text{ст}} = 0$, can be written as:

$$\frac{k_3 v^{IV}}{\left(1-\frac{T}{k_1}\right)^2} + \frac{T v''}{\left(1-\frac{T}{k_1}\right)} = 0. \quad (21)$$

The solution to the equation (21), which is an exact solution to the stability problem for the Euler-Bernoulli beam, taking into account the axial and bending stiffnesses, can be written in the following way:

$$T_{cr} = \frac{k_1}{2}\left(1 - \sqrt{1 - \frac{4T_E}{k_1}}\right). \quad (22)$$

To assess the effect of the shear stiffnesses of an initially rectilinear rod compressed by an axial dead load T, as shown in Figure 1, let us compare the values of the critical load calculated by the exact formula, according to equation (13), taking into account the axial, shear and bending stiffnesses, with values, calculated by equation (22) for the Euler-Bernoulli beam, taking into account the axial and bending stiffnesses. Figure 2 shows the graphs for the strut, made of the I-beam, as an example. For illustrative purposes, the figure 2 also shows the graph of the critical load values for the Timoshenko beam, calculated by equation (16), and the graph of the critical load values for the Euler-Bernoulli beam, calculated by equation (19).

Based on the analysis of the results, we can conclude that the value of the critical load obtained from equation (22) is greater than the value obtained from the exact formula (13) and the value obtained from Euler's formula (19). Thus, the use of equation (22) leads to the risk of loss of the rod's stability even before reaching the critical load calculated by the equation (22). Therefore, as shown in figure 2, it is unacceptable to take into account the axial stiffness without taking into account the shear stiffness, when analyzing the rod's stability.

4. CONCLUSIONS

1. The formulations of the problems are presented in the form of a system of differential equations and variational formulations in the form of the problem of finding the stationarity point functional of the Lagrange type.
2. For the plane problems, equations of equilibrium stability problems are obtained as the Euler equations for the second variation of the Lagrange functional
3. The exact universal solution in equation (13), taking into account axial, shear and bending stiffnesses, which gives the exact value of the critical load was obtained for the problem of the stability of a rod compressed by an axial force.
4. There were made the comparisons of exact solutions which regards all the rod's stiffnesses and solutions, based on three simplified models.
5. It was shown, that considering axial stiffness leads to increasing the values of the critical load. Thus, we take into account the rod's internal "reserves" under the action of the "dead" axial load, adding the axial stiffness to the calculation of the rod's stability.
6. It was shown, that inclusion of the axial and shear stiffnesses significantly reduces the critical load. Thus, the use of the classical Euler formula leads to the risk of loss of stability by the rod even before reaching the critical load calculated by the exact equation.

7. It was shown, that taking into account the axial stiffness, without taking into account the shear stiffness, significantly increases the critical load. Therefore, it is unacceptable to take into account the axial stiffness without taking into account the shear stiffness, when analyzing the rod's stability.
8. It was shown, that the obtained exact value of the critical compressive load, taking into account all rod's stiffnesses, has a lower value than the critical load value calculated by the classical Euler's formula. Since both formulas are equally simple for manual calculation, the resulting exact formula can be recommended for use in all cases in which Euler's formula was previously used.

REFERENCES

1. **Goloskokov D.P., Zhilin P.A.** Obshaja nelinejnaja teorija uprugih sterzhnej s prilozheniem k opisaniju jeffekta Pojntinga. Deposited VINITI No. 1912-V87 Dep. p 20
2. **Eliseev V.V.** Mehanika uprugih sterzhnej. Saint-Petersburg: SPbGPU Press, 1994, 88 pages (in Russian).
3. **ZHilin P.A., Sergeev A.D.** Ravnovesie i ustojchivost tonkogo sterzhnya nagruzhennogo konservativnym momentom//Trudy SPbGTU. Mekhanika i processy upravleniya, SPb.: SPbGPU Press, 1994, Volume 448, pp. 47-56 (in Russian).
4. **ZHilin P.A., Sergeev A.D., Tovstik T.P.** Nelinejnaya teoriya sterzhnej i ee prilozheniya // Trudy XXIV letnej shkoly «Analiz i sintez nelinejnyh mekhanicheskih kolebatelnyh system», Saint-Petersburg: SPbGPU Press, 1997, pp. 313-37 (in Russian).
5. **ZHilin P.A.** Prikladnaya mekhanika. Teoriya uprugih tonkih sterzhnej. Saint-Petersburg: SPbGPU Press, 2007, 102 pages (in Russian).
6. **Eliseev V.V., Zinoveva T.V.** Mekhanika tonkostennyh konstrukcij. Teoriya sterzhnej. Saint-Petersburg: SPbGPU Press, 2008, 96 pages (in Russian).
7. **Jelenic G., Crisfield M.A.** Geometrically exact 3D beam theory: implementation of a strain – invariant finite element for static and dynamics // Comp. Meths. Appl. Mech. Engng, 1999, Volume 171, pp. 141-71.
8. **Shabana A.A., Yakoub R.Y.** Three dimensional absolute nodal coordinate formulation for beam elements: theory // ASME, Journal of Mechanical Design, 2001, Volume 123 (4), pp. 606-613.
9. **Reddy J.N.** An Introduction to Nonlinear Finite Element Analysis. Oxford University Press, 2004, 482 pages.
10. **Antman S. S.** Nonlinear problems of elasticity. Springer, Berlin Heidelberg New York, 2005, 835 pages.
11. **Gerstmayr J**., **Shabana A.A.** Analysis of thin beams and cables using the absolute nodal coordinate formulation // Nonlinear Dynamics, 2006, Volume 45 (1-2), pp. 109-130.
12. **Shabana A.A.** Computational continuum mechanics. Cambridge University Press, 2008, 349 pages.
13. **Wriggers P.** Nonlinear finite element methods. Springer-Verlag Berlin Heidelberg, 2008, 566 pages.
14. **Krenk S.** Non-linear modelling and analysis of solids and structures. Cambridge University Press, 2009, 361 pages.
15. **Ibrahimbegovic A.** Nonlinear Solid Mechanics. Springer Science+Business Media B.V, 2009, 585 pages.
16. **Bigoni D.** Nonlinear solid mechanics: bifurcation theory and material instability. Cambridge University Press, 2012, 550 pages.
17. **Coskun S., Öztürk B.** Elastic Stability Analysis of Euler Columns Using Analytical Approximate Techniques Advances in Computational Stability Analysis ed Dr. Safa Bozkurt Coşkun ISBN: 978-953-51-0673-9, InTech, DOI: 10.5772/45940
18. **Bagmutov V.P., Belov A.A., Stoljarchuk A.S.** Jelementy raschetov na ustojchivost': ucheb. posobie. Volgograd: IUNL VolgGTU, 2010, 56 pages (in Russian).

19. **Lalin V.V.** Razlichnye formy uravnenij nelinejnoj dinamiki uprugih sterzhnej // Trudy SPbGPU, 2004, Volume 489, pp.121-128 (in Russian).
20. **Lalin V.V., Rozin L.A., Kushova D.A.** Variacionnaja postanovka ploskoj zadachi geometricheski nelinejnogo deformirovanija i ustojc``hivosti uprugih sterzhnej // Inzhenerno – stroitel'nyj zhurnal, 2013, Volume 1, pp. 87-96 (in Russian).
21. **Lalin V.V., Zdanchuk E.V., Kushova D.A., Rozin L.A.** Variacionnye postanovki nelinejnyh zadach s nezavisimymi vrashhatel'nymi stepenjami svobody // Inzhenerno – stroitel'nyj zhurnal, 2015, Volume 4, pp. 54-80 (in Russian).
22. **Lalin V.V., Kushova D.A.** Geometricheski nelinejnoe deformirovanie i ustojchivost' ploskih uprugih sterzhnej s uchetom zhestkostej na rastjazhenie-szhatie, sdvig i izgib // International Journal for Computational Civil and Structural Engineering, 2013, Volume 9, pp. 178-185 (in Russian).
23. **Lalin V.V., Kushova D.A.** Reshenie zadachi ustojchivosti szhatogo sterzhnja dinamicheskim metodom s uchetom zhestkostej na sdvig i rastjazhenie // Stroitel'naja mehanika i raschet sooruzhenij, 2014, Volume 5 (256), pp. 49-54 (in Russian).
24. **Perel'muter A.V., Slivker V.I.** Ustojchivost' ravnovesija konstrukcij i rodstvennye problemy. Volume 1. Moscow: SKAD SOFT Press, 2010, 704 pages (in Russian).

СПИСОК ЛИТЕРАТУРЫ

1. **Голоскоков Д.П., Жилин П.А.** Общая нелинейная теория упругих стержней с приложением к описанию эффекта Пойнтинга // Депонироано ВИНИТИ №1912-В87 Деп., 20 с.
2. **Елисеев В.В.** Механика упругих стержней. СПб, Изд-во СПбГПУ, 1994. – 88 с
3. **Жилин П.А., Сергеев А.Д.** Равновесие и устойчивость тонкого стержня, нагруженного консервативным моментом // Механика и процессы управления. Труды СПбГТУ. 1994. № 448. с. 47-56.
4. **Жилин П.А., Сергеев А.Д., Товстик Т.П.** Нелинейная теория стержней и ее приложения // Труды XXIV летней школы «Анализ и синтез нелинейных механических колебательных систем», Санкт-Петербург, 1997, с. 313-37.
5. **Жилин П.А.** Прикладная механика. Теория тонких упругих стержней. СПб, Изд-во СПбГПУ. 2007. – 102 с.
6. **Елисеев В.В., Зиновьева Т.В.** Механика тонкостенных конструкций. Теория стержней. СПб, Изд-во СПбГПУ. 2008. – 96 с.
7. **Jelenic G., Crisfield M.A.** Geometrically exact 3D beam theory: implementation of a strain – invariant finite element for static and dynamics // Comp. Meths. Appl. Mech. Engng, 1999, Volume 171, pp. 141-71.
8. **Shabana A.A., Yakoub R.Y.** Three dimensional absolute nodal coordinate formulation for beam elements: theory // ASME, Journal of Mechanical Design, 2001, Volume 123 (4), pp. 606-613.
9. **Reddy J.N.** An Introduction to Nonlinear Finite Element Analysis. Oxford University Press, 2004, 482 pages.
10. **Antman S. S.** Nonlinear problems of elasticity. Springer, Berlin Heidelberg New York, 2005, 835 pages.
11. **Gerstmayr J**., **Shabana A.A.** Analysis of thin beams and cables using the absolute nodal coordinate formulation // Nonlinear Dynamics, 2006, Volume 45 (1-2), pp. 109-130.
12. **Shabana A.A.** Computational continuum mechanics. Cambridge University Press, 2008, 349 pages.
13. **Wriggers P.** Nonlinear finite element methods. Springer-Verlag Berlin Heidelberg, 2008, 566 pages.
14. **Krenk S.** Non-linear modelling and analysis of solids and structures. Cambridge University Press, 2009, 361 pages.
15. **Ibrahimbegovic A.** Nonlinear Solid Mechanics. Springer Science+Business Media B.V, 2009, 585 pages.

16. **Bigoni D.** Nonlinear solid mechanics: bifurcation theory and material instability. Cambridge University Press, 2012, 550 pages.
17. **Coskun S., Öztürk B.** Elastic Stability Analysis of Euler Columns Using Analytical Approximate Techniques Advances in Computational Stability Analysis ed Dr. Safa Bozkurt Coşkun ISBN: 978-953-51-0673-9, InTech, DOI: 10.5772/45940
18. **Багмутов В.П., Белов А.А., Столярчук А.С.** Элементы расчетов на устойчивость: учеб. пособие. Волгоград: ИУНЛ ВолгГТУ, 2010. – 56с.
19. **Лалин В.В.** Различные формы уравнений нелинейной динамики упругих стержней // Труды СПбГПУ. 2004, №489, с. 121-128.
20. **Лалин В.В., Розин Л.А., Кушова Д.А.** Вариационная постановка плоской задачи геометрически нелинейного деформирования и устойчивости упругих стержней // Инженерно-строительный журнал, 2013, № 1 (36), с. 87-96.
21. **Лалин В.В., Зданчук Е.В., Кушова Д.А., Розин Л.А.** Вариационные постановки нелинейных задач с независимыми вращательными степенями свободы // Инженерно –строительный журнал, 2015, № 4, с. 54-80.
22. **Лалин В.В., Кушова Д.А.** Геометрически нелинейное деформирование и устойчивость плоских упругих стержней с учетом жесткостей на растяжение-сжатие, сдвиг и изгиб // International Journal for Computational Civil and Structural Engineering, 2013, № 9, с. 178-185.
23. **Лалин В.В., Кушова Д.А.** Решение задачи устойчивости сжатого стержня динамическим методом с учетом жесткостей на сдвиг и растяжение // Строительная механика и расчет сооружений, 2014, № 5 (256), с. 49-54.
24. **Перельмутер А.В., Сливкер В.И.** Устойчивость равновесия конструкций и родственные проблемы. Том1. М.: Издательство СКАД СОФТ, 2010. – 704 с.

Daria A. Kuznetsova, Ph.D.; Associate Professor of Department of Geoinformation Technologies of Polytechnic Institute of Far Eastern Federal University; 10 Ajax Bay, Russky Island, Vladivostok 690922, Russia; e-mail: kuznetcova.dal@dvfu.ru. ORCID: 0000-0002-6551-9271; eLibrary.ru SPIN-код: 1399-3200

Vladimir V. Lalin, Professor, Dr.Sc.; Professor of Higher School of Industrial, Civil and Road Construction, Institute of Civil Engineering, Peter the Great St. Petersburg Polytechnic University, Polytechnicheskaya, 29, St. Petersburg 195251, Russia; e-mail: vllalin@yandex.ru. ORCID: 0000-0003-3850-424X

Nikolay M. Malkov, Ph.D. Associate Professor; Associate Professor of Department of Geoinformation Technologies of Polytechnic Institute of Far Eastern Federal University; 10 Ajax Bay, Russky Island, Vladivostok 690922, Russia;

Кузнецова Дарья Александровна, кандидат технических наук; доцент Департамента геоинформационных технологий Политехнического института Дальневосточного Федерального Университета; бухта Аякс, 10, остров Русский, г. Владивосток, 690922, Россия; e-mail: kuznetcova.dal@dvfu.ru. ORCID: 0000-0002-6551-9271; eLibrary.ru SPIN-код: 1399-3200

Лалин Владимир Владимирович, профессор, доктор технических наук, заведующий кафедрой «Строительная механика и строительные конструкции» ФГБОУ ВПО Санкт-Петербургского политехнического университета, 195251, Россия, г. Санкт-Петербург, Политехническая ул., 29. e-mail: vllalin@yandex.ru. ORCID: 0000-0003-3850-424X

Мальков Николай Михайлович, кандидат технических наук, доцент; доцент Департамента геоинформационных технологий Политехнического института Дальневосточного Федерального Университета; бухта Аякс, 10, остров Русский, г. Владивосток, 690922, Россия;

International Journal for Computational Civil and Structural Engineering, 18(4) 71–81 (2022)

DOI:10.22337/2587-9618-2022-18-4-71-81

FORMATION OF COMPUTATIONAL SCHEMES OF ADDITIONAL TARGETED CONSTRAINTS THAT REGULATE THE FREQUENCY SPECTRUM OF NATURAL OSCILLATIONS OF ELASTIC SYSTEMS WITH A FINITE NUMBER OF DEGREES OF MASS FREEDOM, THE DIRECTIONS OF MOVEMENT OF WHICH ARE PARALLEL, BUT DO NOT LIE IN THE SAME PLANE PART 3: THE SECOND SAMPLE OF ANALYSIS AND CONCLUSION

Leonid S. Lyakhovich [1], ***Pavel A. Akimov*** [2], ***Nikita V. Mescheulov*** [1]

[1] Tomsk State University of Architecture and Civil Engineering, Tomsk, RUSSIA
[2] National Research Moscow State University of Civil Engineering, Moscow, RUSSIA

Abstract: For some elastic systems with a finite number of degrees of freedom of masses, in which the directions of mass movement are parallel and lie in the same plane (for example, rods), special methods have been developed for creating additional constraints, the introduction of each of which purposefully increases the value of only one natural frequency and does not change any from the natural modes. The method of forming a matrix of additional stiffness coefficients that characterize such targeted constraint in this problem can also be applied when solving a similar problem for elastic systems with a finite number of degrees of mass freedom, in which the directions of mass movement are parallel, but do not lie in the same plane (for example, plates). At the same time, for such systems, only the requirements for the design schemes of additional targeted constraints are formulated, and not the methods for their creation. The distinctive paper is devoted to solution of corresponding sample of plate analysis with the use of approach that allows researcher to create computational schemes for additional targeted constraints for such systems.

Keywords: natural frequency, natural modes, generalized additional targeted constraint, sample of analysis

ФОРМИРОВАНИЕ РАСЧЕТНЫХ СХЕМ ДОПОЛНИТЕЛЬНЫХ СВЯЗЕЙ, ПРИЦЕЛЬНО РЕГУЛИРУЮЩИХ СПЕКТР ЧАСТОТ СОБСТВЕННЫХ КОЛЕБАНИЙ УПРУГИХ СИСТЕМ С КОНЕЧНЫМ ЧИСЛОМ СТЕПЕНЕЙ СВОБОДЫ МАСС, У КОТОРЫХ НАПРАВЛЕНИЯ ДВИЖЕНИЯ ПАРАЛЛЕЛЬНЫ, НО НЕ ЛЕЖАТ В ОДНОЙ ПЛОСКОСТИ ЧАСТЬ 3: ВТОРОЙ ТЕСТОВЫЙ ПРИМЕР И ЗАКЛЮЧЕНИЕ

Л.С. Ляхович [1], ***П.А. Акимов*** [2], ***Н.В. Мещеулов*** [1]

[1] Томский государственный архитектурно-строительный университет, г. Томск, РОССИЯ
[2] Национальный исследовательский Московский государственный строительный университет, г. Москва, РОССИЯ

Аннотация: Для некоторых упругих систем с конечным числом степеней свободы масс, у которых направления движения масс параллельны и лежат в одной плоскости, (например, стержни) разработаны методы создания дополнительных связей, введение каждой из которых прицельно увеличивает значение только

одной собственной частоты и не изменяет ни одну из форм собственных колебаний. Метод формирования матрицы дополнительных коэффициентов жесткости, характеризующих в этой задаче такую прицельную связь, может быть применен и при решении аналогичной задачи для упругих систем с конечным числом степеней свободы масс, у которых направления движения масс параллельны, но не лежат в одной плоскости (например, пластины). Вместе с тем для таких систем сформулированы лишь требования к расчетным схемам дополнительных прицельных связей, а не методы их создания. В данной статье рассматривается пример применения для пластин разработанного подхода, позволяющего создавать расчётные схемы дополнительных прицельных связей и для таких систем.

Ключевые слова: частота собственных колебаний, форма собственных колебаний, обобщенная прицельная дополнительная связь, пример расчета

THE SECOND SAMPLE OF ANALYSIS

Let us consider a hinged rectangular plate [4, 10-14, 19, 20] 6 *m* by 6 *m* in size, carrying concentrated masses (Fig. 1*a* [4])

$$m[1] = 1000\,kg,\ \ m[2] = 1100\,kg,$$
$$m[3] = 1150\,kg,\ \ m[4] = 1200\,kg\,.$$

The thickness of the plate is 0.12 *m*. The modulus of elasticity of the plate material

$$E = 24 \cdot 10^9\ N/m^2 = 24 \cdot 10^9\ Pa\,.$$

Poisson's ratio $\nu_0 = 0.2$.

Assume that it is required to increase the value of the fourth frequency of natural oscillations up to 250 s^{-1} (or up to 250 *Hz*, respectively). To do this, in accordance with formulas (7), (8), (9) given in [4], we form a matrix of additional stiffness coefficients (4) (see [4]). All the data necessary to use dependencies (7), (8), (9) from [4] are given in Table 1. After forming the matrix of additional stiffness factors, taking into account their influence, we determine from equation (10) given in [4], the modified spectrum eigenfrequencies and their corresponding vibration modes [1-6, 13]. The modified spectrum of natural frequencies and their corresponding forms are shown in Table 2.

It can be seen from the Table 2 that taking into account the additional stiffness factors did not change any of the modes of natural oscillations of the plate, but only increased the value of one of the frequencies from 205.4514 s^{-1} to the specified value of 250 s^{-1}.

The initial variant of the computational scheme of the targeted constraint is shown in Figure 1*a* and Figure 1*b*.

For the base we will take the vertical member of the first node. Let's compute the forces

$$R_0[i] = m[i]v[i,4],\ \ i = 1,..,4$$

were $m[i]$ are given values; $v[i,4]$ are presented at the fourth columns of Table 1 and Table 2.

The forces are shown in Table 3.

It is also necessary to set the force in one of the vertical members. Let's accept

$$N_{st}[1] = R_0[1] = 589.2890kg$$

Let's perform the formation of design schemes of sighting for different values of the lengths of the base vertical member $l_{st0}[1]$. Table 4 contains fifteen variants of lengths of the base vertical member $l_{st0}[1]$.

The development (formation) of computational schemes of targeted constraint was done without taking into account restrictions on the length of the vertical members. Consideration of restrictions will be considered as well.

In each variant, after the development of the computational scheme, the areas of transverse sections of the rods of the targeted constraint were computed. As in the first sample […], when minimizing the volume of the targeted constraint material (formula (16)_from […]), the case is considered when, according to the design conditions, we have $\alpha[i] = 2$ and $\beta[i] = 1$. Let's consider all the rods of a solid circular section. The modulus of elasticity of the material of the rods

is equal to $E = 2.06 \cdot 10^5 MPa$. The cross-sectional areas of the rods and the volume of the bonding material were determined by dependences (13)-(16) from [4].

Table 1. Values of eigenfrequencies (natural vibration frequencies) of the plate and coordinates of their corresponding eigenmodes (natural modes) (the second example).

ω	61.6965	141.4295	146.2905	205.4514
1	0.4908	0.0001	0.7080	-0.5893
2	0.4965	-0.7093	0.0895	0.5154
3	0.5058	-0.0676	-0.7003	-0.4432
4	0.5068	0.7016	0.0181	0.4367

Table 2. Modified frequency spectrum of natural vibrations of the plate and coordinates, corresponding to them natural forms (the second example).

ω	61.6965	141.4295	146.2905	250.00
1	0.4908	0.0001	0.7080	-0.5893
2	0.4965	-0.7093	0.0895	0.5154
3	0.5058	-0.0676	-0.7003	-0.4432
4	0.5068	0.7016	0.0181	0.4367

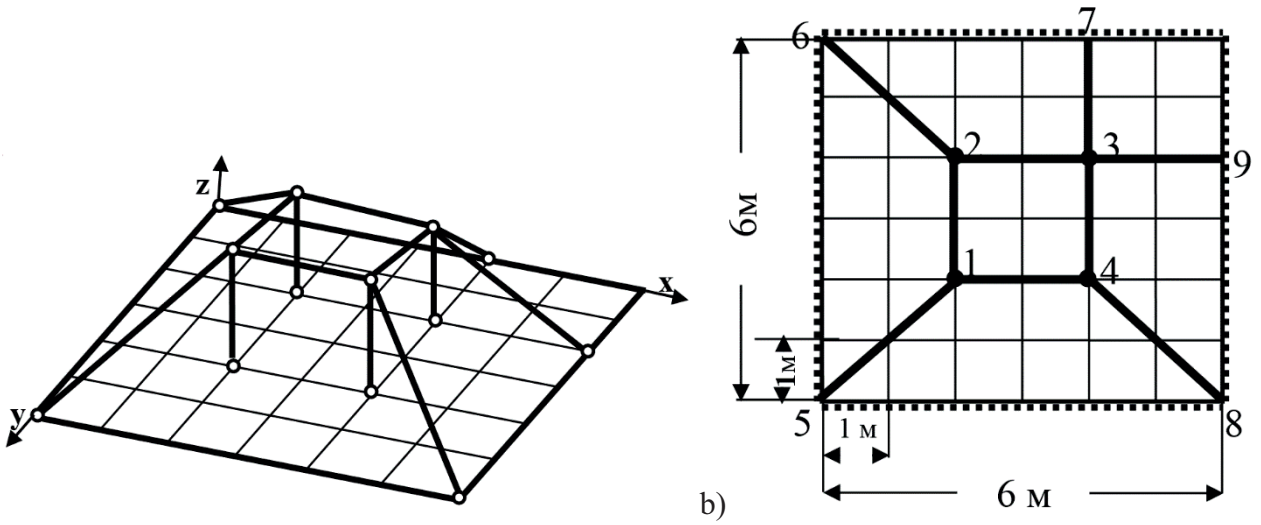

Figure 1. The second sample: variant of the computational targeted constraint: a) three-dimensional visualization; b) top view.

Table 3. To the analysis of the targeted constraint in the computational scheme (the first example).

i	1	2	3	4
$m[i]$	1000	1100	1150	1200
$v[i,1]$	-0.5893	0.5154	-0.4432	0.4367
$R_0[i]$	-589.2890	566.8873	-509.7103	524.0320

For each version of the length of the base vertical member, Table 8 shows the lengths of the remaining vertical members and the amount of targeted constraint material V_{VS}.

In all considered variants, the lengths of the first and third vertical members are positive, and the lengths of second and fourth vertical members are negative.

Table 8 shows that the minimum amount of constraints material is achieved at $l_{st0}[1] = 1.17m$ (highlighted line number 11 from Table 4). The areas and diameters of the cross-sections of the targeted constraint vertical members are equal the following:

$$F_{st} = 0.0004865\,м^2,\ D_{st} = 0.02489\,м,$$

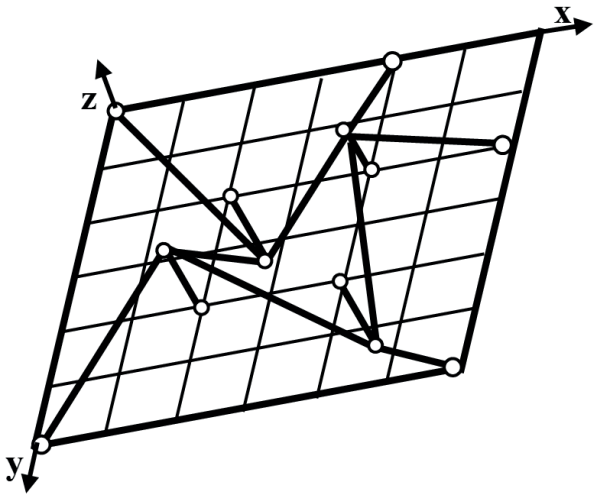

Figure 2. The second sample: general view of this targeted constraint.

Table 4. The parameters of targeted constraint (the first sample).

No.	$l_{st0}[1]$	$l_{st}[2]$	$l_{st}[3]$	$l_{st}[4]$	V_{SV}
1	1	0.9737	0.7968	1.0162	0.02495
2	1.5	1.4606	1.1952	1.5242	0.01567
3	2.15	2.0934	1.7131	2.1848	0.01268
4	2.45	2.3855	1.9521	2.4896	0.01247
5	2.6356	2.5662	2.1000	2.6782	0.01254
6	3.0	2.9211	2.3904	3.0485	0.01300
7	3.25	3.1645	2.5896	3.3025	0.01351

$$F_p = 0.0002432\,м^2,\ D_p = 0.01760\,м.$$

The general view of this targeted constraint is shown in Figure 2.

As we have already noted, structurally, such a computational scheme is almost unrealizable. In these cases, the targeted constraint should be shifted in the direction of movement of the masses in the positive or negative direction of the axis Z by the value at which the values of all lengths of the main vertical members will be of the same sign. When performing a shift, the relationship between the forces in the rods is preserved.

When the constraint is shifted in the positive direction of axis Z by the value of $Z_V = (l_{st}[k])_{\min} + l_{\min}$ the length of all vertical members will become "positive". In this case, the length of the largest vertical member will be $(l_{st}[i])_{\max} + (l_{st}[k])_{\min} + l_{\min}$, and the length of the smallest vertical member will be $l_{\min}$.

When the constraint is shifted in the negative direction of axis Z by the value of $Z_N = (l_{st}[i])_{\max} + l_{\min}$ the length of all vertical members will become "negative". In this case, the largest absolute value of length of all vertical member will be $(l_{st}[i])_{\max} + (l_{st}[k])_{\min} + l_{\min}$, and the smallest absolute value of length of all vertical member will be $l_{\min}$.

When forming restrictions on the lengths of the vertical members and, accordingly, the area of admissible values of the length of the vertical member $l_{st0}[1]$, which is variable when

minimizing the volume of the material of the targeted constraint, it is necessary to determine the value

$$\chi_3 = \frac{l_{st0}[[g]}{(l_{st}[i])_{\max} + (l_{st}[k])_{\min}}.$$

Table 5. Results representing the computational schemes of targeted constraints taking into account shifts in a one-dimensional search for the minimum volume of targeted constraints material (the second sample)

$l_{st0}[1]$	Z_V					
	$l_{st}[1]$	$l_{st}[2]$	$l_{st}[3]$	$l_{st}[4]$	V_{SV}	Z_V
1.07	2.352	0.100	1.901	0.232	0.008941	1.282
1.08	2.373	0.100	1.918	0.233	0.008938	1.293
1.09	2.395	0.100	1.935	0.235	0.008920	1.305
1.10	2.416	0.100	1.952	0.236	0.008910	1.316
1.11	2.437	0.100	1.969	0.237	0.008902	1.327
1.12	2.458	0.100	1.9857	0.239	0.0088961	1.338
1.13	2.479	0.100	2.002	0.240	0.008891	1.349
1.14	2.500	0.100	2.019	0.241	0.008888	1.360
1.15	2.521	0.100	2.036	0.242	0.008887	1.371
1.16	2.542	0.100	2.053	0.243	0.008887	1.382
1.17	2.563	0.100	2.070	0.244	0.008888	1.393
1.18	2.584	0.100	2.086	0.246	0.008890	1.404
1.19	2.605	0.100	2.103	0.2467	0.008895	1.415
1.2	2.626	0.100	2.120	0.248	0.008900	1.426
1.25	2.731	0.100	2.204	0.254	0.008946	1.481

$l_{st0}[1]$	Z_N					
	$l_{st}[1]$	$l_{st}[2]$	$l_{st}[3]$	$l_{st}[4]$	V_{SV}	Z_N
1.07	-0.100	-2.352	-0.551	-2.221	0.009497	-1.17
1.08	-0.100	-2.373	-0.555	-2.240	0.009488	-1.18
1.09	-0.100	-2.395	-0.560	-2.260	0.009481	-1.19
1.10	-0.100	-2.416	-0.564	-2.280	0.009476	-1.2
1.11	-0.100	-2.437	-0.568	-2.300	0.009473	-1.21
1.12	-0.100	-2.458	-0.572	-2.320	0.009471	-1.22
1.13	-0.100	-2.479	-0.576	-2.339	0.009471	-1.23
1.14	-0.100	-2.500	-0.581	-2.359	0.009473	-1.24
1.15	-0.100	-2.521	-0.585	-2.379	0.009476	-1.25
1.16	-0.100	-2.542	-0.589	-2.399	0.009481	-1.26
1.17	-0.100	-2.563	-0.593	-2.419	0.009487	-1.27
1.18	-0.100	-2.584	-0.598	-2.439	0.009495	-1.28
1.19	-0.100	-2605	-0.602	-2.458	0.009504	-1.29
1.2	-0.100	-2.626	-0.606	-2.478	0.009514	-1.3
1.25	-0.100	-2.731	-0.627	-2.577	0.009587	-1.35

It will be the same for all variants, presented in Table 4. If we determine χ_3 from the data of row number 11 of Table 4, then we get

$$\chi_3 = 1.7/(1.17+1.2929) = 0.475 .$$

Let's consider two options for forming restrictions on the lengths of the vertical members and, accordingly, the range of acceptable values for the length of the base vertical member $l_{st0}[1]$, which is variable while minimizing the volume of targeted constraint material:

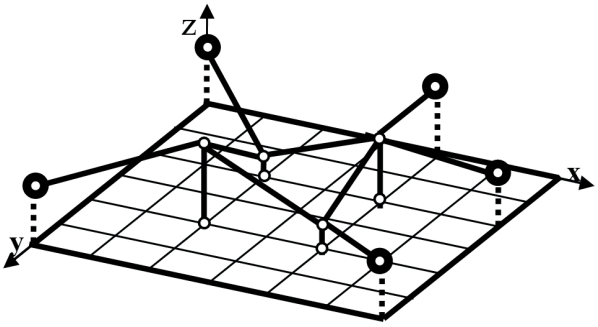

Figure 3. The second sample: general view of this targeted constraint.

1) $l_{\max} = 2.6\,м$, $l_{\min} = 0.1\,м$;
$(l_{\max} - l_{\min}) \cdot \chi_3 \geq l_{st0}[g]$; $1.1875 \geq l_{st0}[1]$;
2) $l_{\max} = 2.4\,м$, $l_{\min} = 0.1\,м$: $1.0925 \geq l_{st0}[1]$.

Let's shift each variant of the computational scheme of targeted constraint from Table 4 both in the positive and in the negative direction of the axis Z. The results representing the computational schemes of targeted constraints, taking into account shifts in a one-dimensional search for the minimum volume of targeted constraint material, are shown in Table 5.

The values of the shift values of the computational schemes Z_V and Z_N were determined according to the data in Table 4 and taking into account the selected option of restrictions.

In the first variant of the restrictions on the length of base vertical member, when $l_{st0}[1] \leq 1.1875\,м$, and the targeted constraint is shifted in the positive direction of the axis Z, the minimum volume of targeted constraint material $V_{SV} = 0.008887\,м^3$ is reached at $l_{st}[g] = 1.16\,м$.

The areas and cross-sectional diameters of the rods of targeted constraint are equal to

$$F_{st} = 0.0005078\,м^2,\ D_{st} = 0.02543\,м,$$
$$F_p = 0.0002539\,м^2,\ D_p = 0.01798\,м .$$

The lengths of the vertical members are given in table 9 at $l_{st}[g] = 1.16\,м$. They are all positive. The optimum is achieved when the restrictions on the length of the base vertical member in the form of inequality ($l_{st0}[1] = 1.16м < 1.1875\,м$) are met. Thus, this extremum is global. A general view of this targeted constraint is shown in Figure 3.

Also, in the first version of the restrictions on the length of base vertical member, constraint is shifted in the negative direction of the axis Z. In this case, the minimum volume of material $V_{SV} = 0.009471\,м^3$ is achieved at $l_{st}[g] = 1.12\,м$, and the areas and diameters of the cross-sections of the rods of targeted constraint are equal to

$$F_{st} = 0.0005298\,м^2,\ D_{st} = 0.02597\,м,$$
$$F_p = 0.0002649\,м^2,\ D_p = 0.01837\,м .$$

The lengths of the vertical members are given in Table 5 at $l_{st}[g] = 1.12\,м$. The lengths of all vertical members are negative in this case. Since the optimum is reached when the restrictions on the length of the base vertical member in the form of inequality $l_{st0}[1] = 1.12м < 1.1875\,м$ are met, this extremum is also global. The general view of this targeted constraint is shown in Figure 4. This version of the computational scheme can also be

implemented when the direction of the axis Z is reversed. It is obvious that this action does not change the targeted properties of the constraint. A general view of the targeted constraint for such a case is shown in Figure 5.

In the second variant of the restrictions on the length of base vertical member with $l_{st0}[1] \le 1.0925\,м$ and shift of the targeted constraint in the positive direction of the axis Z or in the negative, the minimum volume of targeted constraint material is reached at the border of the area of admissible values of the length of the base vertical member at $l_{st0}[1] = 1.0925\,м$ (Table 5).

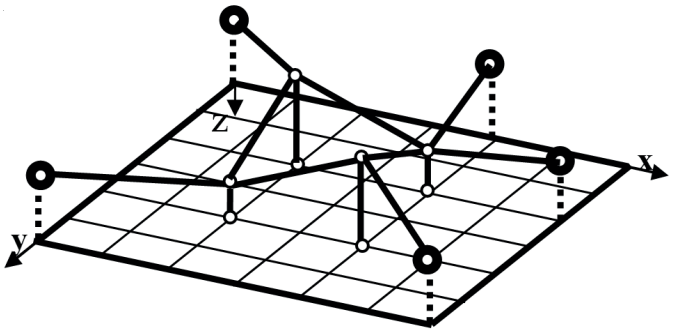

Figure 4. The second sample: general view of this targeted constraint.

When the targeted constraint is shifted in the positive direction of the axis Z, the minimum is $V_{SV} = 0.008920\,м^3$, and the areas and diameters of the sections of the rods of targeted constraint are equal to

$$F_{st} = 0.0005250\,м^2,\ D_{st} = 0.02585\,м,$$
$$F_p = 0.0002625\,м^2,\ D_p = 0.01828\,м.$$

When the targeted constraint is shifted in the negative direction of the axis Z, the minimum is $V_{SV} = 0.009481\,м^3$, and the areas and diameters of the sections of the rods of targeted constraint are equal to

$$F_{st} = 0.0005375\,м^2,\ D_{st} = 0.02616\,м,$$
$$F_p = 0.0002688\,м^2,\ D_p = 0.01850\,м.$$

So, in the second variant of restrictions on the lengths of the vertical members, the minimums of the volume of the targeted constraint material turned out to be boundary. Therefore, their values are somewhat higher than the corresponding values for the first variant of restrictions, in which the minima V_{SV} were implemented as global ones.

CONCLUSION

The first sample, considered in […] confirms the possibility of development of computational scheme of targeted constraint for systems with a finite number of degrees of freedom of masses, in which the directions of mass movement are parallel, but do not lie in the same plane. It also illustrates the possibility of minimizing the volume of material when creating targeted constraint. At the same time, the limitations of the lengths of the main vertical members, which determine the geometry of the targeted constraint, were taken into account. In the first sample the special case is considered – all the lengths of the main vertical members turned out to be positive within development of computational scheme of the targeted constraint.

The second sample illustrates an approach that makes it possible to develop targeted constraints taking into account the restrictions on the lengths of the vertical members and modify the computational schemes for cases where the values of the lengths of some main vertical members turn out to be positive, while others are negative.

So, the distinctive series of papers proposes an approach that allows researcher to create (develop) computational schemes of targeted

constraints for elastic systems with a finite number of degrees of freedom of masses, in which the directions of mass movement are parallel, but do not lie in the same plane. Some special properties of such targeted constraints are revealed. Within development of computational scheme of the targeted constraint, the material consumption for its creation is minimized, and some design limitations are taken into account. Particular attention is paid to the modification of targeted constraints, when, during their development, it becomes necessary to shift the computational scheme.

REFERENCES

1. **Akimov P.A, Lyahovich L.S.** Pricel'noe regulirovanie spektra chastot sobstvennyh kolebanij uprugih plastin s konechnym chislom stepenej svobody mass putem vvedenija dopolnitel'nyh obobshhennyh svjazej i obobshhennyh kinematicheskih ustrojstv [Precision control for eigen-frequency of elastic plates with finite number of mass degrees of freedom by using additional generalized connections and kinematic devices]. // Vestnik Tomskogo gosudarstvennogo arkhitekturno-stroitel'nogo universiteta. Journal of Construction and Architecture, 2021, Vol. 23, No. 4, pp. 57-67 (In Russian).
2. **Giterman D.M., Lyahovich L.S., Nudel'man Ja.L.** Algoritm sozdanija rezonansno-bezopasnyh zon pri pomoshhi nalozhenija dopolnitel'nyh svjazej [Algorithm for creating resonantly safe zones by imposing additional bonds]. // Dinamika i prochnost' mashin, Vypusk 39. – Kharkov, Vishha shkola, 1984, pp. 63-69 (In Russian).
3. **Lyahovich L.S.** Osobye svojstva optimal'nyh sistem i osnovnye napravlenija ih realizacii v metodah rascheta sooruzhenij [Special properties of optimal systems and the main directions of their implementation in the methods of structural analysis]. Tomsk, TGASU, 2009. – 372 pages (In Russian).
4. **Lyakhovich L.S., Akimov P.A.** Formation of Computational Schemes of Additional Targeted Constraints That Regulate The Frequency Spectrum of Natural Oscillations of Elastic Systems With a Finite Number of Degrees of Mass Freedom, the Directions of Movement of Which are Parallel, But Do Not Lie in the Same Plane. Part 1: Theoretical Foundations. // International Journal for Computational Civil and Structural Engineering, 2022, Volume 18, Issue 2, pp. 183-193.
5. **Lyakhovich L.S., Akimov P.A.** Formation of Computational Schemes of Additional Targeted Constraints That Regulate The Frequency Spectrum of Natural Oscillations of Elastic Systems With a Finite Number of Degrees of Mass Freedom, the Directions of Movement of Which are Parallel, But Do Not Lie in the Same Plane. Part 2: The First Sample of Analysis. // International Journal for Computational Civil and Structural Engineering, 2022, Volume 18, Issue 3, pp. 137-146.
6. **Lyahovich L.S., Maletkin O.Ju.** O pricel'nom regulirovanii sobstvennyh chastot uprugih system [On targeted control of natural frequencies of elastic systems]. // Izvestija vuzov. Stroitel'stvo i arhitektura, 1990, No. 1, pp. 113-117 (In Russian).
7. **Nudel'man Ja.L., Lyahovich L.S., Giterman D.M.** O naibolee podatlivyh svjazjah naibol'shej zhestkosti [On the most pliable bonds of the greatest rigidity]. // Voprosy prikladnoj Mehaniki i matematiki. Tomsk, TGU, 1981, pp. 113-126 (In Russian).
8. **An H.H., Jung M.H., Kim N.H., Lee E.B., Shin K.B.** Study on the Automated Size Optimization and Structural Analysis Program for Composite Lattice Structures. // Transactions of the Korean Society of Mechanical Engineers, 2022, Volume 66, Issue 3, pp. 77-83.
9. **Dmitrieva T., Ulambayar Kh.** Algorithm for Building Structures Optimization Based on Lagrangian Functions. // Magazine of

Civil Engineering, 2022, Volume 109, Issue 1, pp. 10910.
10. **Hinz M., Magoules F., Rozanova-Pierrat A., Rynkovskaya M., Teplyaev A.** On the Existence of Optimal Shapes in Architecture. // Applied Mathematical Modelling, 2021, Volume 94, pp. 676-687.
11. **Koreneva E.B.** Analysis of Combined Plates With Allowance for Contact With Elastic Foundation. // International Journal for Computational Civil and Structural Engineering, 2019, Volume 15, Issue 4, pp. 83-87.
12. **Koreneva E.B.** Unsymmetric Oscillations of Anisotropic Plate Having an Additional Mass. // International Journal for Computational Civil and Structural Engineering, 2021, Volume 17, Issue 1, pp. 48-54.
13. **Koreneva E.B., Grosman V.R.** Equation Decomposition Method for Solving of Problems of Statics, Vibrations and Stability of Thin-Walled Constructions. // International Journal for Computational Civil and Structural Engineering, 2020, Volume 16, Issue 2, pp. 63-70.
14. **Lyakhovich L.S., Akimov P.A.** Aimed control of the frequency spectrum of eigenvibrations of elastic plates with a finite number of degrees of freedom of masses by superimposing additional constraints. // International Journal for Computational Civil and Structural Engineering, 2021, Volume 17, Issue 2, pp. 76-82.
15. **Manuylov G.A., Kosytsyn S.B., Grudtsyna I.E.** Influence of Buckling Forms Interaction of Stiffened Plate Bearing Capacity. // International Journal for Computational Civil and Structural Engineering, 2020, Volume 16, Issue 2, pp. 83-93.
16. **Pan C., Han Y., Lu J.** Design and Optimization of Lattice Structures: A Review. // Applied Sciences, 2020, Volume 10, Issue 18, pp. 1-36.
17. **Peleshko I.D., Yurchenko V.V.** Parametric Optimization of Metal Rod Structures Using the Modified Gradient Projection Method. // Internal Applied Mechanics, 2021, Volume 57, Issue 4, pp. 440-454.
18. **Potapov A.N.** The Elastoplastic Calculation of Frames Using the Displacement Method. // International Journal for Computational Civil and Structural Engineering, 2019, Volume 15, Issue 3, pp. 120-130.
19. **Senatore G., Reksowardojo A.P.** Force and Shape Control Strategies for Minimum Energy Adaptive Structures. // Frontiers in Build Environment, 2020, Volume 6, p. 105.
20. **Shitikova M.V., Kandu V.V.** Analysis of Forced Vibrations of Nonlinear Plates in a Viscoelastic Medium Under the Conditions of the Different Combinational Internal Resonances. // International Journal for Computational Civil and Structural Engineering, 2019, Volume 15, Issue 3, pp. 131-148.
21. **Shitikova M.V., Krusser A.I.** Force Driven Vibrations of Nonlinear Plates on a Viscoelastic Winkler Foundation Under the Harmonic Moving Load. // International Journal for Computational Civil and Structural Engineering, 2021, Volume 17, Issue 4, pp. 161-180.
22. **Xu Y., Chen H., Wang X.** Buckling Analysis and Configuration Optimum Design of Grid-Stiffened Composite Panels. // AIAA Journal, 2020, Volume 58, Issue 8, pp. 3653-3664.
23. **Yankovskaya Y., Merenkov A.** Problems of Optimization of Design Solutions of Residential Structures and Their Elements // Lecture Notes in Civil Engineering, 2022, Volume 227, pp. 339-350.
24. **Yurchenko V.V., Peleshko I.D.** Searching for Optimal Prestressing of Steel Bar Structures Based on Sensitivity Analysis. // Archives of Civil Engineering, 2020, Volume 66, Issue 3, pp. 526-540.

СПИСОК ЛИТЕРАТУРЫ

1. **Акимов П.А., Ляхович Л.С.** Прицельное регулирование спектра частот собственных колебаний упругих пластин с конечным числом степеней свободы масс путем введения дополнительных обобщенных

связей и обобщенных кинематических устройств. // Вестник Томского государственного архитектурно-строительного университета, 2021, том 23, № 4, с. 57-67.
2. **Гитерман Д.М., Ляхович Л.С., Нудельман Я.Л.** Алгоритм создания резонансно-безопасных зон при помощи наложения дополнительных связей. // Динамика и прочность машин, Выпуск 39. - Харьков: "Вища школа", 1984, с. 63-69.
3. **Ляхович Л.С.** Особые свойства оптимальных систем и основные направления их реализации в методах расчета сооружений. Монография. - Томск: Издательство ТГАСУ, 2009. - 372 с.
4. **Lyakhovich L.S., Akimov P.A.** Formation of Computational Schemes of Additional Targeted ConstraintsThat Regulate The Frequency Spectrum of Natural Oscillations of Elastic Systems With a Finite Number of Degrees of Mass Freedom, the Directions of Movement of Which are Parallel, But Do Not Lie in the Same Plane. Part 1: Theoretical Foundations. // International Journal for Computational Civil and Structural Engineering, 2022, Volume 18, Issue 2, pp. 183-193.
5. **Lyakhovich L.S., Akimov P.A.** Formation of Computational Schemes of Additional Targeted ConstraintsThat Regulate The Frequency Spectrum of Natural Oscillations of Elastic Systems With a Finite Number of Degrees of Mass Freedom, the Directions of Movement of Which are Parallel, But Do Not Lie in the Same Plane. Part 2: The First Sample of Analysis. // International Journal for Computational Civil and Structural Engineering, 2022, Volume 18, Issue 3, pp. 137-146.
6. **Ляхович Л.С., Малеткин О.Ю.** О прицельном регулировании собственных частот упругих систем. // Известия вузов. Строительство и архитектура, 1990, № 1, с. 113-117.
7. **Нудельман Я.Л., Ляхович Л.С., Гитерман Д.М.** О наиболее податливых связях наибольшей жесткости. // Вопросы прикладной Механики и математики. - Томск: Издательство ТГУ, 1981, с. 113-126.
8. **An H.H., Jung M.H., Kim N.H., Lee E.B., Shin K.B.** Study on the Automated Size Optimization and Structural Analysis Program for Composite Lattice Structures. // Transactions of the Korean Society of Mechanical Engineers, 2022, Volume 66, Issue 3, pp. 77-83.
9. **Dmitrieva T., Ulambayar Kh.** Algorithm for Building Structures Optimization Based on Lagrangian Functions. // Magazine of Civil Engineering, 2022, Volume 109, Issue 1, pp. 10910.
10. **Hinz M., Magoules F., Rozanova-Pierrat A., Rynkovskaya M., Teplyaev A.** On the Existence of Optimal Shapes in Architecture. // Applied Mathematical Modelling, 2021, Volume 94, pp. 676-687.
11. **Koreneva E.B.** Analysis of Combined Plates With Allowance for Contact With Elastic Foundation. // International Journal for Computational Civil and Structural Engineering, 2019, Volume 15, Issue 4, pp. 83-87.
12. **Koreneva E.B.** Unsymmetric Oscillations of Anisotropic Plate Having an Additional Mass. // International Journal for Computational Civil and Structural Engineering, 2021, Volume 17, Issue 1, pp. 48-54.
13. **Koreneva E.B., Grosman V.R.** Equation Decomposition Method for Solving of Problems of Statics, Vibrations and Stability of Thin-Walled Constructions. // International Journal for Computational Civil and Structural Engineering, 2020, Volume 16, Issue 2, pp. 63-70.
14. **Lyakhovich L.S., Akimov P.A.** Aimed control of the frequency spectrum of eigenvibrations of elastic plates with a finite number of degrees of freedom of masses by superimposing additional constraints. // International Journal for Computational Civil and Structural Engineering, 2021, Volume 17, Issue 2, pp. 76-82.
15. **Manuylov G.A., Kosytsyn S.B., Grudtsyna I.E.** Influence of Buckling Forms Interaction

of Stiffened Plate Bearing Capacity. // International Journal for Computational Civil and Structural Engineering, 2020, Volume 16, Issue 2, pp. 83-93.
16. **Pan C., Han Y., Lu J.** Design and Optimization of Lattice Structures: A Review. // Applied Sciences, 2020, Volume 10, Issue 18, pp. 1-36.
17. **Peleshko I.D., Yurchenko V.V.** Parametric Optimization of Metal Rod Structures Using the Modified Gradient Projection Method. // Internal Applied Mechanics, 2021, Volume 57, Issue 4, pp. 440-454.
18. **Potapov A.N.** The Elastoplastic Calculation of Frames Using the Displacement Method. // International Journal for Computational Civil and Structural Engineering, 2019, Volume 15, Issue 3, pp. 120-130.
19. **Senatore G., Reksowardojo A.P.** Force and Shape Control Strategies for Minimum Energy Adaptive Structures. // Frontiers in Build Environment, 2020, Volume 6, p. 105.
20. **Shitikova M.V., Kandu V.V.** Analysis of Forced Vibrations of Nonlinear Plates in a Viscoelastic Medium Under the Conditions of the Different Combinational Internal Resonances. // International Journal for Computational Civil and Structural Engineering, 2019, Volume 15, Issue 3, pp. 131-148.
21. **Shitikova M.V., Krusser A.I.** Force Driven Vibrations of Nonlinear Plates on a Viscoelastic Winkler Foundation Under the Harmonic Moving Load. // International Journal for Computational Civil and Structural Engineering, 2021, Volume 17, Issue 4, pp. 161-180.
22. **Xu Y., Chen H., Wang X.** Buckling Analysis and Configuration Optimum Design of Grid-Stiffened Composite Panels. // AIAA Journal, 2020, Volume 58, Issue 8, pp. 3653-3664.
23. **Yankovskaya Y., Merenkov A.** Problems of Optimization of Design Solutions of Residential Structures and Their Elements // Lecture Notes in Civil Engineering, 2022, Volume 227, pp. 339-350.
24. **Yurchenko V.V., Peleshko I.D.** Searching for Optimal Prestressing of Steel Bar Structures Based on Sensitivity Analysis. // Archives of Civil Engineering, 2020, Volume 66, Issue 3, pp. 526-540.

Leonid S. Lyakhovich, Full Member of the Russian Academy of Architecture and Construction Sciences, Professor, DSc, Head of Department of Structural Mechanics, Tomsk State University of Architecture and Building; 2, Solyanaya St., 2, Tomsk, 634003, Russia;
E-mail: lls@tsuab.ru

Pavel A. Akimov, Full Member of the Russian Academy of Architecture and Construction Sciences, Professor, Dr.Sc.; Rector of National Research Moscow State University of Civil Engineering; 26, Yaroslavskoe Shosse, Moscow, 129337, Russia; phone +7(495) 651-81-85;
Email: AkimovPA@mgsu.ru, pavel.akimov@gmail.com.

Nikita V. Mescheulov, Ph.D., Director of Scientific & Educational Center of Computer Modelling of Structures and Systems, Tomsk State University of Architecture and Building; 2, Solyanaya St., 2, Tomsk, 634003, Russia;
phone +7(962)788-41-21; E-mail: ckm.tsuab@mail.ru.

Ляхович Леонид Семенович, академик РААСН, профессор, доктор технических наук, профессор кафедры строительной механики, Томский государственный архитектурно-строительный университет; 634003, Россия, г. Томск, Соляная пл. 2;
E-mail: lls@tsuab.ru

Акимов Павел Алексеевич, академик РААСН, профессор, доктор технических наук; ректор Национального исследовательского Московского государственного строительного университета; 129337, г. Москва, Ярославское шоссе, д. 26; тел. +7(495) 651-81-85;
Email: AkimovPA@mgsu.ru, pavel.akimov@gmail.com.

Мещеулов Никита Владимирович, кандидат технических наук, директор Научно-образовательного центра «Компьютерное моделирование строительных конструкций и систем», Томский государственный архитектурно-строительный университет; 634003, Россия, г. Томск, Соляная пл. 2; тел. +7(962)788-41-21;
E-mail: ckm.tsuab@mail.ru.

International Journal for Computational Civil and Structural Engineering, 18(4) 82–90 (2022)

DOI:10.22337/2587-9618-2022-18-4-82-90

INFLUENCE OF SURFACE CRACKS ON THE STABILITY OF CRACKED SOIL SLOPE

Mojtaba Hosseini [1], Peyman Beiranvand [2], Mohammad Mohammadiasl [3], Ashkan Hassanvand [4]

[1] Associate Professor, Department of Civil Engineering, Lorestan University, Khorramabad, IRAN
[2] Lecturer, Department of Civil Engineering, Lorestan University, Khorramabad, IRAN
[3] PhD, Department of Civil Engineering, Khorramabad Branch, Islamic Azad University, IRAN
[4] B.Sc., Department of Mechanical Engineering, Khorramabad Branch, Islamic Azad University, IRAN

Abstract. The slope stability is a major concern to geotechnical engineers. Traditional methods of slope stability analysis have potentially ignored the influence of surface cracks. It is also known that seasonal rainfall and seepage through crack are closely related with slope failure. First, surface cracks provide special flow channels which increase the soil permeability and decrease the soil strength. Second, water-filled cracks apply an additional active force on the slope. Finally, cracks can create a part of the critical failure surface that has no shear strength. The objective of this paper is to investigate the influence of existing cracks on the stability of a cracked soil slope in different state. The effects of crack depth, slope angle and water-filled cracks on the stability of the cracked slope are explored. The analysis was conducted using the computer modelling programs Optum G2 to analysis of slope factor of safety. The results show that with increasing of slope angle the factor of safety decreases and this problem is significant in the slope with water filled cracks. Also, Factor of safety for all of slope angles in Dry and water filled cracks states with increasing the crack depth, decrease significantly.

Keywords: surface cracks, in Dry and water filled cracks, Optum G2, slope factor of safety

ВЛИЯНИЕ ПОВЕРХНОСТНЫХ ТРЕЩИН НА УСТОЙЧИВОСТЬ ГРУНТОВОГО СКЛОНА

М. Хоссейни [1], П. Бейранванд [2], М. Мохаммадиасл [3], А. Хассанванд [4]

[1] Доцент, кафедра гражданского строительства, Лорестанский университет, г. Хоррамабад, ИРАН
[2] Преподаватель кафедры гражданского строительства Лорестанского университета, г. Хоррамабад, ИРАН
[3] Кандидат наук, кафедра гражданского строительства, Хоррамабадский филиал, Исламский университет Азада, ИРАН
[4] Бакалавр наук, факультет машиностроения, Хоррамабадский филиал, Исламский университет Азада, ИРАН

Аннотация. Устойчивость склонов является серьезной проблемой для инженеров-геотехников. Традиционные методы анализа устойчивости склонов, как правило, игнорируют влияние поверхностных трещин. Также известно, что сезонные осадки и просачивание их через трещины может приводить к обрушению склона. Во-первых, поверхностные трещины создают специальные каналы для потоков воды, увеличивают проницаемость грунта и снижают его прочность. Во-вторых, трещины, заполненные водой, оказывают на склон дополнительное активное давление. Наконец, трещины могут создать часть критической поверхности разрушения, которая не способна сопротивляться сдвигу. Целью данной работы являлось исследование влияния существующих трещин на устойчивость грунтового откоса в различном состоянии. Исследовано влияние глубины трещины, угла наклона и наличия трещин, заполненных водой, на устойчивость склона. Анализ проводился с использованием программы компьютерного моделирования Optum G2 для оценки коэффициента запаса устойчивости. Результаты показывают, что с увеличением угла откоса коэффициент запаса устойчивости снижается, и эта проблема актуальна для склонов с трещинами, заполненными водой. Также коэффициент запаса устойчивости для всех углов откоса для сухих и водонасыщенных трещин с увеличением глубины трещины значительно снижается.

Ключевые слова: поверхностные трещины, сухие и заполненные водой трещины, Optum G2, коэффициент запаса устойчивости склона

INTRODUCTION

The fact of landslides and instability of slopes is a major concern in many parts of the world. The failure mechanism of slopes and geological history of a slopes can be very complicated and important for a slope stability analysis. Seasonal rainfall is an essential cause for many slope failures and catastrophic landslides. The primary reason for landslide was loss of matric suction of soil due to rainwater infiltration. It is familiar that rain water infiltration into subsurface soil slopes or through soil cracks will start to saturate the soil layers and eventually reduce the matric suction of soil. The notable reduction of matric suction causes the reduction of soil shear parameters. Factors such as soil texture, intensity and rainfall duration and degree of saturation, soil moisture content, surface cover and slope angle also influence rainfall infiltration [1-2].

The classical and primary way to analyze of slope stability is accessed using two methods; either continuum mechanics, or the limit equilibrium approach. Generally cracks are formed at the tension zones and a series of micro cracks is formed at the upper surface and will cause obvious cracks at tension zones at dry periods after a prolonged wet and dry cycle. The cracks usually supply easy pathways for rainfall infiltration into soil mass and subsurface layers [3]. The water head due to the soil cracks causes the additional force for rain water infiltration. The water content in deeper layers is higher in cracked slopes than uncracked slopes due to rain infiltration. Generally higher matric suction will obtain at dry seasons at unsaturated soil zones and it improves the shear strength of the soil [4].

A new approach is used by Stephen and Colin to specify the direct prediction of the tension cracks on a river bank. This tension cracks are assumed to be formed by two essential group of forces. The first group is formed by shrinkage on soil and is caused by desiccation fact. The second is related with gravitational force where the weight of the soil separates a great block on a soil slope. The tension cracks are founded at upper layer failure surface when the tensile strength (σ_s) in the upper soil layer be more than the tensile stress (σ_τ) of the soil [5]. Cai et al. investigated the vertical cut slope stability with using a number of soil parameters such as the geometry of crack at upper slope surface, curves relating the parameter of strain energy density factor and the non-dimensional variable from slope geometry $N = H / C$ ratio of slope height to distance of crack from edge of slopes. In this research, the curves were developed through numerous parametric studies. They concluded that the failure surface is not circular on a simple straight line. However, failure surfaces are regularly in good and suitable agreement with the results of classical slope stability analysis [6].

Fan et al. studied the effects of rainfall infiltration on fractured slopes. The authors showed that rainwater infiltrates into existing fractures in slopes, and that pore water pressure in soil rises correspondingly [7]. Wang et al. illustrated that cracks in soil slopes decrease stability of slope through three effects: (1) water filled cracks exert an additional and active driving force on the slopes (2) Cracks supply particular flow channels which increase permeability of soil and decrease soil strength and (3) cracks can form part of the critical and serious slip surface that has no special shear strength [8].

GUI and Han showed two Malaysian landslides that occurred after heavy rainfall in 1999. They investigated that the stability of this slopes was significantly affected by the rainfall. They concluded rainfall infiltration into existing fractures reduced the matric suction and shear strength of the slope. This was further worsened when rainfall infiltration increased the mobilized shear stress and self-weight of the slopes [9]. Post analyses of landslides phenomenon in the past by Nurly et al. at Air Laya, Indonesia concluded that existing tension cracks caused slope failure. Rainfall infiltration caused in formation of weak planes which activate to failure of slope [10].

More recently, Zeng et al [11] and Mukhlisin and Khiyon [12] investigated the effect of the

characteristics, such as the angle, depth, location and density of surface cracks, on the pore water pressure and stability of slopes under rainfall infiltration by numerical modeling. They concluded that as the crack depth increases, both the pore water pressure in the crack and the infiltration depth increase at the end of rainfall phenomenon, and the safety factor of the slope remarkably decreases. In terms of crack angle, the former research showed that as the crack angle increases, the infiltration depth decreases. The latter described that when the crack angle is parallel to the sliding surface, the safety factor of the slope is clearly decreased, which is consistent with the result of Zhang et al. [13]. Also, Zeng et al. reported that when the crack density increases, the isolated saturated zones with positive pore water pressures attach with each other in the slope gradually. Mukhlisin and Khiyon concluded that the crack distance is to the top of the slope is closer, the safety factor of the slope is lower.

From the above studies, one can note that the distribution characteristics of surface cracks in depth have main and essential influences on the seepage operation and stability of slopes. However, little attention was paid on the influence of cracks on stability of slopes. For this reason, this paper aims to investigate the distribution characteristics, including the crack depth, effect of dry or water filled cracks and slope angle (β) on stability of slopes by numerical calculations. The program "Optum G2" is employed in the analysis of the slope stability in different state.

THEORY AND METHOD

A commercial finite element limit analysis (FELA) software, OptumG2 [14], was employed to analyze of cracks effect on the stability of slope in different state. This rigorous numerical technique has been successfully employed to solve various problems in geotechnical engineering as demonstrated by Ukritchon and Keawsawasvong, Nielsen [15-16].

Darcy's law can be used in the flow of water through both unsaturated and saturated soils. The difference is that the soil permeability (hydraulic conductivity) is no longer a constant value under conditions of unsaturated flow. The hydraulic conductivity varies with changes in water content of soil. According to conservation of flux the partial differential water flow equation in two dimensions can be defined [17].

$$\frac{\partial}{\partial x}\left(k_x \frac{\partial H}{\partial x}\right) + \frac{\partial}{\partial y}\left(k_y \frac{\partial H}{\partial y}\right) + Q = \frac{\partial \theta}{\partial t} \qquad (1)$$

Where, "H" is the total head, k_x and k_y are the hydraulic conductivity in "x" and "y" direction, "Q" is the applied boundary flux, θ is the volumetric water content and "t" is time.

This equation expresses that the difference between the flow entering and leaving an elemental volume of soil at a point in special time is equal to the change in the storage of the soil. More basically, it reveals that the sum of the rates of change of flow in the x and y direction plus the external flux is equal to the rate of change of the water content with respect to time [18].

The safety factor is mostly used to assess whether a slope is stable or not. Many methods are developed to assess the factor of safety. Most of this methods are based on limit equilibrium methods. A potential sliding mass is first divided into many vertical slices in the limit equilibrium state. Then the force and moment of each of this slices are calculated individually. Finally the safety factor of the slope is analyzed by adding up the results of all of the slices. The differences between different methods are the static equations used and inter-slice forces included.

Spencer's method accepts a constant relationship for the inter slice shear to normal force ratio. The critical failure surface of with the lowest safety factor needs to be determined. Finding the critical failure surface involves a trial procedure. There are many ways to describe the positions and shape of trial failure surfaces. Between these methods an auto search method can give circular or combined slip surfaces. A crack can form a part of the combined failure surface using this method [19].

While Limit Analysis method deals with the problem of determining the ultimate magnitude

of reference loads, Strength Reduction analysis (phi-c reduction method) deals the complementary problem of determining the strength necessary to prevent collapse and failure given a set of actual loads. The Strength Reduction analysis in Optum G2 software goes on by computing a strength reduction factor by which the material parameters need to be reduced in order to reach a condition of incipient collapse. A safety factor greater than 1 thus expresses a stable system while a safety factor less than 1 implies that additional strength is required to prevent collapse and failure.

NUMERICAL SIMULATION

The two-dimensional numerical model of clayey soil slope in different state (without crack, Dry crack and water-filled crack) is investigated. In order to examine the influence of the spatial distribution characteristics of cracks on safety factor of slopes, a numerical parametric study is conducted to better understand the performance of this slopes. The slope had a height of 10m, wet density of soil is 20kN⁄m^3, initial cohesion is 60kN⁄m^2 and other investigated parameters are listed in Table 1. Figure 1 presents the model geometry for a slope of without crack, Dry crack and water-filled crack, respectively. In this study, the crack thickness is assumed to be 10cm based on the results of field surveys and shear strength of the cracks is assumed to be zero.

Table 1. Scheme of numerical calculations used in numerical modeling

Parameter	Value	Parameter state
Height of slope (m)	10	constant
Wet density ($\mathbf{kN/m^3}$)	20	constant
cohesion	60	constant
crack depth, D_{crack} (m)	0, 1, 2, 3, 4	variable
Slope angle, β (degree)	30, 45, 60, 75	variable
Crack condition in slope	Without crack, Dry crack, water filled crack	variable

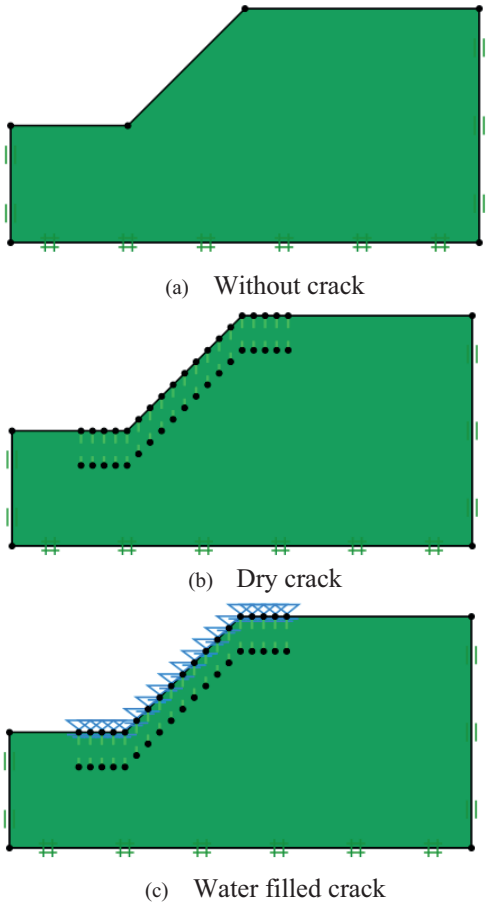

(a) Without crack

(b) Dry crack

(c) Water filled crack

Figure 1. Geometry model of slope in different state of analyses

NUMERICAL RESULTS AND DISCUSSION

To investigate the effect of crack depth on the safety factor of slope with different slope angle, Dry and water filled cracks with 1, 2, 3 and 4m depths located at Longitudinal direction of the slope of the slope is considered. Figures 2 to 5 show the variation of factor of safety with crack depth for the case with slope angle of 30, 45, 60 and 75 degree, respectively. It clearly observe that factor of safety for all of slope angles in Dry and water filled cracks states with increasing the crack depth, decrease significantly. The reason of decreasing of safety factor is that the deep crack does form a part of slip surface. In Figures 6 and 7 are showed the displacement contours for 2m crack depth, 45 degree slope angle in Dry and water filled cracks states respectively.

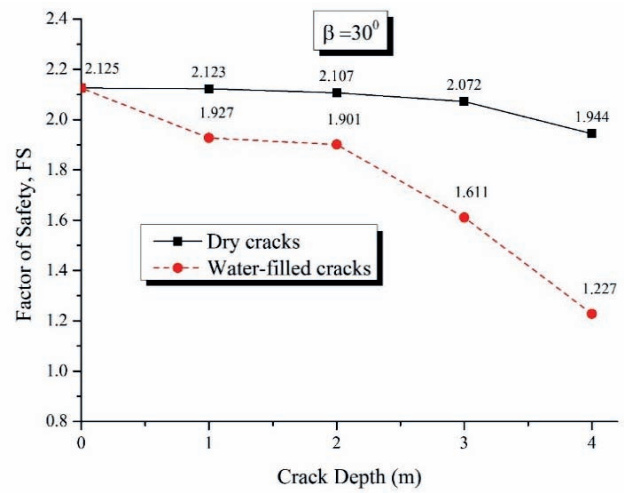

Figure 2. Variation of factor of safety with crack depth for β=30

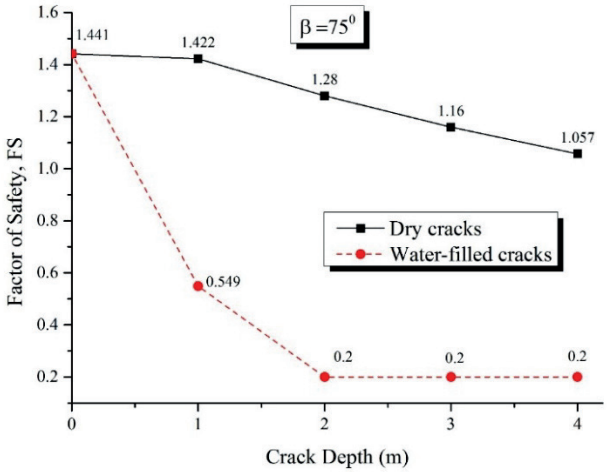

Figure 5. Variation of factor of safety with crack depth for β=75

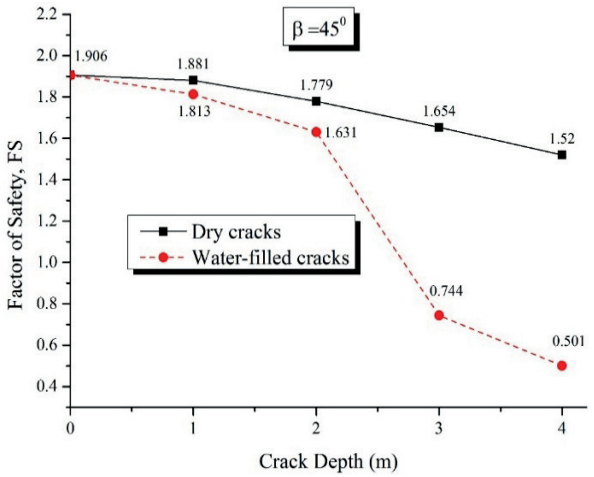

Figure 3. Variation of factor of safety with crack depth for β=45

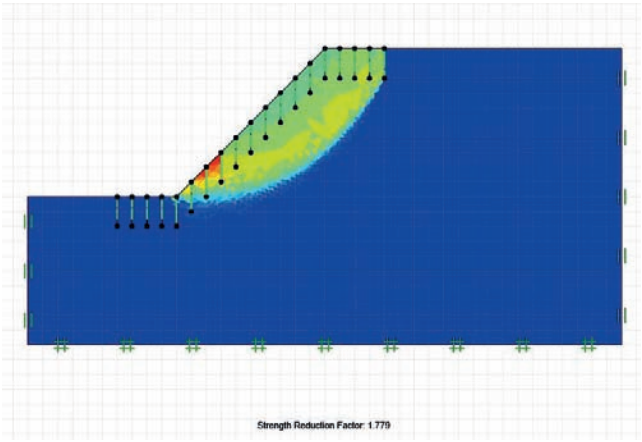

Figure 6. Displacement contour for dry crack state (D_{crack}=2m, β= 45˚)

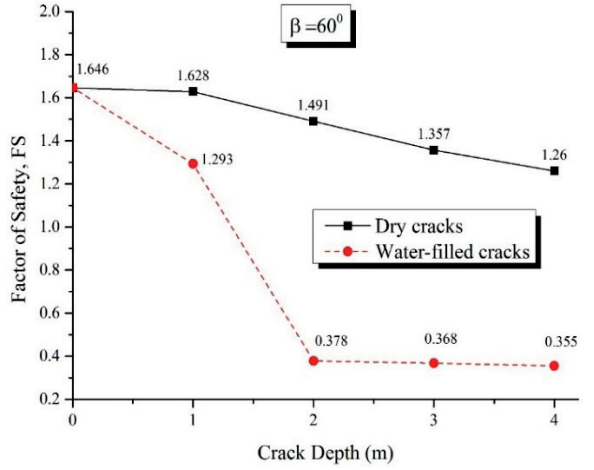

Figure 4. Variation of factor of safety with crack depth for β=60

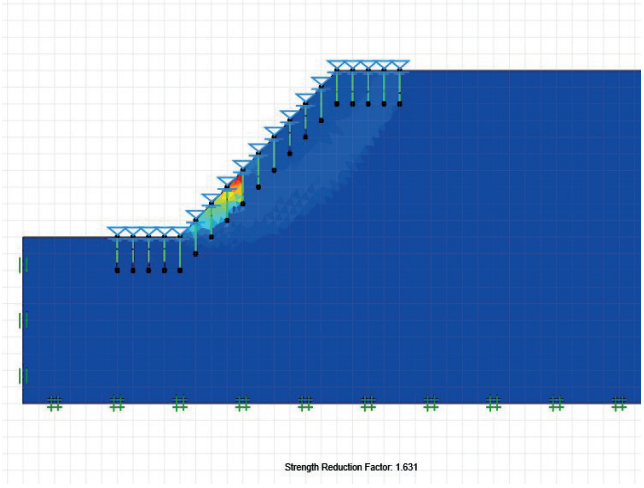

Figure 7. Displacement contour for water filled crack state (D_{crack}=2m, β= 45˚)

To study the effect of slope angle on the slope stability in different crack depth, three conditions are considered: 1) slope without crack, 2) slope with dry cracks, 3) slope with water filled cracks. Figures 8 to 12 show the variation of factor of safety with slope angle for the case with without any crack, crack with depth of 1, 2, 3 and 4 m, respectively. The results of finite element limit analysis using Optum G2 program demonstrated that with increasing of slope angle the factor of safety decreases and this problem is significant in the slope with water filled cracks. As the shear strength of the crack is zero, it is reasonable that the safety factor decreases when the slip surface passes through the crack especially in water filled cracks state. The decrease of slope stability in water filled cracks state is mainly because of the increase in water content, which leads to a decreased shear strength of the slope soil.

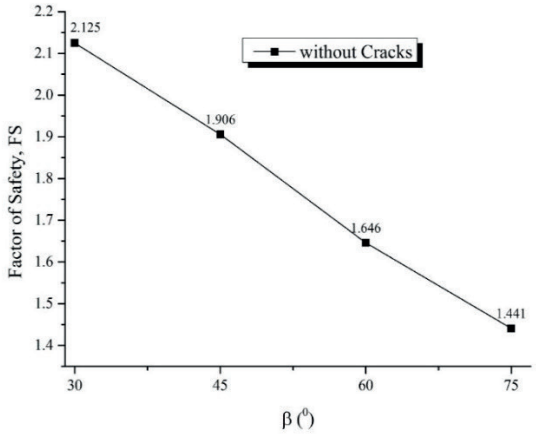

Figure 8. Variation of factor of safety with slope angle in without crack slope

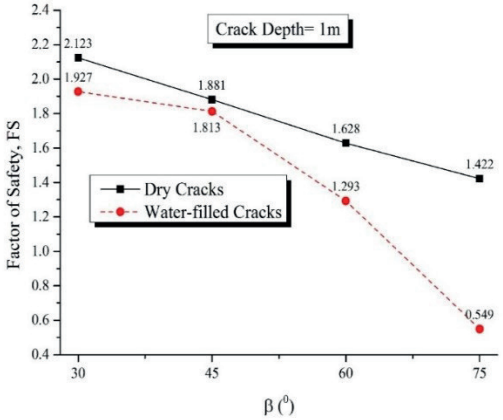

Figure 9. Variation of factor of safety with slope angle in D_{crack}=1m

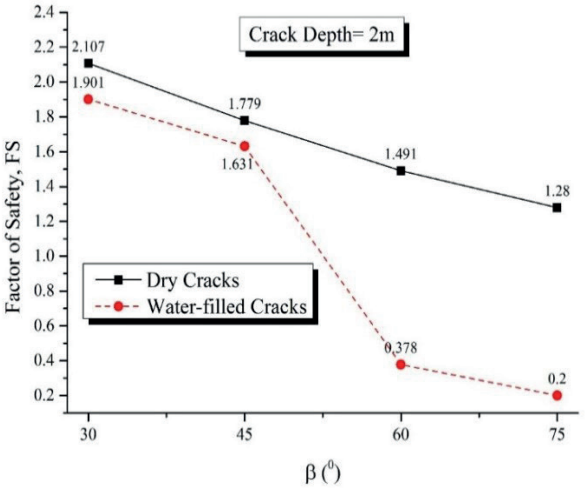

Figure 10. Variation of factor of safety with slope angle in D_{crack}=2m

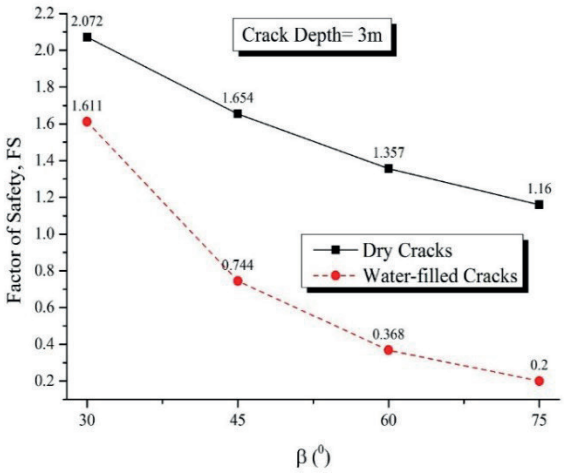

Figure 11. Variation of factor of safety with slope angle in D_{crack}=3m

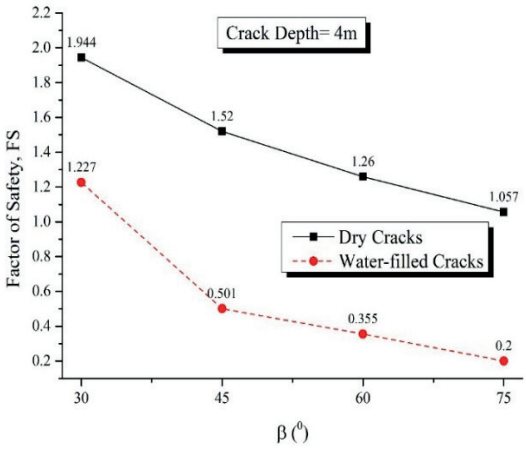

Figure 12. Variation of factor of safety with slope angle in D_{crack}=4m

CONCLUSION

In this study, numerical modeling results of Influence of cracks on the stability of a cracked soil slope were presented using a commercial finite element limit analysis (FELA) software. The effect of crack depth, slope angle on the factor of safety in two state for cracks (dry crack and water filled crack) were examined. Based on the numerical analysis using FELA software conducted in this study, the following results were obtained:

- Factor of safety for all of slope angles in Dry and water filled cracks states with increasing the crack depth, decrease significantly
- The reason of decreasing of safety factor is that the deep crack does form a part of slip surface.
- With increasing of slope angle the factor of safety decreases and this problem is significant in the slope with water filled cracks.
- As the shear strength of the crack is zero, it is reasonable that the safety factor decreases when the slip surface passes through the crack especially in water filled cracks state.

REFERENCES

1. **Bujang, B.K., Huat Faisal, H.J.A. & Low, T.H.** Water infiltration characteristics of unsaturated soil slope and its effect on suction and stability // Geotechnical and Geological Engineering. – 2006. - Vol. 24. – pp. 1293-1306.
2. **Gavin, K., & Xue, J.** A simple method to analyze infiltration into unsaturated soil slopes // Computers and Geotechnics. - 2008. - Vol. 35. - pp. 223-230.
3. **Zhan, L.** Soil-water interaction in unsaturated expansive soil slopes // Frontiers of Architecture and Civil Engineering in China. – 2007. – Vol. 1. – Issue. 2. – pp. 198-204.
4. **Fu, H.Y., Hsun, P.C., Fa, J.C. & Haw, C.L.** Instability of unsaturated soil slopes due to infiltration // International Symposium on Geohazards Mitigation. – 2006. - Taiwan.
5. **Stephen, E.D., & Colin, R.R.** Prediction of tension crack location and riverbank erosion hazards along destabilized channels // Earth surface processes and landforms. – 1994. – Vol. 19. – pp. 233-245.
6. **CAI, W.M., Murti, V., & Valliappan, S.** Slope stability analysis using fracture mechanics approach // Theoretical and applied fracture Mechanics. – 2005. – Vol. 12. – pp. 261-281.
7. **Fan, P., Liu, Q., Li, J., & Sun, J., P.** Numerical analysis of rainfall infiltration in the slope with a fracture // Science in China Series E-Engineering & Materials Science. – 2005. – Vol. 48. – pp. 107-120.
8. **Wang, Z. F.** Unsaturated hydraulic properties of a single crack and its effects on slope stability // MPhil thesis. Harbin Institute of Technology, PRC. – 2011.
9. **GUI, MW. And Han, K.K.** A case study on infiltration effect on the stability of two slopes // Landslides and Engineered Slopes. – 2008. – pp. 1737 -1743.
10. **Nurly, G., Lee, M.L., and Asof, M.** Transient seepage and slope stability analysis for rainfall-induced landslide // A case study Malaysian Jour. Civil Eng. – 2008. – Vol. 18. – Issue. 1. – pp. 1-13.
11. **Zeng, L., Liu, J., Zhang, J.H., Bian, H.B., Lu, W.H.** Effect of colluvial soil slope fracture's anisotropy characteristics on rainwater infiltration process // Adv. Civ. Eng. – 2018.
12. **Mukhlisin, M., Khiyon, K.N.** The effects of cracking on slope stability // Geo Soc India. – 2018. – Vol. 91. – Issue. 6. – pp. 704-710.
13. **Zhang, G., Wang, R., Qian, J., Zhang, J.M., Qian, J.** Effect study of cracks on behavior of soil slope under rainfall

conditions // Soils Found. – 2012. – Vol. 52. – Issue. 4. – pp. 634–643.
14. **Krabbenhoft, K., Lyamin, A., & Krabbenhoft, J.** Optum computational engineering (OptumG2) // [Computer software]. Retrieved from https. – 2015. - www.optumce.com
15. **Ukritchon, B., and Keawsawasvong, S.** Design equations of uplift capacity of circular piles in sands // Applied Ocean Research. – 2019. – Vol. 90. – 101844.
16. **Nielsen, S.D.** Finite element modeling of the tensile capacity of suction caissons in cohesion less soil // Applied Ocean Research. – 2019. – Vol. 90. - 101866.
17. **Daniel, M.** Prediction of steady-state flow of real gases in randomly heterogeneous porous media // Physical D. Nonlinear Phenomena. – 1999. – Vol. 133. – pp. 463-468.
18. **Fredlund, D.G., and Rahardjo, H.** Soil mechanics for unsaturated soils // New York: John Wiley & Sons. – 1993.
19. **Spencer, E.** A method of analysis of embankments assuming parallel interstice forces // Geotechnique. – 1967. – Vol. 17.

СПИСОК ЛИТЕРАТУРЫ

1. **Bujang, B.K., Huat Faisal, H.J.A. & Low, T.H.** Water infiltration characteristics of unsaturated soil slope and its effect on suction and stability // Geotechnical and Geological Engineering. – 2006. - Vol. 24. – pp. 1293-1306.
2. **Gavin, K., & Xue, J.** A simple method to analyze infiltration into unsaturated soil slopes // Computers and Geotechnics. - 2008. - Vol. 35. - pp. 223-230.
3. **Zhan, L.** Soil-water interaction in unsaturated expansive soil slopes // Frontiers of Architecture and Civil Engineering in China. – 2007. – Vol. 1. – Issue. 2. – pp. 198-204.
4. **Fu, H.Y., Hsun, P.C., Fa, J.C. & Haw, C.L.** Instability of unsaturated soil slopes due to infiltration // International Symposium on Geohazards Mitigation. – 2006. - Taiwan.
5. **Stephen, E.D., & Colin, R.R.** Prediction of tension crack location and riverbank erosion hazards along destabilized channels // Earth surface processes and landforms. – 1994. – Vol. 19. – pp. 233-245.
6. **CAI, W.M., Murti, V., & Valliappan, S.** Slope stability analysis using fracture mechanics approach // Theoretical and applied fracture Mechanics. – 2005. – Vol. 12. – pp. 261-281.
7. **Fan, P., Liu, Q., Li, J., & Sun, J., P.** Numerical analysis of rainfall infiltration in the slope with a fracture // Science in China Series E-Engineering & Materials Science. – 2005. – Vol. 48. – pp. 107-120.
8. **Wang, Z. F.** Unsaturated hydraulic properties of a single crack and its effects on slope stability // MPhil thesis. Harbin Institute of Technology, PRC. – 2011.
9. **GUI, MW. And Han, K.K.** A case study on infiltration effect on the stability of two slopes // Landslides and Engineered Slopes. – 2008. – pp. 1737 -1743.
10. **Nurly, G., Lee, M.L., and Asof, M.** Transient seepage and slope stability analysis for rainfall-induced landslide // A case study Malaysian Jour. Civil Eng. – 2008. – Vol. 18. – Issue. 1. – pp. 1-13.
11. **Zeng, L., Liu, J., Zhang, J.H., Bian, H.B., Lu, W.H.** Effect of colluvial soil slope fracture's anisotropy characteristics on rainwater infiltration process // Adv. Civ. Eng. – 2018.
12. **Mukhlisin, M., Khiyon, K.N.** The effects of cracking on slope stability // Geo Soc India. – 2018. – Vol. 91. – Issue. 6. – pp. 704-710.

13. **Zhang, G., Wang, R., Qian, J., Zhang, J.M., Qian, J.** Effect study of cracks on behavior of soil slope under rainfall conditions // Soils Found. – 2012. – Vol. 52. – Issue. 4. – pp. 634–643.
14. **Krabbenhoft, K., Lyamin, A., & Krabbenhoft, J.** Optum computational engineering (OptumG2) // [Computer software]. Retrieved from https. – 2015. - www.optumce.com
15. **Ukritchon, B., and Keawsawasvong, S.** Design equations of uplift capacity of circular piles in sands // Applied Ocean Research. – 2019. – Vol. 90. – 101844.
16. **Nielsen, S.D.** Finite element modeling of the tensile capacity of suction caissons in cohesion less soil // Applied Ocean Research. – 2019. – Vol. 90. - 101866.
17. **Daniel, M.** Prediction of steady-state flow of real gases in randomly heterogeneous porous media // Physical D. Nonlinear Phenomena. – 1999. – Vol. 133. – pp. 463-468.
18. **Fredlund, D.G., and Rahardjo, H.** Soil mechanics for unsaturated soils // New York: John Wiley & Sons. – 1993.
19. **Spencer, E.** A method of analysis of embankments assuming parallel interstice forces // Geotechnique. – 1967. – Vol. 17.

M. Hosseini is an Associate Professor in Civil Engineering Department at Lorestan University, Iran. He received his PhD in Civil Engineering from Tehran University. Ph.: (+98)9163973584, Hosseini.m@lu.ac.ir

P. Beiranvand is a Lecturer in Civil Engineering at Lorestan University. He received his PhD in Civil Engineering from Razi University of Iran. More than 100 journal papers, 10 conference papers, 1 published book are the results of his researches so far. Ph.: (+98)9160199970, peyman51471366@gmail.com

M. Mohammadiasl is a Lecturer in Civil Engineering at Lorestan University. He received his PhD in Civil Engineering from Malayer University of Iran. Ph.: (+98)9126069337.

A. Hasanvand is a student bachelor in Mechanical Engineering. He is B.Sc., Department of Mechanical Engineering, Khorramabad Branch, Islamic Azad University. Ph.: (+98)9167958568.

Моджтаба Хоссейни доцент, кафедра гражданского строительства, Лорестанский университет, Хоррамабад, Иран. Ph.: (+98)9163973584, Hosseini.m@lu.ac.ir

Пейман Бейранванд преподаватель кафедры гражданского строительства Лорестанского университета, Хоррамабад, Иран. Ph.: (+98)9160199970, peyman51471366@gmail.com

Мохаммад Мохаммадиасл кандидат наук, кафедра гражданского строительства, Хоррамабадский филиал, Исламский университет Азада, Иран. Ph.: (+98)9126069337.

Ашкан Хассанванд бакалавр наук, факультет машиностроения, Хоррамабадский филиал, Исламский университет Азада, Иран. Ph.: (+98)9167958568.

International Journal for Computational Civil and Structural Engineering, 18(4) 91–100 (2022)

DOI:10.22337/2587-9618-2022-18-4-91-100

SIMULATION OF THE STRENGTH OF TWO-LAYER PIPE STRUCTURES IMPLEMENTED IN THE TRENCHLESS REPAIR METHOD AND ASSESSMENT ITS ENERGY SAVING DURING WATER SUPPLYING

Vladimir A. Orlov, Sergey P. Zotkin, Dmitry A. Peterburgsky

National Research Moscow State University of Civil Engineering, Moscow, RUSSIA

Abstract. The article proposes approaches for assessing the strength characteristics of two-layer pipelines formed as a result of using a trenchless method for the reconstruction of dilapidated steel pipeline networks by pulling pipes made of unplasticized polyvinyl chloride (UPVC) into them. The results of simulation of filling the annular space between steel and polymer pipes are presented with an analysis of the three states of a two-pipe system in order to ensure strength characteristics. The paper provides an analysis of the possibility of saving energy when using PVC-U pipes in a two-layer pipe structure at various temperatures of supplying water and a stable temperature of the pipeline wall. Besides, it proposes the introduction of a set of developed automated programs for design.

Keywords: underground pipelines, reconstruction, strength analysis, simulation, automated programs, energy saving

МОДЕЛИРОВАНИЕ ПРОЧНОСТНЫХ ХАРАКТЕРИСТИК ДВУХСЛОЙНЫХ ТРУБНЫХ КОНСТРУКЦИЙ ПРИ РЕАЛИЗАЦИИ БЕСТРАНШЕЙНОГО МЕТОДА РЕМОНТА С ОЦЕНКОЙ ЭНЕРГОСБЕРЕЖЕНИЯ ПРИ ТРАНСПОРТИРОВКЕ ВОДЫ

В.А. Орлов, С.П. Зоткин, Д.А. Петербургский

Национальный исследовательский Московский государственный строительный университет, г. Москва, РОССИЯ

Аннотация. Предложены подходы к оценке прочностных характеристик двухслойных трубопроводов, образующихся в результате использования бестраншейной технологии реконструкции ветхих стальных трубопроводных сетей путем протаскивания в них труб из непластифицированного поливинилхлорида (НПВХ). Представлены результаты моделирования процесса забутовки межтрубного пространства между стальной и полимерной трубами с анализом трех состояний двухтрубной системы на предмет обеспечения прочностных характеристик. Выполнены расчета и представлен анализ возможности экономии электроэнергии при использовании труб из НПВХ в двухслойной трубной конструкции при различных температурах транспортируемой воды и стабильной температуре стенки трубопровода с предложениями внедрения комплекса разработанных автоматизированных программ при проведении проектных разработок.

Ключевые слова: подземные трубопроводы, реконструкция, прочностные расчеты, моделирование, автоматизированные программы, энергосбережение

INTRODUCTION

The situation in the field of underground pressure pipelines of water supply systems both in our country and abroad remains very difficult, since almost half of their total number needs to be repaired or replaced (modernized) [1]. This brings the problems of prompt restoration of aging pipeline networks and increasing the reliability of their operation. The ensuring of the strength and hydraulic characteristics required by the project play a dominant role when using various types of repair materials [2, 3].

The trenchless method of reconstruction is the most effective one in terms of saving material and monetary costs, as well as the efficiency of performing restoration work on dilapidated pipeline networks made of various materials that is worn-out structure with reduced deformation and strength characteristics. This method allows not only to eliminate existing defects in the pipeline network, but also to increase their throughput [4, 5]. One of the most popular methods for the reconstruction of aged pipelines in a trenchless way is the pulling and fixing of new pipelines made of polymeric materials into them. That allows obtaining a two-layer pipeline with the required technical indicators, which include, first of all, the high strength characteristics of the new two-pipe structure, as well as the possibility of energy saving during fluid motion due to relatively small specific resistances [6]. However, among the many modern polymeric materials used for the manufacture of pipes (polyethylene, polybutylene, polypropylene, polyvinyl chloride, etc.), it becomes necessary to choose one that has a number of advantages compared to others, in particular, to ensure the required strength characteristics of a new double-pipe structure, lower coefficient of linear elongation, energy savings when supplying liquids, durability and other factors [7]. Such materials include unplasticized polyvinyl chloride (UPVC). The PVC-U pipe dragged into the dilapidated pipeline after the operations of backfilling the annular space with mortars in order to increase the load capacity of the new two-layer pipe structure. Another actual task is introducing electronic models for assessing the integrated operation of water supply systems, including water supply networks and their repair by various methods with the achievement of the energy saving effect [8, 9].

SIMULATION APPROACHES FOR THE STRENGTH CHARACTERISTICS OF TWO-LAYER UNDERGROUND PIPE STRUCTURES.

The pressure pipes manufactured by Chemkor JSC from non-plasticized polyvinyl chloride (UPVC) made in accordance with GOST 32415-2013 and used both for open laying and restoring the performance of dilapidated supplying networks from various materials using trenchless technology for pulling new pipes into the aged pipeline with the formation of a two-layer structure were the materials for research. The low value of the resistivity coefficient of the internal walls of AUPVC = 0.0008d-5.1977 (where d is the diameter of the pipeline in m), as well as a 2.5 times lower coefficient of linear extention compared to traditional ones for use in trenchless technologies repair of pipelines with polyethylene pipes. It reduces the likelihood of a significant curvature of the new pipeline in the old one under the influence of ambient temperature and the supplied liquid. However, this does not exclude the filling of the annular space, which guarantees the provision of the required strength indicators (load capacity) of the two-pipe structure.

The paper provides the methods of computer simulation of the strength characteristics of two-layer pipe structures during the implementation of repair work using the trenchless approach, as well as an assessment of the possibility of energy saving when supplying water through a two-layer pressure system after repair work.

The process of simulation of strength characteristics consists of applying the algorithm developed by the authors of the article and an automated computation program, which analyzes the static and dynamic components of

ensuring the load capacity of the restored pipeline system [10]:
- the strength of the PVC-U pipe, pulled in the aged pipeline;
- allowable deformations of the diameter of the new pipeline in the aged one under the influence of mortars filling the annular space, i.e., compliance with the conditions for not exceeding the degree of ovalization of the circular cross-section of the pipe by a value of not more than 5% in diameter;
- the probability of the PVC-U pipe floating due to the Archimedean force and thereby eliminating the negative case of its support on the inner surface (hard arch) of the old pipeline, which can provoke the early appearance and propagation of cracks near point loads and increase the abrasion of the walls of the new pipeline [11].

Figure 1 shows a cross-sectional diagram of the repair two-layer pipe structure.

The most popular in practice mortars on gravel or crushed stone with a density of 24,000 N/m^3 and, as an alternative, a cement-slag mortar with a density of 8,000 N/m^3, were considered as mixtures used for backfilling during the simulation period. The tasks of modeling, in particular, included the determination of the loads that counteract the mixture. These loads act on the PVC-U pipe with various options for filling the annular space (uniform or uneven) with mortar.

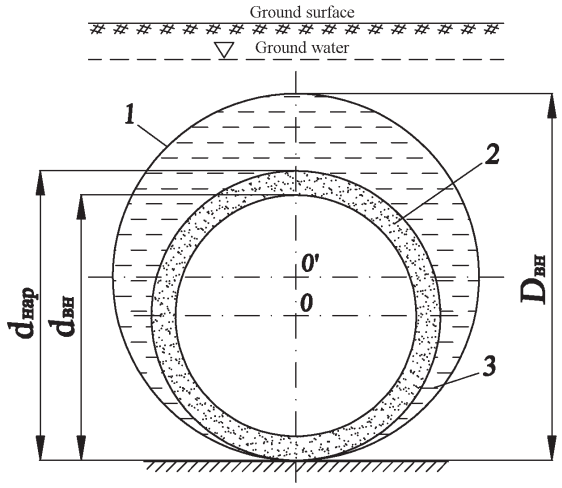

Figure 1. Cross section of a repair pipeline with backfilling of the annulus with mortar
1 - the inner wall of the aged pipeline renovated with an internal diameter $D_{in.}$; 2- PVC-U pipeline with outer diameter d_{out} and inner diameter d_{in}; 3- mortar in the annulus

Table 1 presents the values of the initial parameters of the input information for one of the considered examples of automated simulation.

Table 1. Initial information for strength calculation

Number	Names of parameters and their designation	Values
1.	Inner diameter of the pipeline to be renovated, D_{in}, m	0.6
2.	Diameters of the new pipeline being pulled into the aged one, - *d* external, m - *d* internal, m	 0.476 0.452
3.	Volume weights, N/m^3 - cement mortar *g cm* - pulled pipe *gpp* - supplying liquid (water) *gw*	 24000.0 9500.0 9800.0
4.	The internal pressure of the supplied medium, corresponding to reduced design stresses *P*, *MPa*	0.0
5.	The value of the possible vacuum in the annulus *Pvac*, *MPa*	0.0
6.	Standard service life of the pulled pipeline *t*, years	50.0
7.	Maximum operating temperature of the pulled pipeline *T,°C*	20.00

8.	Characteristic long-term strength of the pipe material (depending on the values of t and T) *R*ch, *MPa*	5.0
9.	Depth of the pipeline from the ground *H*, m	10.00
10.	The value of groundwater pressure on the arch of the pipeline *Pgw*, *MPa*	0.02
11.	Coefficients: - laying conditions k_1 - stability of the pulled pipeline k_2 - working conditions k_y - joint strength k_c 0.90 - influence of temperature on the deformation properties of the material k_e - load distribution and support reaction of the base z	 0.80 0.60 0.60 0.90 0.80 1.30
12.	Maximum permissible value of ovalization of the cross section E, %	5.000
13.	Creep modulus of the pipe material in tension (depending on the values of t and Rch) *E*o, *MPa*	100.0
14.	Backfill deformation modulus, depending on the backfill material *Eg* , *MPa*	0.50

According to the results of the field survey, the aged pipeline under operation is a worn-out structure with reduced deformation and strength characteristics. It is necessary to strengthen the pipe structure operating in these conditions which consists of separate modules of PVC-U socket pipes connected in series. The pipe pulled into the dilapidated pipeline should ensure increase the load capacity of the two-layer pipe structure and be a barrier against the phenomena of groundwater infiltration into the pipeline body and exfiltration of the transported water into the annulus after the operations of filling the annular space with mortars.

Below, paper provides examples of automated calculations and their interpretation based on the results of the reconstruction of an aged pressure steel pipeline with an internal diameter of 600 mm for two selective options for the diameters of PVC-U pipes from among the available products in the range of Chemkor JSC:

- PVC-U SDR 41-500, having a socket with a diameter of 549 mm, an inner diameter of 475 mm and an outer diameter of 487 mm (hereinafter, the term SDR refers to the ratio of the pipeline diameter to its wall thickness);
- PVC-U SDR 21-500, having a socket with a diameter of 578 mm, an inner diameter of a pipe of 452 mm and an outer diameter of 476 mm.

Thus, the pipes presented above differ in wall thickness (for the first example 12 mm and for the second one 24 mm), i.e., it is conventionally considered as thin-walled and thick-walled.

Additional information includes the following: the maximum allowable water pressure in the pipeline is 0.8 MPa;

The significant depth of the pipeline of 10 m (see Table 1) was chosen as extreme one, i.e., it guarantees that compliance with (not exceeding) the basic values of the design parameters will be ensured due to a certain margin of safety at a lower pipe penetration. In addition, it should be noted that a prerequisite for the implementation of the method for pulling new pipes into the old one and backfilling it is performing of preliminary dewatering using wellpoints when there is groundwater above the pipeline.

Table 2 presents the results of automated calculation for two selective pipe options.

Table 2. Summary output information on the results of the strength analysis of two-pipe structures when mortar with a density of 24000 N/m³ is used for backfilling

Name of design indicators of bearing capacity	uPVC pipe	
	SDR 41-500	*SDR* 21-500
1. By strength to the effect of internal water pressure, MPa	0,8	0,8
2. According to the maximum permissible ovalization (deformation) of the cross section of the pipeline, %:		
- for the case of uniform filling of the annular space in the absence of water in the pipeline	13,398	3,438
- the same if there is water in the pipeline	7,073	1,778
- for the case of uneven filling of the annular space in the absence of water in the pipeline	11,309	3,055
- the same if there is water in the pipeline	9,1214	2,526
3. On the stability of the round shape (profile) of the pipeline being pulled to the ascent through the value of the radial pressure on the pipe walls, MPa:		
- for the case of uniform filling and the absence of water in the pipeline	0,019	0,021
- the same if there is water in the pipeline	0,026	0,027
- for the case of uneven filling of the annular space in the absence of water in the pipeline	0,045	0,044
- the same if there is water in the pipeline	0,043	0,043

Analysis of the data presented in Table 2 shows that both pipelines are able to withstand the established pressure standards (0.8 MPa) according to the first condition. There are some discrepancies in terms of the second and third conditions. In particular, ovalization exceeds the established standards by 5% for the PVC-U SDR 41-500 pipeline, and it remains within the normal range for the PVC-U SDR 21-500 pipeline. A similar trend is observed when analyzing data for the third condition, where the value of the radial pressure on the pipe walls for various cases exceeds or does not exceed the critical values. In particular, the ascent resistance has been provided only for the case of uniform backfilling and the absence of water in the pipeline for the PVC-U SDR 41-500 pipe, since in this case the radial pressure on the pipeline walls is 0.019 MPa, i.e., less than critical one which is 0.0254 MPa. The ascent stability is not respected for another cases. According to the third condition, the standards are observed in all cases for PVC-U pipe SDR 21-500, since the critical pressure is 0.074 MPa according to the calculation.

Thus, the option of pulling PVC-U SDR 41-500 pipes into an old pipeline with backfilling of the annular space using trenchless method cannot be considered acceptable due to the relatively small thickness of the pipe wall.

As noted above, the strength characteristics of a two-pipe system were analyzed using a cement-slag mortar with a density of 8000 N/m3 as an alternative backfilling option. This circumstance was due to the fact that the practical application of the option of pulling PVC-U SDR 21-500 pipes into the old pipeline with filling with mortar with a density of 24,000 N/m3 can lead to relatively large deformations of the pipeline cross-section (in the range of 1.778-3.438) as presented in Table 2.

The calculations which have been performed using an automated program showed that a lighter construction backfilling material allows reducing the probability of ovalization of the pipeline cross section according to the second

strength condition for 4 cases under consideration to values of 0.924, 0.735, 0.961 and 1.4638%, respectively. This will affect positively on the durability of the restored two-pipe structure. In addition, all cases also have positive results of 0.029, 0.036, 0.037 and 0.038 MPa, respectively, at a critical pressure of 0.077 MPa according to the third strength condition for checking the stability of a two-pipe structure for ascent.

An intermediate conclusion on the analysis of the results of automated calculation is a recommendation for the use of pipe modules made of PVC-U SDR 21-500 for the reconstruction of an old steel pipeline with backfilling of the annular space with cement-slag mortar.

ASSESSMENT OF THE ELECTRICITY SAVING WHEN USING PVC-U PIPES FOR WATER SUPPLYING DEPENDING ON TEMPERATURE CONDITIONS.

At the present stage of development of underground infrastructure, design, construction, reconstruction and modernization of pipeline transport should be based not only on creating conditions for the strength of structures and their durability, but also on ensuring energy saving during their operation. and, if possible, managing the process of water supplying to achieve an economic effect.

The calculation of electricity consumption E (kWh per year) at water supplying through pressure pipelines made of various materials, as a rule, is performed using the universal formula (1):

$$E=[9{,}81Q^3(A_i \cdot l)/\eta_{pump..}]\cdot 24\cdot 365, \qquad (1)$$

where Q is the supplying water consumption, m^3/s; A_i is the coefficient of specific resistance of the pipeline wall material c^2/m^6; l is the pipeline length, m; $\eta_{pump.}$ is the efficiency of the pumping unit; 24 and 365 are the number of hours in a day and days in a year, respectively.

The presented universal formula does not fully reflect the needs of designers and operating personnel of water utilities when they applied it tothe reconstruction an old pipeline by creating a two-layer pipe structure "steel + PVC-U", since it does not consider temperature conditions, in particular, the temperature of the supplied water. Previously, it was found that the coefficient of hydraulic friction λ of pipelines depends on the temperature of the supplied water and, accordingly, the pipe walls [12]. With an increase in temperature, the value of λ decreases due to a decrease in the viscosity of water, which ultimately creates the possibility of saving energy during the water supplying.

The basic calculation formula for determining the cost of electricity accounting the coefficient of hydraulic friction λ, has the form (2):

$$E=0{,}81\cdot Q^3\cdot l\cdot\lambda\cdot 24\cdot 365/(d^5\cdot\eta_{pump.}), \qquad (2)$$

where d is the internal diameter of the pipeline, m.

Thus, formula (2) allows calculation when a certain inner diameter of the pipeline d and the coefficient of hydraulic friction λ are involved.

A specially developed automated calculation program [13] has been used in order to analyze the consumption of electricity during water supplying. The program allows you to calculate the hydraulic and energy parameters of the pressure pipeline in a wide temperature range. At the same time, the previously identified ranges of restrictions on the recommended range of Reynolds numbers and the ratio of dynamic viscosities related to the fluid flow and the pipe wall, respectively, were observed in the algorithm of the automated calculation program which accounts the non-isothermal movement of fluid in pipes [14].

Computer simulation has been carried out in order to assess the effect of water temperature and the pipeline wall on electricity consumption. We accepted PVC-U pipes for trenchless repair of a dilapidated steel pipeline, and the central areas of the Russian Federation as the place for repair work.

The initial parameters entered into the calculation program were as follows:
- depth of occurrence of the restored pipeline of a two-layer structure "steel + PVC-U SDR 21-500" 1.6 m;
- the length of the pipeline is 3000 m;
- average temperature of the pipeline wall (soil around the pipe) 15.50 C;
- water intake by a pumping unit is carried out from a surface reservoir from a depth of 10 m;
- average water temperature 22.10 C (summer) and 80 C (winter);
- consumption of transported water 0.15 m^3/s;
- efficiency of the pumping unit 0.9.

Table 3 presents summary output information on individual parameters of the calculated parameters of the summer and winter periods.

Table 3. Summary output information based on the results of hydraulic and energy analysis of a two-pipe structure in summer and winter periods

Calculated indicators	Indicator values	
	Summer	Winter
1. Water flow rate in the pipeline, m/s	0.9348	0.9348
2. Dynamic viscosity coefficient related to fluid flow, Pa*s	0.0009703	0.0014065
3. Dynamic viscosity coefficient related to pipe wall temperature, Pa*s	0.0011461	0.0011461
4. Ratio of dynamic viscosities	0.847	1.227
5. Fluid kinematic viscosity coefficient, m2/s	0.00000094	0.00000138
6. Reynolds number	449597.47	306279.24
7. Estimated coefficient of hydraulic friction	0.013787	0.013819
8. Electricity consumption through the coefficient of hydraulic friction, kWh per year	58333.698	58470.157
9. Electricity consumption through the coefficient of resistivity, kWh per year	47962.585	47962.585

An analysis of the calculated data presented in Table 3 for items 8 and 9 is typical for the following two conclusions.

Firstly, electricity consumption in winter increases by 58470.157-58333.698=136.459 kWh per year compared to summer according to the calculations in 8 for the summer and winter periods. With an average cost of 1 kWh of electricity of 9.13125 rubles (at the current time), the savings is 136.459x9.13125=1246.04 rubles per year.

Secondly, a comparison of the values of electricity consumption in 8 and 9, i.e., considering the temperatures of the water and the pipeline wall and without it, shows a significant discrepancy. For example, the difference in electricity consumption is 58470.157-47962.585=10507.572 kWh per year, or 17.97% less for the winter period. This leads to the conclusion that designing, requires considering temperature factors in order to obtain the most probable values of electricity consumption, i.e., it is necessary to include data on the temperature parameters of the pipeline wall and transported water in projects for the construction of pipeline networks and to carry out calculations of electricity consumption. This is facilitated by simulation, which allows identification of the optimal parameters for controlling the process of water transportation based on the search for the minimum values of electricity consumption. Using the capabilities of the automated program, it is possible to calculate the cost of electricity in a wide range of temperatures of the pipe wall (of the appropriate material and diameter) and transported water for both northern and southern

regions at various values of water flow rates and efficiency values of pumping units.

COMCLUSIONS

1. The simulation of the strength characteristics of two-layer pipe structures using an automated program allowed determination of parameters that allow choosing the most acceptable technical solutions for filling the annular space with mortars from alternative options.
2. The values of the permissible ovalization (deformation) of the cross section of the new pipeline dragged into the old pipeline, as well as its resistance to ascent under various conditions through the magnitude of the radial pressure of the mortar on the pipe walls, are proposed as criteria for comparing the options for filling the annular space with mortars.
3. The article substantiated the application of new PVC-U SDR 21-500 pipes during the period of trenchless repair of an old steel pipeline for specific design conditions. This approach has a number of positive properties compared to other polymer pipes, and use cement-slag mortar as a material for backfilling the annular space, which provides less deformations of the cross section of new pipes.
4. An example of designing an underground pressure pipeline network for the conditions of the middle area of the Russian Federation, based on the results of automated calculations, presented the values of saving energy costs for transporting water under various temperature conditions. This allows performing managerial functions of the operation of pipelines from various materials and diameters, varying costs of transported water and the type of pumps used, and during operation to monitor the real effect of reducing cash costs at the stage of design.

REFERENCES

1. **Stepanov M.A., Primin O.G.** The reliability problems of pipelines of water supply, sanitation systems and ways to solve them. // Water supply and sanitary engineering, 2021, No. 10, p. 4-9
2. **Baranov L.A., Yermolin Yu.A.** Assessment of reliability indicators of a "linearly aging" object // Reliability. 2015. No. 4 (55). P. 57–60
3. **Heber Pimentel Gomes, Pedro Augusto Silva Sabino de Farias, Saulo de Tarso Marques Bezerra, Sabrina da Silva.** Efficiency indicator for assessment of water distribution networks carrying capacity //Environmental Engineering and Management Journal. May 2020, Vol. 19, No. 5, 747-753
4. **Kuliczkowski A.** Renovation or reconstruction on the example of water and sewage pipes. // INSTAL, 2012. No 1, pp. 46-49.
5. **Kozlov M.N., Menshchikova O.A., Gavrilov D.V.** The experience of Mosvodokanal JSC in introducing new equipment and technologies // Water Magazine. 2016. No. 10. P. 14–19.
6. **Primin O. G., Orlov V. A.** Reliability of utility pipelines and planning for their restoration // Pipeline transport (theory and practice). 2016. No. 2. p. 21–25
7. **Khramenkov S.V.** Time to manage water. -M.: OJSC Moscow textbooks and cartolithography. 2012. 279 p.
8. **Galperin E.M., Egorova Yu.A., Vaskovskii A.V., Konevskii E.V.** Ways to improve the management of the urban system of water supply and distribution // Water supply and sanitary engineering. 2016. No. 10. p. 23–27
9. **Chupin R.V., Melekhov E.S.** Justification of the parameters of developing water supply and sanitation systems based on their electronic models. // IOP Conference Series: Materials Science and Engineering, 2020. DOI: 10.1088/1757-899X/880/1/012050
10. **Khurgin R.E., Orlov V.A., Zotkin S.P.** "The program for determining the loads on the pipeline with checking its load capacity

during reconstruction." Certificate of state registration of the computer program No. 2013615444 accessed 10.06.2013
11. **Rameil M.** Handbook of pipe bursting practice. Essen: Vulkan Verlag. 2007. 351 p.
12. **Orlov V.A., Peterburgsky D.A.** The influence of the temperature factor on the consumption of electricity during the transportation of water through pressure pipelines. //Plumbing. Heating. Conditioning. (P.H.C.), 2021, No. 12, p. 20-25
13. **Orlov V.A., Zotkin S.P., Inshakova M.A., Petersburg D.A.** "Calculation of hydraulic parameters of pressure pipes at temperature regime changes". Certificate of state registration of the computer program No. 2020661754 dated 30.09.2020
14. **Altshul A.D.** Hydraulic resistance. Moscow: Nedra.1970. 216 p.

СПИСОК ЛИТЕРАТУРЫ

1. **Степанов М.А., Примин О.Г.** Проблемы надежности трубопроводов систем водоснабжения и водоотведения и пути их решения. //Водоснабжение и санитарная техника, 2021, № 10, с. 4-9
2. **Баранов Л.А., Ермолин Ю.А.** Оценка показателей надежности «линейно-стареющего» объекта // Надежность. 2015. № 4 (55). с. 57–60
3. **Heber Pimentel Gomes, Pedro Augusto Silva Sabino de Farias, Saulo de Tarso Marques Bezerra, Sabrina da Silva.** Efficiency indicator for assessment of water distribution networks carrying capacity //Environmental Engineering and Management Journal. May 2020, Vol. 19, No. 5, 747-753
4. **Kuliczkowski A.** Renovation or reconstruction on the example of water and sewage pipes. // INSTAL, 2012. № 1, pp. 46-49.
5. **Козлов М.Н., Меньщикова О.А., Гаврилов Д.В.** Опыт АО «Мосводоканал» по внедрению новой техники и технологий // Вода Magazine. 2016. № 10. С. 14–19.
6. **Примин О.Г., Орлов В.А.** Надежность коммунальных трубопроводов и планирование их восстановления //Трубопроводный транспорт (теория и практика). 2016. № 2. с. 21–25
7. **Храменков С.В**. Время управлять водой. -М.: ОАО Московские учебники и картолитография. 2012. 279 с.
8. **Гальперин Е.М., Егорова Ю.А., Васьковский А.В., Коневский Е.В.** Пути совершенствования управления городской системой подачи и распределения воды // Водоснабжение и санитарная техника. 2016. № 10. с. 23–27
9. **Chupin R.V., Melekhov E.S.** Justification of the parameters of developing water supply and sanitation systems based on their electronic models. // IOP Conference Series: Materials Science and Engineering, 2020. DOI: 10.1088/1757-899X/880/1/012050
10. **Хургин Р.Е., Орлов В.А., Зоткин С.П.** «Программа определения нагрузок на трубопровод с проверкой его несущей способности при реконструкции». Свидетельство о государственной регистрации программы для ЭВМ № 2013615444 от 10.06.2013
11. **Rameil M.** Handbook of pipe bursting practice. Essen: Vulkan Verlag. 2007. 351 p.
12. **Орлов В.А., Петербургский Д.А.** Влияние температурного фактора на потребление электроэнергии при транспортировке воды по напорным трубопроводам. //Сантехника. Отопление. Кондиционирование. (С.О.К.), 2021, № 12, с. 20-25
13. **Орлов В.А., Зоткин С.П. Иншакова М.А., Петербургский Д.А.** «Расчет гидравлических параметров напорных труб при изменении температурных режимов». Свидетельство о государственной регистрации программы для ЭВМ № 2020661754 от 30.09.2020
14. **Альтшуль А.Д.** Гидравлические сопротивления.-М.: Недра.1970. 216 с.

Orlov Vladimir Alexandrovich, professor, doctor of technical sciences; National Research Moscow State University of Civil Engineering (NRU MGSU), Russia, 129337, Moscow, street Yaroslavskoe shosse, 26; tel. +7(917) 538-43-16; E-mail: OrlovVA@mgsu.ru.

Zotkin Sergey Petrovich, professor, candidate of technical sciences; Russia, National Research Moscow State University of Civil Engineering (NRU MGSU), 129337, Moscow, street Yaroslavskoe shosse, 26; tel. +7(980) 187-87-75; E-mail: ZotkinSP@mgsu.ru

Peterburgsky Dmitry Alexandrovich, post-graduate student; National Research Moscow State University of Civil Engineering (NRU MGSU), Russia, 129337, Moscow, street Yaroslavskoe shosse, 26; tel. +7(962) 360-32-91; E-mail: Piter.rus@inbox.ru

Орлов Владимир Александрович, профессор, доктор технических наук; Федеральное государственное бюджетное образовательное учреждение высшего образования «Национальный исследовательский Московский государственный строительный университет» (НИУ МГСУ), Россия, 129337, Москва, Ярославское шоссе, 26; тел. +7(917) 538-43-16; E-mail: OrlovVA@mgsu.ru.

Зоткин Сергей Петрович, профессор, кандидат технических наук; Россия, Федеральное государственное бюджетное образовательное учреждение высшего образования «Национальный исследовательский Московский государственный строительный университет» (НИУ МГСУ), 129337, Москва, Ярославское шоссе, 26; тел. +7(980) 187-87-75; E-mail: ZotkinSP@mgsu.ru.

Петербургский Дмитрий Александрович, аспирант; Федеральное государственное бюджетное образовательное учреждение высшего образования «Национальный исследовательский Московский государственный строительный университет» (НИУ МГСУ), Россия, 129337, Москва, Ярославское шоссе, 26; тел. +7(962) 360-32-91; E-mail: Piter.rus@inbox.ru

International Journal for Computational Civil and Structural Engineering, 18(4) 101–110 (2022)

DOI:10.22337/2587-9618-2022-18-4-101-110

EXPLICIT DIGITAL MODELS OF LINEAR COMPLEXES

Aleksandr N. Rozhkov [1,2], Vera V. Galishnikova [1,2]

[1] People's Friendship University of Russia (RUDN University), Moscow, RUSSIA

[2] National Research Moscow State University of Civil Engineering, Moscow, RUSSIA

Abstract: It is obvious that the interoperability of existing digital models is insufficient. Current research on model view definitions and on their semantic enrichment addresses the issue of good interpretation of the results of existing models to improve interoperability. The alternative research presented in this paper is not concerned with interpretation. Instead, the influence of modifications in the geometric and topological concepts of the digital models themselves on their interoperability is investigated. The geometric and topological attributes of the models are made as explicit as possible. Two-dimensional line drawings are replaced by three-dimensional linear complexes to reduce the need for implicit information. The topology of a complex is described with topological tables containing all elements of the model, thus replacing the geometric neighborhood concept of the industry foundation classes. A highly efficient algorithm for the construction of new topological tables of large buildings is presented. The difficulties encountered in modifying existing topological tables are analyzed and solved. Topological and geometric aspects of linear complexes that cannot be treated explicitly with topological tables are identified and presented.

Keywords: linear complex, cell, polyhedral partition, topological modeling, topological tables, topology, neighborhood

ЯВНЫЕ ЦИФРОВЫЕ МОДЕЛИ ЛИНЕЙНЫХ КОМПЛЕКСОВ

А.Н. Рожков [1,2], В.В. Галишникова [1,2]

[1] Российский университет дружбы народов, Москва, РОССИЯ

[2] Национальный исследовательский Московский государственный строительный университет, Москва, РОССИЯ

Аннотация: следует признать, что функциональная совместимость цифровых моделей, используемых в программных продуктах разных производителей, на данный момент не достигнута. Текущие исследования в этой области нацелены на усовершенствование интерпретации данных существующих моделей и их семантическом обогащении. Альтернативное исследование, представленное в данной статье, посвящено влиянию модификаций геометрических и топологических концепций самих цифровых моделей на их функциональную совместимость. Геометрические и топологические атрибуты моделей сделаны максимально явными. Двумерные линейные чертежи заменяются трехмерными линейными комплексами, чтобы уменьшить потребность в неявной информации. Топология комплекса описывается топологическими таблицами, содержащими все элементы модели, заменяя, таким образом, концепцию геометрического соседства, используемую в системе отраслевых базовых классов (IFC). Представлен высокоэффективный алгоритм построения новых топологических таблиц больших строительных объектов. Проанализированы и решены проблемы, возникающие при модификации существующих топологических таблиц. Выявлены и представлены топологические и геометрические аспекты линейных комплексов, которые не могут быть явно обработаны топологическими таблицами.

Keywords: линейный комплекс, ячейка, полиэдральное разбиение, топологическое моделирование, топологические таблицы, топология, соседство

INTRODUCTION

The information used in the design, construction and operation of buildings must be explicit, reliable and complete. Digital models of the buildings are the tool with which the information is assembled, distributed and applied. The models are constructed with

commercial software based on international standards. A widely used approach in the building industry are boundary representations of the building components and their assembly in a model using the industry foundation classes IFC [1].

The IFC were originally designed to be interoperable. Successful implementation of this concept would have permitted vendor-neutral automatic exchange of building information models in digital networks [2]. Because this goal has not been reached, the concepts on which the IFC are based and the manner, in which digital models based on IFC are interpreted, are the subjects of intensive current research [3–6].

The IFC are complex and voluminous, as they cover a very large number of topics in the building and construction industry. To permit the model users to focus on the specific information, which they require for their tasks, model view definitions MVD have been introduced [7]. A MVD specifies, which parts of an IFC data model needs to be implemented for a specific data exchange scenario. The MVD approach assumes that software companies will develop IFC export and import subroutines tailored for each MVD.

IFC Certification [8] for consistent and reliable implementations of IFC specifications by software vendors for multiple software platforms was developed. The procedure supports checks for collisions and voids using geometric attributes and element identities. The National BIM Standard initiative [9] facilitates information exchange through MVDs [10]. Interoperability is only guaranteed within a single MVD, not between different MVDs.

The semantic enrichment concept for building information models SeeBIM extends the MVD concept [11]. The concept postulates that IFC-based models contain both implicit and explicit information. To interpret both types of information, if-then rules are formulated using a predefined set of object types and operators. The operations include reading the building model, testing for geometrical and topological relationships, and creating new objects, properties, and relationships. The new and the enriched objects conform to the definitions of an MVD defined for the given subdomain.

Tools based on the MVD and SeeBIM concepts support the interpretation of the results of existing IFC-based models, but do not affect the models themselves. The question arises, whether unsatisfactory interoperability may not be due partly to inherent deficiencies of the IFC concept itself [2]. Such deficiencies cannot be remedied by concepts like MVD and SeeBIM. This paper analyzes the treatment of geometry and topology in the IFC concept, as described by Borrmann et al. [1], and investigates the use of topological tables as an alternative concept that promotes interoperability.

The most widely used approach to the modeling of geometric solids with IFC is Boundary Representation (Brep). Classes IfcFacetedBrep and IfcAdvancedBrep implement flat surfaces and surfaces with curved edges respectively for simply connected domains. Corresponding classes for multiply connected domains are

- IfcFactedBrepWithVoids and
- IfcAdvancedBrepWithVoids.

Solids such as walls and doors are constructed individually and aggregated to construct the IFC model.

The neighborhood of solids in an IFC model is described indirectly using classes that inherit from IfcObjectPlacement [1]. Each IFC solid has a local coordinate system, whose location in the model is specified in a common global coordinate system. This method is a geometric specification of neighborhood, which can increase the risk of collision of solids and voids between solids due to imprecise numerical attributes of the solids, especially their node coordinates.

This paper shows that the problematic geometric specification of neighborhood in IFC can be replaced by a truly topological specification of neighborhood: the contact of topological elements is described in topological tables. This is an example of the replacement of implicit information (the IFC user must convert

geometric location to topological neighborhood) to explicit information (the topological tables explicitly name the elements, with which a specified element is in contact).

EXPLICIT AND IMPLICIT INFORMATION FOR BUILDINGS

Buildings are traditionally planned with two-dimensional line drawings showing plans, elevations, sections and details of the project. The line drawing in figure 1 shows the plan and a section of a room. The drawings contain explicit information about the original, such as the dimensions of the building components and their projections to the plane of the drawing. The explicit information in a drawing is not sufficient to create a three-dimensional mental model of the three-dimensional original of the building. For example, building components in a plan are not explicitly associated with the same components in the elevations and sections. Some faces of components are not shown explicitly in the projections. The person reading the drawing must add implicit information to the explicit information to be able to create the mental model. Persons with different background, knowledge and experience add different implicit information. Implicit information is therefore a potential source of inconsistency, inaccuracy and errors in engineering practice. The aim of our research is to make models explicit.

The storage capacity and high speed of the digital environment provide an opportunity to lessen the need for implicit information. The strategy of our research project is to map as many of the topological and geometric properties of the original explicitly to the model as possible. The mapping is bijective, such that the information and insights gained with the model can be applied to the original, and vice versa. Line drawings remain a valuable tool in engineering practice. However, in the digital environment line drawings for selected parts of the project are prepared upon demand and for a specific purpose from a general computer model of the entire original that contains the explicit information describing the original.

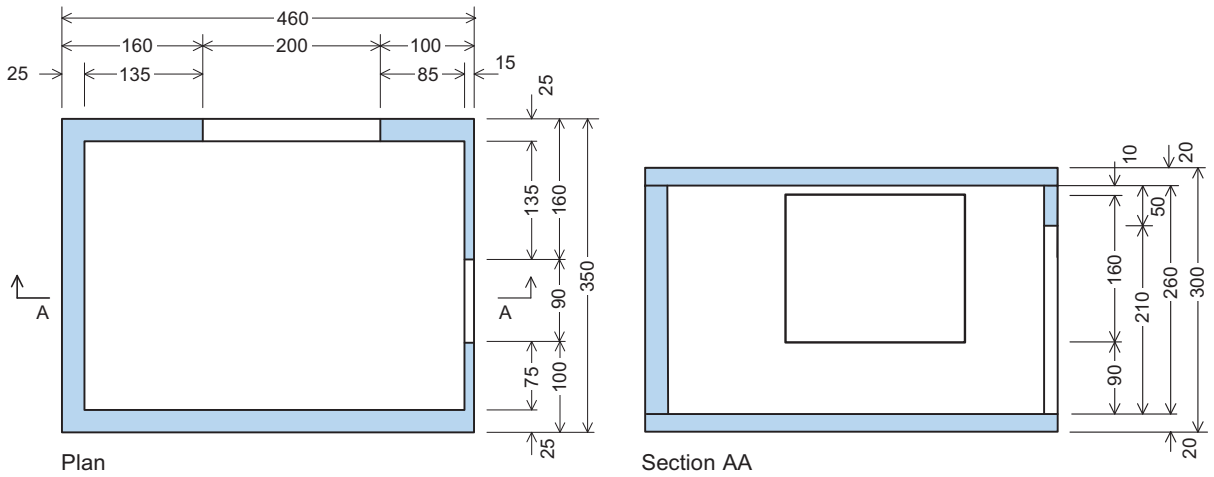

Figure 1. Line drawing showing the plan and a section of a room

LINEAR COMPLEXES

The character of explicit and implicit information is investigated for linear complexes. The linear complex for the room in figure 1 is shown in figure 2. A linear complex is a configuration composed of nodes, edges, faces and cells called the domains of the complex. A node is a single point. An edge is a straight line segment. A face is a plane area bounded by at least one closed polygonal curve composed of edges. A cell is a volume bounded by at least one closed polyhedral surface composed of

faces. A rank from 0 to 3 equal to their dimension is assigned to nodes, edges, faces and cells respectively to create a hierarchy.
A domain is described by its boundary. The boundary of a domain of rank n consists of domains of rank n-1. For example, the boundary of a cell consists of faces. The topology of a complex describes relations between its domains. For example, the topology specifies the edges of a cell. The geometry of a complex is specified with the global coordinates of its nodes and the rules for the shape interpolation between to nodes of the domains.

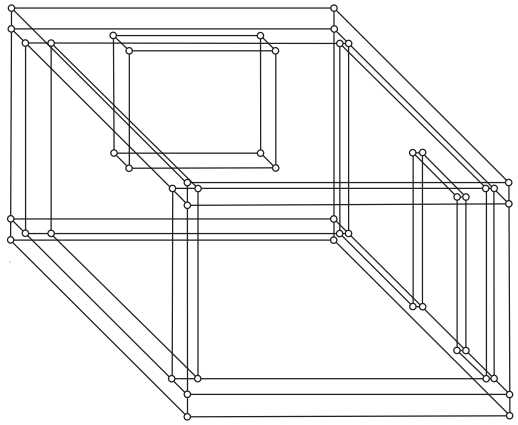

Figure 2. Perspective of the linear complex for the room in figure 1

The topology of a complex is unique. However, complexes with equal topology can have different geometries. For example, four nodes and four edges can form the boundary of a rectangular face. If the coordinates of two adjacent nodes are interchanged, the topology does not change, but two edges intersect at internal points such that they no longer form the boundary of face.

TOPOLOGICAL TABLES OF A COMPLEX

The complex, which is shown graphically in figure 2, is described alphanumerically in a computer model. A unique name is assigned to each domain of the complex. The node objects are collected in a map using the node name as key and the three global node coordinates as value of an entry. The topology of the complex is described with 12 topological tables. The first column of a table contains all components of a given type D_1 in the complex, for example all faces. The other columns of the table contain objects of another type D_2 in the complex, for example nodes. A row of the table contains the objects of type D_2, which are in contact with an object of type D_1. In the example, the table contains the nodes, which are in contact with a face of the complex. A topological table is named with the domain types D_1 and D_2, for example face-node-table.
A complex contains 4 types of domains: nodes, edges, faces and cells, one of which is placed in the first column of a table. Once the type for the first column has been selected, there are three remaining types, one of which is entered in the other columns. Some tables have a constant number of domains per row, for example the edge-node-table, whereas the number varies for others, for example the face-edge-table. The number of type combinations that can be formed for a table in this manner is 3*4. Figure 3 shows the 12 types of topological table arranged in matrix form.
Entry T_{kk} in the matrix is the set of the domains of rank k. It is not a topological table. The entries below the diagonal are tables showing the domains of rank m<k, which are components of the domain of rank k, for example the nodes which are components of a face. The entries above the diagonal are tables showing the domains of rank m>k, which have a common domain of type D_k. For example, T_{13} is the edge-cell-table which contains the cells of the complex that have a common edge.

CONSTRUCTION OF THE TOPOLOGICAL TABLES

Objects that are instances of industry foundation classes IFC describe their own topology. The topological relationship to other objects of the model is specified explicitly in special cases such as a common face of two cells. In general, the overall topology is not specified explicitly. Additional implicit topological information must be derived from the relative location of the

objects. The concept of our project is to describe the topology of all elements of the complex explicitly in common topological tables. This approach demands an efficient algorithm for the construction of large topological tables.
The topological tables in figure 3 are not independent. For example, the edge-node, face-edge and cell-face tables together define the topology of the complex completely. They are called base tables. The other tables can be derived from the base tables.

T_{km}		rank m , domain type			
		0 node	1 edge	2 face	3 cell
rank k, domain type	0 node	T_{00}	T_{01}	T_{02}	T_{03}
	1 edge	T_{10}	T_{11}	T_{12}	T_{13}
	2 face	T_{20}	T_{21}	T_{22}	T_{23}
	3 cell	T_{30}	T_{31}	T_{32}	T_{33}

Figure 3. Matrix of topological tables T_{km} for linear complexes

The base tables are specified by the user with a sequence of commands consisting of a key word *node, edge, face or cell* for the component type, followed by the name of the domain and a set of parameters. Each command defines one domain of the complex. The commands for a complex end with command *do*. The command sequence for the construction of the unit cube in figure 4 is shown in figure 5.

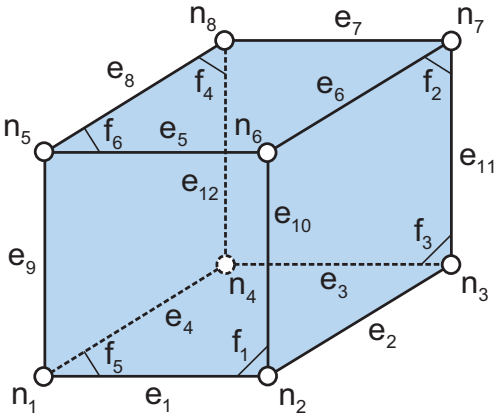

Figure 4. Perspective of a unit cube

Because the commands can be specified in arbitrary order, a command can contain objects that have not yet been defined. For example, the objects for the four edge objects in command *face* f2 (e2, e11, e6, e10) in figure 5 are not yet constructed.

```
cell   c1 (f1, f2, f3, f4, f5, f6)
face   f1  (e1, e10, e5, e9)
face   f2  (e2, e11, e6, e10)
face   f3  (e4, e11, e7, e12)
face   f4  (e2, e12, e8, e9)
face   f5  (e1, e2, e3, e4)
face   f6  (e5, e6, e7, e9)
edge   e1 (n1, n2)
edge   e2 (n2, n3)
edge   e3 (n3, n4)
edge   e4 (n4, n1)
edge   e5 (n5, n6)
edge   e6 (n6, n7)
edge   e7 (n7, n8)
edge   e8 (n5, n8)
edge   e9 (n1, n5)
edge   e10 (n2, n6)
edge   e11 (n3, n7)
edge   e12 (n4, n8)
node   n1 (0.0, 0.0, 0.0)
node   n2 (0.0, 1.0, 0.0)
node   n3 (0.0, 1.0, 1.0)
node   n4 (0.0, 0.0, 1.0)
node   n5 (1.0, 0.0, 0.0)
node   n6 (1.0, 1.0, 0.0)
node   n7 (1.0, 1.0, 1.0)
node   n8 (1.0, 0.0, 1.0)
do
```

Figure 5. Commands for a unit cube

When command *face* is interpreted, a persistent *Face* object is constructed and its edge attributes a persistent *Face* object is constructed and its edge attributes are set to null. The face is entered in a face map with the face name as key and the reference of the *Face* object as value. The names of the edges and the reference of the persistent Face object are stored in a transient shadow edge object. When command *do* is reached, all persistent objects of the complex

have been constructed and entered in the map. The set of shadow objects is traversed. The names of the edges are used to read the references of the persistent *Edge* objects in the map, which are then stored in the persistent *Face* object. After command *do* has been executed, the independent topological tables exist on the data base.

For navigation in the complex, the other topological tables in the matrix in figure 3 must be constructed. An efficient algorithm has been developed to derive the dependent tables form the specified independent tables as follows. Because any object of class *Edge*, *Face* or *Cell* refers only to the objects describing domains of the next lower rank, the 12 tables can be constructed in four nested loops. The algorithm, which is used to add an element to a map, must automatically suppress multiple entries of the same object. The following operations are performed in the loops:

1. Loop over the cells *c* of the complex.
2. Loop over the faces *f* of cell *c*.
   - add face *f* to the cell-face map with key *c*
   - add cell c to the face-cell map with key *f*
3. Loop over the edges *e* of face *f* of cell *c*
   - add edge *e* to the cell-edge map with key *c*
   - add edge *e* to the face-edge map with key *f*
   - add face *f* to the edge-face map with key *e*
   - add cell *c* to the edge-cell map with key *e*
4. Loop over the nodes *n* of edge *e* of face *f* of cell *c*
   - add node *n* to the cell-node map with key *c*
   - add node *n* to the face-node map with key *f*
   - add node *n* to the edge-node map with key *e*
   - add cell *c* to the node-cell map with key *n*
   - add face *f* to the node-face map with key *n*
   - add edge *e* to the node-edge map with key *n*

The innermost loop 4 can be avoided by arranging the six add-operations in a method with node *n* as parameter, and invoking the method twice in loop 3 to treat the two nodes of the current edge. The outer loop over the cells constructs the cell-face and the face-cell tables. The first nested loop over the faces constructs the cell-edge, face-edge, edge-cell and edge-face tables. The second nested loop constructs the remaining tables. As an example, the topological tables for the unit cube in figure 4 are presented in tables 1 to 4.

The complexity of the table construction algorithm is determined by counting the number of add-operations for the tables:

- Loop 1 is performed N_c times, where N_c is the number of cells in the complex
- Loop 2 is performed N_f times per cycle of loop 1, where N_f is the average number of faces per cell. The total number of traversals of loop 2 is $N_c \cdot N_f$. Two domains are added per cycle.
- Loop 3 is performed N_e times per cycle of loop 2, where N_e is the average number of edges per face. The total number of traversals of loop 3 is $N_c \cdot N_f \cdot N_e$. Four domains are added per cycle.
- Loop 4 is performed twice per cycle of loop 3, where 2 is the number of nodes per edge. The total number of traversals of loop 4 is $2 \cdot N_c \cdot N_f \cdot N_e$. Six domains are added per cycle.

Table 1. Node-edge, Node-face and Node-cell Tables

node	edges	faces	cells
n1	e1, e4, e9	f1, f4, f5	c1
n2	e1, e2, e10	f1, f2, f5	c1
n3	e2, e3, e11	f2, f3, f5	c1
n4	e3, e4, e12	f3, f4, f5	c1
n5	e5, e8, e9	f1, f4, f6	c1
n6	e5, e6, e10	f1, f2, f6	c1
n7	e6, e7, e11	f2, f3, f6	c1
n8	e7, e8, e12	f3, f4, f6	c1

Table 2. Edge-node, edge-face and edge-cell tables

edge	nodes	faces	cells
e1	n1, n2	f1, f5	c1
e2	n2, n3	f2, f5	c1
e3	n3, n4	f3, f5	c1
e4	n1, n4	f4, f5	c1
e5	n5, n6	f1, f6	c1
e6	n6, n7	f2, f6	c1
e7	n7, n8	f3, f6	c1
e8	n5, n8	f4, f6	c1
e9	n1, n5	f1, f4	c1
e10	n2, n6	f1, f2	c1
e11	n3, n7	f2, f3	c1
e12	n4, n8	f3, f4	c1

Table 3. Face-node, face-edge, face-cell tables

face	nodes	edges	cells
f1	n1, n2, n5, n6	e1, e5, e9, e10	c1
f2	n2, n3, n6, n7	e2, e6, e10, e11	c1
f3	n3, n4, n7, n8	e3, e7, e11, e12	c1
f4	n1, n4, n5, n8	e4, e8, e9, e12	c1
f5	n1, n2, n3, n4	e1, e2, e3, e4	c1
f6	n5, n6, n7, n8	e5, e6, e7, e8	c1

Table 4. Cell-node, cell-edge, cell-face tables

cell	nodes	edges	faces
c1	n1, n2, n3, n4, n5, n6, n7, n8	e1, e2, e3, e4, e5, e6, e7, e8, e9, e10, e11, e12	f1, f2, f3, f4, f5, f6

The total number N_t of add-operations for the construction of the topological tables is:

$$N_t = 2N_cN_f + 4N_cN_fN_e + 12N_cN_fN_e \approx \approx 16N_cN_fN_e \quad (1)$$

Usually the average number of cells per face N_f and the average number of edges per face N_e are independent of the size of a complex. The complexity of the algorithm then is $O(N_c)$, which is highly efficient.

MODIFICATION OF LINEAR COMPLEXES

Engineering design proceeds in cycles of work steps, during which a complex changes continuously. Three types of modification occur in a design cycle:

- addition of new domains
- removal of old domains
- modification of attributes of old domains.

The identification of the old values of type D_2, which must be removed in the topological tables due to a modification, requires extensive

searches. It is more efficient to group the commands of a modification and to construct new tables for the modified complex defined by the command group. This concept is followed in the project.

An additional command type *remove* nameset is defined for the removal of domains. The entries for the objects in the set are removed from the base tables. The existing command types *node, edge, face* and *cell* are used to add new domains to the base tables and to construct their persistent objects as before. The same command types are used to modify the attributes of old domains whose entries in the base tables already exist. The attributes of these domains are modified in their persistent objects. When command *do* is executed, the modified base tables are used as input stream for the construction algorithm described in section 4. The complexity for a modification group equals the complexity of the construction of the initial topological tables.

Figure 6 shows a modified unit cube. Figure 7 shows the command group for the modification of the unit cube. Node n_6 is removed. Edges e_5, e_6 and e_{10} as well as faces f_1, f_2 and f_6 are modified. Nodes n_9 to n_{15}, edges e_{13} to e_{21} and faces f_7 to f_9 are new.

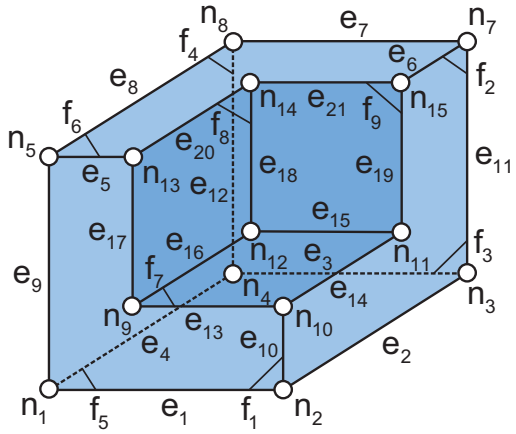

Figure 6. Perspective of the modified unit cube

Cell c_1 is modified. The constructed tables are similar to those shown for the unit cube in tables 1 to 4.

```
remove node n6
edge   e5    (n5, n13)
edge   e6    (n7, n15
edge   e10   (n2, n10)
face   f1    (e1, e10, e13, e17, e5, e9)
face   f2    (e2, e11, e6, e19, e14, e10
face   f6    (e5, e20, e21, e6, e7, e8)
node   n9    (0.5, 0.5, 0.0)
node   n10   (0.5, 1.0, 0.0)
node   n11   (0.5, 1.0, 0.5)
node   n12   (0.5, 0.5, 0.5)
node   n13   (1.0, 0.5, 0.0)
node   n14   (1.0, 0.5, 0.5)
node   n15   (1.0, 1.0, 0.5)
edge   e13   (n9, n10)
edge   e14   (n10, n11)
edge   e15   (n11, n12)
edge   e16   (n12, n9)
edge   e17   (n9, n13)
edge   e18   (n12, n14)
edge   e19   (n11, n15)
edge   e20   (n13, n14)
edge   e21   (n14, n15)
face   f7    (e13, e14, e15, e16)
face   f8    (e16, e17, e18, e20)
face   f9    (e15, e18, e19, e21)
cell   c1    (f1, f2, f3, f4, f5, f6, f7, f8, f9)
do
```

Figure 7. Commands for the modification

CONCLUSIONS

The investigation has shown that topological tables can be constructed efficiently for linear complexes representing entire buildings. The necessity to combine the individual topology of a large set of standardized building components in the model is thus eliminated. The complexity of the table construction algorithm developed in the project is linear in the number of cells and thus very efficient. Topological tables for modified complexes are constructed with the same algorithm as the tables for the initial complex.

Topological tables do not make all of the properties of an original explicit in the model.

The closed polygonal curves of the boundaries of faces and the closed polyhedral surfaces of the boundaries of cells are not specified explicitly in the tables. Faces and cells therefore cannot be oriented in the tables. As a result, topological tables do not show explicitly whether the bounded or the unbounded area defined by a closed curve in a plane is the interior of the face. Similarly, the tables do not show explicitly whether the bounded or the unbounded volume defined by a closed surface is the interior of a cell. Due to these deficiencies, it is not possible to differentiate explicitly between simply and multiply connected faces and cells of complexes. Other topics for further research are the robustness of the algorithms for complexes, unbounded domains for complete models of the environment of buildings and handling of concave domains without the necessity for convex triangulation. These topics are being investigated in an associated research project.

ACKNOWLEDGEMENTS

The research is funded by the Russian Foundation for Basic Research (RFBR) – Project Number 20-57-12006.

REFERENCES

1. **Borrmann A.**, **Beetz J., Koch C., Liebich T., Muhic S.** Section 5.7. Geometric Representations. In: Borrmann A., König M., Koch C., Beetz J., eds. Building Information Modelling. Cham: Springer; 2018, pp. 101-111, DOI: 10.1007/978-3-319-92862-3_5
2. **van Berlo L., Krijnen T., Tauscher H., Liebich T.** Future of the Industry Foundation Classes: towards IFC 5, in: Proc. of the 38th International Conference of CIB W78, 2021, pp. 123-137
3. **Huhnt W., Galishnikova V.** Partitioning of space as basis for data structures to describe digital building models, in: Proc. of the 17th International Conference on Computing in Civil and Building Engineering, 2018, pp. 42-49
4. **Huhnt W.** Reconstruction of edges in digital building models. // Advanced Engineering Informatics, 2018, V. 38, pp. 474-487. DOI: 10.1016/j.aei.2018.08.004
5. **Huhnt W., Hartmann T., Suter G.** Space classification from point clouds of indoor environments based on reconstructed topology. In: Smith I., Domer B., eds. Advanced Computing Strategies for Engineering, 25th EG-ICE International Workshop. Cham: Springer; 2018, V. 10863, pp. 82-102. DOI: 10.1007/978-3-319-91635-4_5
6. **Kraft B., Huhnt W.** Geometrically Complete Building Models // Proc. of the 21th International Workshop of the European Group for Intelligent Computing in Engineering, 2014, pp. 1-11
7. **Belsky M., Sacks R., Brilakis I.** Semantic Enrichment for Building Information Modeling // Computer-Aided Civil and Infrastructure Engineering, 2016, V. 31, No. 4, pp. 261-274. DOI: 10.1111/mice.12128
8. **Steinmann R.** IFC Certification 3.0: Specifications and Terms and Conditions. BuildingSMART International Ltd., UK; 2018. URL https://www.buildingsmart.org
9. National BIM Standard-United States Version 2 (NBIMS-US 2012). The National Institute of Building Sciences
10. **Hietanen J., Find S.** IFC model view definition format, in: Proceedings of the 24th International Conference of CIB W78, 2007, pp. 1-29
11. **Bloch T., Sacks R.** Clustering Information Types for Semantic Enrichment of Building Information Models to Support Automated Code Compliance Checking // J. Comput. Civ. Eng., 2020, V. 34, No. 6, 04020040. DOI: 10.1061/(ASCE)CP.1943-5487.0000922

СПИСОК ЛИТЕРАТУРЫ

1. **Borrmann A.**, **Beetz J., Koch C., Liebich T., Muhic S.** Section 5.7. Geometric Representations. In: Borrmann A., König M., Koch C., Beetz J., eds. Building Information Modelling. Cham: Springer; 2018, pp. 101-111. DOI: 10.1007/978-3-319-92862-3_5
2. **van Berlo L., Krijnen T., Tauscher H., Liebich T.** Future of the Industry Foundation Classes: towards IFC 5, in: Proc. of the 38th International Conference of CIB W78, 2021, pp. 123-137
3. **Huhnt W., Galishnikova V.** Partitioning of space as basis for data structures to describe digital building models, in: Proc. of the 17th International Conference on Computing in Civil and Building Engineering, 2018, pp. 42-49
4. **Huhnt W.** Reconstruction of edges in digital building models. // Advanced Engineering Informatics, 2018, V. 38, pp. 474-487. DOI: 10.1016/j.aei.2018.08.004
5. **Huhnt W., Hartmann T., Suter G.** Space classification from point clouds of indoor environments based on reconstructed topology. In: Smith I., Domer B., eds. Advanced Computing Strategies for Engineering, 25th EG-ICE International Workshop. Cham: Springer; 2018, V. 10863, pp. 82-102. DOI: 10.1007/978-3-319-91635-4_5
6. **Kraft B., Huhnt W.** Geometrically Complete Building Models // Proc. of the 21th International Workshop of the European Group for Intelligent Computing in Engineering, 2014. pp. 1-11
7. **Belsky M., Sacks R., Brilakis I.** Semantic Enrichment for Building Information Modeling // Computer-Aided Civil and Infrastructure Engineering, 2016, V. 31, No. 4, pp. 261-274. DOI: 10.1111/mice.12128
8. **Steinmann R.** IFC Certification 3.0: Specifications and Terms and Conditions. BuildingSMART International Ltd., UK; 2018. URL https://www.buildingsmart.org
9. National BIM Standard-United States Version 2 (NBIMS-US 2012). The National Institute of Building Sciences
10. **Hietanen J., Find S.** IFC model view definition format, in: Proceedings of the 24th International Conference of CIB W78, 2007, pp. 1-29
11. **Bloch T., Sacks R.** Clustering Information Types for Semantic Enrichment of Building Information Models to Support Automated Code Compliance Checking // J. Comput. Civ. Eng., 2020, V. 34, No. 6, 04020040. DOI: 10.1061/(ASCE)CP.1943-5487.0000922

Aleksandr N. Rozhkov, Senior Lecturer at the Department of Fundamental Education, branch of National Research Moscow State University of Civil Engineering in Mytishchi, 129337, Russia, Moscow, Yaroslavskoe Shosse, 26; assistant of the Department of Civil Engineering of the Engineering Academy of the People's Friendship University of Russia, 117198, Russia, Moscow, st. Miklukho-Maclay, 6; phone: +7(925)023-83-76. e-mail: rozhkovalex@hotmail.com.

Vera V. Galishnikova, Professor, Dr.Sc.; Vice-Rector of the National Research Moscow State University of Civil Engineering, 129337, Russia, Moscow, Yaroslavskoe Shosse, 26; Professor of the Department of Civil Engineering of the Engineering Academy of the People's Friendship University of Russia, 117198, Russia, Moscow, st. Miklukho-Maclay, 6; phone: +7 (495) 287-49-14. e-mail: galishni@yandex.ru.

Рожков Александр Николаевич, старший преподаватель кафедры Фундаментального образования филиала НИУ МГСУ в г. Мытищи, 129337, Россия, г. Москва, Ярославское шоссе, д. 26; ассистент департамента строительства инженерной академии Российского университета дружбы народов, 117198, Россия, г. Москва, ул. Миклухо-Маклая, 6; тел. +7(925) 023-83-76. e-mail: rozhkovalex@hotmail.com.

Галишникова Вера Владимировна, профессор, доктор технических наук, проректор Национального исследовательского Московского государственного строительного университета, 129337, Россия, г. Москва, Ярославское шоссе, д. 26; профессор департамента строительства инженерной академии Российского университета дружбы народов, 117198, Россия, г. Москва, ул. Миклухо-Маклая, 6; тел. +7 (495) 287-49-14. e-mail: galishni@yandex.ru.

DOI:10.22337/2587-9618-2022-18-4-111-123

DINAMIC FORCES IN THE ECCENTRICALLY COMPRESSED MEMBERS OF REINFORCED CONCRETE FRAMES UNDER ACCIDENTAL IMPACTS

Sergey Yu. Savin [1], Natalia V. Fedorova [1], Vitaly I. Kolchunov [1,2]

[1]National Research Moscow State University of Civil Engineering, Moscow, RUSSIA
[2]Southwest state university, Kursk, RUSSIA

Abstract: Interest to solving scientific problems related to the evaluation of facilities' resistance and its protection against progressive collapse increases and attracts more and more attention of specialists in the field of structural analysis and design. Therefore, the article presents the results of a computational analysis of dynamic forces in eccentrically compressed reinforced concrete members of structures under accidental impact such as sudden removal of a load bearing member. Using relations for specific deformation energy and integrating it through the cross-section area, the analytical expressions for dynamic strains and curvatures have been obtained for physically and structurally nonlinear RC frame members under eccentric compression. These expressions in some cases allow symbolic solution, for example, in MathCAD software. In contrary, it can be solved with the approximate iterative method. To assess the reliability and effectiveness of the proposed quasi-static method, the analysis of the cast-in-situ reinforced concrete frame resistance to progressive collapse has been performed. The article also provides comparison of the simulation results of the nonlinear quasi-static analysis and the nonlinear dynamic time-history analysis.

Keywords: reinforced concrete, eccentric compression, accidental impacts, energy dissipation, dynamic effect, quasi-static analysis

ДИНАМИЧЕСКИЕ ЭФФЕКТЫ ВО ВНЕЦЕНТРЕННО СЖАТЫХ ЖЕЛЕЗОБЕТОННЫХ ЭЛЕМЕНТАХ МНОГОЭТАЖНЫХ ЗДАНИЙ ПРИ ОСОБЫХ ВОЗДЕЙСТВИЯХ

С.Ю. Савин [1], Н.В. Федорова [1], В.И. Колчунов [1,2]

[1] Национальный исследовательский Московский государственный строительный университет, г. Москва, РОССИЯ
[2] Юго-Западный государственный университет, г. Курск, РОССИЯ

Аннотация: Решение научных задач, связанных с проблемой живучести и защиты зданий и сооружений от прогрессирующего обрушения при особых воздействиях привлекает все более значительное внимание специалистов в области расчета и проектирования строительных конструкций, зданий и сооружений. В рассматриваемой статье приведены результаты расчетного анализа динамических догружений внецентренно сжатых железобетонных элементов конструктивных систем при их структурной перестройке, вызываемой аварийными воздействиями. Для таких физически и конструктивно нелинейных систем, применительно к рассматриваемому напряженному состоянию на энергетической основе путем интегрирования выражений удельной энергии деформации волокна (фибры) по высоте расчетного сечения железобетонного элемента получены аналитические выражения для динамических деформаций и кривизн этого элемента. Структура уравнений в отдельных случаях допускает их решение в символьном виде, например, в ПК MathCAD, либо они решаются одним из приближенных методов. Для оценки достоверности и эффективности предложенного квазистатического метода выполнен расчёт живучести монолитной железобетонной рамы каркаса пятиэтажного здания и приведено сопоставление результатов нелинейного расчетного анализа по квазистатическому методу и методу прямого динамического расчета.

Ключевые слова: железобетон, внецентренное сжатие, особое воздействия, диссипация, динамический эффект, квазистатический метод

INTRODUCTION

Interest to solving scientific problems related to the structures' progressive (disproportional) collapse resistance under special impacts increases and attracts more and more attention of specialists in the field of structural design and analysis as evidenced by the number of research articles published over the past two decades. In many countries including Russia, the theoretical [1-8] and experimental [9-14] studies have been performed that became the basis for development and introduction of new regulatory documents for the facilities' protection against progressive collapse under accidental impacts [15-18]. Currently, the most complex and debatable question in the considered field is the assessment of the dynamic effects in structural systems during forces' redistribution through the alternate load paths, when accidental impact occurred [20].

For the assessment of such a dynamic effect in composite nonlinear deformable bars under instantaneous structural transformation, G.A. Geniyev proposed energy approach [21, 22]. Later, V.I. Kolchunov, N.V. Fedorova, N.B. Androsova, P.A. Korenkov and etc. [22-26] developed this approach. Their papers provide solutions for uniaxial compression and tension, as well as in transverse bending. They obtain the upper limit values of the forces and the lower limits of deformations in absolute value. With regard to cases of a more complex stress-strain state, the assessment of dynamic effects during the instantaneous load bearing member removal requires integrating the expressions for the specific strain energy over the cross-section area. However, such an approach may be associated with some computational difficulties when constructing the energy expressions, especially for structures with inelastic second-order effects. Therefore, we consider a simplified practical method for assessment the dynamic effects in physically nonlinear eccentrically compressed (or eccentrically tensioned) reinforced concrete bars. Due to the phenomenon of buckling in such members, the bending moment acting in cross-sections is a function of the axial force. In this case, the ultimate bending moment perceived by the cross-section also depend on the magnitude of the acting axial force. This leads to the fact that the moment vs. curvature interaction diagram of such element changes during loading. In addition, there is a decrease in the magnitude of the ultimate forces in flexible eccentrically compressed reinforced concrete members in comparison with those one for members of zero slenderness ratio, i.e., for the cross-section pure strength [29], that can be explained as inelastic second-order instability. These circumstances must be considered when constructing a simplified method for estimating the dynamic effects in eccentrically compressed members of frame structures under accidental actions.

MATERIALS AND METHODS

Let us consider an eccentrically compressed reinforced concrete element of unit length subjected to the external axial force N_{ext} and the bending moment M_{ext} as *Figure 1,a* shows. Because of external forces, the internal forces arise in the element cross-sections: $N_{int} = N_{ext}$, $M_{int} = M_{ext}$. For practical purposes, we neglect the increments of the axial force and bending moment along the unit length of the bar under consideration since its size dL is sufficiently small.

Considering the strain diagram in *Figure 1,b*, the internal axial force acting in the cross-section is equal to (1):

$$N_{int} = \varepsilon_{av} B_{N0} = \varepsilon_{av} E_b A_{b,red} = N_{ext}, \qquad (1)$$

where ε_{av} is the average strain value within the cross-section, E_b is the tangent modulus of elasticity of normal weight concrete at a stress of $\sigma = 0$ and at 28 days; $A_{b,red}$ is the reduced cross sectional area. It should be noted, that $A_{b,red}$ is the function of the axil force N.

If we approximate the moment - curvature interaction diagram with the second order

polynomial, the internal bending moment can be obtained from Eq. (2):

$$M_{int} = \chi B_{M0}\left(1 - \frac{\chi}{2\chi_0}\right) = M_{ext}, \qquad (2)$$

where χ is the curvature of the deformed cross-section, $B_{M0} = E_b J_{b,red}$ is the initial (or undeformed) bending stiffness, χ_0 is the curvature corresponding the ultimate moment M_{ult} as *Figure 1,d* shows.

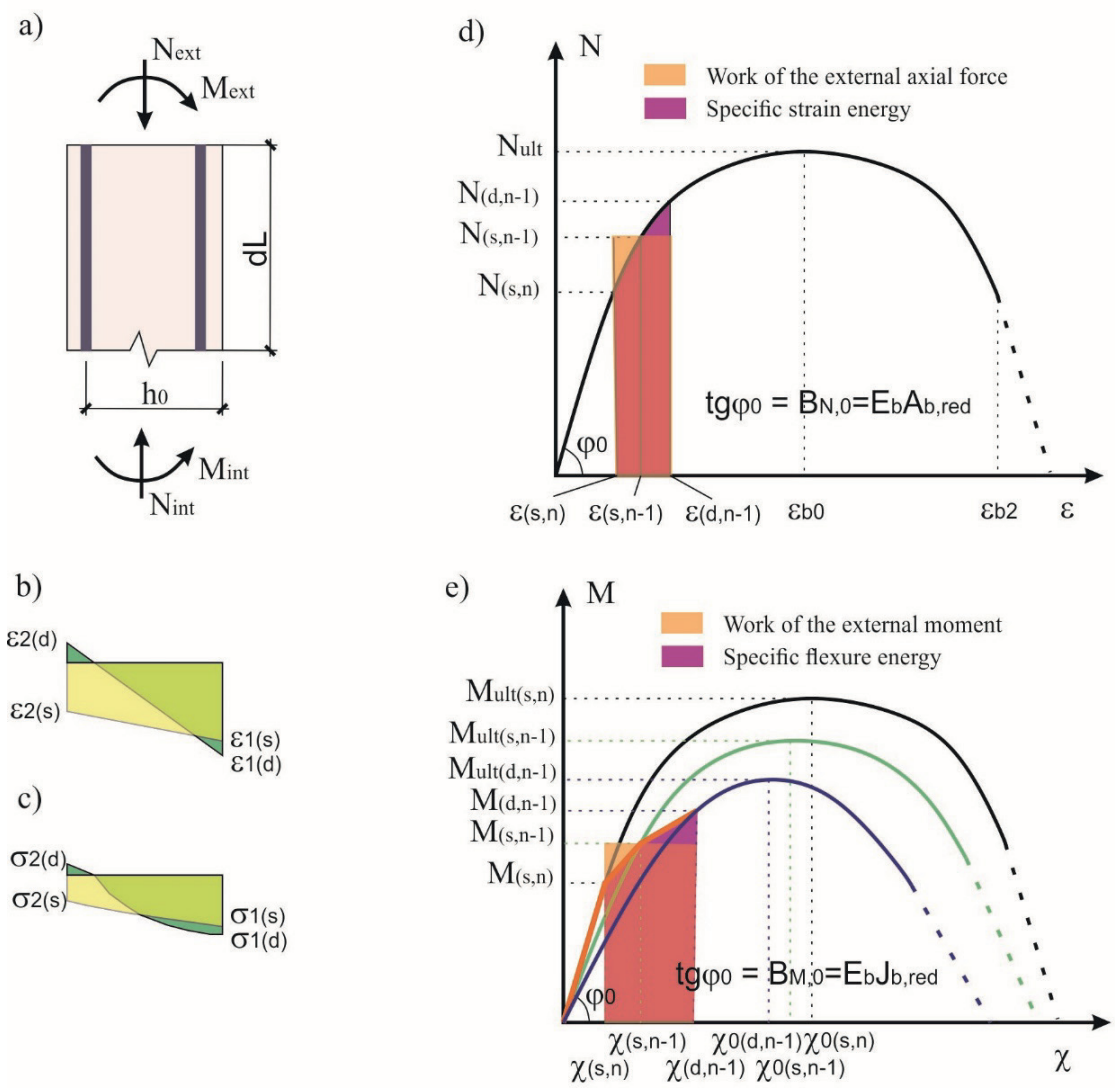

Figure 1. Eccentrically compressed reinforced concrete element: a) design scheme; b) strain diagram; c) normal stresses' diagram; d) scheme of the axial forces vs. strain diagram; e) moment vs. curvature diagram

In the first approximation, we find the curvature χ_0 using the expression for the ultimate bending moment of an eccentrically compressed element, according to SP 63.13330:

$$\chi_0 = \frac{0.8\varepsilon_{b2}}{x}, \qquad (3)$$

where ε_{b2} is the ultimate compressive strain in concrete, x is the neutral axis depth for rectangular compressive stresses diagram in concrete in accordance with 8.1.14 SP63.13330:

$$\begin{cases} x = \dfrac{N + R_{sn}A_s - R_{scn}A'_s}{R_{bn}b} \; for\; \xi \le \xi_R, \\ x = \dfrac{N + R_{sn}A_s\dfrac{1+\xi_R}{1-\xi_R} - R_{scn}A'_s}{R_{bn}b + \dfrac{2R_{sn}A_s}{h_0(1-\xi_R)}} \; for\; \xi > \xi_R. \end{cases} \quad (4)$$

In contrast to SP 63.13330, the formulas (4) adopt characteristic strength of materials in regard with SP 385.132580 requirements for a special limit state criterion. Characteristic compressive strength of steel reinforcement $R_{sc,n}$ corresponds to strain ε_s = 0.0035 which is restricted by ultimate compressive strain in concrete. $\xi = x/h_0$ is the relative depth of the neutral axis, ξ_R is the boundary relative depth of the neutral axis.

The coefficient 0.8 adopted in formula (3) reflects the ratio between the depth of the neutral axis for the rectangular distribution of normal stresses in the compressed zone and the actual depth of the neutral axis. It should be replaced with 0.7 for concrete of compressive strength classes B70-B100. Popov D. [28] provides the values of this coefficient for corrosion-damaged reinforced concrete elements under dynamic loading.

Following the approach proposed by G.A. Geniyev [20], we accept the principle of constancy of the total specific strain energy. In addition, we introduced the assumption that this principle meets to compression and bending separately with an enough accuracy for practical purposes. As a result, we obtain a system of equations in which the first one can be resolved with respect to the strain $\varepsilon_{d,n-1}$, and the second one resolved with respect to the strain $\varepsilon_{d,n-1}$ and curvature $\chi_{d,n-1}$:

$$\begin{cases} \Phi(\varepsilon_{d,n-1}) - \Phi(\varepsilon_{s,n}) = N_{s,n-1}(\varepsilon_{d,n-1} - \varepsilon_{s,n}); \\ \Phi(\chi_{d,n-1}) - \Phi(\chi_{s,n}) = M_{s,n-1}(\chi_{d,n-1} - \chi_{s,n}), \end{cases} \quad (5)$$

where $\Phi(\varepsilon_{d,n-1})$ is the specific strain energy for uniaxial dynamic compression caused by sudden load bearing structural member removal and determined from Eq. (6):

$$\Phi(\varepsilon_{d,n-1}) = B_N \int_0^{\varepsilon_{d,n-1}} \left(\varepsilon - \frac{\varepsilon^2}{2\varepsilon_{b0}}\right) d\varepsilon = \\ = \frac{E_b A_{b,red}\varepsilon^2_{d,n-1}}{2}\left(1 - \frac{\varepsilon_{d,n-1}}{3\varepsilon_{b0}}\right). \quad (6)$$

$\Phi(\varepsilon_{s,n})$ is the specific strain energy for uniaxial compression with service load before sudden load bearing structural member removal and determined from Eq. (7):

$$\Phi(\varepsilon_{s,n}) = B_N \int_0^{\varepsilon_{s,n}} \left(\varepsilon - \frac{\varepsilon^2}{2\varepsilon_{b0}}\right) d\varepsilon = \\ = \frac{E_b A_{b,red}\varepsilon^2_{s,n}}{2}\left(1 - \frac{\varepsilon_{s,n}}{3\varepsilon_{b0}}\right) \quad (7)$$

$\Phi(\chi_{d,n-1})$ is the specific flexure energy for uniaxial dynamic compression caused by sudden load bearing structural member removal and determined from Eq. (8):

$$\Phi(\chi_{d,n-1}) = B_M \int_0^{\chi_{d,n-1}} \left(\chi - \frac{\chi^2}{2\chi_0}\right) d\varepsilon \\ = \frac{E_b J_{b,red}\chi^2_{d,n-1}}{2}\left(1 - \frac{\chi_{d,n-1}}{3\chi_{0,d,n-1}}\right). \quad (8)$$

$\Phi(\chi_{s,n})$ is the specific flexure energy for uniaxial compression with service load before sudden load bearing structural member removal and determined from Eq. (9):

$$\Phi(\chi_{s,n}) = B_M \int_0^{\chi_{s,n}} \left(\chi - \frac{\chi^2}{2\chi_0}\right) d\varepsilon = \\ = \frac{E_b J_{b,red} \chi_{s,n}^2}{2}\left(1 - \frac{\chi_{s,n}}{3\chi_{0,s,n}}\right). \quad (9)$$

$N_{s,n-1}(\varepsilon_{d,n-1} - \varepsilon_{s,n})$ is the specific work under compression after the sudden load bearing structural member removal,

$M_{s,n-1}(\chi_{d,n-1} - \chi_{s,n})$ is the specific work under flexure after the sudden load bearing structural member removal.

The Eqs. (10)…(14) allow determining geometric parameters for the above mentioned relation:

$$A_{b,red} = b \int_{-0.5h}^{0.5h} \left(1 - \frac{\varepsilon}{2\varepsilon_{b0}}\right) dy + \frac{E_{s1}}{E_b} A_s + \frac{E_{s2}}{E_b} A'_s, \quad (10)$$

Where

$$\varepsilon = \varepsilon_{av} + \chi \cdot y, \quad (11)$$

$$S_{b,red} = b \int_{-0.5h}^{0.5h} \left(1 - \frac{\varepsilon}{2\varepsilon_{b0}}\right) y dy - \frac{E_{s1}}{E_b} A_s (0.5h - a) + \frac{E_{s2}}{E_b} A'_s (0.5h - a'), \quad (12)$$

$$y_{g.c.} = \frac{S_{b,red}}{A_{b,red}}, \quad (13)$$

$$J_{b,red} = b \int_{-0.5h+y_{g.c.}}^{0.5h+y_{g.c.}} \left(1 - \frac{\varepsilon}{2\varepsilon_{b0}}\right) y^2 dy + \frac{E_{s1}}{E_b} A_s \left(0.5h + y_{g.c.} - a\right)^2 \\ + \frac{E_{s2}}{E_b} A'_s \left(0.5h - y_{g.c.} - a'\right)^2. \quad (14)$$

Eqs. (10) … (14) apply the following symbols:

y is the current depth from geometrical cross sectional gravity center in Eqs. (10), (12) and from physical cross sectional gravity center in Eq. (14);

ε_{b0} is the compressive strain in concrete at the ultimate compressive stresses $\sigma = R_{b,n}$;

E_{s1}, E_{s2} are moduli of deformation for reinforcement steel in tension and in compression at current strain values in accordance with stress vs. strain curve;

A_s, A'_s are the cross sectional areas of reinforcement steel in tension and in compression respectively;

b is the cross-sectional width out of bending moment plane;

h is the overall cross-sectional depth in the bending plane;

a, a' are the distances from gravity centers of reinforcement in tension and compression respectively to the concrete surfaces;

$S_{b,red}$ is first moment of area for reduced cross-section measured from geometrical gravity center;

$y_{g.c.}$ is the distance between geometrical and physical gravity centers of the cross-section when the positive direction is to the most compressed face;

$J_{b,red}$ is the moment of inertia of the reduced cross-section with respect to physical gravity center.

After substitutions (1), (6), (7) and mathematical operations, the first equation of system (5) transforms into a 4th-oreder polynomial with respect to $\varepsilon_{av(d,n-1)}$ that is the average cross-sectional strain under dynamic loading (15):

$$\varepsilon_{av(d,n-1)}^4 \frac{b \cdot h}{12} - \varepsilon_{av(d,n-1)}^3 \left(\frac{b \cdot h}{6} + \frac{b \cdot h}{4\varepsilon_{b0}} + \frac{A_s \cdot E_{s1}}{6E_b} + \frac{A'_s \cdot E_{s2}}{6E_b} \right) + \\ + \varepsilon_{av(d,n-1)}^2 \left(\frac{b \cdot h}{2} + \frac{A_s \cdot E_{s1}}{2E_b} + \frac{A'_s \cdot E_{s2}}{2E_b} \right) - N_{s,n-1} \cdot \varepsilon_{av(d,n-1)} + \\ + \varepsilon_{av,s,n} \cdot \left(N_{s,n-1} + \frac{E_b \cdot A_{b,red(s,n)} \cdot \varepsilon_{av,s,n}}{6\varepsilon_{b0}} \right) = 0. \quad (15)$$

In few cases, Eq. (15) allows a solution in symbolic form, for example, in the MathCAD Software. However, as a rule, it is more convenient to find its solution using one of the approximate methods. In this case, the solution should correspond to the physical essence of the problem (16):

$$\begin{cases} \varepsilon_{av(d,n-1)} > \varepsilon_{av(s,n-1)}, \text{если } \varepsilon_{av(s,n-1)} > \varepsilon_{av(s,n)}; \\ \varepsilon_{av(d,n-1)} < \varepsilon_{av(s,n-1)}, \text{если } \varepsilon_{av(s,n-1)} < \varepsilon_{av(s,n)}, \end{cases} \quad (16)$$

and provides the minimum value of the strain energy among all physically feasible solutions.

Substituting (8), (9), (14) into the second equation of system (5) with respect to (2), (3), (4) and the value $\varepsilon_{av(d,n-1)}$, we obtain a 7th-order polynomial with respect to $\chi_{d,n-1}$ that is the curvature of an eccentrically compressed element from the axis passes through the physical gravity center:

$$a_1\chi_{(d,n-1)}^7 + a_2\chi_{(d,n-1)}^6 + a_3\chi_{(d,n-1)}^5 + a_4\chi_{(d,n-1)}^4 + a_5\chi_{(d,n-1)}^3 + a_6\chi_{(d,n-1)}^2 + \\ + a_7\chi_{(d,n-1)} + a_8 = 0, \quad (17)$$

where a_1, a_2, …, a_8 are the constants determined from the Eqs. (1) – (15) for given stress-strain state of the primary and secondary design schemes under static loading.

The solution of the polynomial (17) can be found approximately using the MathCAD Software. In this case, the obtained solution should satisfy to the physical essence of the problem (18):

$$\begin{cases} \chi_{(d,n-1)} > \chi_{(s,n-1)}, if\ \chi_{(s,n-1)} > \chi_{(s,n)}; \\ \chi_{(d,n-1)} < \chi_{(s,n-1)}, if\ \chi_{(s,n-1)} < \chi_{(s,n)}, \end{cases} \quad (18)$$

and provides the minimum value of the strain energy among all physically feasible solutions.

If we know the average cross-sectional strain $\varepsilon_{av(d,n-1)}$ and the curvature $\chi_{d,n-1}$ relative to the physical gravity center of the cross-section under dynamic loading, then it is easy to determine the stress - strain state at any point of the cross-section from (11), (13) and evaluate criteria of the special limit state in accordance with SP 385.132580. Expressions (1) and (2) allow determination of the acting in the cross-section.

RESULTS

To evaluate the proposed method, we carried out analysis resistance to progressive collapse of

the 5-storey reinforced concrete frame (Figure 2, a) when the outer column on the first floor in the B-1 axes failured. The spans of the frame are 6 m, the floors' height is 3.3 m. The frame material is concrete of B30 compressive class. The cross-sectional dimensions of the columns are of 300x300 mm (*Figure 2,b*). For the girders, it is of 300x450 mm (*Figure 2,c,d*). A500 was adopted as a longitudinal reinforcement steel bar, and stirrups were made of A240 reinforcement steel. Reinforcement parameters have been choosen in accordance with design requirements of SP 63.13330 and result of structural analysis for combination of characteristic loads according to SP 20.13330 that included death and long-term loads, short-term loads on floors with a characteristic value of 1.5 kN/m^2, snow load with a characteristic value of 1.5 kN/ m^2, wind load for I wind region, terrain type A.

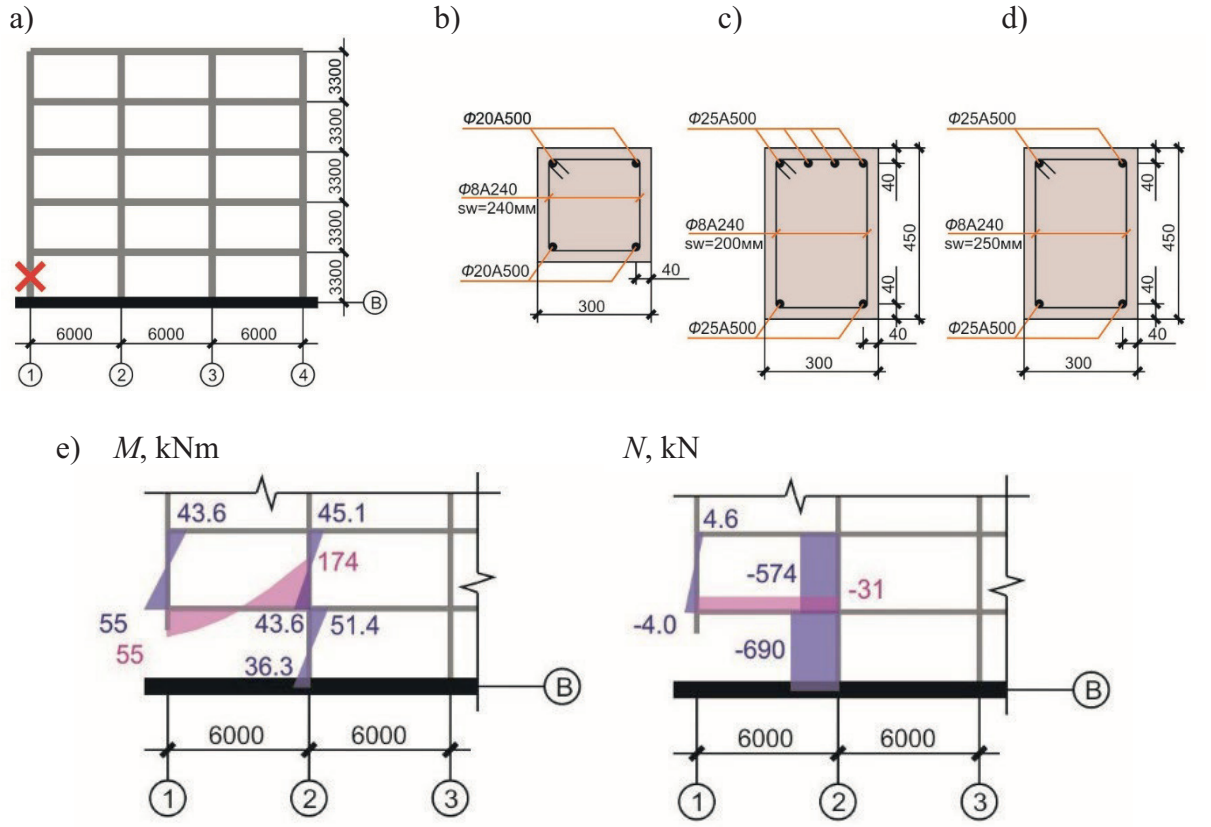

Figure 2. 5-storey reinforced concrete frame: a) primary design scheme; b) cross-section and reinforcement scheme of the columns; c) the same for the supporting sections of the girders; d) the same for girders in the middle of the span, e) the results of a nonlinear dynamic analysis for elements adjacent to the area of initial local failure for the time t = 0.18 s after the impact

We performed the assessment of the frame stress-strain state according to the primary and secondary design schemes [7] after decay of oscillations using nonlinear quasi-static analysis. To assess the reliability of the proposed method, we additionally perform a nonlinear dynamic time-history analysis of the frame. Using modal analysis for secondary design scheme of the reinforced concrete frame (Fig. 2, a), we obtain the period of vibration T = 0.97s for the lower mode which is most similar to the assumed deformed state of the frame after accidental impact. Thus, the time of redistribution of the reaction of the removed column was accepted t = 0.1T = 0.097 s. For comparison, the upper cross-section of the

column on the first floor in the B-2 axes was chosen.

Table 1 provides the computation results of the analysis according to the proposed nonlinear quasi-static and dynamic time-history method. In addition, it provides a comparison of the obtained dynamic amplification factors k_d and coefficients of dynamic overloading θ_d.

Table 1. Comparison of the computation results for nonlinear quasi-static and dynamic time-history analysis

Parameter	Units	Quasi-static analysis	Dynamic time-history analysis	Difference, %
Initial data				
$N_{s,n}$	kN	333	333	-
$\varepsilon_{av,s,n}$	-	$0.118 \cdot 10^{-3}$	$0.118 \cdot 10^{-3}$	-
$M_{s,n}$	kNm	0.794	0.794	-
$\chi_{av,s,n}$	m^{-1}	$3.3 \cdot 10^{-5}$	$3.3 \cdot 10^{-5}$	-
$N_{s,n\text{-}1}$	kN	597.3	597.3	-
$M_{s,n\text{-}1}$	kNm	30.4	30.4	-
Computation results for dynamic effects				
$N_{d,n\text{-}1}$	kN	882	690	27.8
$\varepsilon_{av,d,n\text{-}1}$		$0.29 \cdot 10^{-3}$	$0.25 \cdot 10^{-3}$	16
$M_{d,n\text{-}1}$	kNm	72.5	51.4	41
$\chi_{av,d,n\text{-}1}$	m^{-1}	$3 \cdot 10^{-3}$	$2.59 \cdot 10^{-3}$	15.8
$k_{d,N} = \frac{N_{d,n-1}}{N_{s,n-1}}$	-	1.48	1.15	-
$k_{d,M} = \frac{M_{d,n-1}}{M_{s,n-1}}$	-	2.38	1.69	-
$\theta_{d,N} = \frac{N_{d,n-1}}{N_{s,n}}$	-	2.65	2.07	-
$\theta_{d,M} = \frac{M_{d,n-1}}{M_{s,n}}$	-	91.31	64.74	-

DISCUSSION

Analysis of the data presented in Table 1 indicates that the average cross-sectional strain according to the proposed method is of 16% higher than the value by nonlinear dynamic analysis. Curvatures shows the difference of 15.8%. However, difference between dynamic axial force and bending moment increase to 27.8% and 41% respectively. This indicates a significant influence of the form of stress vs. strain curve. The 2nd order polynomial approximation was adopted in the proposed method, the approximation of the concrete state diagram by a parabola was used. And the nonlinear dynamic analyses applied the exponential approximation of the piece-wise linear diagram. Also, the discrepancy is due to the fact that the dynamic analysis has been performed for certain time, when the proposed method corresponds to instantaneous impact. At the same time, the excess of the stress-strain state parameters for proposed method provides the additional margin of safety of the bearing element. Besides, it allows assessing the special limit state of the reinforced concrete structures using the results of nonlinear static analysis for the primary and secondary design schemes eliminating nonlinear dynamic analysis. This is

especially useful when one conducts structural analysis for the complex structural systems.

CONCLUSION

1. The article provides an approach based on energy relations that allows assessing the bearing capacity of eccentrically compressed physically nonlinear structural elements under accidental impacts caused by sudden failure of a structural member of the facility. The approach uses the results of a nonlinear quasi-static analysis according to the primary and secondary design schemes and eliminate nonlinear dynamic time-history analysis.
2. Structural analysis of 5-storey reinforced concrete frame for progressive collapse resistance shows that the difference between the computational results according to the proposed method and the nonlinear dynamic analysis does not exceed 16% for average strains and curvatures and 41% for internal forces. This discrepancy provides the addition margin of safety.
3. The revealed discrepancy between the computational results is due to the fact that the dynamic analysis has been performed for certain time, when the proposed method corresponds to instantaneous impact, as well as various approximation of stress vs. strain and moment vs. curvature curves adopted in the methods considered in the article.

REFERENCES

1. **Kwasniewski L.** Nonlinear dynamic simulations of progressive collapse for a multistory building. Eng Struct. 2010. Vol. 32(5). pp. 1223-1235. https://doi.org/10.1016/j.engstruct.2009.12.048
2. **Xu G., Ellingwood B.R.** An energy-based partial pushdown analysis procedure for assessment of disproportionate collapse potential. J Constr Steel Res. 2011. Vol. 67(3). pp. 547-555. https://doi.org/10.1016/j.jcsr.2010.09.001
3. **Adam J.M. et al.** Dynamic performance of a real-scale reinforced concrete building test under a corner-column failure scenario. Eng Struct. 2020. Vol. 210. pp. 110414. https://doi.org/10.1016/j.engstruct.2020.110414
4. **Almazov V.O., Kao Z.K.** Dynamics of progressive collapse of monolithic multi-storey frames. Moscow: ASV Publ., 2014. 128 p. (in Russian)
5. **Almazov V.O., Plotnikov A.I., Rastorguev B.S.** Problems of buildings resistance to progressive collapse. Vestnik MGSU. 2011. No 2-1. pp.16-20. (in Russian)
6. **Tamrazyan A.G.** Recommendations for the development of requirements for the survivability of buildings and structures. Vestnik MGSU. 2011. No. 2. pp. 77–83. (in Russian)
7. **Belostotsky A.M., Pavlov A.S.** Long span buildings analysys under phisical, geometic and structural nonlinearities consideration. International Journal for Computational Civil and Structural Engineering. 2010. Vol. 6, № 1 & 2. P. 80–86. (in Russian)
8. **Kabantsev, O.V., Mitrovich, B.** Modeling of a multi-mode failure mechanism of reinforced concrete structures under biaxial stresses. Izvestiya Vysshikh Uchebnykh Zavedenii, Seriya Teknologiya Tekstil'noi Promyshlennosti. 2017. Vol. 369. pp. 225-230 (in Russian)
9. **Fedorova N.V., Korenkov P.A.** Analysis of deformation and crack formation of multistory monolithic reinforced concrete frame-bar structural systems under limit and beyond-limit conditions. Promyshlennoye i grazhdanskoye stroitel'stvo. 2016. no 11. pp. 8-13. (in Russian)
10. **Li S., Shan S., Zhai C. et al.** Experimental and numerical study on progressive collapse process of RC frames with full-height infill walls. Engineering Failure

Analysis. 2016. Vol. 59. pp. 57-68. https://doi.org/10.1016/j.engfailanal.2015.11.020

11. **Yu J., Tan K.H.** Analytical model for the capacity of compressive arch action of reinforced concrete sub-assemblages. Magazine of Concrete Research. 2014. Vol. 66. Issue 3. pp. 109-126. https://doi.org/10.1680/macr.13.00217
12. **Yu J., Tan K.H.** Experimental and numerical investigation on progressive collapse resistance of reinforced concrete beam column sub-assemblages. Engineering Structures. 2013. Vol. 55. pp. 90-106. https://doi.org/10.1016/j.engstruct.2011.08.040
13. **Yi W.J., He Q.F., Xiao Y., Kunnath S.K.** Experimental study on progressive collapse-resistant behavior of reinforced concrete frame structures. ACI Structural Journal. 2008. Vol. 105. Issue 4. pp. 433.
14. **Abdelazim W., Mohamed H.M., Benmokrane B.** Inelastic Second-Order Analysis for Slender GFRP-Reinforced Concrete Columns: Experimental Investigations and Theoretical Study. Journal of Composites for Construction. American Society of Civil Engineers (ASCE). 2020. Vol. 24, Issue 3. https://doi.org/10.1061/(asce)cc.1943-5614.0001019
15. UFC 4-023-03. Design of Buildings to Resist Progressive Collapse. Design of Buildings to Resist Progressive Collapse. 2016. P. 34–37.
16. GSA-2013. General Services Administration Alternate Path Analysis & Design Guidelines for Progressive Collapse Resistance Approved for Public Release; Distribution Unlimited GSA. 2013.
17. GOST 27751-2014 Reliability of building structures and foundations. Basic provisions. Moscow: JSC “Research Center” Construction ", 2019. (in Russian)
18. SP 385.1325800.2018 Protection of buildings and structures against progressive collapse. Design code. Basic statements. Moscow: Ministry of Construction, 2018. 26 p. (in Russian)
19. **Kolchunov V.I., Fedorova N.V., Savin S.Yu.** Dynamic effects in statically indeterminate physically and structurally nonlinear structural systems. Promyshlennoye i grazhdanskoye stroitel'stvo. 2022. No. 9. pp. 51-60. https://doi.org/10.33622/9.2022.09.51-60. (in Russian)
20. **Geniyev G.A.** On dynamic effects in rod systems made of physical non-linear brittle materials. Promyshlennoye i grazhdanskoye stroitel'stvo. 1999. No. 9. pp. 23–24. (in Russian)
21. **Geniyev G.A. et al.** Strength and deformability of reinforced concrete structures under beyond-design impacts. Moscow: ASV Publ., 2004. 216 p. (in Russian)
22. **Kolchunov V.I., Klyueva N.V., Androsova N.B., Bukhtiyarova A.S.** Survivability of building and strctures to undesigned actions. Moscow: ASV Publ., 2014. 208 p. (in Russian)
23. **Ilyushchenko T.A., Kolchunov V.I., Fedorov S.S.** Crack resistance of prestressed reinforced concrete frame structure systems under special impact. Building and reconstruction. 2021. Vol. 93, Issue 1. pp. 74–84. https://doi.org/10.33979/2073-7416-2021-93-1-74-84 (in Russian)
24. **Androsova N.B., Kolchunov V.I.** Survivability of the frame-rod reinforced concrete building framework in accidental action. Building and reconstruction. 2021. Issue 5. pp. 40-50. https://doi.org/10.33979/2073-7416-2021-97-5-40-50 (in Russian)
25. **Fedorova N. V., Vu N. T., Iliushchenko T. A**. Dynamic additional loading of the frame of a multi-story building after the failure of one of the structures. IOP Conference Series: Materials Science and Engineering. – IOP Publishing, 2020. Vol.

896. Issue 1. pp. 012040. https://doi.org/10.1088/1757-899X/896/1/012040
26. **Kolchunov V.I., Fedorova N.V., Savin S.Yu., Kovalev V.V., Iliushchenko T.A.** Failure simulation of a RC multi-storey building frame with prestressed girders. Magazine of Civil Engineering. 2019. 92(8). Pp. 155–162. https://doi.org/10.18720/MCE.92.13.
27. **Klyueva N.V., Korenkov P.A.** Method of Experimental Determination of Parameters of Survivability of Reinforced Concrete Frame-Rod Structural Systems. Promyshlennoye i grazhdanskoye stroitel'stvo. 2016. No 2. pp.44-48. (in Russian)
28. **Popov D.S.** Experimental Studies of Dynamic Properties of Corrosion-Damaged Compressed Reinforced Concrete Elements. Building and reconstruction. 2022. Vol. 100, No 2. P. 55–64. https://doi.org/ 10.33979/2073-7416-2022-100-2-55-64 (in Russian)

СПИСОК ЛИТЕРАТУРЫ

1. **Kwasniewski L.** Nonlinear dynamic simulations of progressive collapse for a multistory building // Eng Struct. 2010. Vol. 32(5). pp. 1223-1235. https://doi.org/10.1016/j.engstruct.2009.12.048
2. **Xu G., Ellingwood B.R.** An energy-based partial pushdown analysis procedure for assessment of disproportionate collapse potential // J Constr Steel Res. 2011. Vol. 67(3). pp. 547-555. https://doi.org/ 10.1016/j.jcsr.2010.09.001
3. **Adam J.M. et al.** Dynamic performance of a real-scale reinforced concrete building test under a corner-column failure scenario // Eng Struct. 2020. Vol. 210. pp. 110414. https://doi.org/10.1016/j.engstruct.2020.110414
4. **Алмазов В.О., Као З.К.** Динамика прогрессирующего разрушения монолитных многоэтажных каркасов. М.: Издательство АСВ, 2014. 128 с.
5. **Алмазов В.О., Плотников А.И., Расторгуев Б.С.** Проблемы сопротивления зданий прогрессирующему разрушению // Вестник МГСУ. 2011. 2-1. С.16-20.
6. **Тамразян А.Г.** Рекомендации к разработке требований к живучести зданий и сооружений // Вестник МГСУ. 2011. № 2. С. 77–83.
7. **Belostotsky A.M., Pavlov A.S.** Long span buildings analysys under phisical, geometic and structural nonlinearities consideration // International Journal for Computational Civil and Structural Engineering. 2010. Vol. 6, № 1 & 2. P. 80–86.
8. **Кабанцев О.В., Митрович Б.** Моделирование многорежимного механизма отказа железобетонных конструкций при двухосном напряженном состоянии // Известия высших учебных заведений. Технология текстильной промышленности. 2017. №. 3. С. 225-231.
9. **Федорова Н.В., Кореньков П.А.** Анализ деформирования и трещинообразования многоэтажных железобетонных рамно-стержневых конструктивных систем зданий в предельных и запредельных состояниях // Промышленное и гражданское строительство. 2016. № 11. С.8-13.
10. **Li S., Shan S., Zhai C. et al.** Experimental and numerical study on progressive collapse process of RC frames with full-height infill walls // Engineering Failure Analysis. 2016. Vol. 59. pp. 57-68. https://doi.org/10.1016/j.engfailanal.2015.11.020
11. **Yu J., Tan K.H.** Analytical model for the capacity of compressive arch action of reinforced concrete sub-assemblages // Magazine of Concrete Research. 2014. Vol. 66. Issue 3. pp. 109-126. https://doi.org/10.1680/macr.13.00217

12. **Yu J., Tan K.H.** Experimental and numerical investigation on progressive collapse resistance of reinforced concrete beam column sub-assemblages // Engineering Structures. 2013. Vol. 55. pp. 90-106. https://doi.org/10.1016/j.engstruct.2011.08.040
13. **Yi W.J., He Q.F., Xiao Y., Kunnath S.K.** Experimental study on progressive collapse-resistant behavior of reinforced concrete frame structures // ACI Structural Journal. 2008. Vol. 105. Issue 4. pp. 433.
14. **Abdelazim W., Mohamed H.M., Benmokrane B.** Inelastic Second-Order Analysis for Slender GFRP-Reinforced Concrete Columns: Experimental Investigations and Theoretical Study // Journal of Composites for Construction. American Society of Civil Engineers (ASCE). 2020. Vol. 24, Issue 3. https://doi.org/10.1061/(asce)cc.1943-5614.0001019
15. UFC 4-023-03. Design of Buildings to Resist Progressive Collapse // Design of Buildings to Resist Progressive Collapse. 2016. P. 34–37.
16. GSA-2013. General Services Administration Alternate Path Analysis & Design Guidelines for Progressive Collapse Resistance Approved for Public Release; Distribution Unlimited GSA. 2013.
17. ГОСТ 27751-2014 Надежность строительных конструкций и оснований. Основные положения. М.: НИЦ «Строительство», 2019.
18. СП 385.1325800.2018 «Защита зданий и сооружений от прогрессирующего обрушения. Правила проектирования. Основные положения». Издание оф. М.: Минстрой России, 2018. 26 с.
19. **Колчунов В.И., Федорова Н.В., Савин С.Ю.** Динамические эффекты в статически неопределимых физически и конструктивно нелинейных системах // Промышленное и гражданское строительство. 2022. №9. С. 51-60. https://doi.org/10.33622/9.2022.09.51-60.
20. **Гениев Г.А.** О динамических эффектах в стержневых системах из физических нелинейных хрупких материалов // Промышленное и гражданское строительство. 1999. № 9. P. 23–24.
21. **Гениев Г.А. и др.** Прочность и деформативность железобетонных конструкций при запроектных воздействиях. М.: Издательство АСВ, 2004. 216 p.
22. **Колчунов В.И., Клюева Н.В., Андросова Н.Б., Бухтиярова А.С.** Живучесть зданий и сооружений при запроектных воздействиях. М.: Издательство АСВ, 2014. 208 с.
23. **Ильющенко Т.А., Колчунов В.И., Федоров С.С.** Трещиностойкость преднапряженных железобетонных рамно-стержневых конструкций при особых воздействиях // Строительство и реконструкция. 2021. Vol. 93, № 1. P. 74–84. https://doi.org/10.33979/2073-7416-2021-93-1-74-84
24. **Андросова Н.Б., Колчунов В.И.** Живучесть рамно-стержневого железобетонного каркаса здания в запредельных состояниях // Строительство и реконструкция. 2021. № 5. С. 40-50. https://doi.org/10.33979/2073-7416-2021-97-5-40-50
25. **Fedorova N.V., Vu N.T., Iliushchenko T. A**. Dynamic additional loading of the frame of a multi-story building after the failure of one of the structures // IOP Conference Series: Materials Science and Engineering. – IOP Publishing, 2020. Vol. 896. Issue 1. pp. 012040. https://doi.org/10.1088/1757-899X/896/1/012040
26. **Kolchunov V.I., Fedorova N.V., Savin S.Yu., Kovalev V.V., Iliushchenko T.A.** Failure simulation of a RC multi-storey building frame with prestressed girders. Magazine of Civil Engineering. 2019. 92(8). Pp. 155–162. https://doi.org/10.18720/MCE.92.13.

27. **Клюева Н.В., Кореньков П.А.** Методика экспериментального определения параметров живучести железобетонных рамно-стержневых конструктивных систем // Промышленное и гражданское строительство. 2016. No 2. С.44-48

28. **Popov D.S.** Experimental Studies of Dynamic Properties of Corrosion-Damaged Compressed Reinforced Concrete Elements // Building and reconstruction. 2022. Vol. 100, № 2. P. 55–64. https://doi.org/10.33979/2073-7416-2022-100-2-55-64

Sergey Yu. Savin, Candidate of Technical Sciences, Docent, Associated Professor of the Department of Reinforced Concrete and Masonry Structures of Moscow State University of Civil Engineering (National Research University) (MGSU); 26 Yaroslavskoe shosse, Moscow, 129337, Russian Federation; Scopus ID: 57052453700, ResearcerID: M-8375-2016, ORCID: 0000-0002-6697-3388; phone +7(495)287-49-14, e-mail: savinsyu@mgsu.ru.

Natalia V. Fedorova, Advisor of RAACS, Professor, Doctor of Technical Sciences, Head of the Department of Architectural and Construction Design, Director of the branch of Moscow State University of Civil Engineering (National Research University) (MGSU) in Mytishchi; Moscow State University of Civil Engineering (National Research University) (MGSU), 26 Yaroslavskoe shosse, Moscow, 129337, Russian Federation; Scopus ID: 57196437054, ResearcerID: O-8119-2015, ORCID: 0000-0002-5392-9150; phone +7(495)287-49-14, e-mail: fedorovaNV@mgsu.ru.

Vitaly I. Kolchunov, Full Member of RAACS, Professor, Doctor of Technical Sciences, Professor of the Department of Reinforced Concrete and Masonry Structures; Moscow State University of Civil Engineering (National Research University) (MGSU), head of the department of Southwest State University; 26 Yaroslavskoe shosse, Moscow, 129337, Russian Federation; Scopus ID: 55534147800, ResearcerID: J-9152-2013, ORCID: 0000-0001-5290-3429; phone +7(495)287-49-14, e-mail: asiorel@mail.ru.

Савин Сергей Юрьевич, кандидат технических наук, доцент, доцент кафедры железобетонных и каменных конструкций; Национальный исследовательский Московский государственный строительный университет (НИУ МГСУ); 129337, г. Москва, Ярославское шоссе, д. 26; Scopus ID: 57052453700, ResearcerID: M-8375-2016, ORCID: 0000-0002-6697-3388; тел. +7(495)287-49-14, e-mail: savinsyu@mgsu.ru.

Федорова Наталия Витальевна, советник РААСН, профессор, доктор технических наук, заведующий кафедрой архитектурно-строительного проектирования, директор филиала НИУ МГСУ в г. Мытищи; 129337, г. Москва, Ярославское шоссе, д. 26; Scopus ID: 57196437054, ResearcerID: O-8119-2015, ORCID: 0000-0002-5392-9150; phone +7(495)287-49-14, e-mail: fedorovaNV@mgsu.ru.

Колчунов Виталий Иванович, академик РААСН, профессор, доктор технических наук, профессор кафедры железобетонных и каменных конструкций Национального исследовательского Московского государственного строительного университета (НИУ МГСУ), заведующий кафедрой уникальных зданий и сооружений Юго-Западного государственного университета; 129337, г. Москва, Ярославское шоссе, д. 26; Scopus ID: 55534147800, ResearcerID: J-9152-2013, ORCID: 0000-0001-5290-3429; тел. +7(495)287-49-14, e-mail: asiorel@mail.ru.

International Journal for Computational Civil and Structural Engineering, 18(4) 124–131 (2022)

DOI:10.22337/2587-9618-2022-18-4-124-131

DYNAMIC MODEL OF BEAM DEFORMATION WITH CONSIDER NONLOCAL IN TIME ELASTIC PROPERTIES OF THE MATERIAL

Vladimir N. Sidorov [1,2], Elena. S. Badina [1,2,3], Roman O. Tsarev [3]

[1] Russian University of Transport (MIIT), Moscow, RUSSIA
[2] Moscow State University of Civil Engineering, Moscow, RUSSIA
[3] Institute of Applied Mechanics of Russian Academy of Sciences, Moscow, RUSSIA

Abstract: In this paper, the problem of numerical dynamic calculation of a beam made of composite material with a developed internal structure is considered. The elastic properties are assumed to be nonlocal in time. A short review of the existing methods for mathematical modeling of the dynamic behavior of elements with a developed internal structure was carried out. A non-local in time model of dynamic deformation of a bending beam is constructed. Since the finite element analysis (FEA) is the most demanded numerical method for mechanical systems analysis, a non-local dynamic deformation model is integrated into the algorithm of this method. The equilibrium equation of the structure in motion is solved by an explicit scheme. The damping matrix is obtained from the condition of stationarity of the total deformation energy of a moving mechanical system. A one-dimensional non-local in time model was implemented in the MATLAB software package.

Keywords: Nonlocal mechanics, nonlocal damping, numerical simulation, finite element method

МОДЕЛЬ ДИНАМИЧЕСКОГО ДЕФОРМИРОВАНИЯ ИЗГИБАЕМОЙ БАЛКИ С УЧЕТОМ НЕЛОКАЛЬНЫХ ВО ВРЕМЕНИ УПРУГИХ СВОЙСТВ МАТЕРИАЛА

В.Н. Сидоров [1,2], Е.С. Бадьина [1,2,3], Р.О. Царёв [3]

[1] Российский университет транспорта (МИИТ), г. Москва, РОССИЯ
[2] Национальный исследовательский Московский государственный строительный университет, г. Москва, РОССИЯ
[3] Институт прикладной механики Российской академии наук, г. Москва, РОССИЯ

Аннотация: В настоящей работе рассматривается задача численного динамического расчета изгибаемой балки из композитного материала с развитой внутренней структурой с учетом нелокальных во времени упругих свойств. Был проведен краткий обзор существующих методов математического моделирования динамического поведения элементов с развитой внутренней структурой. Построена нелокальная модель деформирования изгибаемой балки под действием динамической нагрузки. Поскольку метод конечных элементов (МКЭ) является наиболее востребованным численным методом анализа механических систем, нелокальная модель динамического деформирования интегрирована в алгоритм этого метода. Уравнение равновесия конструкции в движении решается по явной схеме. Матрица демпфирования получена из условия стационарности полной энергии деформирования движущейся механической системы. Одномерная нелокальная во времени модель была реализована в программном комплексе MATLAB.

Ключевые слова: Нелокальная механика, нелокальное демпфирование, численное моделирование, метод конечных элементов

INTRODUCTION

The development of construction technologies and the gradual implementation of new composite and nano-materials with "controllable" physical characteristics in construction require the creation of appropriate mathematical models that allow to reliably describe the behavior of such materials, in particular under the dynamic load.

Generally, in order to obtain sufficient accuracy of the numerical calculation, three-dimensional finite element models are used to take into account the orthotropic properties of the material. However, these models are resource-intensive and difficult to form and analyze. For instance, as a result of computation, only the fields of the stress-strain state in elements and their nodes can be obtained as a result of 3D finite element modelling, which is not always sufficient for engineering analysis of the calculation results. As an alternative to 3D modeling the one dimensional elements can be used, constructed using reasonable mathematical hypotheses that allow to describe the characteristic properties of the material. The special hypotheses turn out to be necessary, since the frequently used classical viscoelastic models proposed in the works of W. Kelvin [1], J. Maxwell [2], J. Rayleigh [3], Voigt [4] no longer allow accurately model the behavior of materials with a complex internal structure.

To simulate the dynamic behavior of structural elements made of composite materials, models based on the principles of non-local mechanics are applicable. Such models may include the models proposed in the works of A. Eringen and D. Edelen [5], D. Russell [6], Banks and Inman. [7], Lei [8] and V. D. Potapov [9].

NON-LOCAL DAMPING MODELS

A wide class of non-local models applicable to describe the dynamic behavior of composite materials are non-local damping models.

In the article [8] Y. Lei proposed a non-local damping model that takes into account the effects of time and spatial hysteresis. This model is used for dynamic analysis of structures consisting of Euler–Bernoulli beams and Kirchhoff plates. Unlike classic local damping models, the damping force in the non-local model is defined as a weighted average of the velocity field in the spatial domain determined by a kernel function based on distance measures. Also, the resulting equation of motion for beam or plate structures is a partial integro-differential equation, in contrast to the partial differential equation for the local damping model. Approximate solutions for complex eigenvalues and modes with nonlocal damping are obtained using the Galerkin method. Numerical examples demonstrate the effectiveness of the proposed method for beam and plate structures with simple boundary conditions, for non-local and inviscid damping models and various core functions.

$$L_e\dot{u}(r,t) = \int_\Omega \int_0^t C_e(r,\xi,t-\tau)\dot{u}(\xi,\tau)d\tau d\xi \quad (1)$$

$$L_i\dot{u}(r,t) = \int_\Omega \int_0^t C_i(r,\xi,t-\tau)L_s\dot{u}(\xi,\tau) \quad (2)$$

The equation of motion in this case is expressed as the following integro-differential equation in partial derivatives

$$\begin{aligned}\frac{\partial^2}{\partial x^2}\left(EI(x)\frac{\partial^2 w(x,t)}{\partial x^2}\right) + \rho A(x)\frac{\partial^2 w(x,t)}{\partial t^2} \\ + \int_{x_1}^{x_2}\int_{-\infty}^{t} C_e(x,\xi,t-\tau)\frac{\partial w(\xi,\tau}{\partial t}d\tau d\xi \\ + \int_{x_1}^{x_2}\int_{-\infty}^{t} C_i(x,\xi,t-\tau)\frac{\partial^2}{\partial \xi^2}\left(\gamma(\xi)\frac{\partial^3 w(\xi,t)}{\partial \xi^2 \partial \tau}\right)d \\ = f(x,t)\end{aligned} \quad (3)$$

Another solution of the problem of non-local damping was proposed in the article by Banks H.T., Inman D.J. [7], where various damping mechanisms are considered for a quasi-isotropic pultruded composite beam. The approach used here is physical. The partial differential equation describes the transverse vibrations of a beam with a mass at the free end. All damping mechanisms considered in the article have an explicit physical basis, in contrast to the usual modal model. Four possible damping mechanisms are considered: one external and three internal. These include: viscous damping (air damping); internal damping depending on strain rates; spatial hysteresis; and time hysteresis. In addition, various combinations of these mechanisms are considered.

These physical damping models are incorporated into the Euler-Bernoulli beam equation, with boundary conditions carefully formulated to be

compatible with different damping models. The resulting partial differential equation (in case of decaying time hysteresis) is approximated using cubic splines. Time histories of the measured experimental responses are then used to estimate the parameters of the models corresponding to the data using the method of least squares. The resulting least squares evaluations of various damping parameters are then used in a partial (integro-partial) differential equation for numerical simulation of the system response. This numerically generated time response of the system being evaluated is then compared with the actual data obtained experimentally. These comparisons allow several conclusions to be drawn regarding the physical damping mechanisms present in a composite beam. In particular, it is shown that the spatial hysteresis model in combination with the external damping model leads to the best fit to the experimental data. The article also notes that the proposed damping models cannot be successfully built using standard damping coefficients in fractions of the critical, since the traditional approach to modal analysis completely masks the physics of damping mechanisms.

The solution for the non-local in space model of damping was made in the article [10]. It is shown that calibrated nonlocal model applied to one-dimensional beam adequately approximate the results of the 3D numerical simulation. An alternative model with damping non-local in time was shown in the article [11]. In comparison to the model from [10] the nonlocal in time model is integrated into the FEA algorithm.

MODELS OF ELASTIC MATERIAL PROPERTIES NON-LOCAL IN SPACE

Historically, one of the first models of an elastic medium that cannot be described within the framework of the classical theory of elasticity is the Cosserat continuum (1909). However, for a long time the work of F. Cosserat remained unnoticed, and only starting from about 1958-60 rr. generalized models of the Cosserat continuum began to be intensively developed. the theory of oriented media, asymmetric, moment, multipolar, micromorphic, etc. theories of elasticity have arisen. The equations of motion for the Cosserat model coincide with the equations of motion for a diatomic chain, and, therefore, in the (x, t)-representation they have the form

$$\begin{gathered} \rho\ddot{u} - \partial y \partial u - \partial x + \eta = q \\ I\ddot{\eta} - \chi\partial u + \Gamma\eta = \mu \end{gathered} \tag{4}$$

here u is the transverse displacement, n is the microrotation, μ is the density of the corresponding micromoments, l is the density of the moments of inertia of the particles. The remaining quantities have the same meaning as in the case of a diatomic chain

Early ideas of non-local elasticity go back to the pioneering work of Kroner [12], Kunin [13], Krumhansl [14]. Improved formulations were then presented in Edelen and Laws [15] and Eringen [16, 17, 18]. Eringen model of a nonlocal elasticity is constructed by integration of an integral member to the Hook`s law:

$$\sigma(t,x) = E \int_{-\infty}^{\infty} C(|x - x`|)\varepsilon(x`)dx`, \tag{5}$$

The stress field at a point x in an elastic continuum not only depends on the strain field at the point but also on strains at all other points of the body.

The Eringen model of non-local elastic material was further developed in works of A.A. Pisano [19]. The article solved the problem of stretching of a bar of finite length, to both ends of which longitudinal forces are applied. This integral-type relation contains a non-local damping function designed to capture the process of diffusion of non-local effects. This article is devoted to finding an exact solution to a simple mechanical problem. The solution of this problem is obtained through the transformation of the second kind Fredholm integral equation, which determines the problem, into two second kind Volterra integral equations. As a result, an exact solution in terms of strains for a non-local elastic rod is obtained.

The article [9] of V.D. Potapov is devoted to the study of the stability of an infinitely long rod lying on an elastic foundation and under the action of a constant or periodically changing longitudinal force. The rod material used in the calculations is characterized by non-local viscoelastic properties. The influence of the parameters characterizing the nonlocality of the viscoelastic properties of the material, as well as the parameters of the load on the buckling and stability of the rod, is analysed. The article assumes that the relationship between stress σ and strain ε for the rod material has the form:

$$\sigma(t,x) = E \int_{-\infty}^{\infty} C(|x-x`|)(1-\mathrm{R})\varepsilon(\tau,x`)dx`, \quad (6)$$

where $C(|x-x`|)$ is the kernel of non-local viscosity along the coordinate, E is the modulus of elasticity, R is the integral viscoelasticity operator:

$$\mathrm{R}\varepsilon(\tau,x`) = \int_{-\infty}^{t} R(t-\tau)\varepsilon(\tau,x`)\,d\tau \quad (7)$$

$R(t,\tau)$ – viscoelasticity kernel, t, τ – time, x, x` – coordinates measured along the rod axis.

It is obvious that, in addition to nonlocality in space, the material considered in the article has the property of memory, since the kernel $R(t,\tau)$ makes it possible to take into account the deformed states of the system over the entire loading history.

THE MODEL OF ELASTIC PROPERTIES OF A MATERIAL IS NON-LOCAL IN TIME

The article [11] shows that a nonlocal in time model of the dissipative properties of the material can be relatively easily integrated into the FEA algorithm. Therefore, the nonlocal model of the elastic properties of the material considered in this work was also implemented in relation to the FEA. Hence, after the calibration such model can be used in solving of applied dynamic problems.

For the model presented in [9], the lower limit of integration over the time domain was taken equal to minus infinity. Strictly speaking, this is mathematically correct, but physically, any system manifests itself for a finite period of time. Yu.N. Rabotnov in [20] notes that the beginning of the real existence of the system has to be chosen as a lower limit. Therefore, in the following equations the initial moment of the oscillatory process *t=0* was used as the lower limit of integration.

DYNAMIC MODEL OF BENDING BEAM DEFORMATION WITH CONSIDERING NON-LOCAL IN TIME ELASTIC PROPERTIES OF THE MATERIAL

Considering the above a nonlocal in time model of the elastic properties of the material can be effectively used for modeling of the composite elements dynamic behavior. In this paper it is assumed that the elastic forces in the structure depend not only on the displacement values at the current time, but also on the previous time history of deformation of the structure. Moreover, the greater the time interval between two moments of time, the less is the influence that one of them has on the other. In the other words, the memory is considered to be fading.

Further calculations were carried out in the MATLAB software package. As a numerical example a 10-meter beam with fixed ends was modeled. The beam material is pultruded fiberglass. The Young's modulus of this material in the longitudinal direction is equal to 28 GPa. The beam cross section is rectangular: 0.3m high and 0.2m wide. The coefficient of relative damping of the material is assumed to be 0.015. The beam is loaded with an instantaneously applied and uniformly distributed load.

In the FEA algorithm, the equilibrium equation for a structure deformed in motion is represented as [21]:

$$M \cdot \ddot{\bar{V}}(t) + D \cdot \dot{\bar{V}}(\tau) + K \cdot \bar{V}(t) = \bar{F}(t) \quad (8)$$

Taking into account the elastic properties nonlocal in time, this expression takes the form:

$$M \cdot \ddot{\bar{V}}(t) + D \cdot \dot{\bar{V}}(\tau) + \\ + K \cdot \int_0^t R(t-\tau) \cdot \bar{V}(t) d\tau = \bar{F}(t) \quad (9)$$

Here $R(t-\tau)$ is the kernel of the elasticity operator used in this work. This function describes the decrease in the influence of the past history of dynamic deformation of the element on the current value of elastic forces in the system. In this case, the normalization condition is satisfied:

$$\int_0^t R(t-\tau)\, d\tau = 1 \quad (10)$$

For numerical calculations, the error function was used as the memory core, which, subject to the normalization condition, takes the form:

$$R(t-\tau) = \frac{2\eta}{\sqrt{\pi}} \cdot e^{-\eta^2 (t-\tau)^2} v \quad (11)$$

Here η is a parameter characterizing the scale of nonlocality of elastic forces in time. The small η parameter conforms to the highly nonlocal properties of the material.

For the numerical solution of the equation of dynamic equilibrium, the method of central differences was used. When converting equation (2) into a computational scheme using the method of central differences, the equation of motion takes the form:

$$\frac{1}{\Delta t^2} \cdot M \cdot (\bar{V}_{i+1} - 2\bar{V}_i + \bar{V}_{i-1}) + \\ + \frac{1}{2\Delta t} D \cdot (\bar{V}_{i+1} - \bar{V}_{i-1}) + K \cdot \bar{Z} = \bar{F}_i \quad (12)$$

where $\bar{Z}$ – is a discrete analogue of the integral kernel $\int_0^t R(t-\tau)d\tau$

$$\bar{Z} = \sum_1^i \frac{2\eta}{\sqrt{\pi}} \cdot e^{-\eta^2 \left(t - \left(\tau - \frac{\Delta t}{2}\right)\right)^2} \bar{V}_i. \quad (13)$$

The computational scheme for the sequential step-by-step calculation of $\bar{V}_{i+1}$ through the vectors $\bar{V}_\text{i}$ and $\bar{V}_{i-1}$, which are calculated in the previous steps, is based on (12)

$$\left(\frac{1}{\Delta t^2} M + \frac{1}{2\Delta t} D\right) \bar{V}_{i+1} + \left(-\frac{2}{\Delta t^2} M\right) \bar{V}_i \\ + \left(\frac{1}{\Delta t^2} M - \frac{1}{2\Delta t} D\right) \cdot \bar{V}_{i-1} + \\ + \mathrm{K} \cdot \bar{Z} = \bar{F}_i. \quad (14)$$

We set in (14):

$$Q = \left(\frac{1}{\Delta t^2} M + \frac{1}{\Delta t} D\right)^{-1}, \\ Q_1 = Q \cdot \left(-\frac{2}{\Delta t^2} M\right), \\ Q_2 = \left(\frac{1}{\Delta t^2} M - \frac{1}{\Delta t} D\right) Q, \\ Q_3 = Q \cdot K. \quad (15)$$

The final scheme for a step-by-step solution in time of the discrete equation of motion (9) using the accepted model of deformation of a material with memory takes the form:

$$\bar{V}_{i+1} = Q \cdot \bar{F}_i - Q_1 \cdot \bar{V}_i - Q_2 \cdot \bar{V}_{i-1} - Q_3 \\ \cdot \bar{Z}. \quad (16)$$

At the first step, for i = 1, $\bar{V}_0 = 0$ and $\bar{V}_1 = 0$ are taken as initial conditions.

Further calculations were carried out in the MATLAB software package.

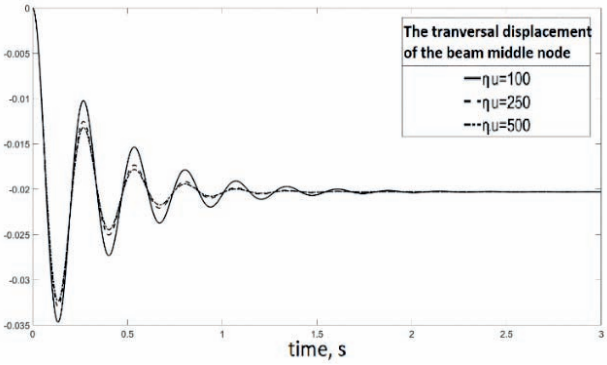

Figure 1. Deflection history of a beam obtained using a model of elastic material properties nonlocal in time for different values of η

As a result of the calculations, graphs of functions with different values of η equal to 100, 250 and 500, were obtained. Analyzing these graphs, we can say that this parameter affects the amplitude of oscillations, but does not affect the frequency of oscillations, a decrease in the parameter η leads to an increase in amplitude. Hence, higher deflection attitude corresponds to the higher level of nonlocality.

CONCLUSION

The article provides a brief overview of existing methods of mathematical modeling of the dynamic behavior of elements made of materials with a developed internal structure. A non-local model of deformation of a bending beam is constructed using the finite element method. The method of central differences was used for the numerical solution of the equation of motion. And the relationship between the scale parameter η and the amplitude of vibrations of the bent beam is shown.

ACKNOWLEDGEMENT

This work was carried out with the financial support of the Ministry of Science and Higher Education of the Russian Federation (project "Theoretical and experimental design of new composite materials to ensure safety during the operation of buildings and structures in conditions of man-made and biogenic threats" No. FSWG-2020-0007).

REFERENCES

1. **Kelvin, (Thomson W.)** Proceedings of Royal Society / Kelvin // Proceedings of Royal Society of London. – 1865.
2. **Maxwell, J. C.** Philosophical Transaction / J. C. Maxwell. - Philosophical Transaction, 1867
3. **Rayleigh, J.** Proceedings of the Mathematical Society / Rayleigh // Proceedings of the Mathematical Society. – 1873. - v.4.
4. **Alexandrov A.V., Potapov V. D., Zylyov V.B.**, 2008, Structural mechanics. In 2 books. Book 2. Dynamic and stability of the elastic systems. Highschool, Moscow (in Russian)
5. **Eringen, A.C.** Nonlocal elasticity / A.C. Eringen, D.G.B. Edelen // International Journal of Engineering Science. – 1972. - 10 (3), 233–248.
6. **Russell, D.L.** On mathematical models for the elastic beam with frequency-proportional damping. / D.L. Russell // Control and Estimation in Distributed Parameter Systems. SIAM, Philadelphia, PA. – 1992. - pp. 125–169.
7. **Banks H. T., Inman D. J.,** 1991, On damping Mechanisms in Beams Journal of Applied Mechanics 58(3) pp 716–723.
8. **Lei Y, Friswell M I and Adhikari S** 2006 A Galerkin Method for Distributed Systems with Non-local Damping Int.Journal of Solids and Structures 43 p 3381–3400
9. **Potapov V.D**. Stability of rods under stochastic loading with allowance for non-local damping. Problems of mechanical engineering and reliability theory. 2012. No. 4. S. 25–31.
10. **E. S. Shepitko, V. N. Sidorov**, 2019, Defining of nonlocal damping model parameters based on composite beam dynamic behaviour numerical simulation results // IOP Conf. Series: Materials Science and Engineering 675 012056
11. **Sidorov, V.N., Badina, E.S., Detina, E.P**, 2021. Nonlocal in Time Model of Material Damping in Composite Structural Elements Dynamic Analysis. International Journal for Computational Civil and Structural Engineering, 17(4), p. 14–21
12. **Kroner, E.**, 1967. Elasticity theory of materials with long range cohesive forces. Int. J. Solids Struct. 3, 731–742
13. **Kunin, I.A**., 1967. The theory of elastic media with microstructure and the theory of dislocation. In: Kroner (Ed.), Mechanics of

Generalised Continua, Proceedings of IUTAM Symposium 1967, Springer, New York, 1968.
14. **Krumhansl, J.A.**, 1968. Some considerations on the relations between solid state physics and generalized continuum mechanics. In: Kroner, E. (Ed.), Mechanics of Generalized Continua. Springer-Verlag, Berlin, pp. 298–331.Эеден
15. **Edelen, D.G.B.**, **Laws, N**., 1971. On the thermodynamics of systems with nonlocality. Arch. Rat. Mech. Anal. 43, 24–35.
16. **Eringen, A.C.**, 1972a. Nonlocal polar elastic continua. Int. J. Engng. Sci. 10, 1–16.
17. **Eringen, A.C.**, 1972b. Linear theory of nonlocal elasticity and dispersion of plane waves. Int. J. Engng. Sci. 10, 425–435.
18. **Eringen, A.C**., 1976. Nonlocal micropolar field theory. In: Eringen, A.C. (Ed.), Continuum Physics, vol. 4. Acadamic Press, New York, pp. 205–267.
19. **Pisno, A.A.** Closed form solution for non-local elastics bar in tension / A.A. Pisno, P. Fuschi // International Journal of Solids and Structures. - 2003. - 40 (1), p. 13–23.
20. **Yu.N.Rabotnov,** 1977. Elements of hereditary mechanics of solids
21. **Bathe K. J., Wilson E.L.,** 1976, Numerical methods in finite element analysis. Prentice Hall, New York.

СПИСОК ЛИТЕРАТУРЫ

1. **Kelvin, (Thomson W.)** Proceedings of Royal Society / Kelvin // Proceedings of Royal Society of London. – 1865.
2. **Maxwell, J.C.** Philosophical Transaction / J. C. Maxwell. - Philosophical Transaction, 1867
3. **Rayleigh, J.** Proceedings of the Mathematical Society / Rayleigh // Proceedings of the Mathematical Society. – 1873. - v.4.
4. **Александров, А.В., Потапов В. Д., Зылёв В.Б.**, 2008, Строительная механика.В 2-х книгах. Книга 2. Динамика и устойчивость упругих систем. Издательство: Высшая школа.
5. **Eringen, A.C.,** 1972 Nonlocal elasticity / A.C. Eringen, D.G.B. Edelen // International Journal of Engineering Science. – 1972. - 10 (3), 233–248.
6. **Russell, D.L.** On mathematical models for the elastic beam with frequency-proportional damping. / D.L. Russell // Control and Estimation in Distributed Parameter Systems. SIAM, Philadelphia, PA. – 1992. - pp. 125–169.
7. **Banks H. T., Inman D. J.,** 1991, On damping Mechanisms in Beams Journal of Applied Mechanics 58(3) pp 716–723.
8. **Lei Y, Friswell M I and Adhikari S** 2006 A Galerkin Method for Distributed Systems with Non-local Damping Int.Journal of Solids and Structures 43 p 3381–3400
9. **Потапов В.Д.** 2012. Устойчивость стержней при стохастическом нагружении с учетом нелокального демпфирования // Проблемы машиностроения и теории надежности. № 4. С. 25–31.
10. **E.S. Shepitko, V.N. Sidorov**, 2019, Defining of nonlocal damping model parameters based on composite beam dynamic behaviour numerical simulation results // IOP Conf. Series: Materials Science and Engineering 675 012056
11. **Sidorov, V.N., Badina, E.S., Detina, E.P** 2021. Nonlocal in time model of material damping in composite structural elements dynamic analysis. International Journal for Computational Civil and Structural Engineering, 17(4), p. 14–21
12. **Kroner, E.**, 1967. Elasticity theory of materials with long range cohesive forces. Int. J. Solids Struct. 3, 731–742
13. **Kunin, I.A**., 1967. The theory of elastic media with microstructure and the theory of dislocation. In: Kroner (Ed.), Mechanics of Generalised Continua, Proceedings of IUTAM Symposium 1967, Springer, New York, 1968.
14. **Krumhansl, J.A.**, 1968. Some considerations on the relations between

solid state physics and generalized continuum mechanics. In: Kroner, E. (Ed.), Mechanics of Generalized Continua. Springer-Verlag, Berlin, pp. 298–331.Эеден
15. **Edelen, D.G.B., Laws, N**., 1971. On the thermodynamics of systems with nonlocality. Arch. Rat. Mech. Anal. 43, 24–35.
16. **Eringen, A.C.**, 1972a. Nonlocal polar elastic continua. Int. J. Engng. Sci. 10, 1–16.
17. **Eringen, A.C.**, 1972b. Linear theory of nonlocal elasticity and dispersion of plane waves. Int. J. Engng. Sci. 10, 425–435.
18. **Eringen, A.C**., 1976. Nonlocal micropolar field theory. In: Eringen, A.C. (Ed.), Continuum Physics, vol. 4. Acadamic Press, New York, pp. 205–267.
19. **Pisno, A.A.** 2003. Closed form solution for non-local elastics bar in tension / A.A. Pisno, P. Fuschi // International Journal of Solids and Structures. - 40 (1), p. 13–23.
20. **Ю.Н.Работнов,** 1977, Элементы наследственной механики твердых тел
21. **Bathe K. J., Wilson E.L.,** 1976, Numerical methods in finite element analysis. Prentice Hall, New York.

Vladimir N. Sidorov, Corresponding Member of Russian Academy of Architecture and Construction Science, Professor, Dr.Sc, Head of the Department of Computer Science and Applied Mathematics, National Research University Moscow State University of Civil Engineering, Professor of «Building Structures, Buildings and Facilities» Department, Institute of Railway Track, Construction and Structures, Russian University of Transport (MIIT), Professor of Department «Engineering Structures and Numerical Mechanics», Perm National Research Polytechnic University; 127994, Russia, Moscow, Obraztsova st., 9, b. 9, phone: +74956814381, e-mail: sidorov.vladimir@gmail.com.

Elena S. Badina, Ph.D, Associate Professor of «Computer Aided Design» Department, Institute of Railway Track, Construction and Structures, Russian University of Transport (MIIT), Senior Researcher at the Scientific and Educational Center for Computer Modeling of Unique Buildings, Structures and Complexes of the Moscow State University of Civil Engineering, Senior Researcher at the Department of Mechanics of Structured and Heterogeneous Environment of the Institute of Applied Mechanics of the Russian Academy of Sciences; 127994, Russia, Moscow, Obraztsova st., 9, b. 9, phone: +74956092116, e-mail: shepitko-es@mail.ru.

Tsarev O. Roman, post-graduate student of the Institute of Applied Mechanics of the Russian Academy of Sciences (IAM RAS); 125040, Russia, Moscow Leningradsky Ave., 7, p. 1 telephone +7 (499) 257-03-58 e-mail: tsarev.r.o@yandex.ru.

Сидоров Владимир Николаевич, член-корреспондент РААСН, профессор, доктор технических наук, заведующий кафедрой информатики и прикладной математики Национального исследовательского Московского государственного строительного университета, профессор кафедры «Строительные конструкции, здания и сооружения» Института пути, строительства и сооружений Российского университета транспорта (МИИТа); 127994, Россия, г. Москва, ул. Образцова, д.9, стр. 9, телефон: +74956814381, e-mail: sidorov.vladimir@gmail.com.

Бадьина Елена Сергеевна, кандидат технических наук, доцент кафедры «Системы автоматизированного проектирования» Института пути, строительства и сооружений Российского университета транспорта (МИИТа), старший научный сотрудник Научно-образовательного центра компьютерного моделирования уникальных зданий, сооружений и комплексов Московского государственного строительного университета, старший научный сотрудник Отдела механики структурированной и гетерогенной среды Института прикладной механики Российской академии наук, 127994, Россия, г. Москва, ул. Образцова, д.9, стр. 9, телефон: +74956092116, e-mail: shepitko-es@mail.ru.

Царев Роман Олегович, аспирант Института прикладной механики Российской академии наук (ИПРИМ РАН); 125040, Россия, г. Москва Ленинградский просп., 7, стр. 1 телефон +7 (499) 257-03-58 e-mail: tsarev.r.o@yandex.ru

DOI:10.22337/2587-9618-2022-18-4-132-137

CONCRETE DEFORMATION MODEL FOR RECONSTRUCTED REINFORCED CONCRETE

Vladimir I. Travush [1], Vasily G. Murashkin [2]

[1] Urban planning institute of residential and public buildings, Moscow, RUSSIA
[2] OOO «Rieltstroy», Samara, RUSSIA

Abstract: During the reconstruction, or upon expiration of the service life, as well as after external impact, reinforced concrete structures require examination and verification calculations. Existing diagrams of concrete deformation are focused on designing new structures and are not adapted to the concretes of the reconstructed structures. Using the world experience in describing alloy deformation, the concrete deformation model based on using the Arrhenius equation is proposed in this article. A technique for creating an individual deformations model during the reconstruction is demonstrated on a specific example. The physical meaning of the coefficients used in the proposed model is illustrated. Examples confirming the adequacy of the proposed concrete deformations model during the reconstruction are given.

Keywords: stress-strain diagram of concrete, reconstruction, reinforced concrete, compressive strain

МОДЕЛЬ ДЕФОРМИРОВАНИЯ БЕТОНА ДЛЯ РЕКОНСТРУИРУЕМОГО ЖЕЛЕЗОБЕТОНА

В.И. Травуш [1], В.Г. Мурашкин [2]

[1] ЗАО «Городской проектный институт жилых и общественных зданий», г. Москва, РОССИЯ
[2] ООО «Риэлтстрой», г. Самара, РОССИЯ

Аннотация: При реконструкции во время эксплуатации сооружения, либо при необходимости продления срока его эксплуатации, железобетонные конструкции требуют обследования и проведения поверочных расчетов. Существующие диаграммы деформирования бетона ориентированы на проектирование новых конструкций и не адаптированы для бетонов реконструируемых сооружений. Используя мировой опыт описания деформирования металлических сплавов, предложена модель деформирования бетона на основе уравнения Аррениуса. Описана методика построения индивидуальной модели деформирования при реконструкции с использованием конкретного примера. Проиллюстрирован физический смыл коэффициентов, используемых в предлагаемой модели. Приведены примеры, подтверждающие адекватность предлагаемой модели деформирования бетона при реконструкции.

Ключевые слова: диаграмма деформирования бетона, реконструкция, железобетон, относительные деформации

INTRODUCTION

The number of structures that require inspection and verification calculations increases every year. One of the most modern and accurate calculation method is the diagram method. The basis of such method is a mathematically described dependence that relates strain to stress (σ–ε) [1]. There are a significant number of different proposals describing the dependence (σ–ε) [2], however all of them are focused on the design of new structures. This means that they are developed for a range of concrete characteristics that fall within the framework established by regulatory documents. During the long-term operation, concrete changes its deformation and strength characteristics, especially when it exposed to an

aggressive environment or high temperatures. For such concretes, the ratio between strength and deformability goes beyond the standard one. Therefore, the existing relations (σ–ε) require adjustment, which is impossible without additional labor-intensive scientific and experimental studies.

METHOD

There are a number of analytical descriptions of the σ–ε curves for metals and alloys based on the well-known Arrhenius equation obtained to describe the kinetic processes occurring in gases:

$$k=A\cdot e^{-Ea/R\cdot T}, \quad (1)$$

where k is the constant for chemical reaction rate; A= (a · $T^{1/2}$) is the total number of molecular interactions; e is base of natural logarithm; Ea is the activation energy J/mol; R is the gas constant 8.31 J/mol·T; T is the temperature measured in K.

Based on the well-known Arrhenius equation, Zeger [3] proposed a logarithmic dependence of the relationship between stresses, temperature and metal strain rate. Davidenkov, using the Arrhenius equation, obtained the relationship between the yield strength of the metal and the strain rate [4]. A number of researchers noted that the logarithmic dependences of strains and stresses are in good agreement with experimental data for aluminum [5] at room temperatures.

Polukhin [5] proposed to use the Arrhenius equations in order to obtain the relationship between temperature, stresses and strains in metals. Besides, he applied a similar equation to determine the number of equilibria point defects in a metal, which allow consideration of microdefects in the material.

Let us focuses on the features of the application of the Arrhenius equation for concrete, which is a more complex multicomponent and inhomogeneous material that has many more structural defects compared to metals.

Taking into account the defects and microcracks in concrete, which close with increasing strains under load, and involve an increasing number of bonds, the coefficient A should obviously be a function of strains.

For concrete, it can be taken in the form

$$A = (a \cdot T^{1/2}) = a \cdot \varepsilon^{b}, \quad (2)$$

where a and b are the coefficients determined from boundary conditions; ε is the strain.

As in equation (1), coefficient *a* reflects the number of connections involved, i.e., actually reflects the strength properties of concrete. In the Arrhenius equation, the total number of bonds involved changes with temperature, which is typical for a gas. If there is no dependence of concrete strain on temperature, the variable T - was replaced by the variable ε similarly to the assumptions of Seger. Thus, the dependence of stresses on strain for concrete can be represented as:

$$\sigma(\varepsilon) = a \cdot \varepsilon^{b} \cdot e^{\frac{-b\cdot\varepsilon}{p}} \quad (3)$$

The resulting expression (3) is recommended to be used to describe the dependence (σ–ε) of concrete during reconstruction. The values of the coefficients *a* and *b* are finded from the survey results.

RESULTS AND DISCUSSION

As an example, a diagram of a concrete specimen cut from a reinforced concrete girder of rectangular cross section of 400 x 200 mm have been constructed using the test results. Design reinforcement consisted of 3 bars of Ø28 placed in one row (Rs=400MPa, Es=200 103MPa). At the time of the survey, the structure had been under operation for over 30 years. The maximum compressive stress in concrete during testing was 32 MPa, the strain

was 0.003. In addition, it was found that compressive stress in concrete of 6.4 MPa corresponded to strain of 0.0005. The expression (3) was written using the data established during the testing of the specimen:

$$32 \cdot 10^6 = a \cdot 0{,}003^b \cdot e^{\frac{-b \cdot 0{,}003}{p}} \qquad (4)$$

$$6{,}4 \cdot 10^6 = a \cdot 0{,}0005^b \cdot e^{\frac{-b \cdot 0{,}0005}{p}} \qquad (5)$$

Having solved equations (4) and (5) together, the values of the coefficients for expression (3) have been determined as follows: $a = 2.958 \cdot 10^{12}$ and $b = 1.679$. The curve σb(εb) has been developed for the reduced values of these coefficients as illustrated in fig. 1.

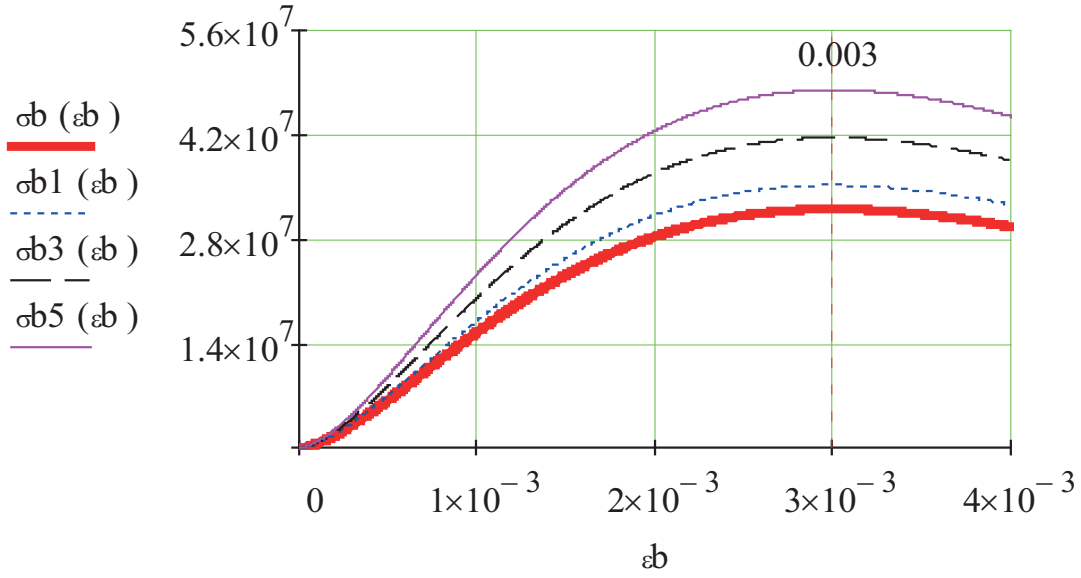

Figure 1. Concrete stress-strain diagrams for various values of the coefficient a

Analysis of equation (3) shows that an increase in the coefficient ***a*** lead to a proportional change in the maximum stresses in the diagram. The curves σ1(ε), σ3(ε), σ5(ε) are plotted for the coefficients ***a*** increased in 1.1; 1.3 and 1.5 times, respectively. As a result, the value of the maximum stresses in the diagram increased to 35.2 MPa, 41.6 MPa, and 48 MPa, respectively. The strain value at the maximum stress did not change.

Concrete is a heterogeneous material with pores and structural defects, which lead to a decrease in the angle of inclination of the tangent to the axis of strain at the initial stage of loading. This fact was demonstrated in the studies of many authors, including Berg [6]. The coefficient b of the proposed deformation model accounts the effects of the physical and mechanical properties of an inhomogeneous material with pores and structural defects.

The effects of the coefficient b on the diagram are illustrated in fig. 2. The curves σ1(ε), σ3(ε), σ5(ε) were constructed for the coefficients ***b*** increased in 1.1, 1.3, and 1.5 times, respectively, with simultaneous proportional correction of the coefficient ***a*** to the initial level of maximum stresses on the diagram. Such correction is necessary due to the fact that the coefficient ***b*** is also included in the first part of equation (3). Respectively, one numerically affects the reflection of the strength characteristic. This does not contradict the meaning of the coefficient b, since pores and structural defects affect the strength of the material. In this case, the correction was aimed to demonstrate the effect of the coefficient ***b***.

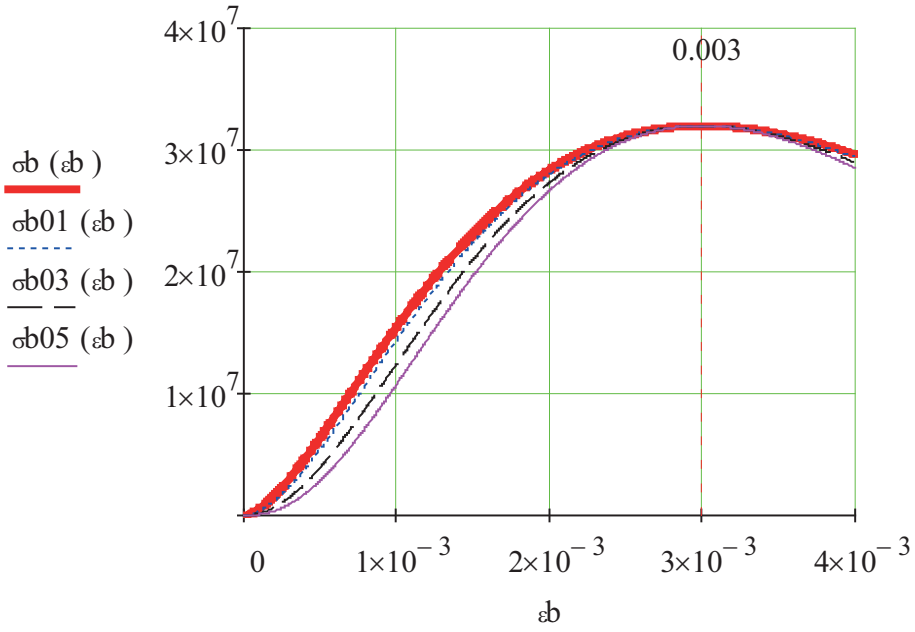

Figure 2. Concrete stress-strain diagrams obtained for variable coefficient b

The more structure defects in concrete, the faster destruction occurs under extreme loads. In such problems, it is often necessary to consider the descending branch. If there is a need to clarify the descending branch on the diagram, the coefficient ***c*** should be added to the analytical expression (3). Its physical meaning is similar to the coefficient ***b*** only on the outrageous section of the diagram. The coefficient c can be obtained from any point on the descending branch of the diagram when testing a specimen.

This ensures correctness of the deformation graph in the most difficult area of the fracture:

$$\sigma(\varepsilon) = a \cdot \varepsilon^{b} \cdot e^{\frac{-c \cdot \varepsilon}{p}}$$

The reliability of the expression (3) to relation (σ–ε) was confirmed by studies that were published in [7] and [8]. The work [7] presents experimental studies confirming the adequacy of using expression (3) for concrete with a strength of 32 MPa after 30 years of operation. The paper [8] provides an analysis of the application of equation (3) for construction of a stress-strain diagram of concrete exposured to fire at temperatures of 400° C and 600° C, according to experimental data obtained by VNIIPO [9] and polymer concrete tested at Mordovian State University [10].

CONCLUSION

Thus, the application of the proposed exponential relation in order to create a concrete deformation model allows approximation of a stress-strain curve (σ–ε) in a fairly simple expression with reflection of the main specific properties of concrete associated with an inhomogeneous structure, the presence of microcracks, pores and other microdefects. Besides, this is urgent in the case of reconstruction, when the strength and deformation properties of concrete are determined during the survey of structures. It allows construct a concrete deformation model based on a small number of test results directly for the reconstructed structure.

REFERENCES

1. **Karpenko S.N., Karpenko N.I., Yarmakovskij V.N.** Diagrammnyj metod rascheta sterzhne-vykh zhelezobetonnykh konstruktsij, ehkspluatiruemykh pri vozdejstvii nizkikh klimati-cheskikh (do -70 °S) i tekhnologicheskikh (do -150 °S) temperature [The Diagram Method of Rod's Reinforced ConcreteStructures Account which are Exploited in the Action of Low Negative Temperatures] *Academia. Arkhitektura i stroitel'stvo*. 2017. No. 1. Pp: 104-108 (in Russ.).
2. **Karpenko N.I.** Obschie modeli mehaniki zhelezobetona [General models of reinforced concrete mechanics] Moskva. Strojizdat. 1996. 416 p. (in Russ.).
3. **Zeger A.** Vozniknovenie defektov reshetki pri dvizhenii dislokacij i ih vliyanie na temperaturnuyu zavisimost' deformiruyushchih napryazhenij GCK kristallov [The emergence of lattice defects during the motion of dislocations and their influence on the temperature dependence of the deforming stresses of FCC crystals] *Problemy sovremennoj fiziki. Dislokacii v kristallah*. Moscow. Izd-vo inostrannoj literatury. 1960. Pp. 179-268 (in Russ.).
4. **Potapova L.B., Yarcev V.P.** Mekhanika materialov pri slozhnom napryazhennom sostoyanii [Mechanics of materials under complex stress state] Moscow. Mashinostroenie – 1. 2005. 244p. (in Russ.).
5. **Poluhin P.I., Gorelik S.S., Voroncov V.K.** Fizicheskie osnovy plasticheskoj deformacii [Physical basis of plastic deformation] Moscow. «Metallurgiya». 1982. 584p. (in Russ.).
6. **Berg O.Y.** Fizicheskie osnovy teorii prochnosti betona i zhelezobetona [Physical foundations of the theory of strength of concrete and reinforced concrete] Moscow. Gosstrojizdat. 1961. 96p. (in Russ.).
7. **Murashkin V.G., Murashkin G.V., Travush V.I.** Raschet nesushhej sposobnosti konstruktsij zdanij tekstil'noj promyshlennosti [Calculation of the bearing capacity of structures of buildings of the textile industry] Izvestiya vysshikh uchebnykh zavedenij. *Tekhnologiya tekstil'noj promyshlennosti*. 2019. No. 5. Pp: 222-228. (in Russ.).
8. **Murashkin V.G.** Osobennosti nelinejnogo deformirovaniya betona [Features of Nonlinear Deformation of Concrete] *Academia. Arkhitektura i stroitel'stvo*. 2019. № 1. Pp. 128-132. (in Russ.).
9. **Fedorov V.S., Levitskij V.E., Molchadskij I.S., Aleksandrov A.V.** Ognestojkost' i pozharnaya opasnost' stroitel'nyh konstrukcij [Fire resistance and fire hazard of building structures] Moscow. ASV. 2009. 408p. (in Russ.).
10. **Selyaev V.P., Nizina T.A., Balykov A.S., Nizin D.R., Balbalin A.V.** Fraktal'nyj analiz krivykh deformirovaniya dispersno-armirovannykh melkozernistykh betonov pri szhatii [Fractal Analysis of Deformation Curves of Dispersed-Reinforced Fine-Grained Concrete under Compression]. Vestnik Permskogo natsional'nogo issledovatel'skogo politekhnicheskogo universiteta. Mekhanika. 2016. No. 1. Pp: 129–146.

СПИСОК ЛИТЕРАТУРЫ

1. **Карпенко С.Н.** Диаграммный метод расчета стержневых железобетонных конструкций, эксплуатируемых при воздействии низких климатических (до -70 °С) и технологических (до -150 °С) температур / Карпенко С.Н., Карпенко Н.И., Ярмаковский В.Н.//Academia. Архитектура и строительство. 2017. № 1. С. 104-108.
2. **Карпенко Н.И.** Общие модели механики железобетона /Карпенко Н.И. - М.: Стройиздат, 1996. 416 с.
3. **Зегер А.** Возникновение дефектов решетки при движении дислокаций и их влияние на температурную зависимость

деформирующих напряжений ГЦК кристаллов / А.Зегер // Проблемы современной физики. Дислокации в кристаллах. - М.: Изд-во иностранной литературы, 1960. — С. 179-268
4. **Потапова Л.Б.** Механика материалов при сложном напряженном состоянии/Потапова Л.Б., Ярцев В.П. – М.: «Издательство Машиностроение – 1», 2005. – С. 244
5. **Полухин П.И.** Физические основы пластической деформации / Полухин П.И., Горелик С.С., Воронцов В.К. – М.: «Металлургия», 1982. – С. 584
6. **Берг О.Я.** Физические основы теории прочности бетона и железобетона / О.Я. Берг. – М.: Госстройиздат, 1961. — С 96.
7. **Мурашкин В.Г.** Расчет несущей способности конструкций зданий текстильной промышленности/ Мурашкин В.Г., Мурашкин Г.В., Травуш В.И. // Известия высших учебных заведений. Технология текстильной промышленности. 2019. № 5 (383). — С. 222-228.
8. **Мурашкин В.Г.** Особенности нелинейного деформирования бетона/Мурашкин В.Г. // Academia. Архитектура и строительство. 2019. № 1. С. 128-132.
9. **Федоров В.С.** Огнестойкость и пожарная опасность строительных конструкций / Федоров В.С., Левитский В.Е., Молчадский И.С., Александров А.В. –М. : АСВ, 2009. – 408 с.
10. **Селяев В.П.** Фрактальный анализ кривых деформирования дисперсно-армированных мелкозернистых бетонов при сжатии / Селяев В.П., Низина Т.А., Балыков А.С., Низин Д.Р., Балбалин А.В. // Вестник Пермского национального исследовательского политехнического университета. Механика. – 2016. – № 1. – С. 129–146.

Vladimir I. Travush, Full Member of Russian Academy of Architecture and Construction Sciences, Professor, Dr.Sc.; Vice-Director, Urban planning institute of residential and public buildings, Nizhnij Susal'nyj per., 5, Moscow; Russia, phone: +7 (495) 775-75-65, e-mail: travush@mail.ru.

Vasily G. Murashkin, docent, candidate in tech. sc., deputy director, OOO «Riehltstroj», 443029 Solnechnay str., 26b, Samara, Russia, phone: +7(846)243-27-26; e-mail: murvag@mail.ru.

Травуш Владимир Ильич, академик РААСН, профессор, доктор технических наук, заместитель генерального директора по научной работе ЗАО «Городской проектный институт жилых и общественных зданий»; Россия, Москва, 105064, Нижний Сусальный пер., д.5; тел.: +7 (495) 775-75-65, e-mail: travush@mail.ru.

Мурашкин Василий Геннадьевич, доцент, к.т.н., заместитель директора, ООО «Риэлтстрой»; г. Самара, 443029, ул. Солнечная, 26Б; тел.: +7 (846)243-27-26; e-mail: murvagr@mail.ru.

International Journal for Computational Civil and Structural Engineering, 18(4) 138–150 (2022)

DOI:10.22337/2587-9618-2022-18-4-138-150

ANALYSIS OF THE DEGREE OF INFLUENCE OF INTERNAL AND EXTERNAL FACTORS ON THE TEMPERATURE REGIME OF A LOW-CEMENT CONCRETE DAM

Nikolay A. Aniskin [1], ***Alexey A. Shaytanov*** [1], ***Mikhail M. Shaytanov*** [2]

[1] National Research Moscow State University of Civil Engineering (MSUCE), Moscow, Russia
[2] Lengiprorechtrans design institute

Abstract: In this paper, we consider the issue of assessing the degree of influence of the selected factors on the temperature regime and the thermally stressed state of a concrete gravity dam being built from low-cement concrete for several possible construction scenarios. The studies were carried out in relation to the design and conditions of the construction area of the Pskem hydroelectric complex in the Republic of Uzbekistan. Variation factors were: cement consumption in the mixture, the initial temperature of the concrete mixture, the heat release of cement, the thickness of the laid concrete layer, the month of commencement of work. The environmental factors were the variable ambient temperature during the year by months and the influence of solar radiation. The calculations were carried out taking into account the seasonality of the moment the construction of the structure began. 2 options were considered: autumn-winter with concreting of the zone at the base of the dam from September to February inclusive; spring-summer with concreting of this zone from March to August inclusive. In addition, options were considered taking into account additional heating from exposure to solar radiation and without it. The studies were carried out using the methodology of experiment planning in the search for optimal solutions (method of factor analysis). The numerical experiment was carried out on the basis of the finite element method using the ANSYS software package. Using the method of factor analysis, the influence of the main acting factors on the temperature regime of a gravity dam made of rolled concrete was studied. A variant of a combination of factors is proposed to obtain the most favorable temperature regime. Regression equations are obtained for predicting the temperature regime of concrete gravity dams being built from low-cement content concrete. The results of studies using the factor analysis technique can be used in the design of concrete dams from rolled concrete.

Keywords: concrete gravity dam, low-cement content concrete, numerical studies, temperature regime, thermal stressed state, factorial analysis, experiment planning theory

АНАЛИЗ СТЕПЕНИ ВОЗДЕЙСТВИЯ ВНУТРЕННИХ И ВНЕШНИХ ФАКТОРОВ НА ТЕРМОНАПРЯЖЕННОЕ СОСТОЯНИЕ ПЛОТИНЫ ИЗ МАЛОЦЕМЕНТНОГО БЕТОНА

Н.А. Анискин [1], ***А.М. Шайтанов*** [1], ***М.В. Шайтанов*** [2]

[1] Национальный исследовательский Московский государственный строительный университет, г. Москва, РОССИЯ
[2] Проектно-изыскательский институт «Ленгипроречтранс»

Аннотация. В настоящей работе рассмотрен вопрос оценки степени воздействия выбранных факторов на температурный режим и термонапряженное состояние плотины из малоцементного бетона при помощи методики факторного анализа для нескольких возможных сценариев учета. Исследования проводились применительно к конструкции и условиям района строительства Пскемского гидроузла в Республике Узбекистан. Факторами варьирования являлись: расход цемента в смеси, начальная температура бетонной смеси, тепловыделение цемента, толщина укладываемого слоя бетона, месяц начала работ. Факторами внешней среды являлись переменная температура окружающей среды в течение года по месяцам и влияние солнечной радиации. Расчеты проведены с учетом сезонности (2 сезона: осенне-зимний с сентября по февраль включительно; весенне-летний с марта по август включительно) для двух

вариантов: с учетом дополнительного разогрева от воздействия солнечной радиации и без него. В результате было определено суммарное температурное воздействие на поверхности возводимого сооружения (среднемесячная температурой окружающей среды совместно с нагревом от солнечной радиации). Основываясь на полученных результатах, были сделаны выводы о вкладе каждого из вышеперечисленного факторов в температурный режим и термонапряженное состояние рассматриваемого сооружения, а также получены уравнения регрессии, позволяющие определить значения искомых показателей в заданных характерных точках, распределенных по сечению плотины. Уравнения применимы для любых массивных плотин из малоцементного бетона с шириной подошвы не менее 20 м, расположенных в любых климатических условиях.

Ключевые слова: бетонная гравитационная плотина, малоцементный бетон, численные исследования, температурный режим, термонапряженное состояние, факторный анализ, теория планирования эксперимента

INTRODUCTION

Forecasting the temperature regime of a gravity dam made of rolled concrete during construction and operational periods is necessary at the design stage of the construction. The solution of this task is rather complicated due to numerous functioning and changing in time factors. The issues of predictive modelling of the temperature regime and thermally stressed state of gravity dams have been considered in a number of works in Russia as well as abroad [1-12]. In recent years there have been significant changes in solving this issue, connected with the development of massive concrete dams' construction technologies as well as calculation methods allowing to take into account various acting factors. Nevertheless, temperature regime control and thermally stressed state of building remain topical today. This article represents results of a temperature regime and thermally stressed state of the gravity dam made of low-cement rolled concrete. The analysis of degree of influence of selected factors on temperature regime and thermally stressed state of the dam is carried out using the method of factor analysis [13-14].

Several possible scenarios for determination and evaluation of influence degree of various factor on stress-deformed state of the building. The calculations were carried out taking into account the seasonality of pouring concrete: starting in March and in September. The effect of solar radiation on the temperature regime is considered in detail. The calculations are provided for two variants: taking into account additional heating of the surfaces of the constructed structure from the influence of the solar radiation and not taking these into account. The solution of the problems of determining the temperature regime and thermally stressed state of the considered variants was obtained using the ANSYS software package on the basis of the finite element method [15-21].

A mathematical model of the structure, which makes it possible to predict the temperature regime and the thermally stressed state of the structure, was obtained from the results of the research. The best and the worst variants of value combinations of the considered factors from the point of view of the temperature regime of the structure were determined.

1. METHODS

1.1. Theoretical basis for solving the temperature problem

Numerical modelling of the temperature nonstationary problem taking into account heat emission by hydration of the cement is based on the solution of the well-known equation of thermal conductivity theory [1-6]:

$$k\nabla^2 T + Q = \rho c \frac{\partial T}{\partial \tau}, \quad (1)$$

where: T – temperature function, ^{0}C; k – thermal conductivity of material, m^2/s; c – material specific heat capacity, kJ/kg · $^\circ$C; ρ – density of

material, kg/m^3; Q – heat released during hydration, kJ/m^3; τ - time, days.
The equation (1) can be written the following way:

$$\frac{k}{c\rho}\nabla^2 T + \frac{Q}{c\rho} = \frac{\partial T}{\partial \tau}, \quad (2)$$

The amount of heat released in the hydration process is defined as:

$$Q = C \cdot E, \quad (3)$$

where: C – cement consumption per cubic meter of concrete, kg/m^3; E – maximum heat release of cement, kJ/kg). Thus, the solution of the temperature problem for a constructed concrete block with thermal insulation of surfaces is reduced to the solution of the basic differential equation of the theory of heat conduction with internal heat sources (2). A boundary condition of the 3rd kind (convective heat exchange) was considered as the limiting condition on the border of the structure.
The heat release of cement was taken into account using the known dependence for the isothermal process (4) [8-9,12,18-19]:

$$Q = Q_{max} \cdot [1 - (1 + A_t \cdot \tau)^{-0{,}833}], \quad (4)$$

where: A_t – coefficient of heat release rate (5):

$$A_t = A_{20} \cdot 2^{\frac{t-20}{\varepsilon}}, \quad (5)$$

where: $\varepsilon = 10$ °C, A_{20} – coefficient of heat release rate at 20 °C [8-9,12,18-19,21].

2. OBJECT OF STUDY

As the object of study, a concrete gravity dam with a height of 197 m made of rolled concrete was considered, designed for the Pskem hydroelectric complex (Republic of Uzbekistan), the site of which is located in the mountains of the Western Tien Shan. The average heights in the construction area there vary between 2 000 m – 4 400 m and decrease from the source to the outlet.

2.1. Climatic conditions of construction area of the facility

The climate of the construction area is characterized by an average annual air temperature of 9,5 ºC. The average long-term air temperature of the coldest month falls on January – minus 3,2 ºC, the warmest – on August – plus 24,4 ºC. The distribution of average monthly temperatures throughout the year is presented in Table 1 and Figure 1 (curve without solar radiation). The data were obtained for the observation period from 1938 to 2016.

Table 1. Average monthly and average annual temperatures in the area of the object

Characteristic	*I*	*II*	*III*	*IV*	*V*	*VI*	*VII*	*VIII*	*IX*	*X*	*XI*	*XII*	*Avg. year*
Average monthly temperature ºC	-4,0	-2,0	3,0	11,0	16,0	21,0	24,0	24,0	19,0	11,0	4,0	-1,1	9,5
Concrete surface temperature taking into account solar radiation, ºC	3,5	10,1	18,1	29,6	33,5	36,2	41,2	40,9	35,4	25,8	13,4	5,9	23,5

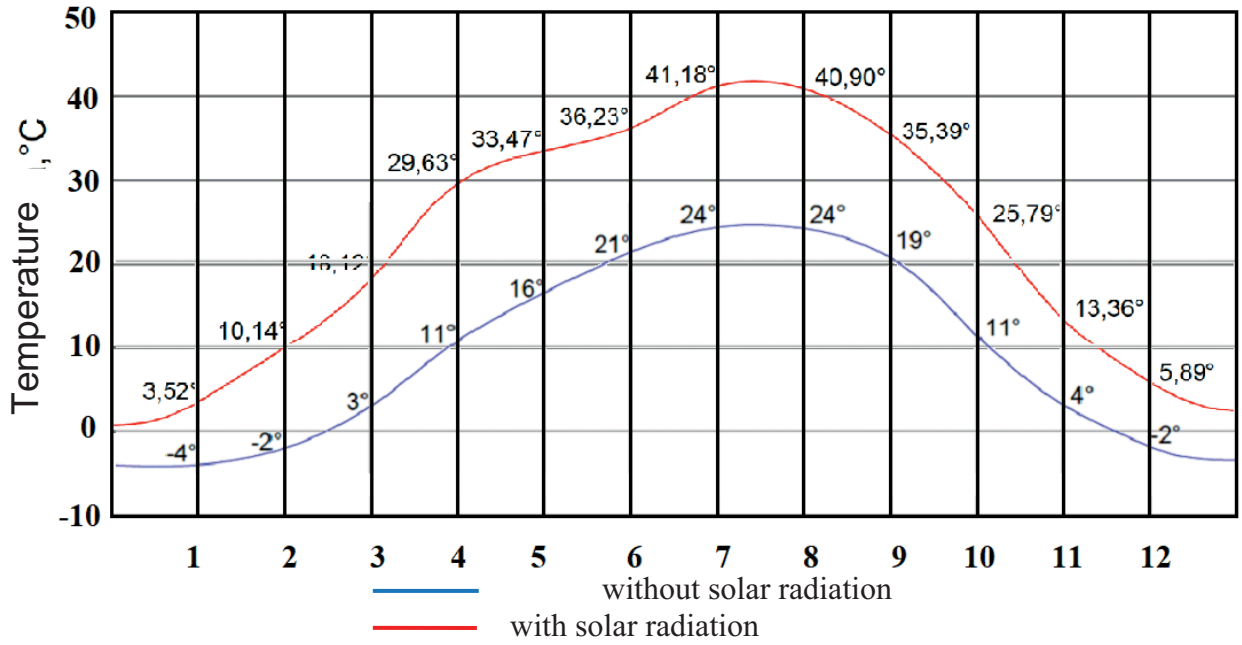

Figure 1. Graph of changes in in the average monthly air temperature in the construction area

The climate in the dam site area is characterized by a large number of sunny days in the year – 250. Therefore, solar radiation was considered as one of the factors influencing the formation of temperature regime of the construction.

The issue of solar radiation effect on the temperature regime of concrete dams in construction and operational periods and the development of a methodology for accounting for this effect has received relatively little attention to date. The works of domestic researchers [1,5-6,8-9,12] contain a number of indications on the need to take into account solar radiation when calculating the temperature regime of concrete constructions. The usual approach, used in hydrotechnical practice is usually to increase the temperature on the construction surface exposed to sunlight using the dependence [22-24]:

$$t_n = t_в + R/\alpha_n, \quad (6)$$

where $t_в$ – air temperature, R – amount of radiant hear absorbed by a unit surface per unit time; α_n – coefficient of heat transfer at the contact of the structure with air.

For the climatic conditions in Russia the average daily value of the surface temperature due to solar radiation R/α_n varies within (4-10) °C [22-24].

The papers [22-24] propose to use some average parameters of thermal heating from solar radiation S_0, $kJ/(m^2 \cdot h)$ depending on the latitude of the considered point of the Earth and the month of the year, obtained on the basis of meteorological observation data.

The value of heating from solar radiation for a day with variable cloudiness can be determined from the dependence:

$$S = S_0 \cdot (1 - k_1 \cdot n), \quad (7)$$

where S – the amount of solar radiation heat on a day with variable cloudiness; S_0 - the amount of heat of solar radiation on a sunny day; n – the cloudiness coefficient; k_1 – coefficient taking into account the latitude.

One of the first objects where much attention was paid to the study of the solar radiation influence was the high concrete dam of the Toktogul hydroelectric power station in the Republic of Kyrgyzstan, where the summer period is characterized by high solar activity.

The determination of solar radiation effect on the temperature regime of the dam on this site was carried out on the basis of data from field actinometric observations directly at the construction site. At the same time, the impact of the scattered solar radiation was assumed to be directly proportional to the impact of direct solar radiation, which led to a decrease in accuracy of the assessment results.

The study of this issue was actively carried out by Chinese researchers in relation to transport facilities [22-24]. In particular, an issue of solar radiation's impact on the temperature regime of bridge supports was considered. However, such facilities are not as massive as concrete dams, which results in more intensive cooling of the structure due to convective heat transfer. The ability of the surfaces of concrete masses to absorb solar energy also needs additional study.

The solar radiation impact will be especially significant for the high gravity dam of rolled concrete considered in this paper. In this case due to the intensive rate of concreting and erecting the structure in fairly thin layers (from 0,5 to 1,5 m) the degree of solar radiation impact on the formation of the temperature regime increases.

The modern approach to assessing the impact of solar radiation, conducted in this paper, allows to take data from both field and satellite observations into account as well as determine the amount of absorbed solar energy and heating of concrete mass connected to it according to seasonality and the terrain around the building site.

The radiation regime of the surfaces under consideration when erecting the dam made of low-cement concrete (the surface of the pressure and downstream faces, the horizontal face of the laid layer) is formed by radiant energy flows. The total solar radiation affecting during the day on a horizontal surface is determined by the formula (8):

$$G = J \cdot sinh_0 + D, \tag{8}$$

where J – intensity of direct solar radiation, W/m^2, determined by means of satellite/field actinometric observations [1]; D – diffused solar radiation, W/m^2, h_0 – angular height of the sun, degrees, determined by the dependence (9):

$$sinh_0 = sin\varphi \cdot sin\delta + cos\varphi \cdot cost \cdot cos\delta, \tag{9}$$

where φ – the latitude of the construction area; δ – declination of the sun, deg; t – hour angle, deg.;

The calculation of the characteristics of solar radiation was conducted taking into account the peculiarities of the location of the hydroelectric complex and the terrain around the site selected specifically for the construction. On Fig. 2 below is a graph for determining the angular height of the sun above the horizon and the solar azimuth, built taking into account the terrain.

As the result the temperatures on the concrete surface of the gravity dam under construction were determined, considering its increase from solar radiation effects by months of the year.

The obtained results are presented on Fig. 2 and Table 1. A significant increase in temperature on the surface due to solar radiation can be noted: for example, it is 17,2 ºC in July.

Data obtained as a result of calculating solar radiation impact temperatures on the surface of concrete structure by months were used in calculating the temperature regime at the next stage.

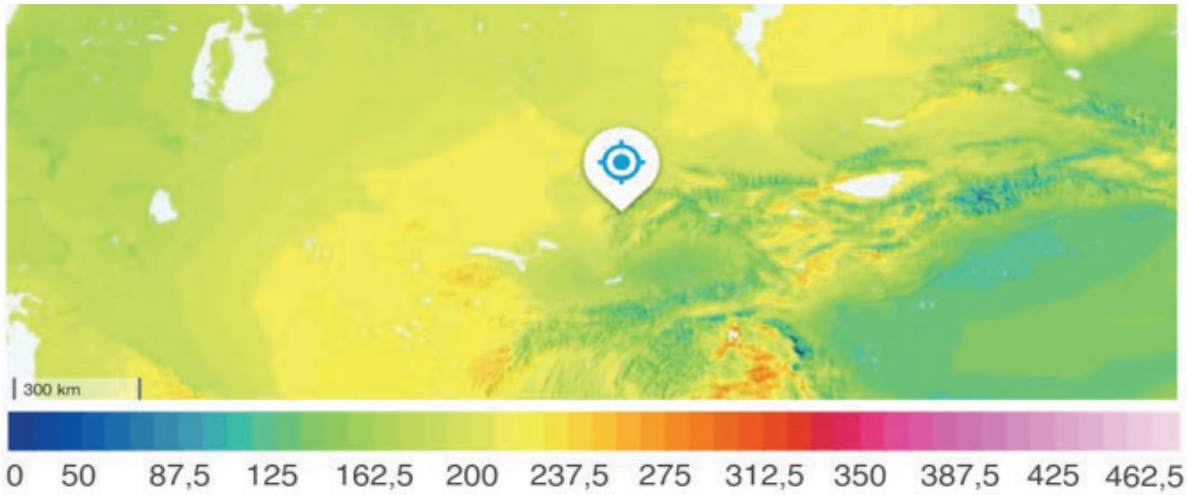

Figure 2. Map of the intensity impact of direct solar radiation, kW/m² in the construction area of the Pskem HPP

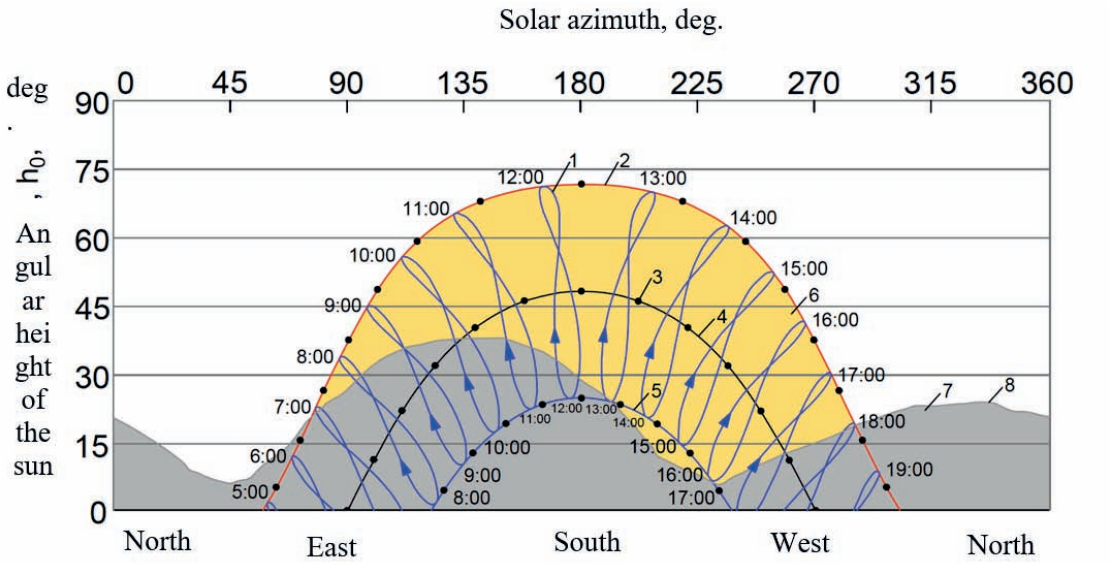

Figure 3. Graph of the change in the angular height h_0 and solar azimuth, where: 1 – local time in the construction area (time zone of Tashkent, Uzbekistan, UTC+05:00); 2 – the movement of the sun on the summer solstice day on 21.06.2021; 3 – true solar time; 4 – the movement of the sun on the spring/autumn equinox day; 5 – the movement of the sun on the winter solstice day on 21.12.2021; 6 – zone of active solar impact; 7 – shading caused by the surrounding terrain; 8 – the contour of the surrounding terrain at the construction site

2.2. Statement of studies using factor analysis.

The main task of studying the temperature regime of a low-cement concrete dam, the results of which are presented in this paper, is to analyze the degree of influence of the selected factors, to assess their favorable or unfavorable effect on the structure. Based on the obtained mathematical model of the temperature regime, recommendations will be developed to achieve a favorable temperature distribution in the structure and a combination of acting factors will be determined to ensure the optimal solution. It must be optimal technologically and economically and meet the stated requirements for the reliability and structural safety. The issues of predictive modeling of the temperature regime and the thermally stressed state of concrete gravity dams

were considered in a number of works performed at NRU MGSU, JSC "VNIIG named after B.E. Vedeneev", in the branch of JSC "Institute Hydroproject" – "NIIES" and other organizations [1-12,16-17,22-24]. Within the framework of this work, numerical studies were performed using the ANSYS software package using the finite element method [15-24]. The result of the work is a mathematical model of the structure, which makes it possible to predict the thermally stressed state of the structure and ensures maximum project efficiency. The analysis of the degree of influence of the selected factors on the temperature regime and the thermally stressed state of the low-cement concrete dam was carried out using the factor analysis technique [13-14]. Several possible scenarios are considered for accounting and assessing the degree of influence of various factors on the stress-strain state of a structure. The calculations were carried out taking into account seasonality (2 seasons: autumn-winter including the September – February period; spring-summer including the March to August period). The effect of solar radiation on the temperature regime is considered in detail. The calculations were carried out for two options: with and without additional heating from exposure to solar radiation.

As an object of study, a gravity dam made of rolled low-cement concrete with a height of 197 m was considered. Fig. 4 presents the cross-section with the position of control points intended to establish temperature values. The formation process of the temperature regime in the process of layer-by-layer construction, filling the reservoir and the start of the operational period (the first year after the completion of construction) was considered.

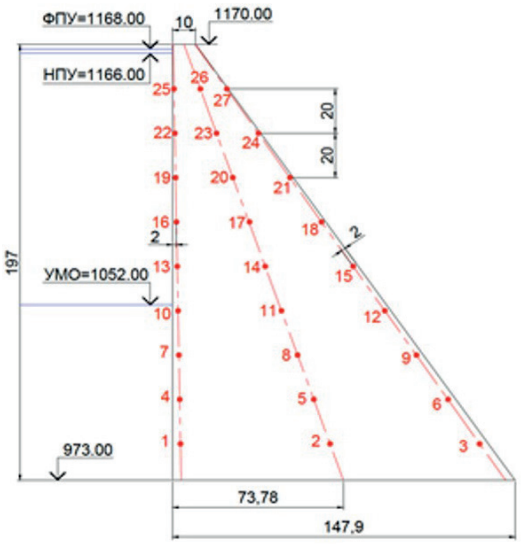

Figure 4. Cross-section of the dam with indication of control points

To create a predictive model for the temperature regime of a gravity dam made of rolled concrete, we used the experimental planning technique [13-14]. To carry out computational studies, the following factors were chosen that affect the formation of the temperature regime: cement consumption (X_1); thickness of the laid-out layer (X_2); heat generation of cement (X_3), temperature of the laid-out concrete mixture (X_4). The selected intervals of factor variation are presented in Table 2.

Table 2. Intervals of factor variation

	Factors of variation	*Factor designation*	*Values*	
			Minimum	*Maximum*
1.	Consumption of cement in the mixture (kg/m^3)	X_1	70	150
2.	Thickness of the laid-out concrete layer (m)	X_2	0,5	1,5
3.	Heat generation of cement (KJ/kg) Q_{28}/Q_{max}	X_3	293/339	335/388
4.	Concrete placement temperature (°C)	X_4	10	30

The heat emission rate of cement was chosen for the most widely used types in the manufacture of low-cement concrete mixes. This choice is associated with a faster build-up of strength, which allows one to speed up the construction of the structure. Calculations in accordance with the compiled planning matrices for the selected factors were performed for the following options:

1. Depending on the month of commencement of construction works: May or October with the corresponding ambient temperatures;
2. Depending on the consideration of solar radiation, the variable temperature of the concrete surface was assumed to be equal to the temperature or the ambient temperature. The following values obtained during the entire considered time period were selected as responses:
    1. Absolute maximum temperature in the concrete array (with indication of the location of the corresponding point), □C;
    2. Maximum temperatures at characteristic points No. 2, No. 8, No. 14, No. 20, No. 26 (Fig. 4), □C.
    3. Maximum temperature gradient between a point in the center of the array and a point on the surface of the pressure face, indicating the corresponding points, □C.

3. RESULTS OF THE STUDY

Let us consider some of the obtained equations and analyze the results obtained from the solution of the temperature problem.

Option 1. Beginning of concreting in May without taking solar radiation into account.

$$y_{i(T_{max})} = 34{,}544 + 4{,}33 \cdot x_1 - 0{,}818 \cdot x_2 + 0{,}787 \cdot x_3 + 2{,}707 \cdot x_4 - \\ -0{,}067 \cdot x_1 \cdot x_2 + 0{,}312 \cdot x_1 \cdot x_3 + 1{,}782 \cdot x_2 \cdot x_4 \quad (10)$$

Option 2. Beginning of concreting in October without taking solar radiation into account.

$$y_{i(T_{max})} = 34{,}541 + 4{,}334 \cdot x_1 - 0{,}821 \cdot x_2 + 0{,}79 \cdot x_3 + 2{,}71 \cdot x_4 - \\ -0{,}064 \cdot x_1 \cdot x_2 + 0{,}307 \cdot x_1 \cdot x_3 + 1{,}785 \cdot x_2 \cdot x_4 \quad (11)$$

Option 3. Beginning of concreting in May, taking solar radiation into account.

$$y_{i(T_{max})} = 47{,}9 + 3{,}396 \cdot x_1 - 2{,}987 \cdot x_2 + 0{,}695 \cdot x_3 + 1{,}619 \cdot x_4 - \\ -0{,}876 \cdot x_1 \cdot x_2 + 0{,}317 \cdot x_1 \cdot x_3 + 0{,}845 \cdot x_1 \cdot x_4 - 0{,}105 \cdot x_2 \cdot x_3 + 0{,}919 \cdot x_2 \cdot x_4 + \\ +0{,}089 \cdot x_3 \cdot x_4 + 0{,}855 \cdot x_1 \cdot x_2 \cdot x_4 + 0{,}101 \cdot x_2 \cdot x_3 \cdot x_4 \quad (12)$$

Option 4. Beginning of concreting in October, taking solar radiation into account.

$$y_{i(T_{max})} = 47{,}9 + 3{,}376 \cdot x_1 - 2{,}976 \cdot x_2 + 0{,}695 \cdot x_3 + 1{,}62 \cdot x_4 - \\ -0{,}884 \cdot x_1 \cdot x_2 + 0{,}313 \cdot x_1 \cdot x_3 + 0{,}865 \cdot x_1 \cdot x_4 - 0{,}092 \cdot x_2 \cdot x_3 + 0{,}908 \cdot x_2 \cdot x_4 + \\ +0{,}089 \cdot x_3 \cdot x_4 + 0{,}863 \cdot x_1 \cdot x_2 \cdot x_4 + 0{,}089 \cdot x_2 \cdot x_3 \cdot x_4 \quad (13)$$

Analyzing the equations obtained from the solution of the temperature problem, we can draw the following conclusions:

– All the selected factors have a significant effect on the maximum temperatures at the selected points. This is most influenced by the cement consumption (factor X_1), the thickness of the laid concrete layer (X_2) and the temperature of the concrete mix (X_4). An increase in cement consumption up to 150 kg/m^3 (the maximum value of factor X_1) leads to an increase in the temperature in the concrete array by ~ (8-12) □C compared to the minimum considered consumption of 70 kg/m^3.

– The degree and sign of the influence of the factor X_2 (thickness of the laid-out concrete layer) has a different effect depending on the laying zone, the seasonality of laying and whether solar radiation is taken into account. In the case when solar radiation is not taken into account and the concreting is begun in May (option 1), in the massive zones of the dam, with an increase in the thickness of the layer of laid concrete, the temperature of the concrete array decreases (the coefficients of the regression equation with a X_2 are negative). However, for this case, the result changes in the near-ridge zone (point 26), where the reverse result is obtained: with an increase in the layer thickness, the temperature increases. At the beginning of concreting in October (option 2), the result is reversed: in the lower massive part of the dam, an increase in the layer thickness leads to an increase in temperature, and vice versa in the zone near the crest.

– For options with taking solar radiation into account (options 3, 4), in most areas of the dam, with an increase in the thickness of the layer, the temperature of the array decreases, which is explained by a decrease in the degree of solar heating for thick layers. An exception here is the zone near the base (point 26) for option 4, which is explained by the influence of low air temperature in the autumn-winter period of the year, when this zone is concreted. When laying out in thin layers, the concrete is intensively cooled by cold air.

– For the considered climatic conditions, taking into account solar radiation makes a significant contribution to the increase in the temperature heating of the structure during its construction. The impact of solar radiation causes an increase in temperature in the concrete array at a maximum of (15-16) □C□

– The choice of the start of dam construction (the options for starting work in May and October are considered) determines the formation of the temperature regime in the most problematic zone of the structures, that is, the one near the contact of the dam with the foundation. Thus, the start of concreting in May leads to an increase in temperature in the area of the dam close to the base by ~ (16-17) □C compared to the option of starting concreting in October.

Based on the results obtained, the worst and the best-case scenarios were determined in terms of the temperature regime of the structure. The degree of heating of the concrete array was considered as an evaluation criterion. The least favorable is the option with the following values of the factors and conditions of construction: cement consumption – 150 kg/m^3, layer thickness – 0,5 m, heat release is increased, initial temperature of the concrete mixture +30 □C, start of work in October, solar radiation is taken into account. The most favorable option corresponds to the following values of the factors: cement consumption – 70 kg/m^3, layer thickness – 1,5 m, heat release is moderate, initial temperature of the concrete mixture +10 □C, with the start of work in May and taking solar radiation into account. The temperature distribution for these options is shown in Fig. 5.

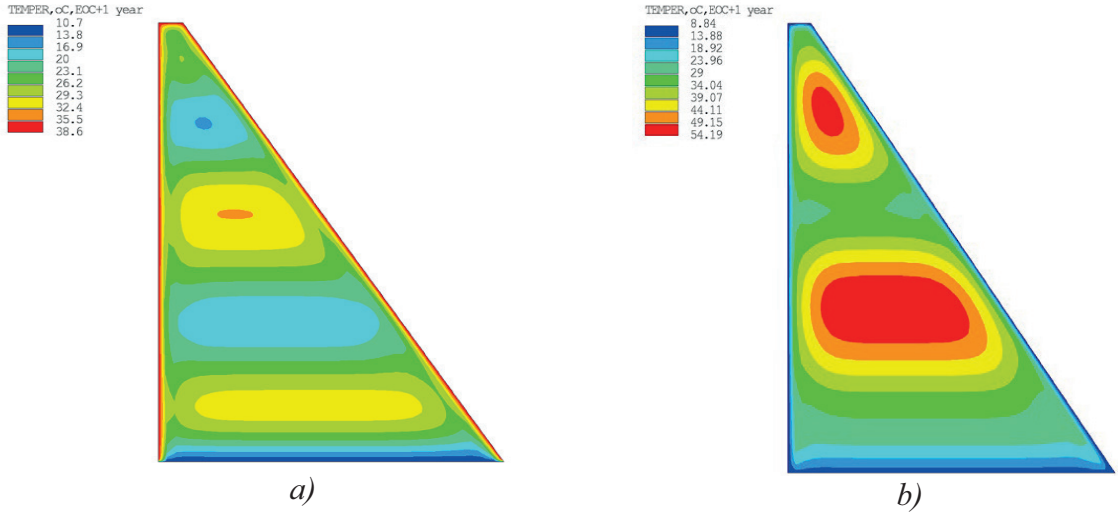

a) *b)*

Figure 5. The results of calculating the maximum temperature in the concrete array: a) the most favorable design case; b) the least favorable design case

The resulting mathematical model of the temperature regime of a gravity dam made of rolled concrete can be used to predict the temperature regime of similar structures and to select the optimal combination of the considered factors. At the next stage of research, the results of solving temperature problems were used to calculate the stress-strain state.

4. CONCLUSIONS AND DISCUSSION

We have presented the practical application of the technique for determining the effect of solar radiation on the temperature regime of the low-cement concrete dam of the Pskem hydroelectric power plant, taking into account the shading of the terrain. Such an impact increases the average annual temperature of the concrete surface by 13,98 ºC or by 147,16%, which is a significant factor that must be taken into account when designing such structures in similar climatic conditions. In the considered example solar radiation causes an increase in temperature in the concrete array, depending on the considered point, by 53,72% – 89,5% (from 8,46 □C – 16,14 □C). Based on the results of variational calculations, the most and least favorable design cases were determined in terms of the temperature regime of the dam. The worst case is the one with the following values of the factors: cement consumption – 150 kg/m^3, layer thickness – 0,5 m, heat release is increased, initial temperature of the concrete mix +30 □C, start of work in October. The most favorable is the case with the following values: cement consumption – 70 kg/m^3, layer thickness – 1,5 m, heat release is moderate, initial temperature of the concrete mixture +10 □C, work begins in May.

Based on the results of the calculations, regression equations were obtained that make it possible to determine the values of the desired indicators at the points under consideration. The equations are applicable to any massive low-cement concrete dams with a base width of at least 40 m in any climatic conditions.

REFERENCES

1. **Aniskin N.A., Shaitanov A.M.** Features of taking into account the influence of solar radiation on the heating of concrete arrays and predictive modeling of the aging of geocomposite impervious screens // Modern problems of hydraulics and hydraulic engineering construction: Collection of abstracts of the IV All-Russian scientific and practical seminar, Moscow, May 26, 2021. - Moscow: National Research Moscow State University of Civil Engineering, 2021. - P. 50.
2. **Plyat, Sh.N.** Calculations of temperature fields of concrete hydraulic structures / Sh.N. Plat - Publishing house "Energy", 1974. - 408 p.
3. **Rtishcheva, A.S.** Theoretical foundations of hydraulics and heat engineering / A.S. Rtishchev. Ulyanovsk: Textbook. - 2007. - 171 p.
4. Consolidated report on the study of the layer-by-layer method of concreting at the construction of the Toktogul HYDROELECTRIC POWER PLANT // Institute Hydroproject JSC. 1971.
5. **Fried, S.A.** Temperature stresses in concrete and reinforced concrete structures of hydraulic structures / S.A. Fried. – M.: Stroyizdat. - 1959. - 72 p.
6. **Semenov, K.V.** The effect of temperature exposure in the calculations of the thermally stressed state of discretely built-up concrete bodies / K.V. Semenov, I.A. Konstantinov, A.V. Savchenko, K.A. Kokoreva, A.A. Nesterov // Construction of unique buildings and structures. - 2015. - No. 5 (32). - S. 18-28.
7. **Isao Nagayama**. 30 years' history of roller compacted concrete dams in Japan / Isao Nagayama, Shigeharu Jikan // Roller compacted concrete dams. – 2003. – Pp. 27-38.
8. **Aniskin N.A., Shaitanov A.M., Shaitanov M.V., Khokhotva S.N.** Influence of solar radiation on the heating of an array of a gravity dam built from low-cement concrete // Gidrotekhnicheskoe stroitel'stvo. 2021. No. 11. From 11-18.
9. **Aniskin, N.A**. Temperature regime and thermal stress state of a concrete array with pipe cooling / N.A. Aniskin, Nguyen Chong Chyk // Hydrotechnical construction. - 2018. - No. 10. – P. 15–20.

10. **Bayagoob K., Bamaga S.** Construction of Roller Compacted Concrete Dams in Hot Arid Regions. materials. 2019 Vol. 12 (19). P. 1-14.
11. **Wanga L., Yang HQ, Zhou SH, Chen E., Tang SW** Mechanical properties, long-term hydration heat, behavior and crack resistance of dam concrete designed with low heat Portland (LHP) cement and fly ash // Construction and Building materials. 2018 Vol. 187. P. 1073-1091.
12. **Aniskin, N.Ch. Chyk, I.A. Bryansky, D.Kh. Hyng.** Determination of the temperature field and the thermal stress state of the laid-out concrete array by the finite element method. Vestnik MGSU. 2018 Vol.13. pp. 1407-1418. https://doi.org/10.22227/1997-0935.2018.11.1407-1418.
13. **Adler, Yu.P.** Planning an experiment in the search for optimal conditions / Yu.P. Adler, E.V. Markova, Yu.V. Granovsky. – M.: Stroyizdat, 1976. – 280 p.
14. **Adler, Yu.P.** Planning an experiment in the search for optimal conditions / Yu.P. Adler. – M.: Stroyizdat, 1976. – 588 p.
15. **Yuxiang Zhang, Jianwen Pan, Xinjian Sun, Jijun Feng, Dengqiang Sheng, Haiyun Wang, Xinjie Zhou, Yinpeng He, Mushuang Diao, Qibing Zhan**. Simulation of thermal stress and control measures for rock-filled concrete dam in high-altitude and cold regions // Engineering Structures. 2021 Vol.230. https://doi.org/10.1016/j.engstruct.2020.111721
16. **Yuqin Zhao, Gaosheng Li, Caixia Fan, Wentai Pang, and Yongtao Wang**. Effect of thermal parameters on hydration heat temperature and thermal stress of mass concrete // Advances in Materials Science and Engineering. 2021. 16p. https://doi.org/10.1155/2021/5541181
17. **Peng Lin, Haoyang Peng, Qixiang Fan, Yunfei Xiang, Zongli Yang & Ning Yang**. A 3D thermal field restructuring method for concrete dams based on real-time temperature monitoring // KSCE Journal of Civil Engineering. 2021 Vol. 25. pp. 1326-1340. https://doi.org/10.1007/s12205-021-1084-8
18. **Nikolay Aniskin, Trong Chuc Nguyen**. Prediction of thermal stress in a concrete gravity dam // IOP Conf. Ser.: Mater. sci. Eng. 2021 Vol. 1030 (012144). doi:10.1088/1757-899X/1030/1/012144
19. **N. Aniskin, Trong Chuc Nguyen**. The thermal stress of roller-compacted concrete dams during construction // MATEC Web of Conferences. 2018 Vol. 196(04059). 8p. https://doi.org/10.1051/matecconf/201819604059
20. MIDAS Information Technology, Heat of Hydration - Analysis Analysis Manual, Version - 2011, 48p.
21. **N.A. Aniskin, N.T. Chuc**. Temperature regime and thermal stress in a concrete massif with pipe cooling // Power Technology and Engineering. 2019.Vol.52(6). pp. 638-643. https://doi.org/10.1007/s10749-019-01009-9.
22. **JR Zhang**, "A test study on the solar radiation absorption coefficient of concrete surface," Building Science, vol. 22, no. 6, pp. 42–45, 2006.
23. **Guadalupe Leon, Hung-Liang (Roger) Chen.** Thermal analysis of mass concrete containing ground granulated blast furnace slag // CivilEng. 2021 Vol. 2(1). pp. 254-270. https://doi.org/10.3390/civileng2010014.
24. **Hoon Moon, Sivakumar Ramanathan, Prannoy Suraneni, Chang-Seon Shon, Chang-Joon Lee, Chul-Woo Chung**. Revisiting the effect of slag in reducing heat of hydration in concrete in comparison to other supplementary cementitious materials // Materials. 2018 Vol.11. 17p. doi:10.3390/ma11101847.

СПИСОК ЛИТЕРАТУРЫ

1. **Анискин Н.А., Шайтанов А.М.** Особенности учета влияния солнечной радиации на разогрев бетонных массивов и прогнозное моделирование старения геокомпозитных противофильтрационных

экранов // Современные проблемы гидравлики и гидротехнического строительства: Сборник тезисов докладов IV Всероссийского научно-практического семинара, Москва, 26 мая 2021 года. – Москва: Национальный исследовательский Московский государственный строительный университет, 2021. – С. 50.

2. **Плят, Ш.Н.** Расчеты температурных полей бетонных гидросооружений / Ш.Н. Плят – Издательство "Энергия", 1974. – 408 с.
3. **Ртищева, А.С.** Теоретические основы гидравлики и теплотехники / А.С. Ртищева. Ульяновск: Учебное пособие. – 2007. – 171 с.
4. Сводный отчет по исследованию послойного метода бетонирования на строительстве Токтогульской ГЭС // АО «Институт Гидропроект». 1971.
5. **Фрид, С.А.** Температурные напряжения в бетонных и железобетонных конструкциях гидротехнических сооружений / С.А. Фрид. – М.: Стройиздат. – 1959. – 72 с.
6. **Семенов, К.В.** Эффект температурного воздействия в расчетах термонапряженного состояния дискретно наращиваемых бетонных тел / К.В. Семенов, И.А. Константинов, А.В. Савченко, К.А. Кокорева, А.А. Нестеров // Строительство уникальных зданий и сооружений. – 2015. – №5(32). – С. 18-28.
7. **Isao Nagayama.** 30 years' history of roller compacted concrete dams in Japan / Isao Nagayama, Shigeharu Jikan // Roller compacted concrete dams. – 2003. – Pp. 27-38.
8. **Анискин Н.А., Шайтанов А.М., Шайтанов М.В., Хохотва С.Н.** Влияние солнечной радиации на разогрев массива гравитационной плотины, возводимой из малоцементного бетона // Гидротехническое строительство. 2021. №11. С 11-18.
9. **Анискин, Н.А.** Температурный режим и термонапряженное состояние бетонного массива с трубным охлаждением / Н.А. Анискин, Нгуен Чонг Чык // Гидротехническое строительство. – 2018. – №10. – С. 15–20.
10. **Bayagoob K., Bamaga S**. Construction of Roller Compacted Concrete Dams in Hot Arid Regions. Materials. 2019. Vol. 12 (19). P. 1-14.
11. **Wanga L., Yang HQ, Zhou SH, Chen E., Tang SW** Mechanical properties, long-term hydration heat, behavior and crack resistance of dam concrete designed with low heat Portland (LHP) cement and fly ash // Construction and Building materials. 2018 Vol. 187. P. 1073-1091.
12. **Н.А. Анискин, Н.Ч. Чык, И.А. Брянский, Д.Х. Хынг.** Определение температурного поля и термонапряженного состояния укладываемого бетонного массива методом конечных элементов // Вестник МГСУ. 2018. Vol.13. Pp. 1407-1418. https://doi.org/10.22227/1997-0935.2018.11.1407-1418.
13. **Адлер, Ю.П.** Планирование эксперимента при поиске оптимальных условий / Ю.П. Адлер, Е.В. Маркова, Ю.В. Грановский. – М.: Стройиздат, 1976. – 280 с.
14. **Адлер, Ю.П.** Планирование эксперимента при поиске оптимальных условий / Ю.П. Адлер. – М.: Стройиздат, 1976. – 588 с.
15. **Yuxiang Zhang, Jianwen Pan, Xinjian Sun, Jijun Feng, Dengqiang Sheng, Haiyun Wang, Xinjie Zhou, Yinpeng He, Mushuang Diao, Qibing Zhan**. Simulation of thermal stress and control measures for rock-filled concrete dam in high-altitude and cold regions // Engineering Structures. 2021 Vol.230. https://doi.org/10.1016/j.engstruct.2020.111721
16. **Yuqin Zhao, Gaosheng Li, Caixia Fan, Wentai Pang, and Yongtao Wang**. Effect of thermal parameters on hydration heat temperature and thermal stress of mass concrete // Advances in Materials Science and Engineering. 2021. 16p. https://doi.org/10.1155/2021/5541181

17. **Peng Lin, Haoyang Peng, Qixiang Fan, Yunfei Xiang, Zongli Yang & Ning Yang**. A 3D thermal field restructuring method for concrete dams based on real-time temperature monitoring // KSCE Journal of Civil Engineering. 2021 Vol. 25. pp. 1326-1340. https://doi.org/10.1007/s12205-021-1084-8
18. **Nikolay Aniskin, Trong Chuc Nguyen.** Prediction of thermal stress in a concrete gravity dam // IOP Conf. Ser.: Mater. sci. Eng. 2021 Vol. 1030 (012144). doi:10.1088/1757-899X/1030/1/012144
19. **N. Aniskin, Trong Chuc Nguyen.** The thermal stress of roller-compacted concrete dams during construction // MATEC Web of Conferences. 2018 Vol. 196(04059). 8p. https://doi.org/10.1051/matecconf/201819604059
20. MIDAS Information Technology, Heat of Hydration - Analysis Analysis Manual, Version - 2011, 48p.
21. **N.A. Aniskin, N.T. Chuc.** Temperature regime and thermal stress in a concrete massif with pipe cooling // Power Technology and Engineering. 2019.Vol.52(6). pp. 638-643. https://doi.org/10.1007/s10749-019-01009-9.
22. **JR Zhang,** "A test study on the solar radiation absorption coefficient of concrete surface," Building Science, vol. 22, no. 6, pp. 42–45, 2006.
23. **Guadalupe Leon, Hung-Liang (Roger) Chen.** Thermal analysis of mass concrete containing ground granulated blast furnace slag // CivilEng. 2021 Vol. 2(1). pp. 254-270. https://doi.org/10.3390/civileng2010014.
24. **Hoon Moon, Sivakumar Ramanathan, Prannoy Suraneni, Chang-Seon Shon, Chang-Joon Lee, Chul-Woo Chung**. Revisiting the effect of slag in reducing heat of hydration in concrete in comparison to other supplementary cementitious materials // Materials. 2018 Vol.11. 17p. doi:10.3390/ma11101847.

Aniskin Nikolai Alekseevich, doctor of Technical Sciences, Professor, National Research Moscow State University of Civil Engineering, 129337, 26, Yaroislavskoye Shosse, Moscow, Russia. e-mail aniskin@mgsu.ru; phone +79104377227.

Shaytanov Aleksey Mihaylovich, graduate student, National Research Moscow State University of Civil Engineering, 129337, 26, Yaroislavskoye Shosse, Moscow, Russia. e-mail shaytanov.alexey@mail.ru; phone +79689887119.

*Shaytanov Mikhail Vladimirovich***,** PhD, Deputy General Director, Lengiprorechtrans Company, 29A, Ivana Chernykh, Saint Petersburg, 198095, e-mail shaytanov-sm@mail.ru; phone +79689887119

Анискин Николай Алексеевич – доктор технических наук, профессор; директор института гидротехнического и энергетического строительства, Национальный исследовательский Московский государственный строительный университет (НИУ МГСУ); 129337, г. Москва, Ярославское шоссе, д. 26; e-mail aniskin@mgsu.ru; тел. +79104377227.

Шайтанов Алексей Михайлович, аспирант, Национальный исследовательский Московский государственный строительный университет (НИУ МГСУ); 129337, г. Москва, Ярославское шоссе, д. 26; e-mail shaytanov.alexey@mail.ru; тел. +79104377227

Шайтанов Михаил Владимирович, заместитель генерального директора, Проектно-изыскательский институт «Ленгипроречтранс»; 198095, Санкт-Петербург, ул. Ивана Черных, д. 29, литер А, e-mail shaytanov-sm@mail.ru; тел. +79689887119